Chromatic interaction between light and optoelectronic multilayer structures

Thesis presented for the degree of

Doctor of Philosophy

To the University of St. Andrews

By

Michael Mazilu

January 2000

I, Michael Mazilu, hereby certify that this Thesis, which is approximately 40000 words in length, has been written by me, that it is the record of work carried out by me and that it has not been submitted in any previous application for a higher degree.

Date 5. 2. 2000 signature of candidate

I was admitted as a research student in 1997 and as a candidate for the degree of Doctor of Philosophy in Physics; the higher study for which this is a record was carried out in the University of St. Andrews between 1997 and 2000.

Date 5. 2. 2000 signature of candidate

I hereby certify that the candidate has fulfilled the conditions of the Resolution and Regulations appropriate for the degree of Doctor of Philosophy in the University of St. Andrews and that the candidate is qualified to submit this thesis in application for that degree.

Date 5 | 2 | 2000 signature of supervisor

In submitting this thesis to the University of St. Andrews I understand that I am giving permission for it to be made available for use in accordance with the regulations of the University Library for the time in force, subject to any copyright vested in the work not being affected thereby. I also understand that the title and abstract will be published, and that a copy of the work may be made and supplied to any bona fide library or research worker.

Date 5 2 2000 signature of candidate

Abstract

In this thesis we study the interaction between monochromatic electromagnetic waves and multilayer structures. The optical properties of this structure are described by its reflection and transmission coefficients. We introduce a combination operator giving the optical properties of two such structures together. More complex structures can be built by "adding" further layers or structures. We also define a simple "multiplication" operator which is useful for calculating the optical effects of periodic multilayer structures. These two operators are used to study the effects of the interface roughness in these structures. Further, this method is used to treat the case of nonlinear intensity-dependent propagation. Within the same formalism we treat the continuous refractive index variation present in interdiffused layers. A direct comparison between the roughness and interdiffusion effects is then possible. One-dimensional photonic bandgap structures are studied using the multiplication operator which calculates the band structure. The formalism is applied to the experimental determination of the roughness of GaAs/AlGaAs multiple quantum well structures.

Using this same formalism one can calculate the energy level in quantum wells and generally in multiple quantum well structures. These energy levels correspond to n-level quantum systems. We study the interaction of a monochromatic wave with this system and show that the classical treatment of this interaction breaks down in the case of high intensity excitations. We introduce a method to describe these high intensity effects which is based on a combination of the continuous fraction and the Floquet method. Within this unique formalism we can treat different nonlinear effects such as the Stark shift, the abnormal high harmonic generation and multi-photon resonance and explain their links. Further, this method is generalised to the case of two beam excitations such as pump-probe and non-degenerate four-wave mixing.

Contents

Chapter 1

Introduction

The optical properties of thin films have their origin in the similarity of the wavelength of the light and the thickness of the thin layer. The interference colours of thin films were first observed by R. Hooke and R. Boyle in the 17^{th} century. Hooke concluded that light consists of vibrations propagated at great speed. Later, the wave nature of light was established and described accurately by Maxwell's equations. Considering this description of light we can understand the optical properties of thin films as the interference between the different reflections in the thin layer.

This same effect can be observed in thin layers of semiconductors. In this case we have the wavelength of the electronic quantum wave which is comparable to the thickness of the quantum well. Schrödinger's wave equation describes this phenomenon and leads to the introduction of discrete localised quantum states in quantum wells. These electronic states correspond to stable stationary waves trapped between the two interfaces of the thin layer.

The interaction between these two effects is an optoelectronic effect. This field of study is very important nowadays because of the increase in telecommunication traffic and the increased use in daily life of optoelectronic devices. The design and development of these devices demands a good understanding of the different effects and interactions between the different components of the device and the electrical and optical waves. One of the practical problems arising in the manufacturing of these thin layer devices is their surface roughness. This roughness affects the optical properties of the device and its electronic performance. Another interesting aspect of thin layers and the electronic systems associated with them is their behaviour when subject to high intensities of light.

In this work we address these two problems from a theoretical point of view. In a first step, we consider only problems in one spatial dimension, that is, the waves are homogeneous in the direction transverse to the direction of propagation and the thin layers are plane. In the time domain the waves are taken as being monochromatic. Within this model, the effects of the interface roughness are treated as a loss of coherence of the monochromatic light wave. Our next step is to generalise our method in order to handle more complex structures. Therefore, we introduce a new method (which we call **LTR**) to calculate the optical properties of multilayered structures which allows the study of distributed roughness effects. This method also allows us to treat various other effects such as the intensity dependent non-linear propagation of light in multilayered structures and the continuous refractive index variation in these same structures. This method can be generalised to handle plane waveguides and one-dimensional photonic structures such as distributed Bragg reflectors.

In the second part we concentrate our research on the electronic states of matter and its interaction with one or two monochromatic waves. Using the equivalence between Maxwell's and Schrödinger's equations we used the **LTR** method to calculate the energy levels in multiple quantum wells. The behaviour of this quantum system under electromagnetic excitation is treated in the density matrix formalism with which we study the systems response to high intensity excitations. This study leads to the definition of a precise method for solving the evolution equations.

The first chapter corresponds to this brief introduction.

In the second chapter, we develop a formalism allowing a study of the optical properties of multilayered structures. This formalism is equivalent to other methods, such as the matrix method or the recursive method. The advantage of our method is the simplicity with which each layer is described. We use directly the **L**eft reflection, the **T**ransmission and the **R**ight reflection coefficients as the definition of the characteristics of a single layer. In order to treat more complex structures we introduce a combination law which takes two layers defined respectively by their **LTR** elements combined to a new total **LTR** element. Further, we define a multiplication operator which is particularly suited to the study of periodic multilayered structures.

In the third chapter, we introduce in the **LTR** formalism three different effects. We start by treating within the **LTR** formalism the cumulative effects of interface roughness in multilayered structures. This is facilitated by the direct physical meaning of the **LTR**

elements. We can thus introduce a special **LTR** element which takes into account the interface roughness. This element can then be combined with any other **LTR** element to calculate the optical coefficients of a multilayered structure including roughness. The roughness itself is described by a statistical distribution of the interface position which for simplicity we take to be Gaussian. We further apply the **LTR** formalism to continuous refractive index variation where we define a combination integral operator which can be used to study any variation in the index with depth. Finally, we treat in this chapter the optical properties of these structures when subject to high intensity monochromatic light. In this case, we assume the dependence of refractive index on the incident light intensity. This study presents a problem because this intensity depends on the number of reflections taken into account. We solve this problem by a physically based method. After defining an intensity dependent combination law we proceed by slowly "turning" up the light intensity. This makes possible the definition of a sequence of **LTR** elements converging towards the **LTR** element at the required intensity.

In the fourth chapter, we show that it is possible to apply the **LTR** formalism to other optical devices. We start with the study of plane waveguides where we use the **LTR** formalism to define the guided modes. This can be achieved by considering an exponentially decreasing wave solution of Maxwell's equations alongside propagating wave solutions. A second interesting study using the **LTR** formalism is the treatment of periodic photonic structures. In the one dimensional case we can directly apply the multiplication operator to one period of the structure. For a better understanding of the effects of this operator we break it into two parts: one takes into account the effective interface of the considered period and the other the effective propagation through the period. Combining n such periods is equivalent to a n-times greater propagation length. This allows the direct introduction of the bandstructure in one dimensional periodic structures. Finally, we show how it is possible to expand the **LTR** formalism to three dimensional photonic structures.

In the fifth chapter, we apply the **LTR** formalism to three different practical cases. We start by considering the dependence of an LED emission as a function of the roughness of its surface semi-transparent mirror. In this case we generalise our formalism to take into account the angular dependence of the wave when its propagation direction is not perpendicular to the multilayered structures. Further, in the case of the LED we take into account the emission of the light from inside the structure. The other two cases

correspond to the experimental determination of the surface and interface roughness in multilayered structures. We start by considering a monolayer of CdZnSe. This case is of special interest because it allows a comparison with the directly measured surface roughness by atomic force microscopy. Another application is GaAs/AlGaAs multiple quantum well structures. In this case we are particularly interested in the roughness introduced by the selective oxidation of the layers.

In the sixth chapter, we study the behaviour of a quantum system interacting with an electromagnetic excitation. We start by defining the Schrödinger equation and its stationary solutions. Any solution can be decomposed into stationary solutions and one can then treat the evolution of the system with the help of the density matrix equation. The stationary solutions themselves correspond to the eigenfunctions of the Hamiltonian operator. In the case of multiple quantum wells we use a variation of the optical **LTR** formalism to search for these eigenfunctions.

In the seventh chapter, we use different methods to find solutions to the density matrix eqautions when subject to a stationary excitation. We start by defining a numerical solution where we use a stationary excitation to simplify the procedure. We show the existence of two distinct solutions: the transient and the stationary solutions. A comparison is then made between this numerical solution and different approximating analytical solutions. These solutions are found by using the perturbation expansion, the rotating wave approximation, the continuous fraction method and the Floquet expansion. All of these methods exhibit a breakdown in the solution when the intensity of the excitation is increased. This breakdown occurs regardless of the order of the expansion.

In the eighth chapter, we introduce a new method for solving the density matrix equation for any intensity. This method is based on a combination between the continuous fraction method and the Floquet method. Using this method we define an approximated recursive solution for which we show the convergence towards the exact solution. This method is then generalised to treat the case of a high intensity bichromatic excitation.

In the nineth chapter, we apply the method to solve the density matrix equation for different excitation configurations. These different configurations correspond to single beam, pump probe and non-degenerate four wave mixing. In all of these cases we determine simple analytical expressions for the optical response of the systems which remains valid in different excitation configurations (high or low intensity, resonant or non-resonant excitation). Further, these recursive solutions are used to show different

non-linear phenomena in optics such as the dynamical Stark shift, the abnormal high harmonic generation and multi-photon resonance. As all of these effects can be modelled in a unique framework, we can explain their link and thus gain a better understanding of the dynamics of an n-level system under high intensity excitation. We proceed in the same way for the pump probe and the non-degenerate four wave mixing configurations.

Chapter 2

LTR Method: Monochromatic light propagation in multi-layered systems

2.1 Introduction

In this chapter we start with Maxwell's equations and deduce the scalar wave equation describing the electric field propagation. Using the continuity conditions of the electrical field and the fundamental solution of the scalar equation we study the behaviour of the electromagnetic field at the interface between two media of different refractive indices. This treatment leads to the definition of the reflection and transmission coefficients for a monochromatic plane wave propagating through the interface.

A monolayer consists of two such interfaces. Because of the multiple reflections between the two interfaces the total reflection and transmission coefficients of such a monolayer is not simply the multiplication of the transmission and reflection coefficients. In order to treat a monolayer and more generally a multilayered structure we introduce two calculation methods.

In the matrix method [1–4] each layer is characterised by a matrix whose elements are derived from the thickness and the refractive index. This matrix defines a linear system of equations which links the transmission and reflection coefficients to the starting and ending indices of refraction. Solving this system leads to the two coefficients. For the calculation of the reflection and transmission coefficients when the monochromatic wave comes from the other direction this equation system has to be redefined and solved again.

The second method treated in this chapter is the recursive method [5, 6] . This is based on the assumption that once the reflection and transmission coefficients are known for one layer it can actually be treated as being a single interface described by these coefficients. In consequence, when adding a single monolayer to the initial layer one has to calculate the transmission and reflection coefficients for only one layer whose initial interface is defined by the transmission and reflection coefficients of the first layer. Thus, one is able to take into account all of the layers in a multilayer structure step by step.

In this chapter, we generalise and simplify this method by defining an **LTR** element consisting of three coefficients: reflection from the left, transmission, and reflection from the right. Thus, our method, simplifies the effective interfaces method [7] which considers the transmission from the right and from the left. This **LTR** element completely defines a multilayered structure. Further, we define a composition law which calculates the global **LTR** element of any two **LTR** elements put together. Thus any multilayered structure can be treated within this framework by combining the different **LTR**s of the monolayers constituting the multilayered structure.

To simplify the calculations of periodical structures in the **LTR** framework we define a multiplication operator. This operator allows the direct calculation of the **LTR** for n periods of a structure when the **LTR** is known for one period.

2.2 Background

The starting point of our study of the propagation of light through multi-layered systems is the Maxwell equations [8]

$$\vec{\nabla} \wedge \vec{B} - \frac{1}{c^2}\frac{\partial \vec{E}}{\partial t} = \mu_0 \left(\vec{j} + \frac{\partial \vec{P}}{\partial t} + \vec{\nabla} \wedge \vec{M} \right), \tag{2.1a}$$

$$\vec{\nabla} \wedge \vec{E} + \frac{\partial \vec{B}}{\partial t} = 0, \tag{2.1b}$$

$$\vec{\nabla} \cdot \vec{E} = \frac{1}{\varepsilon_0} \left(\rho - \vec{\nabla} \cdot \vec{P} \right), \tag{2.1c}$$

$$\vec{\nabla} \cdot \vec{B} = 0. \tag{2.1d}$$

These equations describe the time evolution of the vector fields $\vec{E}$ and $\vec{B}$. The constant $c = 1/\sqrt{\mu_0 \varepsilon_0}$ corresponds to the speed of light in vacuum while ρ and $\vec{j}$ correspond to the

free charge density and current flow. In the following we consider Maxwell's equations in the absence of free charges.

The quantities $\vec{P}$ and $\vec{M}$ are the electrical and magnetic polarisation respectively. These polarisations can have two origins in the materials. They can be permanent as in an electret or a permanent magnet or they can be induced by the external electromagnetic field. It is this second case which interests us. We consider non-magnetic ($\vec{M} = 0$) and dielectric materials ($\vec{P} = \varepsilon_0 \chi \vec{E}$). This second assumption implies a linear response of the material whose polarisation is proportional to the electric field.

Using all this simplification and eliminating the magnetic field in equations (2.1) we can write the wave equation for the electrical vector field

$$\nabla^2 \vec{E} - \frac{1}{c^2} \frac{\partial^2 \vec{E}}{\partial t^2} = \frac{\chi}{c^2} \frac{\partial^2 \vec{E}}{\partial t^2}. \tag{2.2}$$

For multilayer structures we will use scalar versions of this equation, one for each component of the electrical field $\vec{E}$, in the form

$$\nabla^2 U - \frac{n^2}{c^2} \frac{\partial^2 U}{\partial t^2} = 0. \tag{2.3}$$

where $n = \sqrt{1 + \chi}$ is the refractive index of the material. To come back to the vectorial wave equation (2.2) one has to consider three equations (2.3), one for each component of the electrical field $\vec{E}$.

The monochromatic travelling wave solution of this equation is

$$U(z, t) = U_0 e^{ik(ct - nz)}, \tag{2.4}$$

where we consider the $z-$axis as the travelling direction. The wave vector is given by $k = 2\pi/\lambda$ where λ is the wavelength. The electrical field is the real part of the complex solution (2.4).

2.2.1 Matrix method

We describe in the following the propagation of monochromatic light through multilayered structures. In this case the propagation can be characterised by the transmission and reflection coefficients. To find these coefficients one considers an incoming

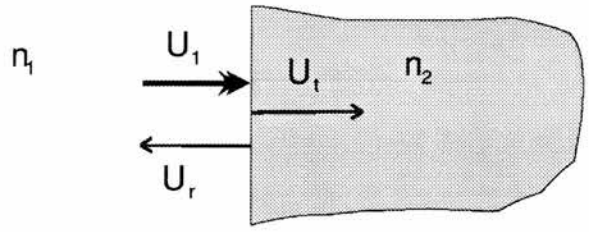

Figure 2.1: Decomposition of the monochromatic field at an interface.

monochromatic wave, $U_1(z,t)$, on to an interface between two layers having different refractive indices n_1 and n_2. At normal incidence this wave splits into two waves: one transmitted, $U_t(z,t)$, and one reflected, $U_r(z,t)$, (see figure 2.1). The scalar fields for these waves are

$$U_1(z,t) = U_0 e^{ik(ct-n_1 z)}, \tag{2.5a}$$

$$U_t(z,t) = t_{12} U_0 e^{ik(ct-n_2 z)}, \tag{2.5b}$$

$$U_r(z,t) = r_{12} U_0 e^{ik(ct+n_1 z)}, \tag{2.5c}$$

where t_{12} and r_{12} correspond to the transmission and reflection coefficients. At the interface we have the continuity condition of the field and its normal derivative (i.e. $\frac{\partial}{\partial z}$)

$$U_1 + U_r = U_t, \tag{2.6a}$$

$$\frac{\partial U_1}{\partial z} + \frac{\partial U_r}{\partial z} = \frac{\partial U_t}{\partial z}. \tag{2.6b}$$

By substituting equations (2.5) into these continuity conditions one finds the following two linear equations

$$1 + r_{12} = t_{12}, \tag{2.7a}$$

$$n_1 - n_1 r_{12} = n_2 t_{12}, \tag{2.7b}$$

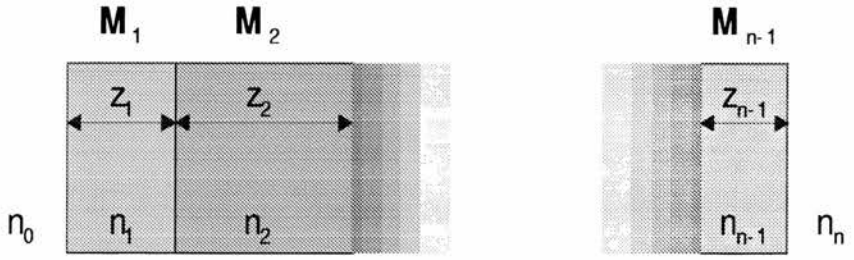

Figure 2.2: Example of a multilayered structure.

which when solved give us the transmission and reflection coefficients

$$r_{12} = \frac{n_1 - n_2}{n_1 + n_2}, \tag{2.8a}$$

$$t_{12} = \frac{2n_1}{n_1 + n_2}. \tag{2.8b}$$

Using the same continuity condition (2.6) one can define the reflection and transmission coefficients, r and t, for a layer of refractive index, n_1, and thickness, z_1. To do this one can introduce the characteristic matrix (for the deduction of this matrix see [9])

$$\mathbf{M} = \begin{pmatrix} \cos(kn_1z_1) & -\frac{i}{n_1}\sin(kn_1z_1) \\ -in_1\sin(kn_1z_1) & \cos(kn_1z_1) \end{pmatrix}. \tag{2.9}$$

Using the characteristic matrix (2.9) the coefficients are defined by the following relation

$$\begin{pmatrix} 1+r \\ n_0(1-r) \end{pmatrix} = \mathbf{M} \begin{pmatrix} t \\ n_2 t \end{pmatrix}, \tag{2.10}$$

where n_0 and n_2 are respectively the refractive indices on the left and right side of the layer. This matrix method takes into account the multiple reflections inside the monolayer and also the interference of the multiple transmitted and reflected electrical fields.

In the case of multiple layers (see figure 2.2) each layer is characterised by a matrix

$$\mathbf{M}_j = \begin{pmatrix} \cos(kn_jz_j) & -\frac{i}{n_j}\sin(kn_jz_j) \\ -in_j\sin(kn_jz_j) & \cos(kn_jz_j) \end{pmatrix}, \tag{2.11}$$

and the total multilayered system is characterised by the matrix product of all the characteristic matrices

$$\mathbf{M} = \mathbf{M}_1\mathbf{M}_2...\mathbf{M}_{n-1}. \tag{2.12}$$

Further, the reflection and transmission coefficients are calculated by using the following relation

$$\begin{pmatrix} 1+r \\ n_0(1-r) \end{pmatrix} = \mathbf{M} \begin{pmatrix} t \\ n_n t \end{pmatrix}, \tag{2.13}$$

where we consider different refractive indices on each side of the multilayered system.

An important property of the matrix $\mathbf{M}$ is that its determinant is equal to 1. This property can be used in the case of a periodical multilayered system. Indeed, the characteristic matrix of such a system is given by $\mathbf{M}^n$ which can be evaluated in this case using the Chebyshev polynomials of the second kind [9,10].

Altogether the characteristic matrix method permits us to calculate the transmission and reflection coefficient of a multilayered system by solving the linear system of equations (2.13). Each time a new layer is added to an already existing structure a new characteristic matrix has to be calculated and the relations (2.13) have to be solved again. The transmission and reflection coefficients of the old structure cannot be re-used. This disadvantage is overcome by using the recursive method which we introduce in the next section.

2.2.2 Recursive method

An alternative method for describing the propagation of a monochromatic wave in a multilayered structure is based on the actual transmission and reflection coefficients for a monolayer of width z_1 index of refraction n_1. To the left of this monolayer we have the refractive index n_0 and to the right the refractive index n_2 (see figure 2.2). Using

the characteristic matrix method we get

$$r_{02} = \frac{r_{01} + r_{12}\exp(2ikn_1z_1)}{1 - r_{10}r_{12}\exp(2ikn_1z_1)} \tag{2.14a}$$

$$r_{20} = \frac{r_{21} + r_{10}\exp(2ikn_1z_1)}{1 - r_{10}r_{12}\exp(2ikn_1z_1)} \tag{2.14b}$$

$$t_{02} = \frac{t_{01}t_{12}\exp(ikn_1z_1)}{1 - r_{10}r_{12}\exp(2ikn_1z_1)} \tag{2.14c}$$

$$t_{20} = \frac{t_{21}t_{12}\exp(ikn_1z_1)}{1 - r_{10}r_{12}\exp(2ikn_1z_1)} \tag{2.14d}$$

where r_{ij} and t_{ij} are the reflection and transmission coefficients at the interfaces between layer i and layer j.

The recurrent method [11] uses the already calculated transmission and reflection coefficients when adding another layer to the structure. Indeed, for $n+1$ layers these coefficients read

$$r_{0n+1} = \frac{r_{0n} + r_{nn+1}\exp(2ikn_nz_n)}{1 - r_{n1}r_{nn+1}\exp(2ikn_nz_n)} \tag{2.15a}$$

$$r_{n+10} = \frac{r_{n+1n} + r_{n0}\exp(2ikn_nz_n)}{1 - r_{n1}r_{nn+1}\exp(2ikn_nz_n)} \tag{2.15b}$$

$$t_{0n+1} = \frac{t_{0n}t_{nn+1}\exp(ikn_nz_n)}{1 - r_{n1}r_{nn+1}\exp(2ikn_nz_n)} \tag{2.15c}$$

$$t_{n+10} = \frac{t_{n+1n}t_{n0}\exp(ikn_nz_n)}{1 - r_{n1}r_{nn+1}\exp(2ikn_nz_n)} \tag{2.15d}$$

where the coefficients r_{1n}, r_{n1}, t_{1n} and t_{n1} correspond to the first n layers.

The advantage of this method is the direct use of the propagation coefficients to define the effects of a multilayered system. On the other hand this method has no advantage in the case of periodical multilayered structures. Further, a single monolayer is not defined as an independent element having some characteristic properties as in the case of the matrix method where each layer is defined by its characteristic matrix. In the following paragraph we solve this problem by introducing an algebra which combines the advantages of the recurrent method with those of the characteristic matrix method.

We wish to mention here another variant of the recursive method which is based on the treatment of transmission lines in the network theory [12–14] as there is an analogy between the two phenomena [15]. Within this method, the results can be graphically evaluated using Smith charts.

2.3 LTR Method

The principal idea of this method is to characterise each element or ensemble of elements of a stratified medium by its transmission and reflection coefficients. First of all we need to count the number of parameters characterising one multilayered structure. In the case of the characteristic matrix method a two by two matrix describes one monolayer or a system of monolayers, which means four parameters are needed for the characterisation of such a system. The determinant of this matrix is always equal to one, thus the four parameters identified are not independent but have to fulfill a condition. This reduces the number of parameters needed for the characterisation of a multilayered structure to three.

Indeed there are three different reflection and transmission coefficients for a given multilayered structure. The field reflection coefficients for an incident wave propagating from the right, r_R, or from the left, r_L, are generally not the same. This counts for two parameters. On the other hand, the transmission coefficient is the same for any stratified medium when coming from the right or from the left. Thus, the field transmission coefficient t is the third parameter needed.

A convenient way of writing the three parameters characterising a multilayered system is to write them in column form. Further we replace the reflection coefficient from the left by L, the transmission coefficient by T and the reflection coefficient from the right by R. As an example of these new definitions we can take a look at the **LTR** element for a single monolayer, $\mathcal{L}$, of refractive index n and width z

$$\mathcal{L}(n,k,z) = \begin{pmatrix} L \\ T \\ R \end{pmatrix} = \begin{pmatrix} r_L \\ t \\ r_R \end{pmatrix} = \begin{pmatrix} r\frac{1-p^2}{1-p^2r^2} \\ p\frac{\left(1-r^2\right)}{\left(1-p^2r^2\right)} \\ r\frac{1-p^2}{1-p^2r^2} \end{pmatrix}, \tag{2.16}$$

with

$$\begin{cases} r = \frac{1-n}{1+n} \\ p = \exp(iknz) \end{cases}. \tag{2.17}$$

In this example we consider a monolayer surrounded by a vacuum of refractive index 1. This points out a further difference between our **LTR** method and the two methods introduced above. Indeed a monolayer is intrinsically described by the **LTR** element

which does not depend on the neighbouring layers. This is not the case for the above mentioned methods. To achieve this, all the layers are characterised with respect to the vacuum even when they are embedded in a multilayered structure. This method corresponds to inserting infinitely small layers of vacuum between the different layers which does not affect the reflectivity and transmission of a multilayer structure [16]. This can also be shown by considering the continuity conditions (2.6).

The **LTR** element $\mathcal{L}(n,k,z)$ defined by (2.16) constitutes the fundamental element of a multilayered structure. To calculate the reflection and transmission coefficients for such a structure from $\mathcal{L}(n_i,k,z_i)$ we need to define the combination law for any two **LTR** elements. Using the definitions of L, T, R and the recurrent method, one can define the effect of combining two **LTR** elements

$$\begin{pmatrix} L_1 \\ T_1 \\ R_1 \end{pmatrix} \oplus \begin{pmatrix} L_2 \\ T_2 \\ R_2 \end{pmatrix} = \begin{pmatrix} L_1 + \frac{L_2 T_1^2}{1-R_1 L_2} \\ \frac{T_1 T_2}{(1-R_1 L_2)} \\ R_2 + \frac{R_1 T_2^2}{1-R_1 L_2} \end{pmatrix}. \tag{2.18}$$

This composition of the two **LTR** elements corresponds to calculating the propagation coefficients of a infinitely narrow vacuum gap limited on the left by (L_1,T_1,R_1) and on the right by (L_2,T_2,R_2). We thus can define a new **LTR** element which can further be combined with another one. The reflection and transmission coefficients of the structure represented in figure 2.2 is given by

$$\mathcal{L}(n_1,k,z_1) \oplus \mathcal{L}(n_2,k,z_2) \oplus \cdots \oplus \mathcal{L}(n_{n-1},k,z_{n-1}), \tag{2.19}$$

where the starting and ending media are considered to be vacuum ($n_0 = n_n = 1$).

As a first example of the composition law we can consider the case of the composition of two layers with identical index of refraction but of different width

$$\begin{aligned}\mathcal{L}(n,k,z_1)\oplus\mathcal{L}(n,k,z_2) &= \begin{pmatrix} r\frac{1-p_1^2}{1-p_1^2r^2} \\ p_1\frac{(1-r^2)}{(1-p_1^2r^2)} \\ r\frac{1-p_1^2}{1-p_1^2r^2}\end{pmatrix}\oplus\begin{pmatrix} r\frac{1-p_2^2}{1-p_2^2r^2} \\ p_2\frac{(1-r^2)}{(1-p_2^2r^2)} \\ r\frac{1-p_2^2}{1-p_2^2r^2}\end{pmatrix} \\ &= \begin{pmatrix} r\frac{1-(p_1p_2)^2}{1-(p_1p_2)^2r^2} \\ p_1p_2\frac{(1-r^2)}{(1-(p_1p_2)^2r^2)} \\ r\frac{1-(p_1p_2)^2}{1-(p_1p_2)^2r^2}\end{pmatrix} \\ &= \mathcal{L}(n,k,z_1+z_2). \end{aligned} \tag{2.20}$$

where $p_1 = \exp(iknz_1)$ and $p_2 = \exp(iknz_2)$.

To define a group using the "additive" composition (2.18) we need to define a neutral **LTR** element that does not change anything when combined with any other **LTR** element. In our case this corresponds to an infinitely narrow vacuum layer

$$N = \begin{pmatrix} 0 \\ 1 \\ 0 \end{pmatrix}, \tag{2.21}$$

which has no reflectivity from either side and a transmission coefficient of one. Further, we need to show that there is always an inverse **LTR** element for every given **LTR**. This inverse element is defined by

$$-\begin{pmatrix} L \\ T \\ R \end{pmatrix} = \begin{pmatrix} -L/(T^2-LR) \\ T/(T^2-LR) \\ -R/(T^2-LR) \end{pmatrix}, \tag{2.22}$$

where with the minus sign we indicate the inverse. In the discussion we will see what happens when $T^2 - LR = 0$. When combining a **LTR** element with its inverse one finds

as expected the neutral element

$$\begin{pmatrix} L \\ T \\ R \end{pmatrix} \oplus - \begin{pmatrix} L \\ T \\ R \end{pmatrix} = \begin{pmatrix} 0 \\ 1 \\ 0 \end{pmatrix}. \tag{2.23}$$

Thus the set of **LTR** elements forms a group with respect to the composition law (2.18). This group is non-abelian because it does not commute (i.e. the result depends on the order of the composition). Indeed one can easily think of two different layers that would show a difference in the optical properties displayed depending on the order in which they are put together.

2.3.1 Multiplication (polynomial method)

In the case of a periodic structure we are interested in calculating the optical effects of a sequence of n identical layered structures. This can be determined by the composition of n **LTR** elements which defines a multiplication law in the **LTR** group

$$\underbrace{\begin{pmatrix} L \\ T \\ R \end{pmatrix} \oplus \begin{pmatrix} L \\ T \\ R \end{pmatrix} \oplus ... \oplus \begin{pmatrix} L \\ T \\ R \end{pmatrix}}_{\text{n times}} = n \begin{pmatrix} L \\ T \\ R \end{pmatrix}. \tag{2.24}$$

To define an operator that acts like a multiplication we need to show first that the **LTR** element 'multiplied' by an integer number is of the form

$$n \begin{pmatrix} L \\ T \\ R \end{pmatrix} = \begin{pmatrix} L\frac{s_n}{d_n} \\ \frac{t_n}{d_n} \\ R\frac{s_n}{d_n} \end{pmatrix}, \tag{2.25}$$

where the quantities s_n, t_n and d_n are polynomials of L, T and R. Further, we consider the following property of these polynomials

$$t_n^2 = d_n^2 + (T^2 - RL - 1)s_n d_n + RLs_n^2, \tag{2.26}$$

to hold. As we will see this property is necessary in order for the polynomials s_n, t_n and d_n to exist.

In the following we show that this property and the polynomial form is true for any integer multiplication factor n. To do this we use the recursive theorem which states that if a relation holds for $n = 1$ and the assumption of being true for n implies it to be true for $n + 1$, then this relation holds for all $n \in \mathbb{N}$. In the case of $n = 1$ (neutral element for the multiplication) we have indeed $s_1 = d_1 = 1$ and $t_1 = T$. Further, we can verify that the relation (2.26) is fulfilled for s_1, t_1 and d_1. Let us presume that the relations (2.25) and (2.26) are true for the integer n and show that they imply these relations to be valid for $n + 1$

$$\begin{aligned}(n+1)\begin{pmatrix} L \\ T \\ R \end{pmatrix} &= n\begin{pmatrix} L \\ T \\ R \end{pmatrix} \oplus \begin{pmatrix} L \\ T \\ R \end{pmatrix} \\ &= \begin{pmatrix} L\frac{s_n}{d_n} \\ \frac{t_n}{d_n} \\ R\frac{s_n}{d_n} \end{pmatrix} \oplus \begin{pmatrix} L \\ T \\ R \end{pmatrix} \\ &= \begin{pmatrix} L\frac{s_n d_n - RLs_n^2 + t_n^2}{d_n^2 - RLs_n d_n} \\ \frac{t_n T}{d_n - RLs_n} \\ R\frac{d_n - RLs_n + T^2 s_n}{d_n - RLs_n} \end{pmatrix}. \end{aligned} \tag{2.27}$$

We have to use the property (2.26) on (2.28) to show that we can define a unique set of polynomials s_n, t_n and d_n. We have then

$$(n+1)\begin{pmatrix} L \\ T \\ R \end{pmatrix} = \begin{pmatrix} L\frac{d_n - RLs_n + T^2 s_n}{d_n - RLs_n} \\ \frac{t_n T}{d_n - RLs_n} \\ R\frac{d_n - RLs_n + T^2 s_n}{d_n - RLs_n} \end{pmatrix}. \tag{2.28}$$

Using the recursive theorem this shows that the polynomial property is true for all $n \in \mathbb{N}$. Further we can identify the link between the polynomials of different order

$$s_{n+1} = d_n - RLs_n + T^2 s_n, \tag{2.29a}$$

$$t_{n+1} = Tt_n, \tag{2.29b}$$

$$d_{n+1} = d_n - RLs_n. \tag{2.29c}$$

To finish our deduction we have to show also that the property (2.28) holds for the order $n+1$. Indeed using the above definitions one can show after simplification that

$$t_{n+1}^2 = d_{n+1}^2 + (T^2 - RL - 1)s_{n+1}d_{n+1} + RLs_{n+1}^2. \tag{2.30}$$

In the following we study the series s_n, t_n and d_n which are defined in a recursive manner. In the case of the polynomial d_n we have the following five terms which we use to define the general form of the sequence

$$d_1 = 1, \tag{2.31a}$$

$$d_2 = 1 - RL, \tag{2.31b}$$

$$d_3 = (1 - RL + T^2)^2 - T^2(2 + T^2 - RL), \tag{2.31c}$$

$$d_4 = (1 - RL + T^2)^3 - T^2(1 - RL + T^2)(3 + T^2 - RL) + T^4, \tag{2.31d}$$

$$\begin{aligned} d_5 = {} & (1 - RL + T^2)^4 - T^2(1 - RL + T^2)^2(4 + T^2 - RL) \\ & + T^4(3 + 2(T^2 - RL)), \end{aligned} \tag{2.31e}$$

$$\vdots$$

$$\begin{aligned} d_n = {} & (1 - RL + T^2)^{n-1} - T^2(1 - RL + T^2)^{n-3}(n - 1 + T^2 - RL) \\ & + \cdots . \end{aligned} \tag{2.31f}$$

Indeed, after searching a little one finds that the coefficients in this polynomial can be expressed as factors of binomial coefficients. The general expression of the series d_n is

$$d_n = \sum_{i=0}^{n-1} (-T^2)^i (1 - RL + T^2)^{n-2i-1} \left(\binom{n-i}{i} + (T^2 - RL)\binom{n-i-1}{i} \right). \tag{2.32}$$

In the same way we can find the general expression of the s_n series

$$s_n = \sum_{i=0}^{n-1} (-T)^i (1 - RL + T)^{n-2i-1} \binom{n-i-1}{i}, \tag{2.33}$$

where the binomial coefficient is defined by

$$\binom{n}{m} = \frac{n!}{m!\,(n-m)!}, \tag{2.34}$$

and where we consider the binomial coefficient to be zero if $m > n$. The series t_n turns out to be a simple geometrical sequence that can be expressed by

$$t_n = T^n. \tag{2.35}$$

We have thus defined the integer multiplication operator which has the form of a rational fraction (2.25) with the numerators given by the series (2.33) and (2.35) and the denominator by the series (2.32). This rational fraction can be generalised to take into account the multiplication with non-integer numbers by using the following generalised binomial coefficient

$$\binom{n}{m} = \frac{\Gamma(n+1)}{\Gamma(m+1)\Gamma(n-m+1)}, \tag{2.36}$$

where $\Gamma(n)$ is the Euler gamma function.

2.3.2 Multiplication

Although the multiplication formalism is easy to understand and apply, the operator that defines the multiplication as a rational expression of the parameters L, T and R is rather complicated. To simplify this operator we have to introduce the parameters a, b and c which we define later as functions of L, T and R.

Indeed, inspired by the composition of two monolayer **LTR** elements as defined by equation (2.20) we find that for any parameters a, b and c the **LTR** element

$$\begin{pmatrix} L_n \\ T_n \\ R_n \end{pmatrix} = \begin{pmatrix} ca\frac{1-b^{2n}}{1-a^2b^{2n}} \\ \frac{b^n(1-a^2)}{1-a^2b^{2n}} \\ \frac{a}{c}\frac{1-b^{2n}}{1-a^2b^{2n}} \end{pmatrix}, \tag{2.37}$$

has a very interesting property. The composition of two such **LTR** elements gives

$$\begin{pmatrix} L_n \\ T_n \\ R_n \end{pmatrix} \oplus \begin{pmatrix} L_m \\ T_m \\ R_m \end{pmatrix} = \begin{pmatrix} ca\frac{1-b^{2(n+m)}}{1-a^2b^{2(n+m)}} \\ \frac{b^{n+m}(1-a^2)}{1-a^2b^{2(n+m)}} \\ \frac{a}{c}\frac{1-b^{2(n+m)}}{1-a^2b^{2(n+m)}} \end{pmatrix} \tag{2.38a}$$

$$= \begin{pmatrix} L_{m+n} \\ T_{m+n} \\ R_{m+n} \end{pmatrix}. \tag{2.38b}$$

This means that for the **LTR** elements defined by (2.37) the composition law simplifies to a simple normal addition. Further, a given set of **LTR** elements based on the same parameters a, b and c forms a subgroup where each element is defined by its order number n. Within this subgroup the multiplication operator simplifies to a simple multiplication of the order number by the multiplication factor

$$m\begin{pmatrix} L_n \\ T_n \\ R_n \end{pmatrix} = \begin{pmatrix} ca\frac{1-b^{2(nm)}}{1-a^2b^{2(nm)}} \\ \frac{b^{nm}(1-a^2)}{1-a^2b^{2(nm)}} \\ \frac{a}{c}\frac{1-b^{2(nm)}}{1-a^2b^{2(nm)}} \end{pmatrix} = \begin{pmatrix} L_{m*n} \\ T_{m*n} \\ R_{m*n} \end{pmatrix}. \tag{2.39}$$

In order to use this subgroup to define the general multiplication operator we must make the first order element of the subgroup equal to any given **LTR** element. We have to chose the parameters a, b and c so that the following relation is true

$$\begin{pmatrix} L_1 \\ T_1 \\ R_1 \end{pmatrix} = \begin{pmatrix} ca\frac{1-b^2}{1-a^2b^2} \\ \frac{b(1-a^2)}{1-a^2b^2} \\ \frac{a}{c}\frac{1-b^2}{1-a^2b^2} \end{pmatrix} = \begin{pmatrix} L \\ T \\ R \end{pmatrix}. \tag{2.40}$$

This relation implies that the composition of any integral number of layers can be calculated using the relation (2.38). This relation implies the following equation for the parameter a

$$\sqrt{RL}a^2 - (1 + RL - T^2)a + \sqrt{RL} = 0. \tag{2.41}$$

We can thus deduce the parameters a, b and c to be equal to

$$a = \frac{1 + RL - T^2 + \sqrt{(1 + RL - T^2)^2 - 4RL}}{2\sqrt{RL}}, \tag{2.42a}$$

$$b = \frac{1 - RL + T^2 + \sqrt{(1 - RL + T^2)^2 - 4T^2}}{2T} \tag{2.42b}$$

$$= \frac{T^2 - RL + \sqrt{RL}a}{T}, \tag{2.42c}$$

$$c^2 = \frac{L}{R}. \tag{2.42d}$$

The root of (2.41) is chosen so that in the case of a monolayer the parameter a corresponds to r in (2.17). The other possible solution gives $a = 1/r$ and $b = 1/p$.

Using the property (2.38) with the parameters (2.42) we can define, with the help of (2.37), a multiplication operator. This operator reads

$$n \begin{pmatrix} L \\ T \\ R \end{pmatrix} = \begin{pmatrix} ca\frac{1-b^{2n}}{1-a^2b^{2n}} \\ \frac{b^n(1-a^2)}{1-a^2b^{2n}} \\ \frac{a}{c}\frac{1-b^{2n}}{1-a^2b^{2n}} \end{pmatrix}, \tag{2.43}$$

which is much simpler than the preceding definition of this operator (2.25) using the rational functions.

The definition of the multiplication operator by (2.43) implies other interesting properties. The multiplication by zero gives the neutral element for the composition law,

while the multiplication by minus one gives the inverse element as follows

$$0\begin{pmatrix} L \\ T \\ R \end{pmatrix} = \begin{pmatrix} 0 \\ 1 \\ 0 \end{pmatrix}, \tag{2.44a}$$

$$-1\begin{pmatrix} L \\ T \\ R \end{pmatrix} = \begin{pmatrix} -L/(T-LR) \\ T/(T-LR) \\ -R/(T-LR) \end{pmatrix}. \tag{2.44b}$$

Another benefit of this definition of the multiplication operator is its direct applicability to the multiplication by non-integer numbers without the use of complicated functions such as the Euler gamma function. One use of the multiplication operator in its non-integer form is the possibility of easily modelling the reflectivity coefficient of a multilayered structure during growth. For example, the **LTR** element for n and a half layers is given by the composition of the **LTR** element of n layers and one last layer multiplied by one half. Another possible use of the multiplication with a non-integral number is the backwards calculation of the reflectivity coefficient of one period from the measure of the optical properties of n periods of multilayered structures. In this case the measured **LTR** element is simply multiplied by $1/n$. We must note here that this multiplication operator is based on the parameter b to the power of n. If n is not an integer, b^n is not uniquely defined and special care must be taken because the power function is multi-valued.

2.4 Discussion

We start our discussion with the study of the domain of definition of the **LTR** method. This is important in that it gives insight into the different special cases that can be encountered while using this method and thus a better understanding of the method itself can be gained. Further, we can deduce some general conclusions about the behaviour of multilayered systems. Indeed, in the preceding section we have five cases whereby, for the calculation of the **LTR** element, we use a division by a denominator that can in some cases be zero. Consequently, in the following we will study the definition of the **LTR** element for a single monolayer (2.16), the composition law (2.18), the definition

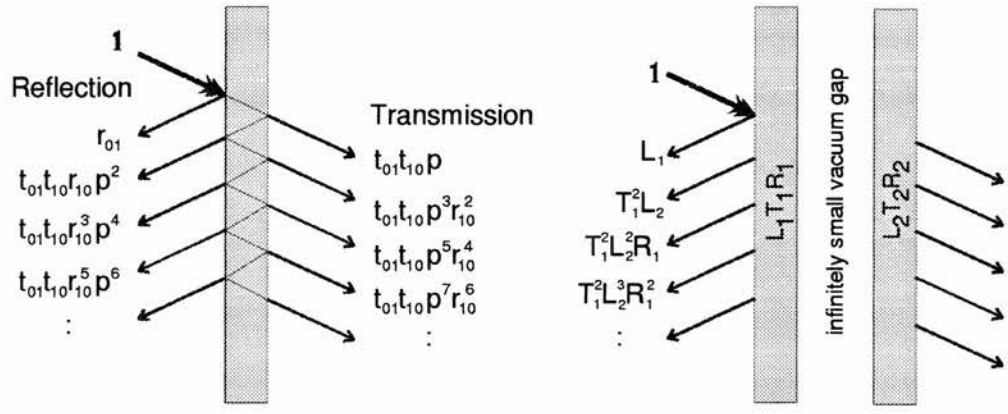

Figure 2.3: Decomposition into multiple reflections for a monolayer and for the composition of two multilayered structures.

of the inverse element (2.22), the multiplication operator using the binomial coefficients (2.25) and finally the multiplication as defined by equation (2.43).

In the case of a single monolayer (2.16) the **LTR** element is not defined when we have

$$1 = r^2p^2. \tag{2.45}$$

If we consider only absorbing materials (i.e. whose imaginary part of the index is positive $\mathrm{Im}(n) > 0$) then this can never be the case. We then have $|p^2| < 1$ and thus $1 > |r^2p^2|$.

On the other hand, the treatment of materials exhibiting gain with the **LTR** method must be carried out with some caution. To better understand the implications of this statement let us take a closer look at the transmission and reflection of a monochromatic wave by a single monolayer. The total field reflected and transmitted can be decomposed into a sequence of multiple waves travelling back and forth in the layer reflected by its two interfaces (see figure 2.3). It is the sum of all these fields coming out of the layer that gives the resultant reflected and transmitted wave. As an example we consider the reflected wave and calculate this sum for an incident field of amplitude one. This gives us the reflection coefficient to the left

$$L = r - t_{12}t_{21}p^2r - t_{12}t_{21}p^4r^3 - t_{12}t_{21}p^6r^5 - \cdots \tag{2.46a}$$

$$= r - t_{12}t_{21}p^2r(1 + p^2r^2 + p^4r^4 + p^6r^6 + \cdots). \tag{2.46b}$$

We can now see directly that the reflection coefficient is not defined when the above geometric series is not converging. This is the case for $1 \leq |r^2p^2|$. Physically this would mean that during the multiple reflection in the monolayer the amplitude of the wave is increasing. For this to occur, not only has the material to amplify the wave but also the losses due to the reflection at the interface must be small. Whereas for an absorbing layer we can always calculate the **LTR** element.

The second case that we consider is the actual composition law (2.18). Indeed the composition of two **LTR** elements is not defined when $1 = R_1 L_2$. This case can be easily dismissed when considering only absorbing material. Their reflection coefficients have a modulus less than one and thus the denominator of (2.18) can not physically be zero. To understand why this problem arises let us consider the two reflection coefficients with a modulus equal to one ($1 = R_1 = L_2$). This would correspond to a case where the composition law is not defined and would arise when the light wave is trapped between two totally reflecting interfaces.

An alternative approach would consider the multiple reflection picture (see figure 2.3), similar to the case of a monolayer. We have then

$$L = L_1 + T_1^2 R_1 L_2 + T_1^2 R_1^2 L_2^2 + T_1^2 R_1^3 L_2^3 + \cdots \tag{2.47a}$$

$$= L_1 + T_1^2 R_1 L_2 (1 + R_1 L_2 + R_1^2 L_2^2 + \cdots). \tag{2.47b}$$

Again this coefficient is defined by a geometric series which converges only if $1 > |R_1 L_2|$. To be complete we have to show next that any two **LTR** elements whose coefficients have a modulus less than one will, when combined, give a **LTR** element of the same kind. The actual mathematical demonstration of this property is beyond the scope of this chapter.

The study of the case where the **LTR** elements have no inverse, leads to an interesting observation. Indeed the inverse (2.22) is not defined when $T^2 - LR = 0$. Let us consider therefore a multilayered structure defined by an **LTR** element. We can then calculate the reflected light to the left and to the right of this structure while it is monochromatically illuminated from the left and from the right (see figure 2.4). We have then

$$E_1' = TE_1 + RE_2, \tag{2.48a}$$

$$E_2' = LE_1 + TE_2. \tag{2.48b}$$

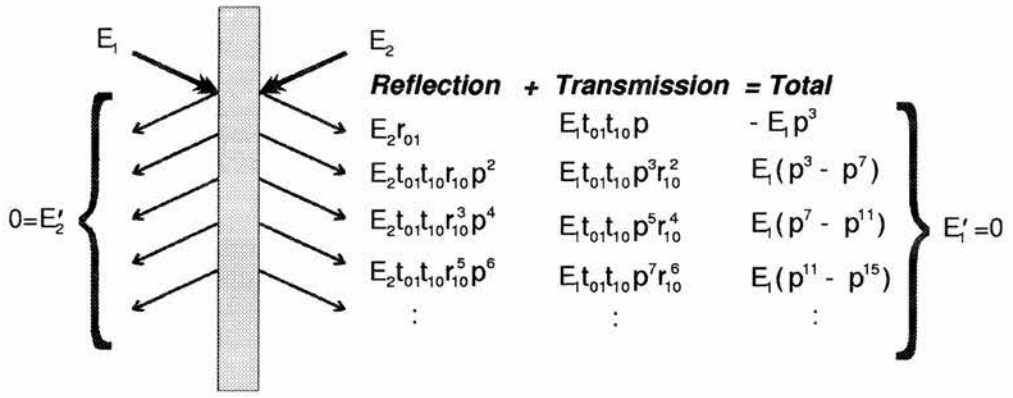

Figure 2.4: Decomposition into multiple reflections in the case of total absorption. To calculate the total outgoing field on the right side of the monolayer we considered the total absorption conditions $r_{10} = -r_{01} = p$ and $E_1 = E_2$. By symmetry the left hand side of the monolayer leads to the same results.

This corresponds to a linear system of equations linking the incident field amplitudes with the amplitudes of the field leaving the multilayered structure. When the above mentioned condition $T^2 - LR = 0$ is fulfilled there exists a family of fields E_1 and E_2 such that no light comes out of the structure. One can say that the transmitted wave from the left is destructively interfering with the reflected wave from the right and vice versa. This can be seen also in the decomposition of the fields into the multiple reflection scheme (see figure 2.4).

Further using (2.16) the definition of the **LTR** element for one monolayer, one can deduce the conditions imposed on the coefficients r and p by the condition $T^2 - LR = 0$. We then have the simple relation $r = p$ which states that the losses through reflection are equal to the losses due to the absorption while propagating through the material. Using this derived condition we can graphically illustrate the index of refraction, absorption coefficients and length of such a monolayer. Figure 2.5 shows that there is a complete family of complex indices for which a monolayer of a certain length would be totally absorptive. The optical length indicated corresponds to $2\pi z/\lambda$ where z is the actual thickness of the monolayer. Further, one can easily imagine more complicated structures where the condition of total absorption is fulfilled.

The intuitive explanation of the impossibility of defining an inverse element for a total absorptive structure is as follows. Having an inverse element means that one can mathematically conceive an inverse structure that, combined with the first real structure, will give something that has no effect (neutral element). If the initial structure has the

property of total absorption then the light going through the inverse structure would be totally absorbed by the real structure and thus cannot go through. It is then impossible to conceive a structure that would allow the light to be transmitted.

We now consider the case of the multiplication operator for a positive integer. This can be treated using the rather heavy formalism (2.25) of the sequence of polynomials s_n, t_n and d_n. For the operator to be defined, the denominator sequence d_n has to be different from zero. We can split the multiplication by n into the multiplication by $(n-1)$ and the combination with one further **LTR** element. We have already treated this last combination at the beginning of this section and showed that it is defined when the multilayered structures are absorptive.

Finally, we discuss the multiplication operator as defined by (2.43). From this definition of the multiplication the following property holds

$$m\left[n\begin{pmatrix} L \\ T \\ R \end{pmatrix}\right] = (m * n)\begin{pmatrix} L \\ T \\ R \end{pmatrix}. \tag{2.49}$$

Thus if the multiplication (2.43) is not defined for $n_1(\mathbf{LTR}_1)$ then it will not be defined for the inverse of $-n_1^{-1}$ $(\mathbf{LTR}_1)$. This brings us to the case already studied beforehand where we showed that the **LTR** elements corresponding to the total absorption cannot be multiplied by minus one.

2.5 Summary

In this chapter we started with the Maxwell equations to show the effects of an interface between two materials with different refractive indices. These effects are considered for a monochromatic wave and can be represented in the simplest case by the reflectivity and transmission coefficients. The determination of these coefficients becomes more difficult when considering a multilayered structure. To illustrate this, we showed two different methods normally used to calculate these coefficients. While the matrix method is easy to apply, the parameters employed to calculate this matrix are not straightforward physical parameters. This property also implies a complicated definition of the optical transmission and reflection coefficients in the case of a periodic multilayered system (use of the Chebyshev polynomials of the second kind). The second method considered is the

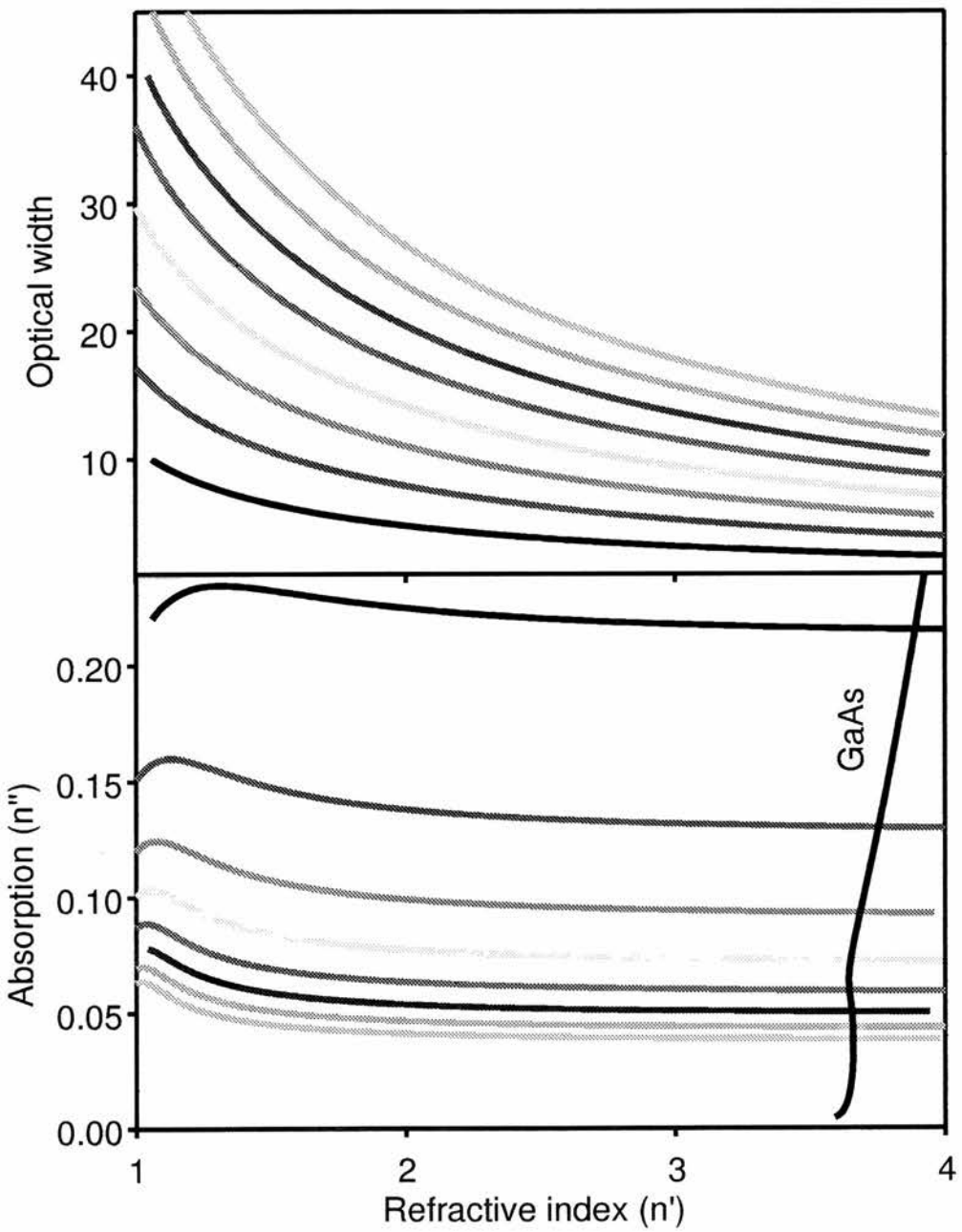

Figure 2.5: Graphical representation of the total absorption condition (only some possible conditions are considered). As an example the lower graph includes also the complex index of GaAs as a function of wavelength from 600nm to 900nm [17] (900nm is at the bottom of the figure).

iterative method. This method, while using only physical parameters (transmission and reflection coefficients), is difficult to generalise directly to consider periodic structures, that is, the periodicity does not simplify the problem.

We thus introduced a formalism that allows a very simple calculation of the reflectivity and transmission coefficients in the case of periodic multilayered structures and at the same time it uses only physical parameters. This formalism consists of a combination law which enables us to calculate the optical properties of two successive multilayered structures when the optical properties of each of them is individually known. Further the formalism comprises a multiplicative operator which allows the direct calculation of the optical properties of a periodic structure when they are known for one period.

We finished this chapter by reviewing the different special cases which can arise when using this formalism. We showed that all of these cases have a physical meaning. Using these special cases we deduced the existence of total absorption in multilayered structures under certain conditions.

Chapter 3

Roughness, continuous refractive index variation and non-linear propagation in multilayered structures

3.1 Introduction

In this chapter we show how to include three different effects into the **LTR** (**L**eft reflection, **T**ransmission and **R**ight reflection) formalism. We begin by defining an **LTR** element which corresponds to interface roughness. This element can be used between two layers in order to model the effects of interface roughness on the transmission and reflection coefficients. Further we generalise the **LTR** formalism to treat continuous refractive index variation. This is the case when the layers interdiffuse for example. Another phenomenon that we study in this chapter is the response of a multilayered structure to a high intensity monochromatic wave. In this case the refractive index and the absorption coefficient depend on the intensity of the light and thus the transmission and reflection coefficients change with intensity.

The roughness of an interface influences greatly the optical properties of a multilayered structure [18]. Its quantitative measure is very important for assessing the quality of such a structure. Too much roughness implies a large amount of scattered light which is no longer available for transmission, reflection or absorption. This can be seen on an unpolished surface where the interface becomes opaque because of the roughness of the surface. This opacity is due to the large amount of scattered light but also to the phase

change of the reflected or transmitted light. In its turn, the phase change is induced by the passage of the light through this uneven surface. In this chapter we model statistically, in one dimension, the effects of an uneven surface on the phase of a monochromatic wave. This phase change leads to the interference between the light interacting with the different parts of the surface which in turn changes its reflection and transmission.

Another application of the **LTR** formalism is the easy calculation of the continuous refractive index variation in multilayered structures (for a similar study see [19]). This variation can be achieved by induced partial disorder through annealing. In this case two adjacent layers interdiffuse implying a gradual change of refractive index between the two layers. In order to treat this continuous refractive index variation we use the multiplication operator discussed in the preceding chapter.

In the third part of this chapter we study the effects of a high intensity monochromatic wave on a multilayered structure [20,21]. By high intensity we mean the intensity needed to induce a change in the refractive index of the material. The problem in modelling such an interaction arises from the change of intensity during the light propagation through the structure. Thus, as it propagates it will change the refractive index by different amounts and consequently more or less light propagates. This effect couples the reflection and transmission coefficients to the light intensity and vice-versa. In a multilayered structure the major problem has its source in the multiple reflections between the different layers. Thus, knowing the transmission and reflection coefficients for the incident intensity is useless because after multiple reflections the incident intensity might change and induce a different amount of transmission. Due to this change, the multiple reflections have to be recalculated because of the different intensity and so on. We solve this problem by not using specific transmission and reflection coefficients during the calculation but by defining a dependence for each layer. This dependence is then used to define a composition law for the dependence in the **LTR** frame-work. Using this generalised composition law we can calculate, for example, the effects of combining two non-linear elements to determine a new intensity dependence for the combined element.

3.2 Roughness effects

This section starts with the theoretical treatment of the surface roughness as a statistical distribution of the depth of the interface. To simplify the calculations we take this

distribution to be a normalised Gaussian function centred on the mean position of the interface. The width of the Gaussian corresponds to the measure of the roughness. At the same time this uneven interface induces different optical path lengths to a perfect monochromatic wave transmitted or reflected by it. Knowing the roughness distribution we are then able to calculate the distribution of the phase and amplitude after such an interaction. When this beam interacts with a second rough surface its phase and amplitude distributions change again. The resulting distribution turns out to be the convolution between the phase-amplitude distribution of the wave and the distribution characterising the second rough surface. After some mathematical treatment we are then able to characterise the propagation through a rough monolayer including the effects of the multiple reflections on the boundaries of the monolayer. The transmission and reflection coefficients deduced by this method are then used to define the fundamental **LTR** element for one monolayer including roughness.

3.2.1 Model

To a first approximation, the roughness is modeled by a succession of parallel planes (see figure 3.1) which are located at different positions. The effects of the different slopes of the planes are neglected here. The positions of the planes are characterised by the distribution function $s(\zeta)$ which corresponds to the proportion of the surface at the position ζ. This distribution function is normalised

$$\int_{-\infty}^{\infty} s(\zeta)d\zeta = 1. \tag{3.1}$$

The origin of the position variable ζ is chosen so that the distribution is centered. This means that the average position of the surface is at $\zeta = 0$, that is, the first order momentum of the distribution is

$$0 = \int_{-\infty}^{\infty} \zeta s(\zeta)d\zeta. \tag{3.2}$$

The parallel planes are distributed around this mean position. The roughness is then characterised by the width of this distribution which corresponds to the second order

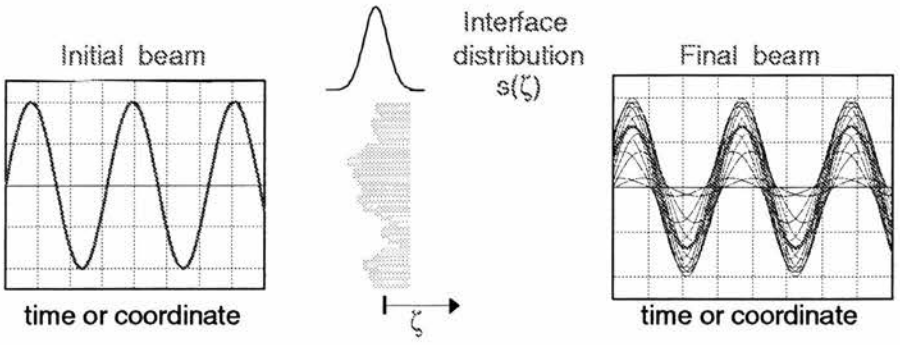

Figure 3.1: Interface roughness distribution and its effects.

momentum of $s(\zeta)$

$$\Delta\zeta^2 = \int_{-\infty}^{\infty} \zeta^2 s(\zeta) d\zeta. \tag{3.3}$$

On the other hand the monochromatic wave is characterised by a complex amplitude distribution $A(\zeta)$. This distribution gives the amplitude and phase of the wave which has travelled the distance ζ with respect to the the centre of the distribution. For example, a coherent and monochromatic wave corresponds in this description to an amplitude distribution function given by the Dirac delta function $A_0\delta(\zeta)$ since the wave is composed of only one amplitude and phase. When such a wave meets with a rough surface it loses its coherence and consequently the amplitude distribution gets wider. Indeed, after passing through the interface the beam is made up of different parts each having passed through a different portion of the interface and thus having acquired different amplitudes and phases. This process repeats itself on each passage through an interface. We must note here that this is an empirical model and the propagation of the wave treated in this manner is not a solution of Maxwell's equations because it does not take into account the light scattered off-axis.

In order to calculate the effects of the roughness on a monochromatic wave with a general amplitude distribution we determine its effects on a normalised Dirac amplitude distribution (coherent wave $A_i(\zeta) = \delta(\zeta)$). We start with a study of the reflection from an interface characterised by the roughness distribution $s(\zeta)$.

The amplitude of the wave reflected from the interface at the position ζ is

$$A_{reflection}(\zeta) = rs(\zeta)e^{2ik\zeta}, \tag{3.4}$$

where k is the wave vector of the monochromatic wave. The first coefficient $r = (1 - n)/(1 + n)$ corresponds to the normal reflection coefficient which is independent of the actual position of the interface. The last two terms correspond to the ratio of the interface at the position ζ and to the phase change undergone by the wave when reflected from this position. If the refractive index n is complex then the last coefficient gives the phase and amplitude change of the reflected wave.

In the same manner, the phase distribution for the transmitted wave can be determined

$$A_{transmission}(\zeta) = ts\,(\zeta)\, e^{i(1-n)k\zeta}, \tag{3.5}$$

where n is the index of refraction on the other side of the interface and $t = 2/(1 + n)$ the transmission coefficient. The difference between the two refractive indices appears here because we defined the phase with respect to the mean position of the interface.

When the incident wave has an initial amplitude distribution then the amplitude distribution of the reflected wave is given by the convolution between (3.4) and the initial amplitude distribution

$$\begin{aligned} A_f(\zeta) &= \int_{-\infty}^{\infty} A_i(\zeta_1) A_{reflection}(\zeta - \zeta_1) d\zeta_1 \\ &= A_i \star A_{reflection}, \end{aligned} \tag{3.6}$$

where $\star$ corresponds to the convolution operator. To handle the transmission, one simply replaces $A_{reflection}(\zeta)$ by $A_{transmission}(\zeta)$.

After several reflections and transmissions through the optical system, the final wave is defined by a final amplitude distribution $A(\zeta)$. To determine from this distribution the received intensity, we suppose that all parts of the beam interfere in a point (i.e. focal point of a lens). At this point, the intensity is given by

$$I = \left| \int_{-\infty}^{\infty} A(\zeta) d\zeta \right|^2 \tag{3.7}$$

$$= \left| \hat{A}(0) \right|^2, \tag{3.8}$$

where $\hat{A}(\nu)$ corresponds to the Fourier transform of $A(\zeta)$. In the next section we use this property to find the transmission and reflection coefficients for a rough monolayer.

3.2.2 Application to a monolayer

In the following we apply this model to the case of a single monolayer. This gives us a better insight into the influence of the roughness on the optical properties. Further it will show us the usefulness of the above mentioned property namely the writing of the measured intensity as a Fourier transformation. The results of this subsection will give us the starting point for the generalisation of the **LTR** formalism to include roughness.

As already shown in the preceding chapter, in a monolayer we have multiple reflections inside the layer (see figure 2.3). The transfer function for the transmission of this monolayer is given by the sum of convolutions of the multiple reflections between the two interfaces

$$A_{final}(\zeta) = e^{iknz}(A_{t01} \star A_{t10}) + e^{3iknz}(A_{t01} \star A_{r10} \star A_{r10} \star A_{t10}) + \cdots .$$

where z corresponds to the thickness of the monolayer and n to its index of refraction. The distributions A_{t01}, A_{t10} and A_{r10} correspond to the transmission from the medium 0 to 1, from 1 to 0 and to the reflection when going from medium 1 to 0.

To evaluate this series of convolutions we use the properties of the Fourier transformation which transforms a convolution into a multiplication. This is further very convenient because the actual measurement of the resulting intensity (3.7) is defined using the Fourier transformation. After the transformation, the transfer function reads

$$\begin{aligned} \hat{A}_{final}(\nu) &= e^{iknz}\hat{A}_{t01}(\nu)\hat{A}_{t10}(\nu) \\ &\quad + e^{3iknz}\hat{A}_{t01}(\nu)\hat{A}_{r10}(\nu)\hat{A}_{r10}(\nu)\hat{A}_{t10}(\nu) + \cdots \qquad (3.9) \\ &= e^{iknz}\hat{A}_{t01}(\nu)\hat{A}_{t10}(\nu)\frac{1}{1 - e^{2iknz}\hat{A}^2_{r10}(\nu)}. \qquad (3.10) \end{aligned}$$

which is nothing but a normal geometrical series that can be easily evaluated.

If we consider the roughness to be characterised by a Gaussian distribution one can calculate the intensity transmission coefficient

$$s(z) = \frac{1}{\Delta z\sqrt{2\pi}} e^{-\frac{z^2}{2\Delta z^2}}. \qquad (3.11)$$

The width of the distribution Δz gives the amount of roughness for the interface and corresponds to the second order momentum of this distribution (root mean square). The

Fourier transformation of this distribution is

$$\hat{s}(\nu) = e^{-2\pi^2\Delta z^2\nu^2}, \tag{3.12}$$

and thus the different transformed transfer functions read:

$$\hat{A}_{r01}(0) = r_{01}\hat{s}(k/\pi) = r_{01}e^{-2k^2\Delta z^2}, \tag{3.13a}$$

$$\hat{A}_{r10}(0) = r_{10}\hat{s}(nk/\pi) = r_{10}e^{-2n^2k^2\Delta z^2}, \tag{3.13b}$$

$$\hat{A}_{t12}(0) = t_{01}\hat{s}((1-n)k/2\pi) = t_{01}e^{-(1-n)^2k^2\Delta z^2/2}, \tag{3.13c}$$

$$\hat{A}_{t21}(0) = t_{10}\hat{s}((1-n)k/2\pi) = t_{10}e^{-(1-n)^2k^2\Delta z^2/2}. \tag{3.13d}$$

Considering the above definitions the intensity transmission and reflection coefficients are:

$$\mathcal{T} = \left|\frac{t_{01}t_{10}e^{-(1-n)^2k^2\Delta z^2}e^{inzk}}{1 - r_{10}^2e^{-4n^2k^2\Delta z^2}e^{2inzk}}\right|^2, \tag{3.14a}$$

$$\mathcal{R} = \left|r_{01}e^{-2n^2k^2\Delta z^2} + \frac{t_{01}t_{10}r_{10}e^{-(1-2n+3n^2)k^2\Delta z^2/2}e^{2inzk}}{1 - r_{10}^2e^{-4n^2k^2\Delta z^2}e^{2inzk}}\right|^2. \tag{3.14b}$$

Interpreting these coefficients is easy if one notes the resemblance to the transmission and reflection coefficients in the absence of roughness. The effects of the roughness can be seen here as a change of the internal transmission and reflection coefficients. The amount by which these coefficients change is linked to the ratio between the optical length of the roughness, $n\Delta z$, and the wavelength of the incident wave, $\lambda = 2\pi/k$. For example, given a roughness of 2nm in a monolayer of $1\mu m$ thickness having a refractive index of 3 at a wavelength of 600nm, the transmission coefficient will change by 2%. For a roughness twice as large the change is about 6%. This small example also shows the non linearity of the response. In the case of reflectivity, the sensitivity of this method is much greater. Under the same conditions as above, but this time at a wavelength of 570nm and for a roughness of 1nm, the change in reflectivity coefficient is 4% whereas for a roughness of 2nm the change is 15%.

An important characteristic of a monolayer is its finesse, $\mathcal{F}$. This can be defined by calculating the transmission coefficient as the thickness of the monolayer is increased. One then observes selective transmission of the monochromatic light when the thickness

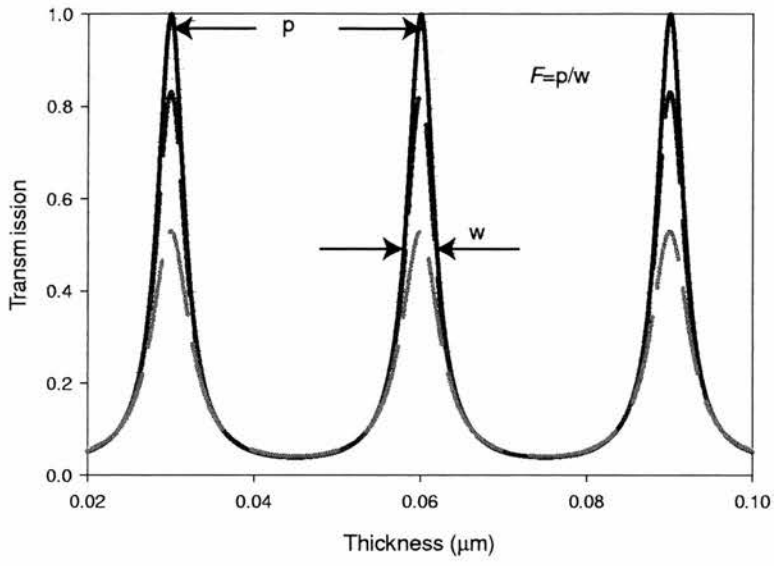

Figure 3.2: Transmission coefficient as function of the monolayer thickness for different roughness.

of the monolayer leads to constructive interference of the wave (see figure 3.2). The finesse is defined as the ratio between the separation of the fringes and their half-width. From the definition of the transmission (3.14a) we can determine the finesse

$$\mathcal{F} = \frac{\pi}{2\sinh(k^2\Delta z^2(1+n^2) + \ln(r))}, \tag{3.15}$$

where $r = |r_{01}|$ is the reflectivity coefficient. The expression for the finesse simplifies to the normal definition when there is no roughness, that is $\mathcal{F} = \pi r/(1-r^2)$. In figure 3.2 we also remark that increasing the roughness of the monolayer decreases the finesse. This relation links the finesse coefficient not only to the optical properties of a monolayer but also to its optical quality.

Finally, we remark that the equations (3.14) giving the intensity and transmission coefficients are not conserving the energy of the field. Indeed, in presence of roughness their sum is not unity. This is due to the treatment of the problem in one dimension, neglecting the diffraction of the wave in other directions at the edges of the roughness steps. Our model is a first order approximation which takes into account only the directionality non-scattered light. The directional scattered light makes up the intensity lost due to the roughness.

3.2.3 The roughness in the LTR formalism

The **LTR** formalism is based on the combination law acting on two **LTR** elements. In the case of the roughness we introduce a statistical distribution of these elements, that is, they depend on the optical path length. In order to include the roughness effects in the **LTR** calculations we have to deduce the combination law for two **LTR** elements that each have a different distribution. Let us consider two layers defined by

$$\begin{pmatrix} L_1(\zeta_1) \\ T_1(\zeta_1) \\ R_1(\zeta_1) \end{pmatrix} \quad \text{and} \quad \begin{pmatrix} L_2(\zeta_2) \\ T_2(\zeta_2) \\ R_2(\zeta_2) \end{pmatrix}. \tag{3.16}$$

The combination law for the left reflection in its expanded form reads

$$L(\zeta) = L_1 + T_1 \star L_2 \star T_1 + T_1 \star L_2 \star R_1 \star L_2 \star T_1 + \cdots . \tag{3.17}$$

This expression can be simplified when using the Fourier transformation

$$\hat{L}(\nu) = \hat{L}_1(\nu) + \frac{\hat{T}_1^2(\nu)\hat{L}_2(\nu)}{1 - \hat{R}_1(\nu)\hat{L}_2(\nu)}. \tag{3.18}$$

In the same manner one can deduce the transmission and the second reflection coefficient. Consequently in the **LTR** formalism the combination law including a roughness distribution is

$$\begin{pmatrix} \hat{L}(\nu) \\ \hat{T}(\nu) \\ \hat{R}(\nu) \end{pmatrix} = \begin{pmatrix} \hat{L}_1(\nu) \\ \hat{T}_1(\nu) \\ \hat{R}_1(\nu) \end{pmatrix} \oplus \begin{pmatrix} \hat{L}_2(\nu) \\ \hat{T}_2(\nu) \\ \hat{R}_2(\nu) \end{pmatrix}. \tag{3.19}$$

The second step necessary to include the interface roughness effects in the **LTR** calculations is to define the roughness in this formalism. One can use the transmission and reflection coefficients calculated in the preceding section in the case of a rough monolayer. This approach has the disadvantage that when two such rough monolayers are combined by the **LTR** method the roughness between them is taken into account twice. Indeed, each layer has at its common interface a roughness variation independent of the other layer. These two roughness are not correlated. This implies that the

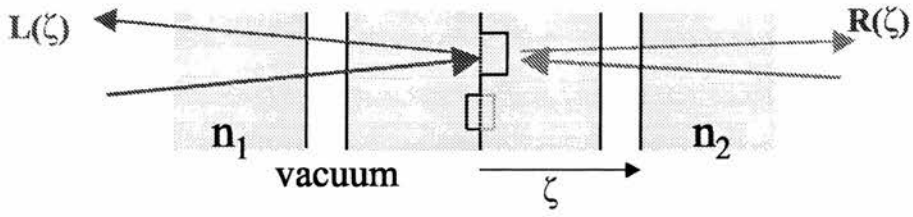

Figure 3.3: Schematic representation of the rough element.

straight forward method of combining two rough monolayers leads automatically to considering small vacuum layers of random thickness between the two layers which implies an overestimation of the roughness effects.

To avoid the above mentioned problem, we introduce a new **LTR** element which corresponds to a "rough" element. This element placed between two adjacent perfect layers takes into account their common roughness. It is formed by the materials of the two layers separated by an internal rough interface (see figure 3.3) with no vacuum layer between them. In a first approximation the interface is represented as an ensemble of parallel steps, neglecting the effects of different step slopes as already defined for the case of the monolayer treated above. The depth of the steps are statistically distributed with a distribution function $s(\zeta)$. This distribution is normalised and its mean value, which corresponds to the position of the ideally flat interface, is chosen for the origin of the ζ-axis. The standard deviation of $s(\zeta)$ is a measure of the roughness.

Using the combination law described in equation (3.19) together with a Gaussian interface distribution (3.11) and a monochromatic incident wave, the rough **LTR** element can be written

$$X_{rough} = \begin{pmatrix} r_{01} \\ \sqrt{t_{01}t_{10}} \\ r_{10} \end{pmatrix} \oplus \begin{pmatrix} r_{12}e^{-2n_1^2k^2\Delta z^2} \\ \sqrt{t_{12}t_{21}}e^{-(n_1-n_2)^2k^2\Delta z^2/2} \\ r_{21}e^{-2n_2^2k^2\Delta z^2} \end{pmatrix} \oplus \begin{pmatrix} r_{20} \\ \sqrt{t_{02}t_{20}} \\ r_{02} \end{pmatrix} \tag{3.20}$$

where the subscripts 1 and 2 stand for the two adjacent media split by the rough interface. Further, for the sake of simplicity, we have written this rough element as the combination of three elements. We remark here also that the **LTR** element has no width as it begins and ends at the same place. This property makes the insertion of the rough element between any two layers possible.

3.3 Continuous refractive index variation

In this section we apply the **LTR** formalism to continuous refractive index variations. This case is a generalisation of the multilayered structures which treats only the case of constant refractive index with a discontinuity at the interface between two layers. The continuous refractive index variation consists in the dependence of the refractive index with depth in a layer. This is obtained by many growth techniques or post growth treatments.

In order to treat the refractive index variation we define by "quadrature" a **LTR** integral. This integral is based on the **LTR** composition law and on the multiplication operator. With its help one can formally calculate the **LTR** of a layer with refractive index variations. This **LTR** integration is then used in the case of a linearly varying refractive index where the result is graphically compared to the direct analytical solution of Maxwell's equations.

3.3.1 The LTR integral

In the case of the combination of N layers (see figure 2.2) we can introduce a combination operator which combines all the layers

$$\bigoplus_{j=1}^{N} \begin{pmatrix} L_j \\ T_j \\ R_j \end{pmatrix} = \begin{pmatrix} L_1 \\ T_1 \\ R_1 \end{pmatrix} \oplus \begin{pmatrix} L_2 \\ T_2 \\ R_2 \end{pmatrix} \oplus \ldots \oplus \begin{pmatrix} L_N \\ T_N \\ R_N \end{pmatrix}. \tag{3.21}$$

We then use this notation to define the **LTR** integral

$$\lim_{\Delta z \to 0} \bigoplus_{j=1}^{N} \Delta z \mathcal{L}(n(z_0 + j\Delta z)) = \oint_{z_0}^{z_1} dz \mathcal{L}(n(z)) \tag{3.22}$$

where $\mathcal{L}(n)$ is the **LTR** element for a monolayer of unit thickness as defined by equation (2.16) and $N = (z_1 - z_0)/\Delta z$. The refractive index is given by the function $n(z)$. This integral gives the transmission and reflection coefficients for a layer whose refractive index is changing with depth. In order to calculate this integral the layer is decomposed into thin layers each having a constant refractive index (see figure 3.4). These layers are

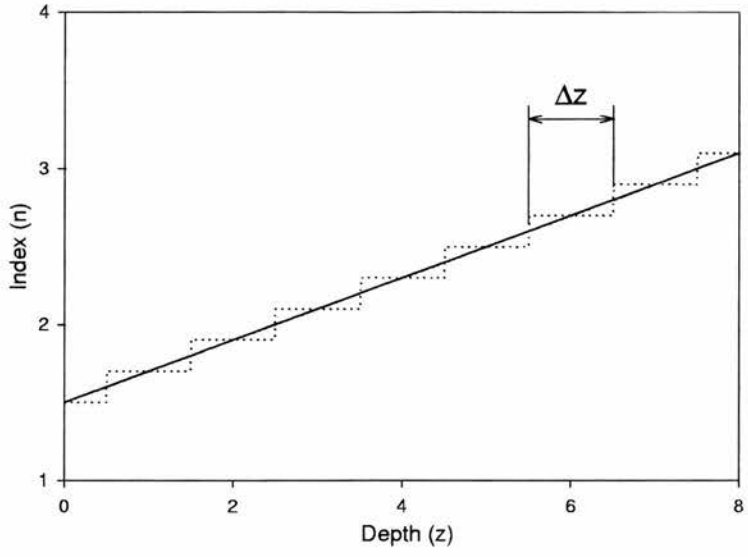

Figure 3.4: Decomposition of a linear varying index into small layers of constant refractive index.

then combined using the combination operator (3.21). In the following application we show that as the thickness of the thin layers decreases, this integral operator gives the same results as the analytical solution of Maxwell's equations.

3.3.2 Application to a linear refractive index change

We can apply the integral defined above to the case of a layer with linear refractive index change. The transmission and reflection coefficients of such a layer can be deduced by considering the solution of Maxwell's equation

$$\frac{\partial^2 E(z,t)}{\partial z^2} - \frac{(n_0 + n_1 z)^2}{c^2}\frac{\partial^2 E(z,t)}{\partial t^2} = 0, \tag{3.23}$$

where n_0 is the starting index of refraction and n_1 is the rate of change of the refractive index of the layer with depth. The solution of this equation is

$$E(z,t) = \sqrt{n_0 + n_1 z}\left(C_1 \mathrm{I}_{1/4}\left(\frac{i\omega\,(n_0 + n_1 z)^2}{2n_1 c}\right) + C_2 \mathrm{K}_{1/4}\left(\frac{i\omega\,(n_0 + n_1 z)^2}{2n_1 c}\right)\right) e^{i\omega t}, \tag{3.24}$$

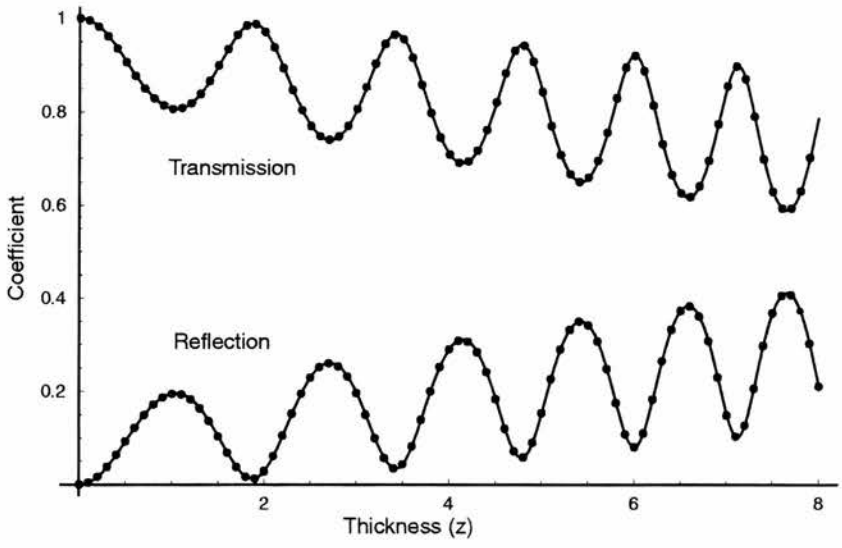

Figure 3.5: Transmission and reflection coefficients for a layer with a linear varying index (see figure 3.4) as a function of the layer thickness. The continuous line corresponds to the exact solution of Maxwell's equation and the dots to the LTR method.

where $\mathrm{I}_{1/4}(z)$ and $\mathrm{K}_{1/4}(z)$ are the modified Bessel functions of the first and second kind. The integration constants C_1 and C_2 correspond to the two waves travelling in opposite directions and can be determined by considering the continuity relations (2.6) of the field at the layer interface. The fields outside the layer can then be decomposed into incident, transmitted and reflected parts defining the transmission and reflection coefficients.

On the other hand one can treat the problem of a layer with continuously varying refractive index by using the integral formalism already introduced. This formalism leads directly to the transmission and reflection coefficients

$$\oint_{z_0}^{z_1} dz\mathcal{L}(n_0 + n_1 z) = \begin{pmatrix} L \\ T \\ R \end{pmatrix}. \tag{3.25}$$

In figure 3.5 we have represented the transmission and reflection coefficients for a layer with a constant refractive index gradient as a function of its thickness. These coefficients are calculated using the two methods described above, that is, the exact solution of Maxwell's equations and the **LTR** integral. One notes the good agreement.

Beyond the graphical verification of the **LTR** integral it is possible to show the convergence of equation (3.22) towards the exact solution but this is beyond the scope of this work. A possible procedure to show this convergence could use the **LTR** formalism

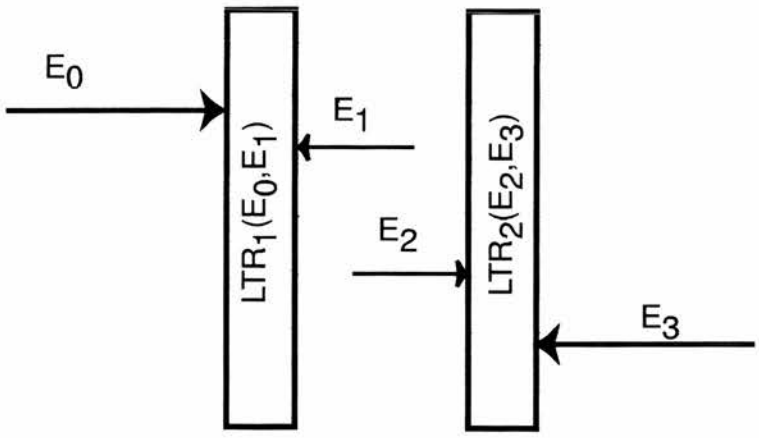

Figure 3.6: Field definitions when combining two intensity dependent **LTR** elements.

to define the exact solutions to Maxwell's equation for a step-function refractive index. One can show that as the step-function tends towards the continuously varying refractive index function, the solution defined by the **LTR** method tends towards the exact solution.

3.4 Intensity dependent propagation in multilayered structures

When the index of refraction depends on light intensity the simple **LTR** method does not work directly. The normal **LTR** method is built on the assumption that the system is linear with respect to the incident fields. If the refractive index depends on the intensity, the reflection and transmission coefficients depend also on the incident intensity. This has no further consequence in the case of a single layer if the dependence of the coefficients is known. The problem arises when one combines two or more intensity dependent **LTR** elements. Indeed, one has to know in this case the intensity of the fields between the layers (see figure 3.6).

The composition law can then be written

$$\begin{pmatrix} L_1(E_0,E_1) \\ T_1(E_0,E_1) \\ R_1(E_0,E_1) \end{pmatrix} \oplus \begin{pmatrix} L_2(E_2,E_3) \\ T_2(E_2,E_3) \\ R_2(E_2,E_3) \end{pmatrix} = \begin{pmatrix} L'(E_0,E_1,E_2,E_3) \\ T'(E_0,E_1,E_2,E_3) \\ R'(E_0,E_1,E_2,E_3) \end{pmatrix}, \tag{3.26}$$

where E_0, E_1, E_2 and E_3 are the fields incident on the two layers. On the other hand the inter-layer field can be calculated with the help of the **LTR** coefficients of each of the layers

$$E_1 = \frac{T_1(E_0, E_1)L_2(E_2, E_3)E_0 + T_2(E_2, E_3)E_3}{1 - L_2(E_2, E_3)R_1(E_0, E_1)}, \tag{3.27a}$$

$$E_2 = \frac{T_1(E_0, E_1)E_0 + T_2(E_2, E_3)R_1(E_0, E_1)E_3}{1 - L_2(E_2, E_3)R_1(E_0, E_1)}. \tag{3.27b}$$

This system of equations links the four incident fields. Solving leads to two solutions $E_1(E_0, E_3)$ and $E_2(E_0, E_3)$. Substituting these solutions into equation (3.26) gives the final **LTR** coefficients depending only on the external incident fields

$$\begin{pmatrix} L_1(E_0, E_1) \\ T_1(E_0, E_1) \\ R_1(E_0, E_1) \end{pmatrix} \oplus \begin{pmatrix} L_2(E_2, E_3) \\ T_2(E_2, E_3) \\ R_2(E_2, E_3) \end{pmatrix} = \begin{pmatrix} L(E_0, E_3) \\ T(E_0, E_3) \\ R(E_0, E_3) \end{pmatrix}. \tag{3.28}$$

Thus the number of parameters does not increase as one combines more and more nonlinear **LTR** elements. At each combination one can eliminate the internal fields by the use of the equations (3.27). This combination law is again self-consistent as its result has the same form as the individual elements of the combination.

The difficulty of this method consists of finding the solution of (3.27). Indeed, this system of equations is nonlinear and there is no general method for finding solutions. An analytical solution can only be found in special cases for nonlinear **LTR** elements. In the following we show a practical method which can be used to solve this problem.

As for the **LTR** method itself, the solution of this problem has a physical meaning. Indeed the principal idea is to increase the amplitude of the incident field slowly thus going gradually from the linear state to the non-linear state. This approach is based on a knowledge of the linear response of the multilayered structure. This can be calculated by the normal **LTR** method. We then use the internal fields found in the linear case to deduce the **LTR** elements for the same incident intensity. This step is repeated until the **LTR** element converge. This self-consistent method ensures the correct result in the case of bistability where a small change in the incident intensity induces a jump in the transmission coefficient. We use this self-consistent **LTR** elements to start the whole

process with a slightly higher incident intensity. We can thus increase the intensity to the desired level step by step.

Practically, the effects of the slow increase of the incident power can be expressed with the help of a sequence of **LTR** combinations. We consider here an increasing sequence, E_m, of incident fields

$$\text{for } E_m \; : \; \begin{pmatrix} L_1^{m-1} \\ T_1^{m-1} \\ R_1^{m-1} \end{pmatrix} \oplus \begin{pmatrix} L_2^{m-1} \\ T_2^{m-1} \\ R_2^{m-1} \end{pmatrix} \oplus \cdots \oplus \begin{pmatrix} L_n^{m-1} \\ T_n^{m-1} \\ R_n^{m-1} \end{pmatrix}, \tag{3.29}$$

where the **LTR** coefficients for the E_m input field are calculated with the interlayer fields resulting from the E_{m-1} input field. The sequence E_m can be an algebraic sequence or one could change the step size of the sequence depending on how rapid the **LTR** coefficients are varying with E. The first element of this sequence is given by the linear **LTR** coefficients

$$\begin{pmatrix} L_i^0 \\ T_i^0 \\ R_i^0 \end{pmatrix} = \begin{pmatrix} L_i(0,0) \\ T_i(0,0) \\ R_i(0,0) \end{pmatrix}. \tag{3.30}$$

In figure 3.7 we are comparing the solution of the nonlinear Maxwell equation with the solution defined by the nonlinear **LTR** method. The Maxwell equation in this case reads

$$\frac{\partial^2 E(z,t)}{\partial z^2} - \frac{(n_1 + n_2|E(z,t)|^2)^2}{c^2} \frac{\partial^2 E(z,t)}{\partial t^2} = 0, \tag{3.31}$$

and for the **LTR** method we use $\mathcal{L}(n_1 + n_2(|E_1|^2 + |E_2|^2))$ as defined by equation (2.16). This figure shows that the two methods give the same resulting transmission and reflection field as a function of input intensity. We remark here that in order to find the solution of the nonlinear Maxwell equation one has to use a backwards calculation method, that is, to presume that the output field is known. This is not the case for the **LTR** method where one gets directly the transmission and reflection coefficients for a given input intensity.

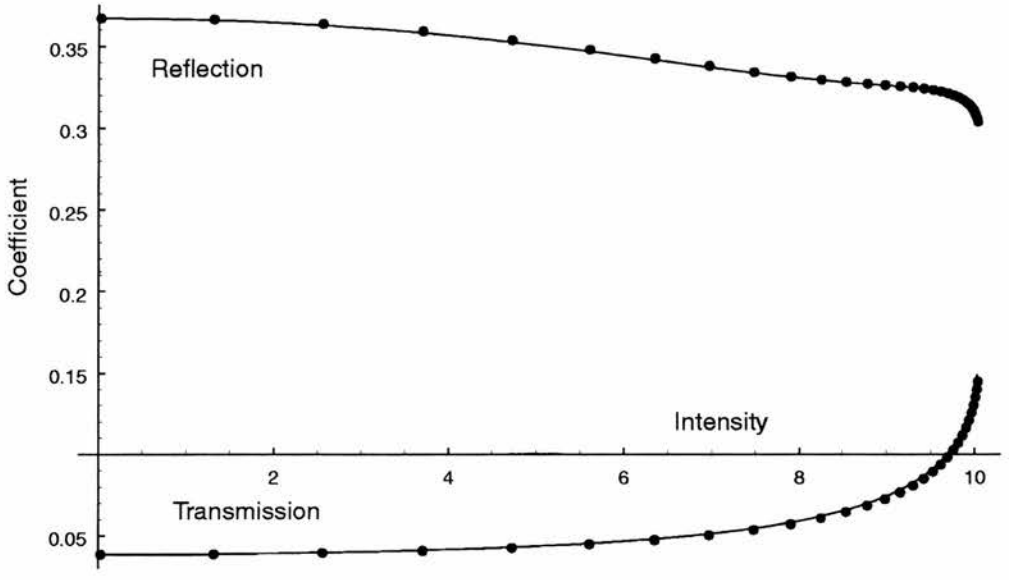

Figure 3.7: Transmission and reflection coefficients as a function of the incident power calculated by the two methods. The continuous line corresponds to the solution to Maxwell's equations and the dots to the LTR method.

3.5 Summary

In this chapter we have generalised the **LTR** method to be able to treat three other cases. We started by considering the effects of the roughness on the optical properties of a monolayer. In this case the transmission and reflection coefficients must be generalised to distributions which take into account the roughness distribution. Their effect can be described by the convolution of their distribution with the phase-amplitude distribution of the wave. By using the properties of the Fourier transformation one can evaluate this convolution while taking into account the multiple reflections inside the monolayer. The resulting distribution gives the final phase-amplitude distribution of the wave after the interaction. The experimental measure of the intensity integrates the interference of all parts of the wave. We can define an **LTR** element which models the roughness when combined between two successive perfect layers. This rough **LTR** element takes the correlated roughness at the interface of the two layers into account. Once this rough element is introduced, one can build more complex multilayered structures having roughness at internal as well external interfaces.

The second application of the **LTR** method treated the case of a continuously varying refractive index. Compared to the multilayered structures composed of layers with constant refractive index, the continuously varying case corresponds to a refractive index

which varies with depth. Its treatment consists of introducing an **LTR** integral which can be evaluated by quadrature. Effectively, this integral considers the refractive index variation as a succession of infinitesimal thin layers of constant refractive index. As the thickness of these layers tends toward zero, the integral defined by quadrature converges towards the solution of Maxwell's equations with varying refractive index as a function of depth. We showed this graphically in the case of a linear refractive index variation.

Finally, the **LTR** formalism was generalised to include the change of refractive index with the intensity of the monochromatic wave. In this case we have to introduce the dependence of the **LTR** elements on the two incident fields (from the right and from the left). When combining two or more of such intensity dependent **LTR** elements, one has to know the internal fields "trapped" between the layers. The next step was to consider a slow variation of the intensity of the incident wave thus passing from the linear to the non-linear case and stopping at the desired intensity. In the linear case, we could calculate the internal fields as the **LTR** elements are not actually intensity dependent in this case. Knowing these fields, we use them to calculate **LTR** elements for the next higher incident intensity. In this way, we can reach the desired intensity step by step. Physically, this method corresponds to slowly turning up the power. We showed graphically that the solution found by this method gives the same result as the solution to the nonlinear Maxwell equation.

With these three examples of generalisation of the **LTR** method we have shown the versatility of our formalism and the ease with which one can apply it to very different cases.

Chapter 4

LTR formalism for waveguides and photonic structures

4.1 Introduction

In this chapter we generalise the **LTR** formalism in order to treat wave propagation in more complex situations. Originally the **LTR** approach treats the case of plane waves propagating through plane multi-layered structures. These plane waves are solutions of Maxwell's equations in homogeneous and isotropic media. In this case, the **LTR** formalism links through the transmission and reflection coefficients these solutions at the interface between two such media.

Without changing anything in the **LTR** formalism we can generalise it by considering other solutions of Maxwell's equations. This is the case of plane waveguides. In a waveguide mode the field outside the guide is described by an evanescent wave and not by a plane wave of constant amplitude [22]. The **LTR** method gives the coefficients linking these evanescent waves and the plane waves inside the waveguide. A particular solution corresponding to a waveguide mode is achieved when the divergent evanescent field has zero amplitude. Another possible generalisation is based on the change of the considered solutions to cylindrical waves. This is the case for cylindrical symmetry waveguides such as optical fibres.

In the case of periodic structures we can distinguish between the one dimensional case [23] and the two [24, 25] and three dimensional cases [26–28]. The one dimensional case can be treated by the normal **LTR** formalism. We use this case to show some of the

features present in periodic structures. The generalisation to two and three dimensional periodic structures leads to the consideration of more complex solutions of Maxwell's equations (i.e. more than one plane wave corresponding to the different diffraction orders). The "link" at an interface between two such solutions can no longer be described by simple transmission and reflection coefficients. We have to use matrices in order to ensure the continuity of the solutions at the interface. These matrices link two families of solutions on either side of the interface. We can continue using the **LTR** formalism after generalising it by changing the transmission and reflection scalar coefficients to matrices. Special care must then be taken because of the non-commutativity of the matrix multiplication.

4.2 Waveguides

We can generalise the **LTR** method to treat the case of plane waveguides. Our approach is based on classical methods for calculating the waveguide modes [22, 29]. In order to take these modes into account we must consider a different solution of Maxwell's wave equation (2.2). Contrary to the plane waves (2.4) this solution has to depend on more then one spatial coordinate. The general solution has the form

$$U(x, y, z, t) = U_0 \exp(i(\omega t - \vec{k}\vec{r}) + \vec{\alpha}\vec{r}), \tag{4.1}$$

where $\vec{r}$ is the position vector and the vector pair $\vec{k}$ and $\vec{\alpha}$ are the real and imaginary part of the wave vector. In order for this function to be a solution of the wave equation, the wave vector must comply with the following dispersion relations

$$\frac{n^2\omega^2}{c^2} - k^2 + \alpha^2 = 0, \tag{4.2}$$

$$\vec{k}\vec{\alpha} = 0. \tag{4.3}$$

In the following we consider a specific case of this dispersion relation i.e. the real part $\vec{k}$ of the wave vector is parallel to the waveguide and the imaginary part $\vec{\alpha}$ is perpendicular to it (see figure 4.1). In this case, the second dispersion relation is automatically fulfilled.

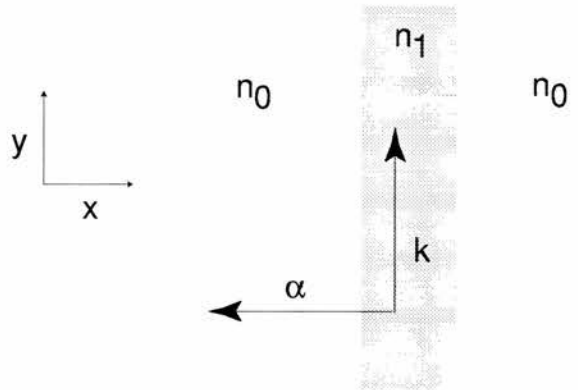

Figure 4.1: The waveguide configuration.

As for travelling waves we can define the reflection and transmission coefficients connecting the solutions on either side of the interface

$$U_1(x,y,z,t) = U_0 \exp(i(\omega t - ky) + \alpha x), \tag{4.4a}$$

$$U_t(x,y,z,t) = t_{12} U_0 \exp(i(\omega t - ky) + \alpha_2 x), \tag{4.4b}$$

$$U_r(x,y,z,t) = r_{12} U_0 \exp(i(\omega t - ky) - \alpha x), \tag{4.4c}$$

where α_2 is so chosen that the dispersion relation is fulfilled in the second medium having the refractive index n_2. In order to satisfy the continuity condition ω and k must be the same on both sides of the interface. We remark here that α_2 can also be purely imaginary without affecting the form of the solutions. This can be the case when $\frac{n_2^2\omega^2}{c^2} < k^2$.

Further, the continuity condition implies the following transmission and reflection coefficients

$$t_{12} = \frac{\alpha - \alpha_2}{\alpha + \alpha_2}, \tag{4.5a}$$

$$r_{12} = \frac{2\alpha}{\alpha + \alpha_2}. \tag{4.5b}$$

We can now define the **LTR** element corresponding to a layer of thickness Δx

$$\mathcal{L}_{wg} = \begin{pmatrix} L \\ T \\ R \end{pmatrix} = \begin{pmatrix} r_L \\ t \\ r_R \end{pmatrix} = \begin{pmatrix} r\frac{1-p^2}{1-p^2r^2} \\ p\frac{(1-r^2)}{(1-p^2r^2)} \\ r\frac{1-p^2}{1-p^2r^2} \end{pmatrix}, \tag{4.6}$$

with

$$\begin{cases} r = \frac{\alpha - \alpha_2}{\alpha + \alpha_2} \\ p = \exp(\alpha_2 \Delta x) \end{cases} . \tag{4.7}$$

Having obtained the definition of the **LTR** for one layer we can calculate the general transmission and reflection coefficients for any composite waveguide. In order to ascertain whether the structure is waveguiding or not we must define a waveguide condition. This condition is the same as the totally absorbing condition described in the preceding chapter i.e. $T^2 - LR = 0$. This implies that there is no wave emerging from the waveguide. In our definitions of the solution these emerging waves diverge at infinity. The remaining incoming waves correspond to the evanescent waves on either side of the waveguide. Further, we remark that all of the above treatment can be generalised to the case where the vectors $\mathbf{k}$ and α are not in this specific configuration.

Practicaly speaking, in order to find the guided modes in such a multilayered structure one starts with the dispersion relation (4.2). Knowing the pulsation frequency ω and choosing the exponential decay coefficient α one can determine the wave vector k. As the frequency and the wave vector must be the same inside and outside the structure one can use the dispersion relation inside each layer with the corresponding index of refraction to calculate the internal exponential coefficient α_2. This coefficient can also be imaginary in which case we have a stationary wave inside the layer. Once the coefficients α and α_2 are known one can calculate the transmission and reflection coefficient for each interface. Using these coefficients in (4.6) one can define the **LTR** element for one layer. The whole structure can then be calculated using the addition and multiplication algebra. Finally, this structure is wave guiding at this frequency and wavelength if the total **LTR** elements fulfils the total absorbsion condition $T^2 - LR = 0$. In order to find all guiding modes of a fibre one has to scan the exponential decay coefficient α.

4.3 Photonic bandstructures in one dimension

Another application of the **LTR** formalism is the study of periodic multilayered structures. These kinds of structures are very useful for the control of the propagation of optical beams [30,31]. A good example is the Distributed Bragg Reflectors (DBR) used as high reflectance mirrors. These mirrors are usually fabricated out of non-absorbing

dielectric films. One can engineer a periodic structure made of such films so that it is highly reflective at a given wavelength. This reflection is only due to the constructive and destructive interference of the multiple reflections from the different interfaces of the periodic structures. The origin of this high reflection explains also its dependence with respect to the wavelength.

In this section we will use the already introduced **LTR** multiplication operator in order to show the different properties of the periodic multilayered structures such as DBRs. Our first step consists in redefining the operator in a form more suitable for this study.

In order to find an analytical form of the multiplication operator we have used the **LTR** elements of a monolayer as a starting point. Applied to a monolayer the multiplication operator should only give the **LTR** element of the same monolayer having a different thickness. The new thickness of the layer is given by the original thickness multiplied by the multiplication factor. This corresponds to the change of the propagation length of the layer by this factor without changing the interface transmission or reflection. This can be observed in the **LTR** formalism when the **LTR** element of one monolayer (2.16) is expressed in a different form

$$\mathcal{L}(n,k,z) = \begin{pmatrix} r \\ \sqrt{(1-r^2)} \\ -r \end{pmatrix} \oplus \begin{pmatrix} 0 \\ p \\ 0 \end{pmatrix} \oplus \begin{pmatrix} -r \\ \sqrt{(1-r^2)} \\ r \end{pmatrix}, \tag{4.8}$$

where r and p are defined by (2.17). We can now distinguish the different parts comprising the **LTR** element for one monolayer. The left and right elements in (4.8) stand for the transmission and reflection coefficients at the interface of the monolayer. The middle part corresponds to the propagation through the monolayer. Applying the multiplication operator to equation (4.8) is equivalent to changing the power of the propagation coefficient p.

Using the decomposed definition of the **LTR** element for a monolayer we can define a decomposed operator for the multiplication

$$n\begin{pmatrix} L \\ T \\ R \end{pmatrix} = \begin{pmatrix} ac \\ \sqrt{(1-a^2)} \\ -a/c \end{pmatrix} \oplus \begin{pmatrix} 0 \\ b^n \\ 0 \end{pmatrix} \oplus \begin{pmatrix} -ac \\ \sqrt{(1-a^2)} \\ a/c \end{pmatrix} \tag{4.9}$$

where the factors a, b and c are defined by the equations (2.42). As for the decomposed monolayer operator we notice here two distinct elements: the free propagation through the medium described by the middle term $(0, b^n, 0)$ and the interface effects described by the outer elements.

In the following we discuss the properties implied by the propagation term. This is equivalent to treating an infinite periodic structure where the interfaces are at infinity and have no effect on the propagation through the structure. One can interpret the properties of this propagation without the interfaces as the bulk properties of the structure.

There are several possibilities for the propagation coefficient b. This complex number can have an absolute value smaller than, greater than or equal to one. The first two cases correspond to an exponentially increasing or decreasing wave. These solutions are divergent in the case of a perfect periodic structure. In the presence of a local breakdown of the periodicity this solution can represent a non-diverging solution, as we will see below.

In the case where the modulus of the propagation factor is unity the only useful information is conveyed by its phase. This phase is equivalent to the phase acquired by the wave while propagating through one period of the structure. Simple multiplication by n gives the phase of the wave after n periods.

In order to study the different possibilities of the propagation factor b in more detail we can rewrite it in the following form

$$b = q + \sqrt{q^2 - 1} \tag{4.10}$$

where $q = (1 - RL + T^2)/2T$. Here we consider only non absorbing refractive indices. In this case the coefficient q is real. Indeed, for real refractive indices we have the following

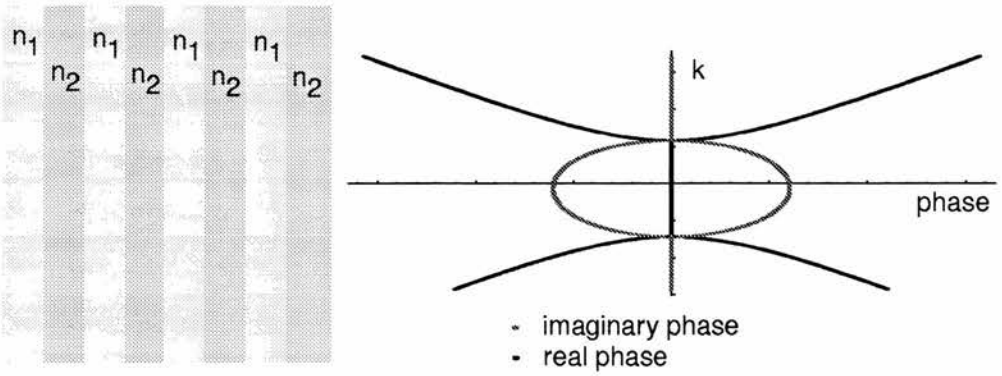

Figure 4.2: Periodic structure constructed with layers of different refractive indices. Real and imaginary phase of the wave while propagating over one period.

relation

$$1 = |T^2 - LR| = |T^2| + |R^2| = |T^2| + |L^2|. \tag{4.11}$$

This implies directly the following properties for the transmission and reflection coefficients

$$T = i|T|e^{i(\alpha+\beta)}, \tag{4.12a}$$

$$R = |R|e^{i\alpha}, \tag{4.12b}$$

$$L = |R|e^{i\beta}. \tag{4.12c}$$

Using these relations we can show that the coefficient q must be a real number. We then have the following three cases:

$$\begin{cases} q > 1 & \text{then} \quad b > 1, \\ q = 1 & \text{then} \quad b = 1, \\ q < 1 & \text{then} \quad |b| = 1. \end{cases} \tag{4.13}$$

The first case corresponds to the divergent solutions of the wave equation whereas the last two cases give periodic solutions. In the more general case of complex refractive indices we have complex coefficients implying a complex propagation coefficient. The divergent solution, for example, is then defined by an exponentially growing solution having a changing phase at the same time.

To illustrate this, let us consider a periodic succession of two layers of different refractive indices in the absence of absorption. In figure 4.2 we represented such a structure where we judiciously choose the basic period so that the **LTR** for one period is symmetric. This does not influence the bulk propagation coefficient but does influence the interface **LTR** element ($c = 1$ in this case). In this configuration one can easily calculate the propagation coefficient and its phase. Figure 4.2 shows the phase introduced while propagating over one period as a function of the wave vector of the pulse.

One observes in figure 4.2 the succession of regions where the introduced phase is real and where it is imaginary. The latter correspond to the divergent solutions. The imaginary phase gives the characteristic exponential coefficient with which the solution increases or decreases. These domains are the so called band gaps. Light cannot propagate through the structure at this wavelength. The domain in which the phase is real corresponds to the cases where light can propagate through the structure. The phase change over one period corresponds to the associated wave vector in the structure. Therefore, figure 4.2 gives the photonic band structure of the periodic multilayers. From the study of this structure one can introduce the effective index (equivalent to the effective mass in the electronic band structures) and the group velocity. It is also possible to define a $k \cdot p$ approach [32].

In the case of absorbing media the phase over one period is no longer either real or imaginary but has a complex value. Its real part gives the phase change over one period, and the imaginary part its decrease or increase (there are always two solutions; one increasing and one decreasing). These solutions can be seen as damped oscillations.

When composing two different periodic structures one has to include in the composition the interface **LTR** elements. Further, depending on the frequency of the light, one can be led to consider the divergent solutions. For example, one can have localised solutions when considering a structure having n periods embedded in another periodic structure. If for a given wavelength the interior structure allows propagating solutions whereas the exterior structure has a forbidden gap at this wavelength then we can have a localised solution [33, 34]. These solutions have an exponential decay in the exterior structure (evanescent wave) and would correspond to a waveguide mode of the structure.

4.4 Photonic bandstructures in 2 and 3 dimensions

4.4.1 Propagation in periodic structures

In order to treat more than one spatial dimension we have to take into account the transverse direction in the complete Maxwell wave equation. As a first step we consider only one transverse direction

$$\frac{\partial^2 U}{\partial x^2} + \frac{\partial^2 U}{\partial z^2} - \frac{n(x,z)^2}{c^2}\frac{\partial^2 U}{\partial t^2} = 0 \tag{4.14}$$

where z is the principal propagation direction and x the transverse direction. We remark here that the refractive index depends on the transverse direction. In this section we study the effects of periodic structures. In the case of two spatial dimensions we take into account the transverse periodicity of the structure

$$n(x + \Lambda_x, z)^2 = n(x,z)^2 \tag{4.15}$$

where Λ_x is the period in the transverse direction. Further we search sinusoidal oscillating fields of the form

$$U(x,z,t) = u(x,z)e^{i\omega t}. \tag{4.16}$$

Inserting this function in equation (4.14) we can obtain a differential equation for the amplitude $u(x,z)$

$$\frac{\partial^2 u}{\partial x^2} + \frac{\partial^2 u}{\partial z^2} + \frac{n(x,z)^2\omega^2}{c^2}u = 0. \tag{4.17}$$

To simplify this differential equation further we can take advantage of the periodicity in the transverse direction of the refractive index. This can be done by taking the Fourier transform of the equation in this direction

$$-k_x^2 u(k_x,z) + \frac{\partial^2 u(k_x,z)}{\partial z^2} + \sum_j N_j(z)u(k_x - jk', z) = 0 \tag{4.18}$$

where k_x and $k' = 2\pi/\Lambda_x$ are the wave vectors of the field and of the periodic refractive index. The sequence $N_j(z)$ corresponds to the coefficients of the Fourier series of $\frac{n(x,z)^2\omega^2}{c^2}$

and the summation corresponds to the convolution between this series and the Fourier transform of the amplitude. This convolution couples the different Fourier components of the amplitude. More precisely the Fourier component with a wave vector k_x is linked through this differential equation to the Fourier components having the wave vectors $k_x - jk'$ where j is an integer. We see here that we have to take into account only the starting wave vectors k_x lying between $-k'/2$ and $+k'/2$. All other wavevectors can be defined in this domain by adding or substracting multiples of k'.

Further, for every starting wave vector k_x we can introduce a Fourier series defined by $u_j(z) = u(k_x - jk', z)$. The propagation equation can then be written

$$\frac{\partial^2 u_i(z)}{\partial z^2} + m_{ik}(z) m_{kj}(z) u_j(z) = 0 \tag{4.19}$$

where the matrix $m_{ik}(z)m_{kj}(z) = N_j(z) - \delta_{ij}(k_x - jk')^2$. Here we have used the convention of the summation over the repeating subscript. This gives us a system of differential equations which is a generalisation of the scalar equation valid for one spatial dimension.

One can also use an alternative approach to the Fourier transformation in order to take into account the periodicity in the transverse direction. This can be done by decomposing the amplitude in the transverse direction into the one-dimensional eigen solutions in this direction. These solutions form a base and can be found by using the one-dimensional periodic multilayer approach. The matrix equation has the same form in this alternative decomposition except that the matrix $m_{ij}(z)$ can have a simpler form. The results expressed in the two bases are equivalent and there is always a transformation between the different representations. In the following we will use the Fourier space representation.

This method can be generalised to the three dimensional case by taking into account the Fourier series terms in the two transverse directions. The amplitude of the field is then described by two series having two indices. The convolution thus corresponds to a summation over the two indices of the two dimensional series.

4.4.2 Matrix LTR

The first step in the study of the propagation through this three dimensional medium is to find the solution of equation (4.19) when the matrix $m_{ij}(z)$ is constant with respect to z. Once the solution is established we can determine the effects of an interface between

two regions of constant m_{ij}. This will give us the transmitted and reflected solution at a discontinuity between two different media. We can then implement the **LTR** formalism step by step and this can then be used to find the optical response of more complicated structures.

Equation (4.19) is a first order differential equation which can be solved in an analytical manner by using the exponential function of matrices. Indeed, in the case of a constant m_{ij} we have

$$u_i(z) = \exp(im_{ij}z)u_j^{0+} + \exp(-im_{ij}z)u_j^{0-} \tag{4.20}$$

where u_j^{0+} and u_j^{0-} correspond to the initial conditions. We recognise here the two solutions propagating in the two directions. At the interface we have two such solutions with different propagation matrices m_{ij}

$$1^{\text{st}} \text{ medium}: \quad \exp(im_{kj}z)u_j^0 + r_{ki}\exp(-im_{ij}z)u_j^0 \tag{4.21a}$$

$$2^{\text{nd}} \text{ medium}: \quad t_{ki}\exp(-im'_{ij}z)u_j^0 \tag{4.21b}$$

where m'_{ji} is the propagation matrix in the second medium. The matrices r_{ki} and t_{ki} are the reflection and transmission matrices.

The continuity equations give us the relations between the transmitted and reflected waves. Placing the interface at $z = 0$ simplifies the equations and the continuity equations lead to

$$\delta_{ki} + r_{ki} = t_{ki}, \tag{4.22a}$$

$$m_{ki} - r_{kj}m_{ji} = t_{kj}m'_{ji}. \tag{4.22b}$$

The first equation corresponds to the field continuity whereas the second equation corresponds to the derivatives continuity. Solving this system of equations gives the two matrices

$$r_{kj} = (m_{ki} - m'_{ki})(m_{ij} + m'_{ij})^{-1}, \tag{4.23a}$$

$$t_{kj} = 2m_{ki}(m_{ij} + m'_{ij})^{-1}. \tag{4.23b}$$

The determinant of the matrix $(m_{ij} + m'_{ij})$ must be non-zero for the reflection and transmission matrices to exist.

This matrix approach of the propagation through periodic media can be used as a starting point for the definition of a three dimensional **LTR** formalism. This generalised formalism is very similar to the one dimensional case except that one has to take special care of the different operations permitted as the matrices are generally not commutating. This implies the introduction of two transmission matrices, that is one from the left and one from the right.

The advantage of the **LTR** formalism for three dimensional photonic structures is that it gives the possibility of introducing concepts from plane multilayer systems. The roughness for example can be used to simulate the uneven boundary of a photonic crystal. One can also introduce an effective index of refraction variation. This would model the lattice displacements in the photonic crystal.

4.5 Summary

In this chapter we have shown two interesting generalisations of the **LTR** formalism to different optical structures. We started with the treatment of plane waveguides. By using the definition of general evanescent waves we determined their transmission and reflection coefficients and thus the **LTR** element for one layer of the waveguide. The normal addition and multiplication operator can then be used with such layers to give a total **LTR** element. If the **LTR** element of the waveguide structure fulfils the totally absorbing condition for one particular wavelength than it is waveguiding for this wavelength.

Further, in this chapter we treated the case of periodic structures in one, two and three spatial dimensions. In one dimension we could define the conditions in which a wave can propagate through the structure. This is made possible by rewriting the multiplication operator and splitting it into two parts: the surface or interface and the propagation part. Using the latter we could determine the phase added to the propagating wave when travelling one period of the structure. The plot of this phase as a function of wave vector gives the optical band structure. When this phase is imaginary we have an evanescent wave which can only exist at the interface. This property can be used when combining two or more periodic structures.

Finally we showed how to generalise the **LTR** formalism in order to treat periodic structures in two or three dimensions. This generalisation is based on the decomposition of the solution into propagating modes. When a wave is incident onto such a periodic structure there is more than one transmission and reflection coefficient. Each of the transmission and reflection coefficients shows the amount the wave is "reflected and transmitted" (generally speaking diffracted) in the different modes. As the incident wave can itself be composed into more than one mode, it is necessary to introduce transmission and reflection matrices which show the coupling between them while interacting with the periodic structure. These matrices could be used to define a new kind of **LTR** elements. In the same way as for the multilayered structures one can introduce addition and multiplication operators for these elements. This will be treated in future work.

Chapter 5

Applications: LTR formalism

5.1 Introduction

In this chapter, we apply the **LTR** formalism to three practical cases. In each of them we concentrate on the effects of interface roughness. We begin by treating the effects of the roughness of one interface, followed by a study of the interaction of the roughness of the two interfaces of a monolayer. We finish by treating the cumulative effects of a distributed roughness in a periodic structure.

In the first case, we analyse the effects of the roughness in a Light Emitting Diode (LED). The roughness is assumed to be situated at the interface between the top electric contact and the actual LED device. Further, we change the **LTR** formalism in order to take into account the emission of light from inside the device (active region of the LED). Another interesting study in the case of an LED is the angular dependence of the light emission. We therefore generalise the **LTR** formalism to include the angle of incidence of the incoming or emitted electromagnetic wave. The roughness effects are then studied either in the emission spectrum or in the angular dependence of the emission at a given wavelength.

In the second section of this chapter, we treat the effects of the roughness of a thin layer of zinc cadmium telluride. This example is interesting because using this sample we can compare two different methods of measuring the surface roughness. One is the determination of the roughness by optical means where we measure the transmission spectrum of the sample. Knowing the thickness and refractive index of the sample

we could fit the spectrum by varying the roughness. The second method is the direct measurement of the roughness by Atomic Force Microscopy (AFM).

Finally, we study the roughness effects introduced in selectively oxidised multilayered semiconductor structures. The samples studied are GaAs/AlGaAs multiple quantum wells containing oxidised AlGaAs as barrier layers around each quantum well. The incentive for this study was to determine the roughness introduced by the oxidation process which is important for the operation of VCSEL and other optoelectronic devices. Another aspect of this study is the utilisation of the multiplication operator in combination with the roughness because the sample is made up of 35 identical periods.

5.2 Roughness in an LED

In the following we study the effects of roughness on the angular dependence and the cavity mode of a Light Emitting Diode (LED) in the framework of the **LTR** formalism. In order to treat the case of an LED with the **LTR** formalism we have to generalise it to include the emission of the light in the active region inside the LED device. Further, it is necessary to be able to treat the case of angled propagating light waves in the **LTR** formalism.

Generally, an LED is constructed out of a highly reflecting substrate, an active layer and a low reflection top layer (see figure 5.1). This structure ensures a directional emission of the light. Light emitted from the active layer is transmitted by the semi-transparent top layer and reflected back from the highly reflecting substrate. One of the problems in LEDs is the electrical contact on the top. This contact can introduce extra roughness in the structure and thus diminishes its performance. Once the **LTR** formalism is generalised to treat the new aspects of the LED we study the effects of this roughness on the emission of the LED.

The major difference from the normal **LTR** procedure is in the position of the light source. In the case of the LED, the light source is between two multi layered structures. In order to calculate the response of the LED to the emission of the light we need to consider the multiple reflections between the two **LTR** structures. This can be done by using the same method applied for defining the combination law for the **LTR** elements.

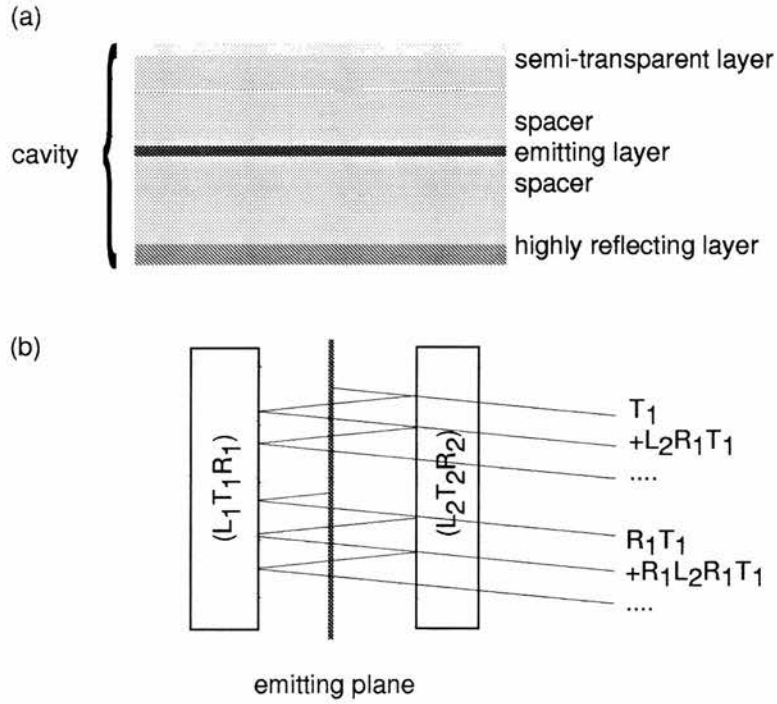

Figure 5.1: (a) Structure of an LED and (b) its corresponding **LTR** structure.

The emitted field coefficients to the left and right are:

$$\begin{aligned} E_L &= T_2 + L_2R_1T_2 + \cdots + R_1T_2 + L_2R_1R_1T_2 + \cdots \\ &= \frac{T_2(1+R_1)}{1-L_2R_1}, \end{aligned} \tag{5.1}$$

$$E_R = \frac{T_1(1+L_2)}{1-L_2R_1}. \tag{5.2}$$

This method takes into account the multiple reflections between the right and the left layers in the case of normal incidence. We remark here that the maximum emission coefficient is two in field and four in intensity. This takes into account the case where we have total reflection on one of the sides and constructive interference on the other.

In a second step, we generalise the **LTR** method to include the angular dependence. This can be done by using Snell's law (law of refraction) linking the angle of incidence to the angle of transmission (see figure 5.2)

$$\frac{\sin(\theta_i)}{\sin(\theta_t)} = \frac{n_2}{n_1}. \tag{5.3}$$

The origin of this relationship is the continuity equations for the vector field. In the case of absorption, these angles are complex and a geometrical representation is more complicated.

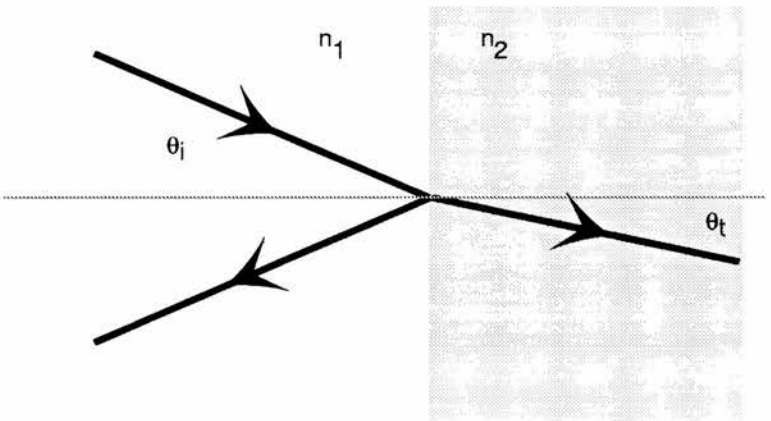

Figure 5.2: Refraction and reflection for a non-normal incident plane wave.

Further, we have to consider the Fresnel formulae for the parallel (denoted by subscript $\|$) and perpendicular (denoted by subscript $\perp$) components of the vector field with respect to the plane of incidence

$$t_{\|} = \frac{2n_1\cos(\theta_i)}{n_2\cos(\theta_i) + n_1\cos(\theta_t)}, \tag{5.4a}$$

$$t_{\perp} = \frac{2n_1\cos(\theta_i)}{n_1\cos(\theta_i) + n_2\cos(\theta_t)}, \tag{5.4b}$$

$$r_{\|} = \frac{n_2\cos(\theta_i) - n_1\cos(\theta_t)}{n_2\cos(\theta_i) + n_1\cos(\theta_t)}, \tag{5.4c}$$

$$r_{\perp} = \frac{n_1\cos(\theta_i) - n_2\cos(\theta_t)}{n_1\cos(\theta_i) + n_2\cos(\theta_t)}. \tag{5.4d}$$

Using equations (5.3) and (5.4) we can deduce the **LTR** element $\mathcal{L}$ for a single layer for a plane wave with an angle of incidence, θ. For the TE wave we have

$$\mathcal{L}_{\perp}(n,k,z,\theta) = \begin{pmatrix} r\frac{1-p^2}{1-p^2r^2} \\ p\frac{(1-r^2)}{(1-p^2r^2)} \\ r\frac{1-p^2}{1-p^2r^2} \end{pmatrix}, \tag{5.5}$$

with

$$\begin{cases} r = \frac{\cos(\theta)-\sqrt{n^2-\sin^2(\theta)}}{\cos(\theta)+\sqrt{n^2-\sin^2(\theta)}} \\ p = \exp(ikz\sqrt{n^2-\sin^2(\theta)}) \end{cases} . \tag{5.6}$$

Taking a closer look at $\mathcal{L}_\perp(n,k,z,\theta)$ we see that it is equal to $\mathcal{L}(n,k,z)$ as defined in equation (2.16) with a small change. The refractive index of vacuum has been replaced by $\cos(\theta)$ and the material index n by $\sqrt{n^2-\sin^2(\theta)}$. In the same manner, one can deduce the **LTR** coefficients for the perpendicular component of the field. In this case, we have to replace the material index n by $\sqrt{n^2-\sin^2(\theta)}$ and the vacuum refractive index by $n^2\cos(\theta)$.

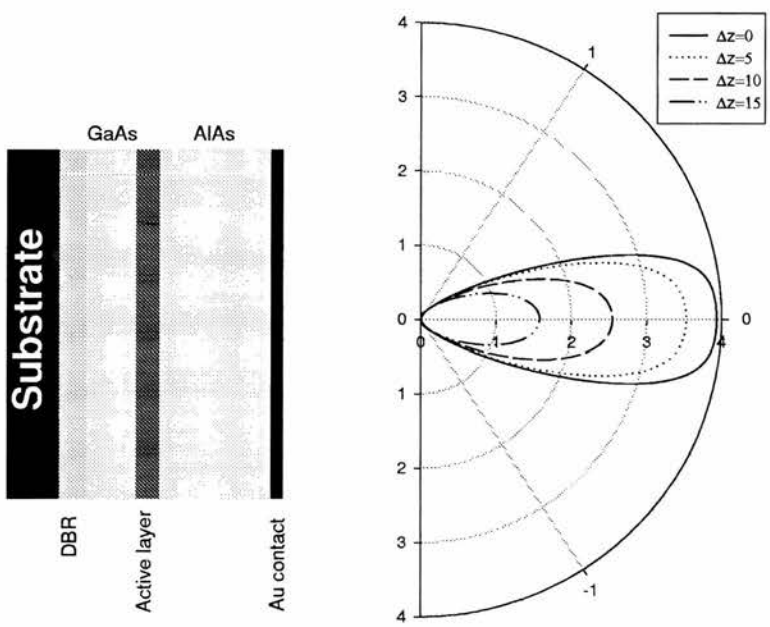

Figure 5.3: (a) Multi layered structure of the LED under consideration. (b) Angular emission coefficient at 900nm in a polar representation. The Δz coefficient corresponds to the effective roughness of the Au contact as defined by equation (3.11).

Using relations (5.2) and (5.1) we can calculate the angular emission of an LED. In figure 5.3 we show emission rates for perfect interfaces and for different levels of roughness. In order to take into account the roughness element with an angle of incidence

we consider the generalisation of the roughness element

$$X_{rough\perp}(\theta) = \begin{pmatrix} r_0 \\ \sqrt{1-r_0^2} \\ -r_0 \end{pmatrix} \oplus \begin{pmatrix} r_1 \exp\left(-2(n_1^2 - \sin^2(\theta))k^2\Delta z^2\right) \\ \sqrt{1-r_1^2}\exp\left(-\frac{\left(\sqrt{n_1^2-\sin^2(\theta)}-\sqrt{n_2^2-\sin^2(\theta)}\right)^2 k^2\Delta z^2}{2}\right) \\ -r_1 \exp\left(-2(n_2^2 - \sin^2(\theta))k^2\Delta z^2\right) \end{pmatrix} \oplus \begin{pmatrix} r_2 \\ \sqrt{1-r_2^2} \\ -r_2 \end{pmatrix} \tag{5.7}$$

with

$$\begin{cases} r_0 = \frac{\cos(\theta)-\sqrt{n_1^2-\sin^2(\theta)}}{\cos(\theta)+\sqrt{n_1^2-\sin^2(\theta)}} \\ r_1 = \frac{\sqrt{n_1^2-\sin^2(\theta)}-\sqrt{n_2^2-\sin^2(\theta)}}{\sqrt{n_1^2-\sin^2(\theta)}+\sqrt{n_2^2-\sin^2(\theta)}} \\ r_2 = \frac{\cos(\theta)-\sqrt{n_2^2-\sin^2(\theta)}}{\cos(\theta)+\sqrt{n_2^2-\sin^2(\theta)}} \end{cases} . \tag{5.8}$$

This is equivalent to the normal incidence roughness element (3.20) where all the refractive indices have been replaced in the same manner as for (5.5).

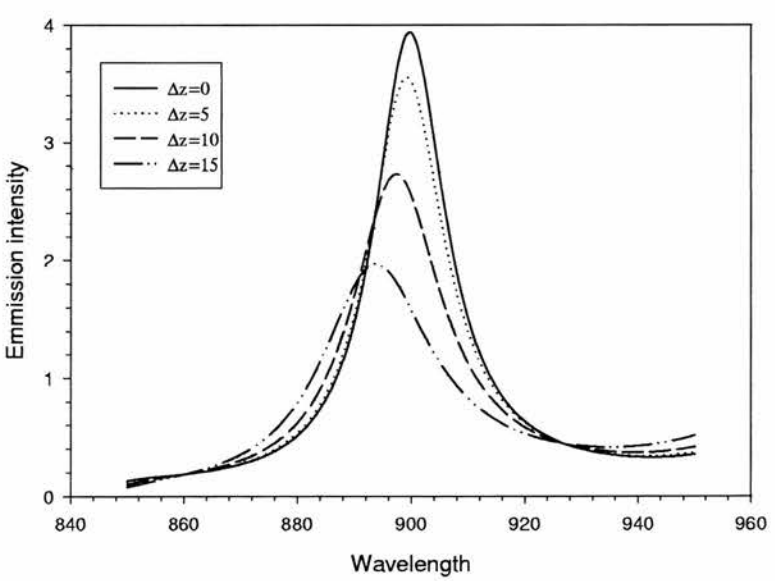

Figure 5.4: Emission spectra for different effective roughness of the metallic contact.

Figure 5.3 shows also the limitation of the roughness model in the case of the angular dependence of the emitted light. As remarked in the third chapter the roughness model loses energy due to the directional scattered light which is no longer in the direction of propagation of the plane wave. In the case of the LED, the emitted light is not a plane wave but has an angular distribution. When the light is scattered this angular distribution changes. This effect cannot be modelled considering only a one-dimensional structure. Figure 5.3 shows only the part of the light which has not changed direction while going through the rough interfaces.

Another interesting feature of an LED is the emission spectra as a function of the roughness. This gives insight on the cavity modes and their change with the introduction of roughness. In figure 5.4 we showed that with increasing roughness the mode corresponding to the resonance of the cavity diminishes in amplitude and broadens. This is similar to the effects measured in high-speed resonant cavity enhanced Schottky photodiodes [35]. It also corresponds to the results from the preceding chapter where we showed the link between the roughness and the finesse coefficient of a Fabry-Perot cavity.

5.3 Roughness measure for a monolayer

5.3.1 Samples

The samples studied in this section are thin layers of zinc cadmium telluride ($Zn_xCd_{1-x}Te$). This material shows large nonlinear optical properties [36, 37]. Furthermore, its band gap can be adjusted between 1.49eV and 2.26eV (830nm and 550nm) by changing the relative Zn/Cd ratio [38,39]. At the same time, varying this ratio in the alloy allows the lattice constants to be matched to a variety of other II-VI compounds e.g. HgCdTe and HgZnTe. It is thus a material with good potential for optoelectronic devices.

Here we consider optical quality thin films. These can be prepared by many sophisticated methods such as molecular beam epitaxy, electrodeposition, liquid phase epitaxy etc.. The sample characterised in this section is prepared as a polycrystalline thin film in a simple evaporation chamber, using the ternary compound as source. Its zinc telluride content is 85% so that the final thin layer is $Zn_{0.85}Cd_{0.15}Te$. In order to characterise the

optical quality of the samples prepared by this method we use its transmission spectra to determine the optical roughness of the surface of the thin layer.

5.3.2 Results

The optical transmission spectra of the films are measured in the range of 550nm to 800nm using a Beckman spectrophotometer. The measured transmission spectrum (figure 5.5) show the position of the band gap and Fabry-Perot fringes in the transparent region. It is mostly these fringes which give information about the optical properties of the thin layer. Indeed, their absolute value and the difference between maxima and minima can be used to determine the absorption coefficient and the roughness of the thin layer. Further, the spectral position of the fringes is linked to the refractive index and the thickness of the sample.

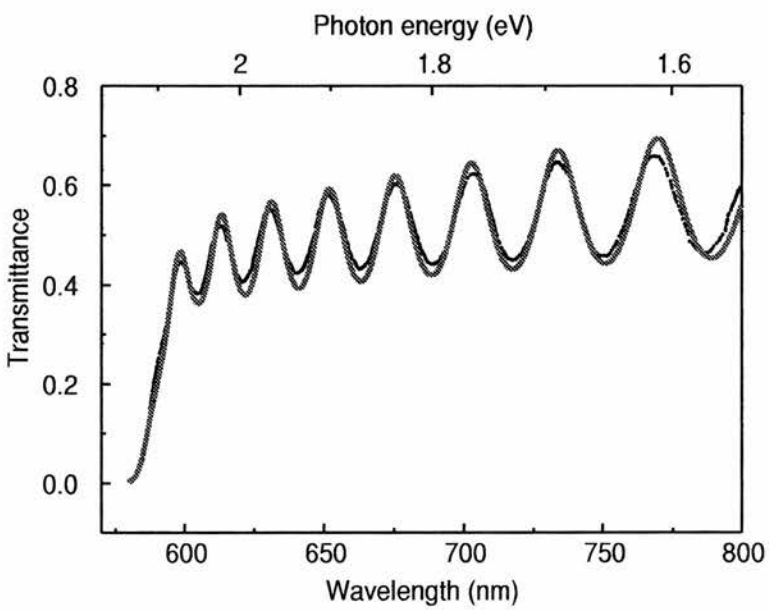

Figure 5.5: Transmission spectrum of $Zn_{0.85}Cd_{0.15}Te$. The dots correspond to measured data and the continuous line to the fit.

Using the above mentioned parameters we are able to fit the transmission spectra in figure 5.5 to a remarkable degree. Further, it is possible to compare the roughness measured by the optical method with the roughness measured by atomic force microscopy for this same sample [40]. Measurements over a distance of $1\mu m$ with the AFM indicate a roughness of 13nm and the optical transmission measurement gives the best fit for a value of 18nm. The overestimation of the roughness by the optical method can be

explained by the size of the light beam on the sample which is of the order of $1mm^2$. In this example we determined that we can distiguish between the roughness and absorbtion effects. Increasing the roughness diminishes the contrast of the Fabry-Perot fringes. Whereas, increasing the absorbtion coefficient diminishes the contrast of the fringes and the overall transmission coefficient.

5.4 Roughness measurement in multilayered structures

The interface between different materials in multilayered semiconductor structures has received considerable attention recently. The interface roughness in such structures is an important parameter limiting both the optical and the electrical performance of devices [41–46]. In particular, this problem is crucial to selectively oxidised Al(Ga)As/GaAs multilayers, which are now becoming widely used to form high reflectivity and wide-bandgap distributed Bragg reflectors (DBRs) in vertical cavity optoelectronics devices, such as lasers, LEDs, modulators and detectors. The scattering loss by interface roughness decreases the maximum reflectivity of DBRs, thus deteriorating the device performance.

Several authors have studied the Al(oxide) layers and the interface quality of Al(oxide)/AlGaAs structures [46–51]. Transmission electron microscopy (TEM) has revealed a granular structure of the Al(oxide) [47, 48] and the grain size has been estimated to be about 8nm [48]. A porous interface between Al(oxide) and AlGaAs has been observed [48,49] and an interface transition width of 2nm has been reported in [47].

The reflectance method used in our measurement is a simple, non-destructive and direct way to study the optical properties of selectively oxidised Al(Ga)As/GaAs multilayers [46, 50, 51]. In this work we measure the reflectivity spectra of GaAs/AlGaAs multiple quantum well structures with and without oxidation of the barrier layers. The **LTR** method is then used for calculating the reflectivity and transmission spectra of these multilayer optical structures. The simple statistical roughness model introduced in the preceding chapter is used to describe the effect of interface roughness. By fitting the experimental reflectivity spectrum using this model we have assessed the interface

roughness of the oxidised layers, as well as the Al(oxide) parameters (refractive index and thickness) [52–54].

5.4.1 Samples

The samples were grown by molecular beam epitaxy on (100) semi-insulating GaAs substrates with 2^o misorientation towards (110). A GaAs (400nm) buffer layer was followed by 35 periods with each period containing an $Al_{0.98}Ga_{0.02}As$ (50nm) barrier layer, an $Al_{0.4}Ga_{0.6}As$ (7.5nm) spacer, a GaAs (7nm) quantum well and another $Al_{0.4}Ga_{0.6}As$ (7.5nm) spacer. An $Al_{0.98}Ga_{0.02}As$ (50nm) barrier layer and a GaAs (30nm) cap layer completed the structure. Three samples were used. The first (2408uu) is as-grown. The other two (2408e and 2408c) were patterned and etched (RIE, 36 min) to obtain $20\mu m$ strips spaced by $2\mu m$ grooves (see figure 5.6). The $Al_{0.98}Ga_{0.02}As$ layers in sample 2408c have been laterally oxidised at 398^oC for 70 minutes. Scanning electron microscopy has shown that these conditions ensure a complete oxidation of the $Al_{0.98}Ga_{0.02}As$ layers.

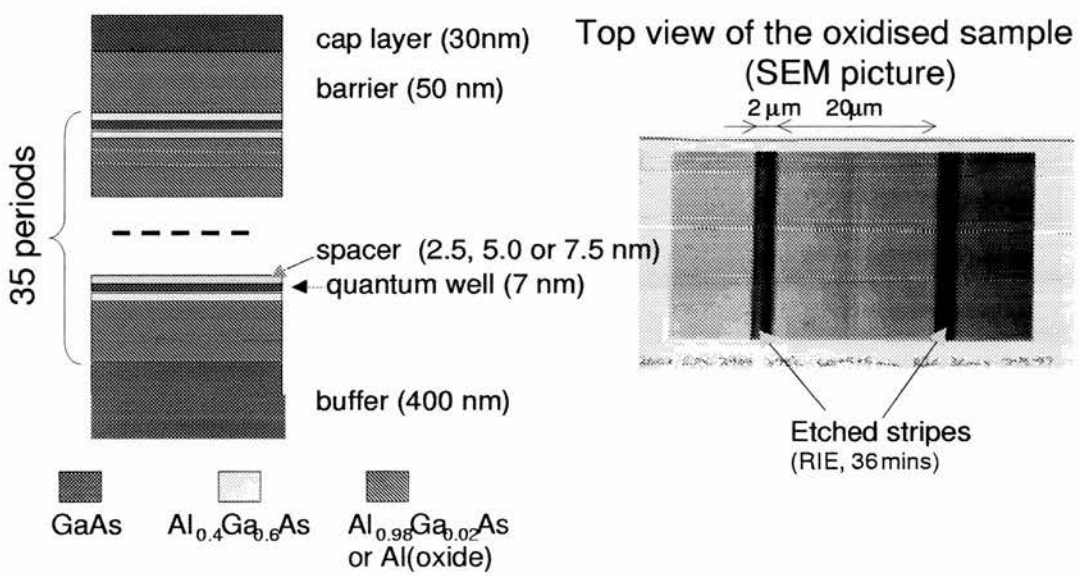

Figure 5.6: Structures of the selectively oxidised Al(Ga)As/GaAs multilayers

5.4.2 Experimental Setup

Measurement of the optical properties of materials must be corrected for spectral dependencies of the light source, any optical elements and the detector sensitivity. Dark

current and parasitic light must also be taken into account. In single beam configurations this is achieved by measuring two successive spectra. To overcome the necessity of spectral calibration and to improve the signal to noise ratio, dual beam techniques are commonly used where the same detector samples alternately a reference beam and a beam from the sample [55]. Using a lock-in amplifier eliminates the parasitic noise. A simultaneous measurement of both beams by using a double frequency optical chopper and two lock-in amplifiers achieves both corrections.

In our set-up for reflectivity measurements we used a simple technique for simultaneous recording of two optical beams using a single optical chopper, detector and lock-in amplifier [56]. The new feature of our method is based on chopping the two beams with the same frequency but with a phase shift of $\pi/2$ or $3\pi/2$. The corresponding electrical signals from the detector are measured as the in-phase and the quadrature signal by the lock-in amplifier.

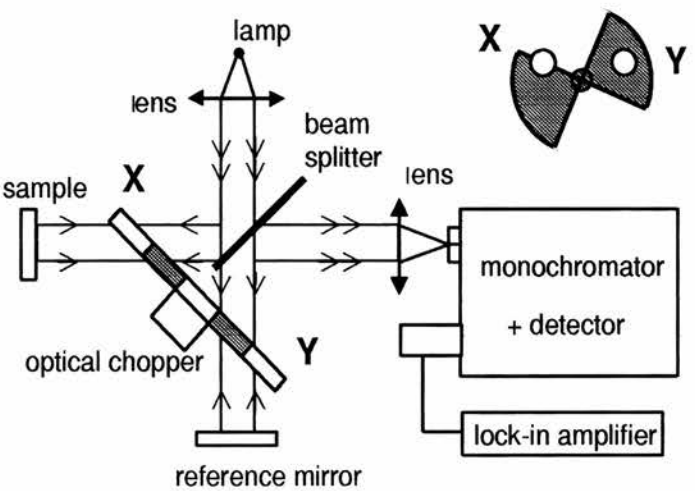

Figure 5.7: The setup used to measure simultaneously the reference and reflectivity signal. The inset in the upper right corner shows the relative position of the beams and the optical chopper, which corresponds to a relative phase shift of $3\pi/2$.

Figure 5.7 illustrates schematically our technique, applied to the case of reflectivity measurements. The collimated beam from the lamp is split into two beams, which are reflected from the sample (beam X) and from the reference mirror (beam Y), respectively. The beams are recombined and focused on the entrance slit of the monochromator, coupled to a Si photodetector. By moving the optical chopper in a direction perpendicular to the plane of rotation it is possible to tune the phase shift between the two

beams until it becomes $\pi/2$ or $3\pi/2$ The ratio between the X and Y outputs of the lock-in amplifier gives the relative reflectivity of the sample with respect to the reference mirror.

The simultaneous detection of X and Y beams reduces considerably the noise compared to a successive detection of the two beams. To illustrate this, we have measured two time dependencies of the signal using the same sample (GaAs/AlGaAs multiple quantum wells with oxidised AlAs layers) under identical conditions recording twice 8000 (X,Y) pairs at 4Hz. The light source was a tungsten lamp with a stabilised power supply.

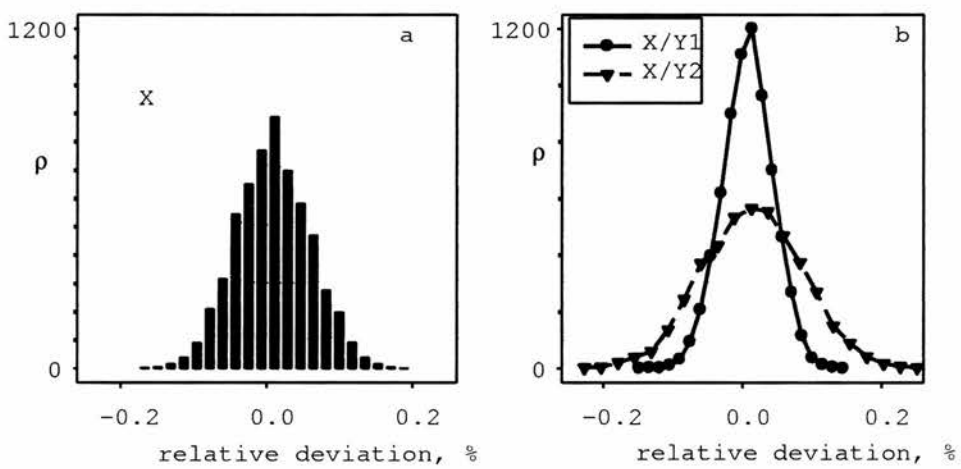

Figure 5.8: Normalised frequency distributions ((ρ) of a: X and b: X/Y1 and X/Y2. The relative deviation is calculated with respect to the mean value.

Let X be the X signal obtained during the first run and Y1 and Y2 be the corresponding signals from the first and the second run, respectively. The single recording of X does not take into account any spectral or noise corrections. The ratio X/Y1 is the reflectivity measured by our technique, while X/Y2 corresponds to the case of successive detection of the sample and the reference beams, as in a single beam set-up. The frequency distributions of X, X/Y1 and X/Y2 around their mean values are shown on Fig. 5.8. It may be observed that the standard deviation is the largest for X/Y2 and smallest for X/Y1. This implies that in the case of a single beam configuration the spectral corrections introduce noise, while in our technique they decrease the noise. This improvement is a result of the simultaneous detection of the X and Y beams.

This simple dual optical beam measurement technique with simultaneous detection of the two beams significantly reduces the noise compared to the single beam configurations

while having many of the advantages of using a double frequency optical chopper and two lock-in amplifiers. Applications could be in spectral measurements such as reflectivity, transmission and excitation spectroscopies. Further, our technique can be generalised to a three-beam configuration in laser pump-probe experiments using a dual frequency chopper.

5.4.3 Results

In the calculations we have used the Afromowitz model [57] for the refractive index of GaAs and $Al_{0.4}Ga_{0.6}As$, while for $Al_{0.98}Ga_{0.02}As$ the model of Fern and Onton [58] has been applied. No excitonic effects have been considered. The reflectivity spectrum of the as-grown sample (2408uu) is shown in Fig.5.9. A series of interference fringes is observed with a period of 30-40nm, which increases with wavelength as expected. In order to achieve optimal matching in the simulation we have assumed a small deviation of the refractive indices over the whole spectral range considered. This is +1.5% for GaAs and $Al_{0.4}Ga_{0.6}As$ and +0.3% for $Al_{0.98}Ga_{0.02}As$. We fix these values in the analysis of the other samples. No roughness has been considered in this case. For multilayers with close refractive indices such as in the GaAs/AlGaAs system, the effect of the roughness in our model becomes noticeable for σ>4-5nm.

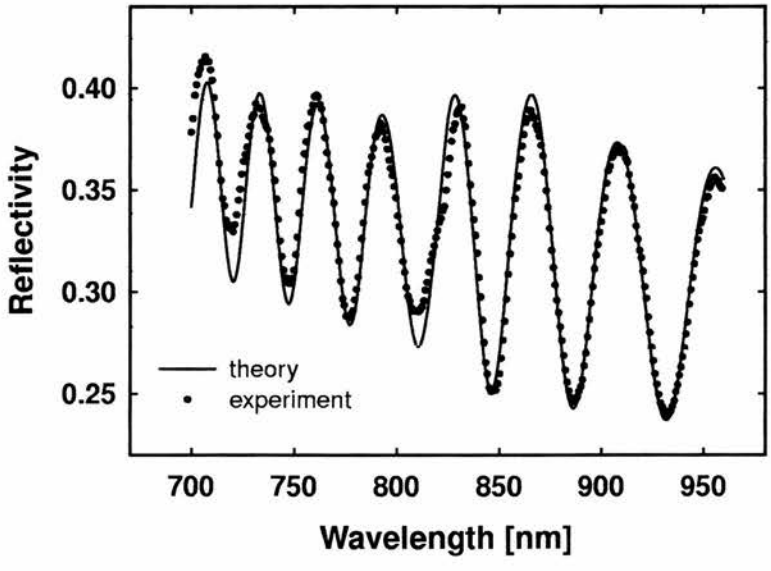

Figure 5.9: Measured and calculated reflectivity spectrum of the as-grown GaAs/AlGaAs multiple quantum well sample.

When simulating the reflectivity of a single layer with the thickness of the whole of the structure (2600nm without the buffer layer) and a refractive index averaged in proportion to the thicknesses of the different materials we obtain fringes which are shifted along the Y-axis, but have the same wavelength positions. This means that the observed fringe pattern is determined predominantly by the interference of the light reflected from the front surface and from the last interface ($Al_{0.98}Ga_{0.02}As/GaAs$).

In the case of etched samples the contribution of the layers at the bottom of the grooves has been added into the simulations in proportion to their area. Unlike the work of MacDougal [50] we have not been able to fit the experimental curves without considering these layers. Their effect is revealed as a modulation of the whole of the spectrum with a period of about 100nm, which corresponds to a groove depth d_{gr}. The extent of the modulation depends on the roughness σ_{gr} of their surfaces. The reflectivity spectrum of the etched, but non-oxidised sample (2408e) is displayed in Fig.5.10. The fringes are at the same positions as for the as-grown sample, but their amplitudes and the mean reflectivity value are modulated, because of the groove layers. Optimal fitting is obtained for d_{gr}=3335nm and σ_{gr}=80nm.

The oxidation of AlGaAs layers changes their parameters considerably [47–51]. Shrinkage of layer thickness is commonly observed. TEM [47, 49] and reflectance [51] studies have found different values for the extent of this shrinkage, which range between 3% and 13%. The refractive index decreases by approximately a factor of 2. Values in the range 1.5-1.65 have been obtained by ellipsometric and reflectance measurements [50, 51]. It is usually assumed to be wavelength independent in the visible and the near-infrared regions.

Figure 5.11 represents the reflectivity spectrum of the oxidised sample (2408c). In comparison with the two previous cases the period of the fringes is increased by about 1.5 times, which corresponds to the decrease of the effective refractive index and thickness of the structure after oxidation. Besides, the fringe amplitude is smaller and the mean reflectivity value is lower. This is attributed to light scattering by interface roughness of the oxidised layers. The modulation of the spectrum due to the groove layers has a similar extent as in Fig.5.10, but is more clearly observed, because of the smaller fringe amplitude.

In the simulations we have varied the index and the thickness of the oxidised layers and the roughness of their interfaces. An optimal fit is obtained with an oxide index of

1.54, oxide thickness of 44.5nm, or 89 % of the initial value and a roughness of 8.4nm. The groove parameters in this case are slightly different: d_{gr}=3247nm and σ_{gr}=70nm, which can be explained by changes due to the oxidation. The values obtained for the refractive index and the shrinkage extent are in good agreement with the findings of other authors [47,49–51]. The interface roughness of Al(oxide) layers is larger than the result obtained in [46], but corresponds to the reported grain size of the oxide granular structure [48].

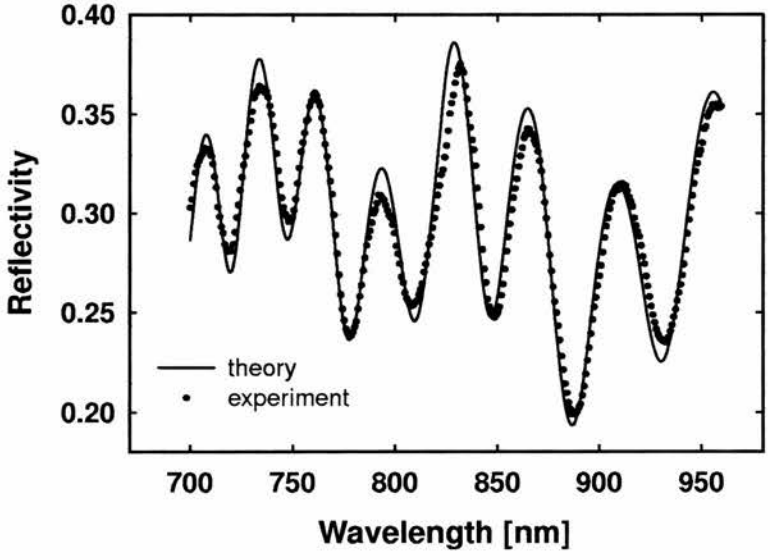

Figure 5.10: Measured and calculated reflectivity spectrum of the GaAs/AlGaAs multiple quantum well sample which has been patterned, but not oxidised.

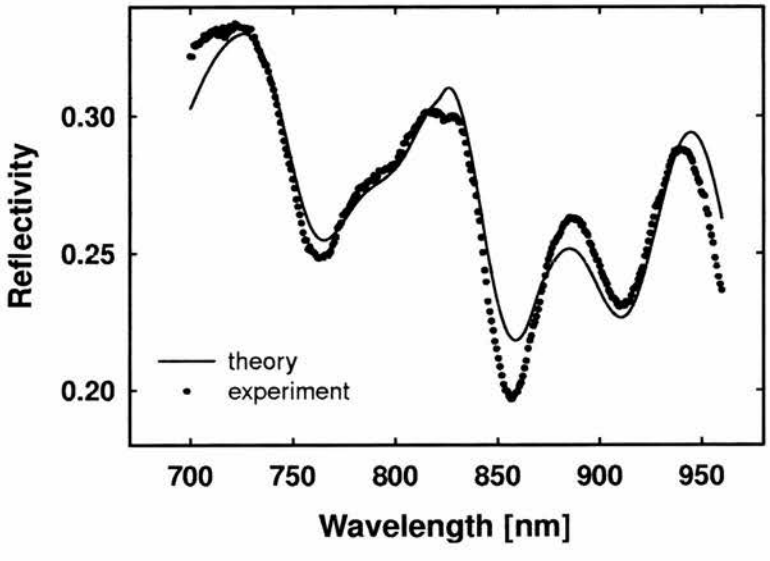

Figure 5.11: Measured and calculated reflectivity spectrum of the GaAs/AlGaAs multiple quantum well sample, which has been patterned and oxidised.

In conclusion the effects of interface roughness can be easily included in the **LTR** calculations of multi-layered structures by introducing a "rough" element between adjacent layers. The model is applied to GaAs/AlGaAs multiple quantum well structures with and without oxidation of the barrier layers. The fits to the reflectivity spectra have given important parameters for the oxidised layers such as the interface roughness, the refractive index and the thickness.

5.5 Summary

In this chapter, we have applied the **LTR** formalism in three different cases. We studied the effects of the electric contact roughness on the light emission of a LED. The introduction of the roughness showed a deterioration of the emission efficiency and a broadening of the emission mode. In the second case we treated the effects of the surface roughness in transmission experiments measured on a thin layer of zinc cadmium telluride. The comparison with the roughness measured by AFM showed that the optical method gives a good estimation of the surface roughness. Finally, we studied the changes in the reflectivity spectra when selectively oxidising layers in GaAs/AlGaAs multiple quantum well structures. We could assess in this case the effective roughness of the oxidised layers. Further, the **LTR** method could be used to evaluate the shrinkage factor of these same layers.

Chapter 6

Multiple quantum well n-level systems

6.1 Introduction

In this chapter, we introduce the quantum n-level system and its theoretical treatment in the framework of the density matrix equation. As an example of an n-level system we use multiple quantum well structures. Taking advantage of the similarities of Maxwell's electromagnetic wave equation and Schrödinger's quantum wave equation we can change the **LTR** formalism (Left reflection, Transmission and Right reflection) and apply it to the multiple quantum well case. Using this formalism we determine the eigen-levels of such a system which can then be used in the density matrix formalism to study the system evolution under excitation.

6.2 Definitions

In the first section, we consider Schrödinger's equation [59,60] and its eigen-states to define an n-level system. Based on these definitions, we introduce the different relaxation times leading towards thermodynamical equilibrium of the n-level system in the density matrix formalism [61]. In this formalism, the relaxation has its origins in the coupling between the quantum system and its environment that can be treated using the Markovian approximation [62] which we use as a working hypothesis. Finally, we show briefly the link between the n-level systems and the optical properties of semiconductors [63,64].

6.3 Evolution equations in n-level systems

In quantum mechanics, the evolution of any system is determined if one knows its wave function $\psi(t, \vec{r})$ as a function of time (where $\vec{r}$ represents the generalised coordinates). The equation of evolution of this wave function is Schrödinger's equation [60, 61, 65]

$$i\hbar \frac{\partial \psi(t, \vec{r})}{\partial t} = \mathbf{H}\psi(t, \vec{r}). \tag{6.1}$$

The linear and Hermitian operator $\mathbf{H}$ is associated with the total energy of the system and is called the Hamiltonian operator. The constant $\hbar$ is Planck's reduced constant linking the energy to the frequency.

The eigen-functions of the Hamiltonian operator $\mathbf{H}$ can be used to solve equation (6.1) for a time-independent Hamiltonian. The equation giving the eigen-values and functions of the Hamiltonian is

$$E_j \psi_j(\vec{r}) = \mathbf{H}\psi_j(\vec{r}), \tag{6.2}$$

where E_j are the eigen-values which correspond to the energy of the system in the state $\psi_j(\vec{r})$. The set of eigen-values of $\mathbf{H}$ can be seen as the spectra of the Hamiltonian. They can be degenerate (several eigen-functions having only one eigen-value) or non-degenerate (one to one relation) and the spectrum can be continuous or discrete. In this work, we study the case of a discrete set of eigen-values.

The complete solution of (6.1) can be found by separation of time and space variables. Then, to each eigen-function is associated a solution of (6.1) having the form

$$\psi_j(t, \vec{r}) = \exp\left(-i\frac{E_j}{\hbar}t\right)\psi_j(\vec{r}). \tag{6.3}$$

The general solution is represented by a linear combination of all the eigen-functions of the Hamiltonian

$$\psi(t, \vec{r}) = \sum_{j=1}^{\infty} c_j(t)\psi_j(\vec{r}). \tag{6.4}$$

where $c_j(t)$ are the probability amplitudes for each of the states. Introducing (6.4) in (6.1) one obtains the evolution equations of the probability amplitudes

$$i\hbar\frac{dc_j(t)}{dt} = H_j^i c_i(t), \tag{6.5}$$

where

$$H_j^i = \delta_j^i E_j, \tag{6.6}$$

which corresponds to the projection of the Hamiltonian operator on its eigen-function base. The square of the modulus of the probability amplitude gives the probability of finding the system in the associated eigen-state. In the case of a discrete, finite and non-degenerate set of eigen-values the Hamiltonian operator defines n eigen-states. This system is an n–level system.

Another equivalent description of quantum mechanics uses the density matrix formalism. This approach is very useful for the phenomenological introduction of the relaxation because the density matrix describing the state of the system gives the probability of each state directly as well as its coherence. Thus we have direct access to the global probability of the system and so we are able to keep this probability constant in time when introducing the relaxation phenomena. Besides, this formalism allows the treatment of statistically mixed states in a simple manner. In the following, this formalism is defined and we introduce the operator corresponding to the relaxation of the system.

Above, the general solution of Schrödinger's equation is projected on an eigen-function base of the Hamiltonian. After this decomposition (6.4), the population ρ_{nn} of state n is defined by

$$\rho_{nn}(t) = c_n^*(t)c_n(t). \tag{6.7a}$$

These terms are the diagonal elements of the density matrix and represent the probabilities for the system to be in the state n. The sum of these probabilities over all states is equal to $\sum_n \rho_{nn} = 1$, which is the normalisation condition of the wave function.

Another important quantity in the study of the evolution of a quantum system is the coherence ρ_{mn} between the different states

$$\rho_{mn}(t) = c_n^*(t)c_m(t), \tag{6.7b}$$

which gives the phase between the populations of the two states. These terms are the non diagonal elements of the density matrix. The derivative with respect to time of the argument of the coherence corresponds to the energy difference between the two states.

The definitions of the population (6.7a) and coherence (6.7b) are given in the "pure case" where the initial state is known perfectly. Mathematically, this implies a knowledge of the initial conditions of the Schrödinger equation. In the case of an incomplete knowledge of the initial conditions, this state is described by the probabilities p_k of the different initial conditions. This case is a statistical mixture and its populations and coherence can be defined from the probabilities of the mixture and the definitions of the pure case

$$\begin{aligned}\rho_{mn}(t) &= \overline{c_n^*(t)c_m(t)} \\ &= \sum_k p_k \rho_{mn}^k(t).\end{aligned} \tag{6.8}$$

With the help of the density matrix, Schrödinger's equation (6.1) can be cast into the form

$$i\hbar\frac{d\rho_{ij}}{dt} = \mathcal{H}_i^k\rho_{kj} - \rho_{ik}\mathcal{H}_j^k, \tag{6.9}$$

where the summations are done using Einstein's convention. The Hamiltonian operator $\mathcal{H}$, considered here, includes the states of the studied system as well as those of the surrounding thermal bath. The right hand side corresponds to the commutator between the Hamiltonian and the density matrix.

The Hamiltonian in (6.9) can be decomposed into two parts: a part giving the internal energy of the studied system and another taking into account the interactions with the surrounding thermal bath. This last part induces an energy dissipation [66] and generally is described by a random interaction adding a supplementary term to

equation (6.9)

$$i\hbar\frac{d\rho_{ij}}{dt} = H_i^k\rho_{kj} - \rho_{ik}H_j^k + i\hbar\left(\frac{\partial\rho_{ij}}{\partial t}\right)_{relaxation}. \tag{6.10}$$

This relaxation term is written with the help of the relaxation coefficients Γ describing the relaxation of the different populations and coherence towards their thermodynamical equilibrium[1] $\rho^{(0)}$ [67]. Thus, the relaxation of the populations, is given by

$$\left(\frac{\partial\rho_{nn}}{\partial t}\right)_{relaxation} = -\Gamma_{nn}^{mm}\left(\rho_{mm} - \rho_{mm}^{(0)}\right), \tag{6.11a}$$

where $(\Gamma_{nn}^{mm})^{-1}$ is the longitudinal relaxation time and corresponds to the dissipation of energy to the thermal bath (inelastic collisions). The relaxation of the coherence is given by

$$\left(\frac{\partial\rho_{ij}}{\partial t}\right)_{relaxation} = -\Gamma_{ij}^{ij}\rho_{ij}, \tag{6.11b}$$

which defines the transverse relaxation time $\left(\Gamma_{ij}^{ij}\right)^{-1}$ constituted from energy dissipation (inelastic collisions) as well as losses due to the interaction between the different populations (elastic collisions).

Considering the two relaxation terms (6.11a) and (6.11b), the density matrix equation can be written as

$$i\hbar\frac{d\rho_{ij}}{dt} = H_i^k\rho_{kj} - \rho_{ik}H_j^k - \Gamma_{ij}^{kl}\left(\rho_{kl} - \rho_{kl}^{(0)}\right). \tag{6.12}$$

In this work, we study the stationary and dynamical response of n-level quantum systems in the framework of this relaxation model.

As the energy dissipation is towards the thermal bath, the different relaxation coefficients Γ as well as the balance state $\rho^{(0)}$ depend on the temperature. The populations at thermodynamical equilibrium $\rho^{(0)}$ are given by the Boltzmann distribution [68]

$$\rho_{nn}^{(0)} = ce^{-H_n^n/(kT)}, \tag{6.13}$$

[1] The phenomenological introduction of the relaxation times can also be achieved by starting from the causality and inertia principles. In this case, the deduced relaxation coefficients matrix Γ generalises the one in equation (6.12)

where k is the Boltzmann constant. The proportionality coefficient c can be determined from the normalisation condition $\sum_n \rho_{nn}^{(0)} = 1$.

Once the density matrix evolution is known we can deduce the polarisation of the system. Indeed, knowing the electronic wave function, the microscopic polarisation can be determined by calculating the first order momentum of the wave function

$$\vec{p}(t) = q \int\int\int \psi^*(t,\vec{r})\vec{r}\psi(t,\vec{r})d^3r. \tag{6.14}$$

The matrix corresponding to the dipolar momentum of the system can be introduced, using the eigen-functions ψ_i and ψ_j in the case of the dipolar approximation [69],

$$\vec{\mu}_j^i = q \int\int\int \psi_i^*(\vec{r})\vec{r}\psi_j(\vec{r})d^3r. \tag{6.15}$$

Symmetry considerations simplify the general form of this matrix. For example, if the eigen-states ψ_i and ψ_j have the same parity, the corresponding matrix element is zero.

With the help of the dipolar momentum matrix, the interaction Hamiltonian between the system and the field can be written as

$$W_j^i(t) = \vec{\mu}_j^i \cdot \vec{E}(t). \tag{6.16}$$

In the density matrix representation, the evolution equation is

$$i\hbar\frac{d\rho}{dt} = \mathbf{H_0}\rho - \rho\mathbf{H_0} + \mathbf{W}(t)\rho - \rho\mathbf{W}(t) - \Gamma\left(\rho - \rho^{(0)}\right), \tag{6.17}$$

and the macroscopic polarisation is given by the trace of the dipolar momentum applied to the density matrix including the statistical distribution (6.8)

$$\vec{P}(t) = \frac{N}{V} Tr(\vec{\mu}_i^k \rho_{kj}), \tag{6.18}$$

where N and V are respectively the number of n-level systems and their total volume.

From the polarisation and excitation field, a new quantity corresponding to the amplitude of the response of the system can be introduced. This is the dielectric susceptibility that is composed of a linear and non-linear part. The linear susceptibility χ is defined as the proportionality factor between the macroscopic polarisation $\vec{P}$ and the

excitation field $\vec{E}$ at the same wavelength

$$\vec{P}(\omega) = \chi(\omega)\vec{E}(\omega). \tag{6.19}$$

The susceptibility is in general a second order tensor, which means that the polarisation and the external field are not necessarily colinear.

The dielectric susceptibility as a function of time is given by a convolution between the transfer function $\hat{\chi}(t)$ and the field $\vec{E}(t)$

$$P(t) = \int_{-\infty}^{\infty} \hat{\chi}(t-\tau)E(\tau)d\tau. \tag{6.20}$$

In order to fulfil the causality condition [67] (no polarisation induced before the excitation), the transfer function $\hat{\chi}(t')$ must be zero for all $t' = t - \tau$ negative. This condition is written in real time as

$$\hat{\chi}(t') = \hat{\chi}(t')\Theta(t'), \tag{6.21}$$

where $\Theta(t')$ is the Heaviside distribution[2]. Using the Fourier transformation of the Heaviside distribution one finds

$$\int_{-\infty}^{\infty} e^{-i\omega t'}\Theta(t')dt' = -i\text{p.v.}\frac{1}{\omega} + \frac{1}{2}\delta(\omega)$$

where p.v. is Cauchy's principal value. Therefore, the causality condition (6.21) can be written in reciprocal space as

$$\begin{aligned}\chi(\omega) &= \chi(\omega) * \left(-i\text{p.v.}\frac{1}{\omega} + \frac{1}{2}\delta(\omega)\right) \\ &= -i\text{p.v.}\int_{-\infty}^{\infty} \frac{\chi(\omega_1)}{\omega - \omega_1}d\omega_1 + \frac{1}{2}\chi(\omega),\end{aligned}$$

where $f * g$ represents the convolution between functions f and g. This equality links up through a Hilbert transformation the real χ' and imaginary χ'' parts of the susceptibility

[2]The Heaviside distribution is defined as $\Theta(t') = 0$ for $t' < 0$, $\Theta(0) = 1/2$ and $\Theta(t') = 1$ for $t' > 0$.

in the following manner

$$\chi'(\omega) = \text{p.v.} \int_{-\infty}^{\infty} d\omega_1 \frac{\chi''(\omega_1)}{\omega - \omega_1}, \tag{6.22a}$$

$$\chi''(\omega) = \text{p.v.} \int_{-\infty}^{\infty} d\omega_1 \frac{\chi'(\omega_1)}{\omega_1 - \omega}. \tag{6.22b}$$

These two equations are called Kramers-Kronig relations. The transfer function of all causal systems must fulfill these conditions.

The Kramers-Kronig relations can be generalised to include the non-linear responses of matter. In this case, the polarisation is written as

$$\begin{aligned} P(\omega) &= \chi^1(\omega)E(\omega) \\ &+ \int_{-\infty}^{\infty} d\omega_1 \int_{-\infty}^{\infty} d\omega_2 \chi^2(\omega_1, \omega_2)E(\omega_1)E(\omega_2)\delta(\omega - \omega_1 - \omega_2) + \cdots \end{aligned} \tag{6.23}$$

where χ^1 and χ^2 are respectively the linear and the lowest order non-linear susceptibility. The generalisation of the Kramers-Kronig condition for the non-linear susceptibilities of higher orders can be found in the literature [70, 71].

6.4 Multiple quantum well n-level systems

In this section we use the **LTR** formalism (Left reflection, Transmission and Right reflection) to calculate the energy levels in semiconductor multiple quantum wells. In order to do this we have to write the quantum wave function in the same form as the electromagnetic wave used in the optical **LTR** formalism.

This can be achieved by using the effective mass approximation which treats the carriers as free particles (i.e. particles in a constant potential) having an effective mass determined by the $\mathbf{k} \cdot \mathbf{p}$ method at the band edge [72, 73]. In this approximation the band structure at the band edge is given by a parabola whose quadratic coefficient is inversely proportional to the effective mass. The band gap energy itself corresponds to the constant potential in which the free carriers are moving.

In the case of multiple quantum wells, we have a succession of different semiconductor layers each having different effective masses and band gaps. The stationary Schrödinger

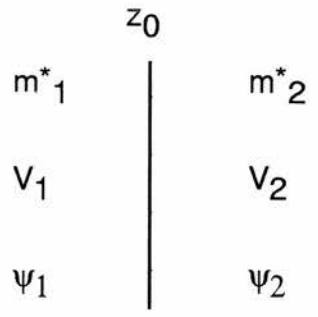

Figure 6.1: Interface between two crystals.

equations for the quantum wave function in each crystal is

$$-\frac{\hbar^2}{2m^*}\frac{d^2}{dz^2}\psi + V\psi = E\psi \tag{6.24}$$

where m^* is the effective mass, E the eigen-energy and V the potential of the crystal.

This stationary equation has two fundamental solutions which lead to the following wave solutions

$$\psi_+(z,t) = \exp\left(i\sqrt{2m^*\frac{E-V}{\hbar^2}}z - i\frac{E}{\hbar}t\right), \tag{6.25a}$$

$$\psi_-(z,t) = \exp\left(-i\sqrt{2m^*\frac{E-V}{\hbar^2}}z - i\frac{E}{\hbar}t\right). \tag{6.25b}$$

These solutions correspond to a travelling wave to the left and to the right.

In order to define the equivalent wave vector and refractive index we have to consider the continuity conditions of the quantum wave in the envelope approximation at the interface between two different media (see figure 6.1)

$$\psi_1(z_0,t) = \psi_2(z_0,t), \tag{6.26a}$$

$$\frac{1}{m_1^*}\frac{d}{dz}\psi_1(z_0,t) = \frac{1}{m_2^*}\frac{d}{dz}\psi_2(z_0,t). \tag{6.26b}$$

We see here a slight difference with the continuity conditions of the electromagnetic wave. In this case the relation giving the continuity of the derivative is a function of the effective mass.

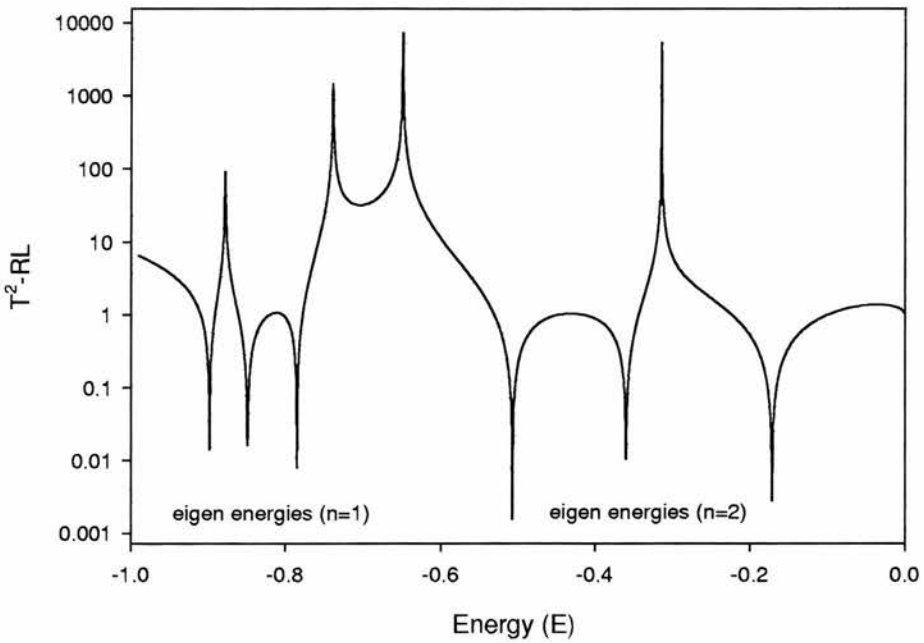

Figure 6.2: The "total absorbing condition" ($T^2 - LR = 0$) as a function of the energy for three coupled quantum wells for the following parameters: width 4 units, separation 0.5 units, effective mass 1, $\hbar = 1$ and crystal potential inside the wells -1.

We consider at the interface an incident, a transmitted and a reflected wave

$$\begin{aligned} \psi_1(z,t) &= \exp\left(i\sqrt{2m_1^*\frac{E-V_1}{\hbar^2}}z - i\frac{E}{\hbar}t\right) \\ &\quad + r_{12}\exp\left(-i\sqrt{2m_1^*\frac{E-V_1}{\hbar^2}}z - i\frac{E}{\hbar}t\right), \qquad (6.27a) \\ \psi_2(z,t) &= t_{12}\exp\left(i\sqrt{2m_2^*\frac{E-V_2}{\hbar^2}}z - i\frac{E}{\hbar}t\right). \qquad (6.27b) \end{aligned}$$

where the coefficients r_{12} and t_{12} correspond to the reflection and transmission coefficients of the quantum wave function. Inserting the solutions (6.27) into the continuity conditions (6.26) we get two equations giving us the relative amplitudes of the reflected and transmitted waves.

$$\begin{aligned} 1 + r_{12} &= t_{12}, \qquad (6.28a) \\ \sqrt{\frac{E-V_1}{m_1^*}} - r_{12}\sqrt{\frac{E-V_1}{m_1^*}} &= t_{12}\sqrt{\frac{E-V_2}{m_2^*}}. \qquad (6.28b) \end{aligned}$$

We can now define an effective refractive index by comparing this equation to (2.7). This effective refractive index in defined up to a multiplicative coefficient. We choose this coefficient so as to have an effective refractive index of unity in the absence of the crystal potential

$$n_q = \sqrt{m_0^* \frac{E - V_1}{m_1^* E}} \tag{6.29}$$

where m_0^* corresponds to the electronic mass in vacuum. Further we can now define the effective quantum wave vector

$$k_q = \frac{m_1^*}{\hbar} \sqrt{\frac{2E}{m_0^*}}. \tag{6.30}$$

We can see here the difference between the electromagnetic wave and the quantum wave in the envelope function approximation. The wave vector and the refractive index changes in each material. This is due to the dependence of the continuity relation of the derivative on the effective mass.

Using the definition of the effective quantum refractive index we can define the reflection and transmission coefficients

$$r_{12} = \frac{n_{1q} - n_{2q}}{n_{1q} + n_{2q}}, \tag{6.31a}$$

$$t_{12} = \frac{2n_{1q}}{n_{1q} + n_{2q}}. \tag{6.31b}$$

Finally, we can define the **LTR** element for a quantum well of effective refractive index n and width z

$$\mathcal{L}_q(n, k, z) = \begin{pmatrix} L \\ T \\ R \end{pmatrix} = \begin{pmatrix} r_L \\ t \\ r_R \end{pmatrix} = \begin{pmatrix} r\frac{1-p^2}{1-p^2r^2} \\ p\frac{(1-r^2)}{(1-p^2r^2)} \\ r\frac{1-p^2}{1-p^2r^2} \end{pmatrix}, \tag{6.32}$$

with

$$\begin{cases} r = \frac{1-n_q}{1+n_q} \\ p = \exp(ik_q n_q z) \end{cases}. \tag{6.33}$$

Using this definition of the **LTR** element $\mathcal{L}_q$ we can now construct more complicated structures such as multiple quantum wells. Once the total **LTR** element is known for the structure we have a localised solution of the stationary Schrödinger equations when the "total absorbing condition" is fulfilled as defined in the second chapter ($T^2 - LR = 0$). Further, one can use all the properties of the optical **LTR** formalism in the case of multiple quantum wells. A good example is the treatment of intentionally disordered quantum wells [74, 75].

Figure 6.2 shows graphically the eigen-energies of a multiple quantum well structure having three wells. The eigen-energies correspond to the positions of the minima in the logarithmic plot.

6.5 Summary

In this chapter we described the interaction between an electromagnetic wave and a quantum system. We started with the general Schrödinger equation which treats the evolution of the wave function. The solution of this equation can be written as the superposition of the eigen-functions of the Hamiltonian operator. This standard procedure leads directly to the density matrix formalism treating the population and the coherence of each eigen-state.

In the second part, we expanded the optical **LTR** formalism in order to treat the stationary Schrödinger equation in the case of multiple quantum wells. Using this formalism one can easily determine the eigen-energies of these structures. They correspond to the energies where the total LTR fulfils the "total absorbing condition".

Chapter 7

Solution breakdown in n-level systems at high intensities

7.1 Introduction

The study of the evolution of a n-level system under excitation is interesting because it shows in a straightforward manner the quantum behaviour of such a system. In the case of the interaction between a monochromatic electromagnetic field and an n-level system we observe resonance phenomena when the photonic energy equals the energy levels of the systems. Further, when the amplitude of the field is increased we observe again resonance phenomena when the interaction energy equals the energy levels of the n-level system or their multiples. It is the treatment of these cases where approximating approaches breakdown. After showing the limitation of the different methods we continue by developing an analytical method that gives the exact solution to the density matrix equations when the excitation is monochromatic. This solution is valid for any excitation amplitude. A possible application of the high intensity part of the exact solution is treating the response of noble gases under high intensity. This kind of excitation is not possible in the case of semiconductors because the absorbed light would melt them before reaching this high intensity region. Further, this monochromatic approach can not be applied in the case where the pulse duration is too short compared to different time constants of the n-level system.

In this chapter, we show the problems that arise when searching for solutions of the density matrix equation describing the evolution of the n-level system under excitation.

Several methods that can be used for solving this equation are presented for the case of monochromatic excitations and we discuss the limits of these methods. The methods treated include perturbation expansion, the rotating wave approximation, the continuous fraction method and the Floquet expansion. These different methods are compared to the numerical solutions that we develop in the case of periodic excitations.

Here we present different methods for the solution of the evolution equation of an n-level system. The advantages and disadvantages of each of the methods are discussed as well as compared to the results obtained with the help of a numerical integration. We start by describing this numerical method which we use to treat a two level system in the density matrix framework. The other approximating techniques, widely used in the literature, can be classified in two categories, following the evolution equations that they solve.

In the first category are those that can be applied to Schrödinger's equation as well as to the density matrix equation. In the following paragraphs, we introduce two of them, that is the perturbation expansion and the rotating wave approximation. The first one consists of a power expansion of the excitation field. We show that this expansion has a finite convergence radius and that, for an excitation amplitude higher than the amplitude corresponding to this radius the method does not converge. In the case of the rotating wave approximation, the result is valid for a greater domain but not for all intensities. Nevertheless, these two methods taken together are able to explain a great number of phenomena experienced at low intensities of excitation [76]. In the case of the density matrix equations, we compare graphically the solutions found using these methods to the solution found by numerical integration. The comparison for Schrödinger's equation without relaxation can be found in [77] in the case of the rotating wave approximation.

The other two methods presented here are only applicable to Schrödinger's equation without relaxation terms. The first method is based on the continuous fraction determined for a two level system. It shows a good correlation with the exact solution of the equations of the density matrix, but it is not applicable in the case of resonance with the system. This is due to the absence of relaxation terms in Schrödinger's equation. Furthermore, it cannot be used to determine the response of the system at the fundamental harmonic of the excitation. This response must be determined by another procedure. Finally, we introduce the method based on a Floquet expansion. This has the same disadvantage as the continuous fraction method, namely it gives correct

results only away from resonance. On the other hand, the Floquet expansion, shows the stationary Schrödinger equation of the complete system, composed of the excitation wave in interaction with the n-level system. The Floquet method can also be used in conjunction with the perturbation expansion [78].

7.2 Numerical integration of the density matrix equation for a two-level system

In order to be able to compare the different resolution methods of the dynamical equations of the n-level systems we develop a numerical resolution method of the density matrix equations for a two level system. This method takes into account the periodic character of the excitation and thus allows us to distinguish between the transient part of the solution and its periodic part. This is an advantage when compared with a complete numerical integration as one can see in the case of the two level system [79] but also in the case of the more complex atomic models [80, 81]. In fact, in these two cases, the rate of increase of the excitation amplitude is important because the calculated solution depends on this parameter. Our method is independent of such a parameter. Furthermore, the Fourier transformation of the periodic solution corresponds to the solution found directly in the frequency space and described in the next chapter of this work.

First the temporal evolution of a two-level system is studied in a numerical approach. More precisely, the solution of the Bloch equations [67] for a two-level system is treated by decomposing it into a homogeneous part and a non-homogeneous part. The solutions of these two parts are calculated numerically by the [82] Runge-Kutta method for one excitation period. From there, the general solution is constructed using the periodic properties of the excitation. We also deduce the necessary initial conditions so that the evolution is periodic. We show that this particular solution is an attractive solution towards which all other solutions converge in an exponential manner. Besides, we show that this attractive and periodic solution does not exist in the absence of the relaxation terms in the density matrix equation. Thus, this method is not valid without relaxation.

7.2.1 Transient solution

In this section, we use the Runge-Kutta [82] integration method to describe the temporal evolution of a two-level system while subject to an excitation $E(t)$

$$E(t) = \begin{cases} 0 & \text{for } t < 0 \\ f(t) & \text{for } t \geq 0 \end{cases} \tag{7.1}$$

with $f(t) = f(t+T)$ being a periodic function of period T.

The density matrix equation for a two-level system in Bloch space representation can be written as follows

$$\frac{dx}{dt} = -\Gamma_2 x + \Omega_0 y, \tag{7.2a}$$

$$\frac{dy}{dt} = -\Omega_0 x - \Gamma_2 y + \frac{2E(t)\mu}{\hbar} z, \tag{7.2b}$$

$$\frac{dz}{dt} = -\frac{2E(t)\mu}{\hbar} y - \Gamma_1 (z - z_0), \tag{7.2c}$$

where x and y are respectively the real and imaginary parts of the coherence ρ_{ab}. The variable z is the population inversion $z = \rho_{bb} - \rho_{aa}$, and z_0 the same but at thermodynamical equilibrium. Using vectorial notation the system of equations (7.2) becomes

$$\frac{d\overrightarrow{R(t)}}{dt} = \overrightarrow{W(t)} \times \overrightarrow{R(t)} - \Gamma \left(\overrightarrow{R(t)} - \overrightarrow{R^0} \right), \tag{7.3}$$

where $\vec{R}$, $\vec{W}$ and $\overrightarrow{R^0}$ represent respectively (x, y, z), $(2\mu E(t)/\hbar, 0, \Omega_0)$ and $(0, 0, z_0)$, while the operator Γ is the relaxation matrix

$$\Gamma = \begin{pmatrix} \Gamma_2 & 0 & 0 \\ 0 & \Gamma_2 & 0 \\ 0 & 0 & \Gamma_1 \end{pmatrix}.$$

With the help of the Bloch equation, the evolution of the state of the system can be followed in three dimensional space. The coordinates (x, y, z) of the vector $\vec{R}$ describe in time a trajectory in this Bloch space.

In the following, we study the solution of the Bloch equations (7.3) while considering a periodic excitation. This solution can be decomposed into two parts. The first part of the solution is the solution of the homogeneous equation, which means that $\overrightarrow{R^0} = 0$.

The second part is a particular solution. The sum of these two gives us the general solution.

Before the numerical integration of the homogeneous equation, it is necessary to introduce the solution in a matrix form

$$\overrightarrow{R(t)} = \mathbf{C}(t)\overrightarrow{R_{t=0}}, \tag{7.4}$$

where $\overrightarrow{R(t)}$ is determined by a certain matrix $\mathbf{C}(t)$ and by its initial conditions $\overrightarrow{R_{t=0}}$. The matrix $\mathbf{C}(t)$ corresponds then to the homogeneous evolution operator of the state of the system. Considering the periodicity of the excitation, we do not need to know the evolution operator for more than one period. The differential equation for this operator can be written

$$\frac{d\mathbf{C}(\mathbf{t})}{dt} = \mathbf{M}(t)\mathbf{C}(t), \tag{7.5}$$

where the matrix $\mathbf{M}$ containing both the excitation and the relaxation term is

$$\mathbf{M}(t) = \begin{pmatrix} -\Gamma_2 & \Omega_0 & 0 \\ -\Omega_0 & -\Gamma_2 & \frac{2E(t)\mu}{\hbar} \\ 0 & -\frac{2E(t)\mu}{\hbar} & -\Gamma_1 \end{pmatrix}.$$

For $\overrightarrow{R(t)}$ defined by the equation (7.4) to be a solution of (7.3) it is necessary that the matrix $\mathbf{C}(t)$ fulfils the following initial condition

$$\mathbf{C}(t=0) = \mathbb{I}$$

where $\mathbb{I}$ represents the identity matrix.

The particular solution $\overrightarrow{S_p(t)}$ is determined numerically for one period from the Bloch equation (7.3). The initial condition for this special solution is the zero vector.

To construct the general solution of Bloch's equations, we have at our disposal the following functions known over one period

$$\begin{aligned} &\mathbf{C}(t), && \text{for } 0 \leq t \leq T, \\ &\overrightarrow{S_p(t)}, && \text{for } 0 \leq t \leq T. \end{aligned}$$

The general solution can be written as a sequence of vector solutions in Bloch space each valid over one period

$$\overrightarrow{R_n(t)} = \mathbf{C}(\Delta t)\overrightarrow{R_{n-1}(nT)} + \overrightarrow{S_p(\Delta t)}, \qquad \text{for } nT \leq t \leq (n+1)T, \tag{7.6}$$

with

$$\Delta t \equiv t \ \ [T],$$
$$\overrightarrow{R_{-1}(0)} = \overrightarrow{R_{t=0}}.$$

In figure 7.1a, the evolution of the solution is represented in the Bloch space during the first periods of the excitation. For initial conditions, the thermodynamic equilibrium state is used.

7.2.2 Stationary solution

Figure 7.1 shows that the general solution of Bloch's equation is not necessarily periodic when the excitation is periodic. Nevertheless, there exists a special initial condition that implies a periodic solution. We determine this initial condition using expression (7.6). The solution found with the help of this initial condition is the asymptotic solution towards which all other solutions converge. The "speed" with which a solution approaches the asymptotic solution depends on the relaxation times.

To determine the initial conditions corresponding to the periodic solution we specify the relation (7.6) at the end of each period

$$\overrightarrow{R_n((n+1)T)} = \mathbf{C}(T)\overrightarrow{R_{n-1}(nT)} + \overrightarrow{R_p(T)}. \tag{7.7}$$

This relation, between the states of the system at times nT and $(n+1)T$, corresponds to a recursive sequence. Figure 7.2 shows the series $\overrightarrow{R_n((n+1)T)}$ in Bloch space. The periodical initial condition is solution of the linear equation

$$\overrightarrow{R} = \mathbf{C}(T)\,\overrightarrow{R} + \overrightarrow{R_p(T)}. \tag{7.8}$$

This implies that the initial condition is self-consistent. The iteration over one period of the solution starting with this initial state leaves the system in this same state.

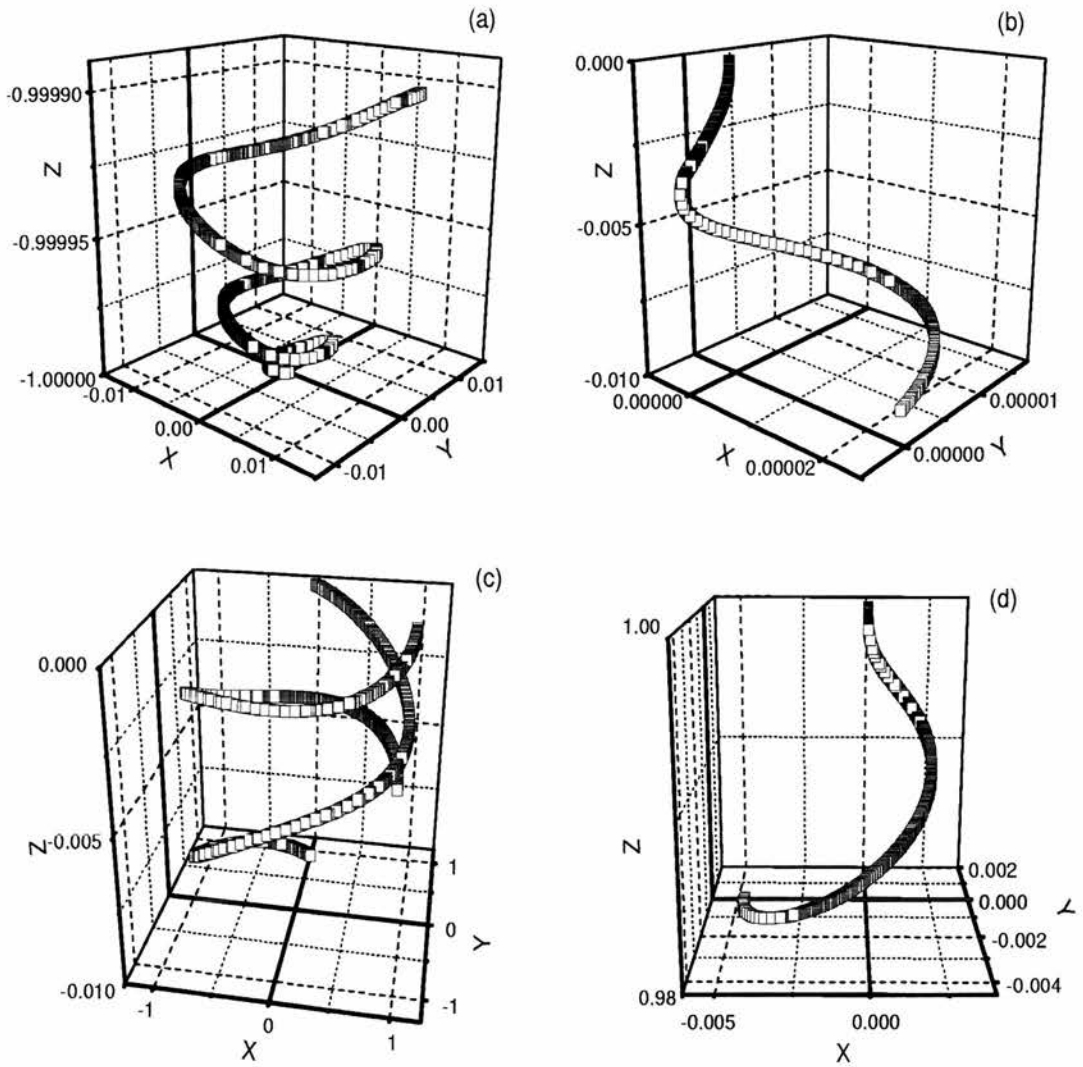

Figure 7.1: Evolution of the state of the system in the Bloch space for the three first periods of the excitation ($f(t) = A\sin(\omega_1 t)$). The figures (b), (c) and (d) are used for the determination of this evolution with the help of the equation (7.6) (b) particular solution $\vec{R}_p(\Delta t)$ for one period (c) homogeneous solutions with the initial conditions $(x = 1, y = 0, z = 0)$ and $(x = 0, y = 1, z = 0)$. These two solutions form two lines of the matrix $\mathbf{C}$. (d) Homogeneous solution with the initial condition $(x = 0, y = 0, z = 1)$. This solution forms the last line of the matrix $\mathbf{C}$.

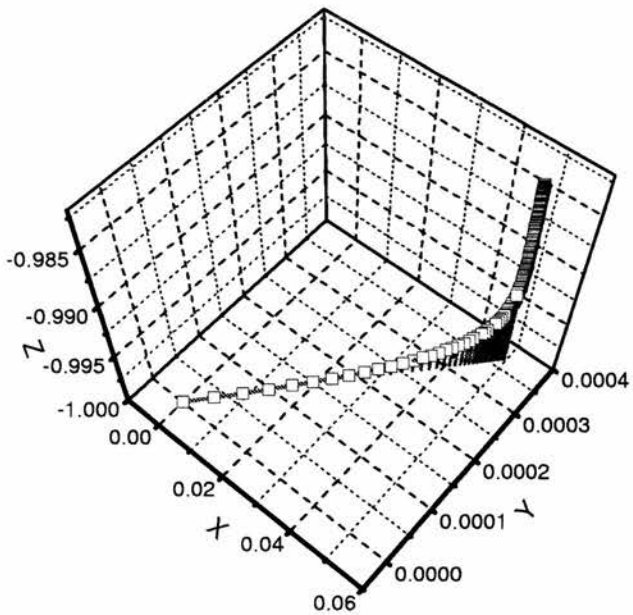

Figure 7.2: Poisson [83] section, (the state of the system after one excitation period) for a two-level system under excitation ($f(t) = Asin(\omega_1 t)$).

We remark that usually the relation (7.8) does not have any non-zero solution $\overrightarrow{R}$ if $\overrightarrow{R_p(T)} = 0$. This corresponds to the absence of the thermodynamical equilibrium term $\overrightarrow{R^0}$ in equation (7.3) and thus also in the case of Schrödinger's equation (relaxation terms are empirically introduced into the density matrix formalism). Consequently, Schrödinger's equation for an n-level system, under periodic excitation, generally does not have any periodic solution. In the case where it has one (matrix $\mathbf{C}(T)$ accepts unity as eigen-value), it is not attractive.

Figure 7.2 shows graphically the convergence of the iterative sequence (7.7) towards the solution of (7.8). In fact, the convergence can be shown mathematically when returning to the Bloch equation (7.3). Let $\overrightarrow{P(t)}$ be the periodic solution and $\overrightarrow{\Delta R(t)} = \overrightarrow{R(t)} - \overrightarrow{P(t)}$. Then $\overrightarrow{\Delta R(t)}$ is a solution of

$$\frac{d\overrightarrow{\Delta R(t)}}{dt} = \overrightarrow{W(t)} \times \overrightarrow{\Delta R(t)} - \Gamma \overrightarrow{\Delta R(t)}. \tag{7.9}$$

When multiplying equation (7.9) by $\overrightarrow{\Delta R(t)}$, the behaviour of the difference between any given solution and the periodical solution can be studied

$$\overrightarrow{\Delta R(t)} \frac{d\overrightarrow{\Delta R(t)}}{dt} = \frac{1}{2} \frac{d\Delta R^2(t)}{dt} = -\overrightarrow{\Delta R(t)} \Gamma \overrightarrow{\Delta R(t)}. \tag{7.10}$$

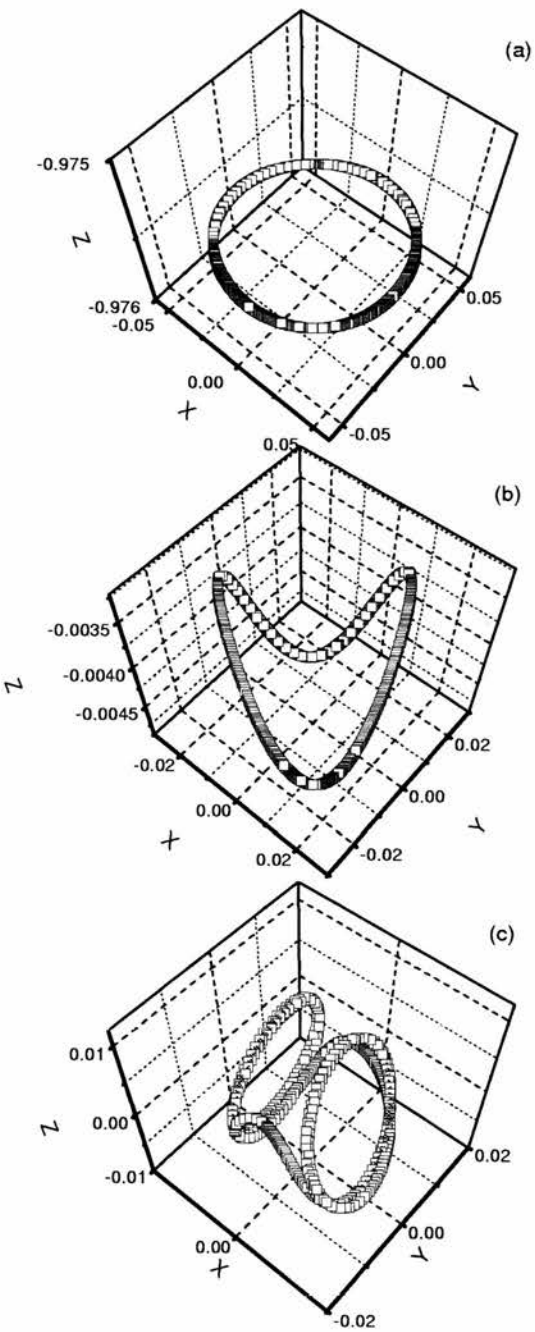

Figure 7.3: The evolution of the system is represented in Bloch space for one period of excitation. The initial condition is the one giving a periodic solution $\overrightarrow{R}$ calculated with the help of equation (7.8). Three typical intensities for the excitation are considered: (a) linear domain of excitation, (b) saturation of the system, (c) domain of the characteristic oscillations.

This differential equation shows the behaviour of the norm of this difference. As the matrix Γ is diagonal and the smallest element is Γ_1, the norm has an upper limit given by the solution of the equation

$$\frac{1}{2}\frac{df(t)}{dt} = -\Gamma_1 f(t), \tag{7.11}$$

with the initial condition $f(0) = |\overrightarrow{\Delta R(0)}|^2$. The solution of the equation (7.11) decreases exponentially. Consequently, the limit

$$\lim_{t\to\infty} |\overrightarrow{\Delta R(t)}| = 0, \tag{7.12}$$

implies the convergence of any solution towards the periodic solution. This means that after a large number of excitation periods the solution approaches asymptotically the periodic solution. Figure 7.3 shows the periodic solution for different intensities of excitation. For weak intensities, the cycle done by the system is very nearly circular. This response of the system corresponds to a linear behaviour where the different approximate resolution methods give satisfactory results. When excitation intensity is increased saturation effects appear. We observe then in Bloch space a deformation of the cycle in the z direction corresponding to an oscillation of the population. For even higher intensities, the energy received by the system cannot any more be stored in the excited population. The cycle described then by the system shows higher harmonic components that are visible in Bloch space as supplementary circular movements.

By comparison, the evolution of a two-level system in Bloch space in the absence of relaxation terms implies that the trajectories are located on the unity sphere [84]. Consequently we observe important differences in Bloch space between the trajectories in absence and in presence of the relaxation terms.

To summarise, we deduced a numerical integration method for the density matrix equation including the relaxation terms for a two level system. Such a study is necessary in order to have a reference solution of these equations so that we are able to compare the different resolution methods. Finally, this method is also necessary for the verification of the properties determined in the next chapter when we will solve the equation in an analytical manner.

The philosophical question of the "why" if one has a numerical solution one should continue searching for an analytical solution, can be replied to as follows. The deduced property of a numerical solution cannot be general for they are only the property of a special case. More precisely, the numerical solution of these equations shows a complex behaviour of these systems when periodically excited. This behaviour was not treated in the literature to its correct value and consequently a deeper study of these equations is necessary. The advantage of an analytical study in comparison to a numerical study is its ability to determine the limiting cases of this behaviour. Furthermore, once the exact and general solution is known it is possible to particularise it for the problem treated. This particularisation can take into account justified approximations and consequently leads to simple and easy formulas for use in practice. Finally, the analytical methods allow us to find the solution in the more general case of an n-level system in the presence of two monochromatic fields.

7.3 Perturbation expansion

There is no general solution of Schrödinger's equation if the Hamiltonian operator is time dependent. In the case when the Hamiltonian operator can be divided into a constant part and a relatively small time dependent part we can use the perturbation approach which uses a Taylor expansion with respect to the excitation. For Taylor expansion, there exists around each point of expansion a convergence radius. This is the same in the case of the perturbation expansion. In this section, we introduce this method without worrying about the convergence radius. In the next section, we will return to this problem to show the importance of this convergence radius when the amplitude of the time dependent part increases.

The starting point for the perturbation expansion is the general density matrix equation

$$i\hbar\frac{d\rho}{dt} = \mathbf{H_0}\rho - \rho\mathbf{H_0} + \lambda\mathbf{W}(t)\rho - \lambda\rho\mathbf{W}(t) - \Gamma\left(\rho - \rho^{(0)}\right), \tag{7.13}$$

where $\lambda\mathbf{W}(\mathbf{t})$ corresponds to the part of the Hamiltonian depending on time. This part can be seen as a perturbation of the Hamiltonian $\mathbf{H_0}$ corresponding to the system at

rest. The solution then is searched in the form of the sum of powers of λ

$$\rho(t) = \rho_0(t) + \lambda\rho_1(t) + \lambda^2\rho_2(t) + \cdots . \tag{7.14}$$

When inserting this sum (7.14) into the density matrix equation, we can identify one equation for each power of λ. The constant part corresponds to the solution in absence of excitation

$$i\hbar\frac{d\rho_0}{dt} = \mathbf{H_0}\rho_0 - \rho_0\mathbf{H_0} - \Gamma\left(\rho_0 - \rho^{(0)}\right), \qquad n = 0. \tag{7.15a}$$

For the n^{th} order density matrix the equation is

$$i\hbar\frac{d\rho_n}{dt} = \mathbf{H_0}\rho_n - \rho_n\mathbf{H_0} + \mathbf{W}(t)\rho_{n-1} - \rho_{n-1}\mathbf{W}(t) - \Gamma\rho_n \qquad n \geq 1. \tag{7.15b}$$

This system of differential equations can be solved in a recursive manner. Each of these equations (7.15) is simpler to solve than the general equation (7.13) because the excitation term appears in the equation as a free term and not as a time dependent coefficient (7.13).

In order to be able to compare the solution (7.14) defined by the system of equations (7.15) and the one calculated by the numerical method, we develop in more detail this solution for a two level system. More particularly, the system considered is symmetric with respect to its origin. Then, the interaction between the system and the field is given by the matrix

$$\begin{aligned}\mathbf{W}(t) &= \mu E(t) \\ &= \begin{pmatrix} 0 & \mu_{ab} \\ \mu_{ba} & 0 \end{pmatrix} E(t)\end{aligned} \tag{7.16}$$

where μ is the matrix corresponding to the dipole momentum of the system (6.15) and $E(t)$ with excitation field

$$E(t) = \begin{cases} 0 & \text{for } t < 0 \\ \sin(\omega_1 t) & \text{for } t \geq 0. \end{cases} \tag{7.17}$$

The Hamiltonian operator of the system is

$$\mathbf{H_0} = \begin{pmatrix} 0 & 0 \\ 0 & \hbar\Omega_0 \end{pmatrix} \tag{7.18}$$

where $\hbar\Omega_0$ corresponds to the energy difference between the eigen-states of the two levels. The equilibrium state of the system is given by the relation (6.13)

$$\rho^{(0)} = \begin{pmatrix} \rho_{aa}^{(0)} & 0 \\ 0 & \rho_{bb}^{(0)} \end{pmatrix}. \tag{7.19}$$

As the initial condition for equation (7.13) at the instant $t = 0$ we consider the system in its thermodynamical equilibrium state $\rho(t = 0) = \rho^{(0)}$. Starting with this general initial condition it is necessary to define the initial conditions for all equations (7.15). In order for this sequence of initial conditions to be valid for any amplitude parameter λ, we choose the following initial conditions

$$\rho_0(t = 0) = \rho^{(0)} \tag{7.20a}$$

$$\rho_n(t = 0) = 0 \quad \text{for } n > 0. \tag{7.20b}$$

The zero and first order solutions of equations (7.15) are

$$\begin{aligned}
\rho_0(t) &= \rho^{(0)} \\
\rho_1(t)_{aa} &= 0 \\
\rho_1(t)_{ab} &= -\rho_D^{(0)} \frac{\mu_{ab}}{D}(i\omega_1 e^{(-\Gamma_2 + i\Omega_0)t} - i\omega_1 \cos(\omega_1 t) + (i\gamma_2 + \Omega_0)\sin(\omega_1 t)) \\
\rho_1(t)_{ba} &= -\rho_D^{(0)} \frac{\mu_{ba}}{D^*}(-i\omega_1 e^{(-\Gamma_2 - i\Omega_0)t} + i\omega_1 \cos(\omega_1 t) - (i\gamma_2 - \Omega_0)\sin(\omega_1 t)) \\
\rho_1(t)_{bb} &= 0
\end{aligned}$$

where $\rho_D^{(0)}$ represents the difference of populations $\rho_{bb}^{(0)}$ and $\rho_{aa}^{(0)}$ at thermodynamical equilibrium. The coefficient Γ_2 corresponds to the inverse of the transverse relaxation time (6.11b) of the two level system and the coefficient Γ_2 to the inverse of the longitudinal one (6.11a). The denominator D is

$$D = \hbar(\Gamma_2^2 - 2i\Gamma_2\Omega_0 - \Omega_0^2 + \omega_1^2))$$

and D^* is its complex conjugate.

We notice that the first order solution is composed of two parts. A transient part defined by an exponentially decreasing term and a stationary part whose amplitude remains constant as a function of time. These two parts are also observed when searching the numerical solution of the density matrix equations where we have a unique periodic and "attractive" solution. All other solutions are approaching this in a exponential manner. Consequently, the transient term can be neglected when searching for the stationary solution. Besides, we can easily verify that the solution, in the absence of the exponential term, remains a solution of equation (7.15b) for $n = 1$. The difference between the stationary solutions and the transient ones resides in the initial conditions (cf. discussion of the numerical solution).

Before calculating the solution for the higher order perturbation, we verify that the defined susceptibility at the first order verifies the Kramers-Kronig conditions (6.22). For that, the polarisation is determined with the help of relation (6.18)

$$\begin{aligned} P_1(t) &= 2\lambda \Re e \left(\mu_{ab}\rho_1(t)_{ba}\right) \\ &= 2\lambda \mu_{ab}\mu_{ba}\Omega_0\rho_D^{(0)} \left(\frac{\Omega_0^2 \sin(\omega_1 t) - \Gamma_2\omega_1 \cos(\omega_1 t) - \omega_1^2 \sin(\omega_1 t)}{\hbar(\Gamma_2^2 + \Omega_0^2 - 2\Omega_0\omega_1 + \omega_1^2)(\Gamma_2^2 + \Omega_0^2 + 2\Omega_0\omega_1 + \omega_1^2)} \right). \end{aligned}$$

From the polarisation, we can define the linear susceptibility at the frequency of excitation

$$\chi_1(\omega) = \frac{-i\mu_{ab}\mu_{ba}\Omega_0\rho_D^{(0)}}{\hbar(\Gamma_2 + i(\Omega_0 + \omega))(\Gamma_2 - i(\Omega_0 - \omega))}. \tag{7.21}$$

We notice that the linear Kramers-Kronig relation is fulfilled by this susceptibility. This can be easily verified by looking for the poles of the susceptibility in the complex plane (the frequency ω is treated as a complex variable). In fact, these two first order poles are located in the inferior half of the complex plane divided by the real axis. Consequently, the perturbation expansion to the first order fulfils the Kramers-Kronig condition [67] and therefore the causality principle.

The formal dependency between the density matrix elements at the different orders of the expansion are:

$$\rho_{2n-1}(t)_{aa} = \rho_{2n-1}(t)_{bb} = 0, \tag{7.22a}$$

$$\rho_{2n-1}(t)_{ab} = \rho^*_{2n-1}(t)_{ba} = \frac{-i}{\hbar}\int_0^t d\tau e^{-(\Gamma_2 - i\Omega_0)(t-\tau)}\sin(\omega_1\tau) (\mu_{ab}\rho_{2n-2}(t)_{bb} - \mu_{ab}\rho_{2n-2}(t)_{aa}), \tag{7.22b}$$

$$\rho_{2n}(t)_{aa} = -\rho_{2n}(t)_{bb} = \frac{-i}{\hbar}\int_0^t d\tau e^{-\Gamma_1(t-\tau)}\sin(\omega_1\tau) (\mu_{ab}\rho_{2n-1}(t)_{ba} - \mu_{ba}\rho_{2n-1}(t)_{ab}), \tag{7.22c}$$

$$\rho_{2n}(t)_{ab} = -\rho_{2n}(t)_{ba} = 0, \tag{7.22d}$$

for $n > 0$. With the help of these relations, it is possible to describe the solution at any order. These solutions can all be divided into a transient part and a stationary one exactly as the first order solution. The stationary parts are:

$$\rho_{2n-1}(t)_{aa} = \rho_{2n-1}(t)_{bb} = 0, \tag{7.23a}$$

$$\rho_{2n-1}(t)_{ab} = \rho^*_{2n-1}(t)_{ba} = \frac{-i}{d\hbar}\int_t^{t+T} d\tau e^{-(\Gamma_2 - i\Omega_0)(t+T-\tau)}\sin(\omega_1\tau) (\mu_{ab}\rho_{2n-2}(t)_{bb} - \mu_{ab}\rho_{2n-2}(t)_{aa}), \tag{7.23b}$$

$$\rho_{2n}(t)_{aa} = -\rho_{2n}(t)_{bb} = \frac{-i}{d\hbar}\int_t^{t+T} d\tau e^{-\Gamma_1(t+T-\tau)}\sin(\omega_1\tau) (\mu_{ab}\rho_{2n-1}(t)_{ba} - \mu_{ba}\rho_{2n-1}(t)_{ab}), \tag{7.23c}$$

$$\rho_{2n}(t)_{ab} = -\rho_{2n}(t)_{ba} = 0, \tag{7.23d}$$

where $T = 2\pi/\omega_1$, $d_1 = 1 - \exp(-(\Gamma_2 - i\Omega_0)T)$ and $d_2 = 1 - \exp(-\Gamma_1 T)$. The stationary solution at the order n is defined in an iterative manner with the help of the solution at the order $n-1$. If the solution at order $n-1$ is periodic then the solution to the order n is also periodic.

Figure 7.4 shows graphically the behaviour of the solution found with the help of the perturbation expansion for a two level system. For this graphical study, we represent the solution in different manners in order to show the differences when comparing the perturbation solution with the solution obtained numerically. First, the two solutions are compared in Bloch space in figures 7.4a and 7.4b. In this representation, we observe

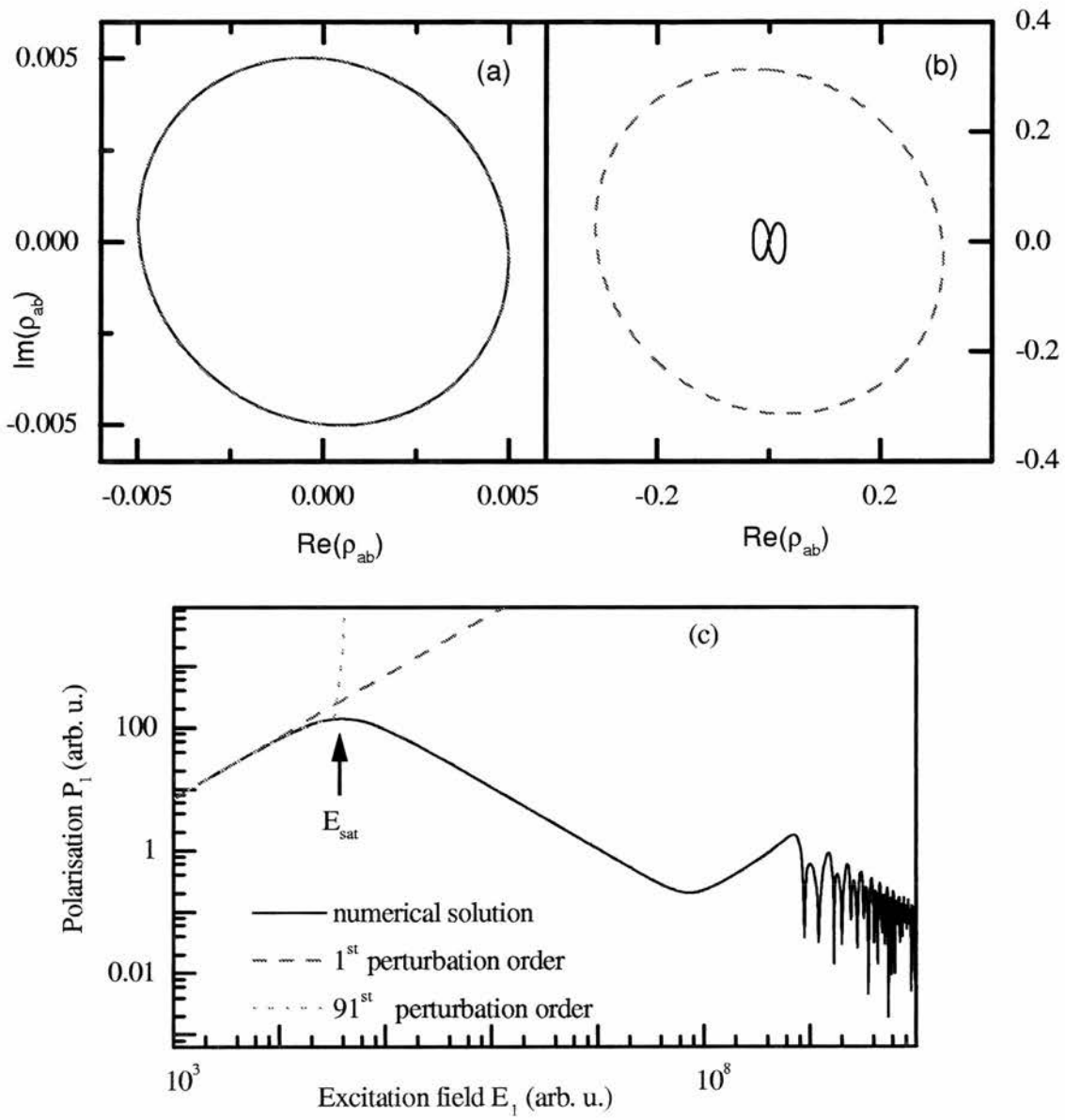

Figure 7.4: Comparison between the solutions found by the perturbation method and the numerical solution for a two level system. The evolution of the two solutions in the Bloch space is represented for a weak excitation intensity in figure (a) and for a strong excitation intensity in figure (b). Figure (c) shows the behaviour of the polarisation at the fundamental frequency according to the excitation amplitude.

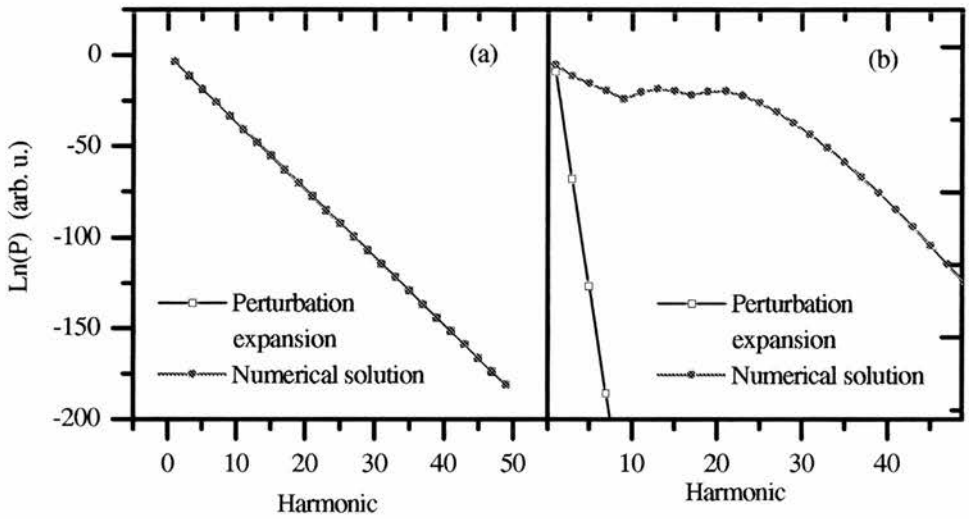

Figure 7.5: Comparison between the solutions found by the perturbation method and the numerical solution for a two level system. The figure shows the amplitude of the response at the harmonic frequencies for a weak (a) and a strong (b) amplitude of excitation.

that for weak excitation intensities, figures 7.4a, the two solutions are in very good agreement. This corresponds to the linear domain of excitation. On the other hand, for high intensity excitations, figures 7.4b, this is not the case. While the numerical solution remains inside the unity sphere where it makes complicated cycles during an excitation period; the one determined with the help of the perturbation expansion is divergent. The cycle described by this last remains circular even for high intensities but it increases in radius beyond the unity sphere.

In order to understand the basic differences between these two solutions we show in figure 7.4c the amplitude of the polarisation at the fundamental harmonic when the excitation amplitude varies. The amplitude of the polarisation gives the energy absorbed by the two level system while excited. The log-log representation is useful because one can visualise more easily the transition from the linear behaviour to the non-linear one. Further, this representation is equivalent to the linear one [77]. In this figure we observe that for excitation amplitudes smaller than the saturation amplitude E_{sat} the two solutions are equal. From the amplitude of saturation E_{sat} onwards, the perturbation expansion is no longer valid. This amplitude corresponds to the convergence radius of the Taylor expansion meaning that the series (7.14) does not converge towards the exact solution for excitation amplitudes greater than E_{sat}. This divergent behaviour explains the abnormal increase of the radius in the Bloch space. We determine in an analytical

manner this convergence radius in the following section with the help of the rotating wave approximation.

Finally, to explain the absence of oscillations (see figures 7.3) in Bloch space, we represent in figure 7.5 the amplitudes at the harmonic frequencies of the polarisation for a weak excitation and a strong one. For the weak excitation intensity, the amplitude of the harmonic response decreases as the power of the order of the harmonic. This behaviour is visible in the case of the perturbation expansion as well as for the numerical solution. When the excitation amplitude corresponds to a non-linear domain of the system this is no longer the case. The perturbation expansion continues to show the same decrease as for the weak intensities while the numerical solution shows a saturation of this response for the small harmonic orders followed by a decrease of the response for the higher harmonics. This explains the characteristic oscillations of the system in Bloch space for the numerical solution and their absence in the case of the perturbation expansion.

In conclusion, the perturbation expansion is not usable for stronger excitation amplitudes than the convergence radius of this expansion. This is not astonishing, because strong excitation intensities can no longer be treated as a perturbation of the Hamiltonian of the system at rest. On the other hand, in the considered example, this convergence radius of the expansion corresponds to the saturation amplitude of the system namely the intensities where the non-linear effects appear.

7.4 Rotating wave approximation

The rotating wave approximation neglects the fast varying terms in the density matrix equation. The starting point of this approximation is the density matrix equation (6.17) for a two level system in the form of the Bloch equations (7.2). Originally this approxiamtion was used when describing the evolution of a $1/2$ spin subject to the superposition of two magnetic fields composed of a constant and an oscillating part. The first part of the field corresponds to the Hamiltonian of the system at rest while the oscillating part corresponds to the excitation field. The excitation in this case is monochromatic

$$E(t) = E_1 \sin(\omega_1 t).$$

Once excited, the spin 1/2 shows a precession movement. It is by placing oneself in the rotating reference frame of the spin that the evolution equations of the spin are resolved when neglecting the oscillation terms.

In the case of the density matrix equation, the change in frame of reference corresponds to the following changes

$$\rho_{ab} = \sigma_{ab} e^{i\omega_1 t},$$
$$\rho_{ba} = \sigma_{ba} e^{-i\omega_1 t},$$
$$\rho_D = \rho_{bb} - \rho_{aa}.$$

These changes of variables allow us to show the "slowly" varying terms (that rotate with the reference frame) and the "fast" varying terms (that rotate with a harmonic frequency of ω_1).

The density matrix equation (6.17) for a two level system in the rotating reference frame are

$$\frac{d\rho_D}{dt} = +\frac{2}{i\hbar} E_1(\mu_{ab}\sigma_{ba} - \sigma_{ab}\mu_{ba}) - \Gamma_1(\rho_D - \rho_D^{(0)}), \tag{7.24a}$$
$$\frac{d\sigma_{ab}^*}{dt} = \frac{d\sigma_{ba}}{dt} = i(\omega_1 - \Omega_0)\sigma_{ba} + \frac{iE_1}{\hbar}\mu_{ba}\rho_D - \Gamma_2\sigma_{ba}, \tag{7.24b}$$

where the fast varying terms $\exp(2i\omega_1 t)$ and $\exp(-2i\omega_1 t)$ are neglected. From these equations we can find the exact analytical solution in the stationary case by solving the system of linear equations (7.24) when the derivatives are zero. The real and imaginary part of the dielectric susceptibility at the excitation frequency can be determined:

$$\chi' = \frac{\mu^2\Gamma_1\Gamma_2\rho_D^{(0)}}{\hbar} \frac{1}{\Gamma_1\Gamma_2^2 + \Gamma_1(\omega_1 - \Omega_0)^2 + 4a_1^2\Gamma_2}, \tag{7.25a}$$
$$\chi'' = \frac{\mu^2\Gamma_1\rho_D^{(0)}}{\hbar} \frac{(\Omega_0 - \omega_1)}{\Gamma_1\Gamma_2^2 + \Gamma_1(\omega_1 - \Omega_0)^2 + 4a_1^2\Gamma_2}, \tag{7.25b}$$

where $a_1 = \mu E/\hbar$ represents the "precession" frequency. The rotating wave approximation is valid for a greater range of excitation intensity than the perturbation expansion, but it does not take into account effects that appear at higher excitation intensity. Further, the susceptibility determined with the help of the rotating wave approximation does not fulfil the Kramers-Kronig condition. This condition is fulfilled only if the

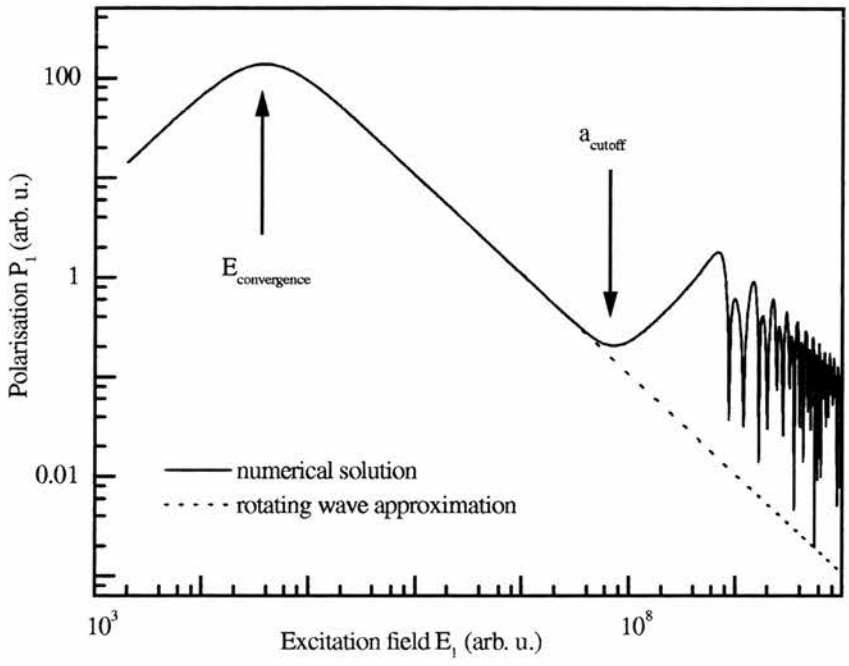

Figure 7.6: Comparison between the solutions found by the rotating wave approximation and the numerical solution for a two level system. The amplitude of the polarisation of the system at the fundamental frequency is represented as a function of the excitation amplitude.

terms containing the excitation amplitude are neglected in the denominator in equations (7.25). The origin of this problem lies in the non-linear aspect of the density matrix equations implying a non-linear solution. In fact, the susceptibility (7.25) is not only composed of the linear susceptibility $\chi^1(\omega)$ but also of the higher order susceptibility (see definition 6.23) as $\chi^3(\omega, \omega, -\omega)$ (there is no polarisation at the second order for a centro-symmetric system). The linear part of the susceptibility satisfies the linear Kramers-Kronig relations. Besides, a direct verification of the differential equations (7.24) generalised to any excitation field shows their causal character; thus it is during the approximation that the causality is lost.

In figure 7.6, we represent the amplitude of the response at the fundamental frequency as a function of the excitation amplitude. This figure shows that the rotating wave approximation remains valid for excitation intensities where the perturbation approach diverges. We also observe the amplitude where the rotating wave approximation is no longer valid

$$a_{1\,cutoff}^2 = 8\sqrt{4\omega_1^2\Gamma_2^2 + (\Omega_0^2 - \omega_1^2)^2}.$$

This cutoff amplitude is due to the relative increase of the anti-resonant terms (the fast varying terms) in comparison with the resonant terms. To determine this cutoff amplitude we use the solution methods presented in the next chapter.

Contrary to the perturbation expansion, the rotating wave approximation cannot model the high harmonic generation as in figure 7.4d. Further, the Bloch space representation of the solution shows only a perfect circle without any special point. From this remark, we can conclude that the complicated cycles shown by the numerical solution in Bloch space have their origin in the high harmonic generation. This hypothesis is reinforced by the observation of the perturbation solution behaviour in Bloch space. In this case, the cycles are more or less circles with small deviations. Besides, the high harmonic generation for the perturbation expansion is much smaller for high intensities than for the numerical solution.

One of the advantages of the rotating wave approximation is its compatibility with the perturbation expansion, that is to say the result found when using these two approximations successively, does not depend on the order in which they are done. In fact, we can use this property to calculate the convergence radius of the perturbation expansion. For that, the solution of equation (7.24) is written as a Taylor expansion with respect to the excitation amplitude (7.14). The polarisation of the system can be determined with the help of relation (6.18) and of the solutions to the different orders of equations (7.24)

$$P = \chi_1 E + \chi_2 E^2 + \chi_3 E^3 + ... \tag{7.26}$$

with

$$\begin{aligned}
\chi_1 &= \frac{\mu^2 \rho_D^{(0)}}{\hbar} \frac{1}{\Gamma_2 + i(\omega_1 - \Omega_0)}, \\
\chi_2 &= 0, \\
\chi_3 &= -\chi_1 \frac{\Gamma_2 \mu^2}{\hbar^2 \Gamma_1} \frac{1}{\Gamma_2^2 + (\omega_1 - \Omega_0)^2}.
\end{aligned}$$

The convergence radius (7.26) of this series can be calculated from the ratio between two consecutive odd terms of this series. Indeed, the convergence radius thus found

corresponds to the excitation amplitude giving the maximum of polarisation

$$E_{convergence} = \frac{\hbar}{\mu}\sqrt{\frac{\Gamma_1(\Gamma_2^2 + (\omega_1 - \Omega_0)^2)}{\Gamma_2}}. \tag{7.27}$$

In conclusion, the combination of the perturbation expansion with the rotating wave approximation allows the definition of the linear and non-linear susceptibility in a very simple manner. On the other hand, this expansion is no longer valid for excitation amplitudes higher than the convergence radius.

7.5 Continuous fraction method

In the following we describe briefly the continuous fraction method as proposed by Plaja et al. [85]. This method applies particularly to the two level systems without relaxation terms. They are treated in the framework of Schrödinger's equation and thus they do not take into account the relaxation terms. A monochromatic wave is used as excitation. The equations of the probability amplitudes of the two states deduced from Schrödinger's equation are:

$$\frac{d}{dt}a_0 = -iVa_1 \cos\omega_1 t, \tag{7.28a}$$

$$\frac{d}{dt}a_1 = -i\Omega_0 a_1 - iVa_0 \cos\omega_1 t. \tag{7.28b}$$

The quantum state of the system is determined by the two complex functions $a_0(t)$ and $a_1(t)$. The wave function is given by $\Psi(t) = a_0(t)\psi_a + a_1(t)\psi_b$. This quantum system has an eigen-frequency Ω_0. Further, ω_1 is the excitation wave frequency and V the coupling between the two level quantum system and this wave.

The dipole moments of the system normalised to the excitation amplitude and the population inversion are defined by:

$$p(t) = V[a_0^*(t)a_1(t) + a_0(t)a_1^*(t)], \tag{7.29a}$$

$$\rho_D(t) = |a_1(t)|^2 - |a_0(t)|^2. \tag{7.29b}$$

With the help of these two definitions, the system of complex differential equations can be written in the form of a purely real system where only the inversion population and

the polarisation intervene:

$$\frac{d^2p(t)}{dt^2} + \Omega_0^2 p(t) = 2\Omega_0 V^2 \rho_D(t)\cos(\omega_1 t), \tag{7.30a}$$

$$\frac{d\rho_D(t)}{dt} = -\frac{2}{\Omega_0}\cos(\omega_1 t)\frac{p(t)}{dt}. \tag{7.30b}$$

The Fourier transformation transforms equations (7.30) into a system of equations linking the dipole moment at the q^{th} harmonic to the dipole moments at the $(q+2)^{th}$ and $(q-2)^{th}$ harmonics

$$-p_q\left(\frac{2q^2}{q^2-1} + \frac{\Omega_0^2 - q^2\omega_1^2}{V^2}\right) = p_{q-2}\frac{q-2}{q-1} + p_{q+2}\frac{q+2}{q+1}, \qquad q \geq 3, \tag{7.31}$$

with

$$p(t) = \sum_q p_q e^{iq\omega_1 t}. \tag{7.32}$$

The solution of this relation implies a continuous fraction, that is to say a fraction whose denominator is a fraction whose denominator is also a fraction and so on

$$z_q = \frac{-(q-2)/(q-1)}{2q^2/(q^2-1) + (\Omega_0^2 - q^2\omega_1^2)/V^2 + [(q+2)/(q+1)]z_{q+2}}, \tag{7.33}$$

with $z_q = p_q/p_{q-2}$. In order to evaluate this continuous fraction (7.33), it is necessary to begin with a high index, q_{max} while neglecting p_q in comparison with p_{q-2} that is to say that $z_{q_{max}} = 0$. The continuous fraction method gives the ratios between the different odd harmonic dipole moments.

To determine completely the values of these harmonics, it is necessary to calculate the response at the fundamental frequency with another method. For that, the difference of populations is evaluated at the moment t_0 where the excitation field $V\cos(\omega_1 t)$ is zero

$$\begin{aligned}\rho_D(t_0) &= -1 \\ &= \sum_q \rho_D^q e^{iq\pi/2} \\ &\approx \rho_D^0 - 2\rho_D^2,\end{aligned}$$

where ρ_D^q is the population difference at the frequency $q\omega_1$. Using this relation, the polarisation of the fundamental harmonic can be written

$$p^1 = -\frac{V^2\Omega_0}{(\Omega_0^2 - \omega_1^2) + (3/2)V^2}. \tag{7.34}$$

This polarisation corresponds to the one determined with the help of the rotating wave approximation applied to the differential equation system (7.28). Consequently, the comparison of the response of the system with the response calculated numerically gives the same result as the one presented in figure 7.6.

In figure 7.7, the response of the system at odd harmonics is represented and compared to the one calculated with the help of the numerical solution. The differences appear when the amplitude of the excitation occurs in resonance with one of the harmonic responses. In this case, the continuous fraction method shows more pronounced resonance effects. This is due to the fact that this method does not include the relaxation phenomena implying that the complex poles of the polarisation are closer to the real axis[1] and therefore more pronounced. Generally, the method of the continuous fraction gives good results for centro-symmetric two level systems. Its defect resides in the impossibility of treating the n-level systems and the relaxation phenomena. Furthermore, the solution found is as good as the term giving the polarisation at the fundamental harmonic (7.34). The response of the system at this harmonic can be very complicated for strong excitation amplitudes as we noticed in the numerical solution (see figures 7.6 and 7.4c). The continuous fraction method does not take into account these effects.

Figure 7.7c shows that the behaviour in Bloch space of the continuous fraction solution differs with respect to the numerical solution (figures 7.7d) for resonant excitation amplitudes. This behaviour difference has its origin in the use of the rotating wave approximation at the time of the determination of the response at the fundamental frequency.

Another interesting detail in figure 7.7c is the periodicity of the solution in Bloch space. When determining the numerical solution we showed that the solutions of equation (7.28) are not periodic generally. By constructing the solution with the help of definition (7.32) and the continuous fraction (7.33), we notice that it is periodic for any

[1] A polarisation of the type $P(\omega) = 1/(\Gamma - i(\omega_0 - \omega))$ is resonant when $\omega = \omega_0$. Its pole is at $\omega = i\Gamma + \omega_0$. The closer the pole is to the real axis, the smaller is the relaxation coefficient and consequently the maximum of the polarisation is larger.

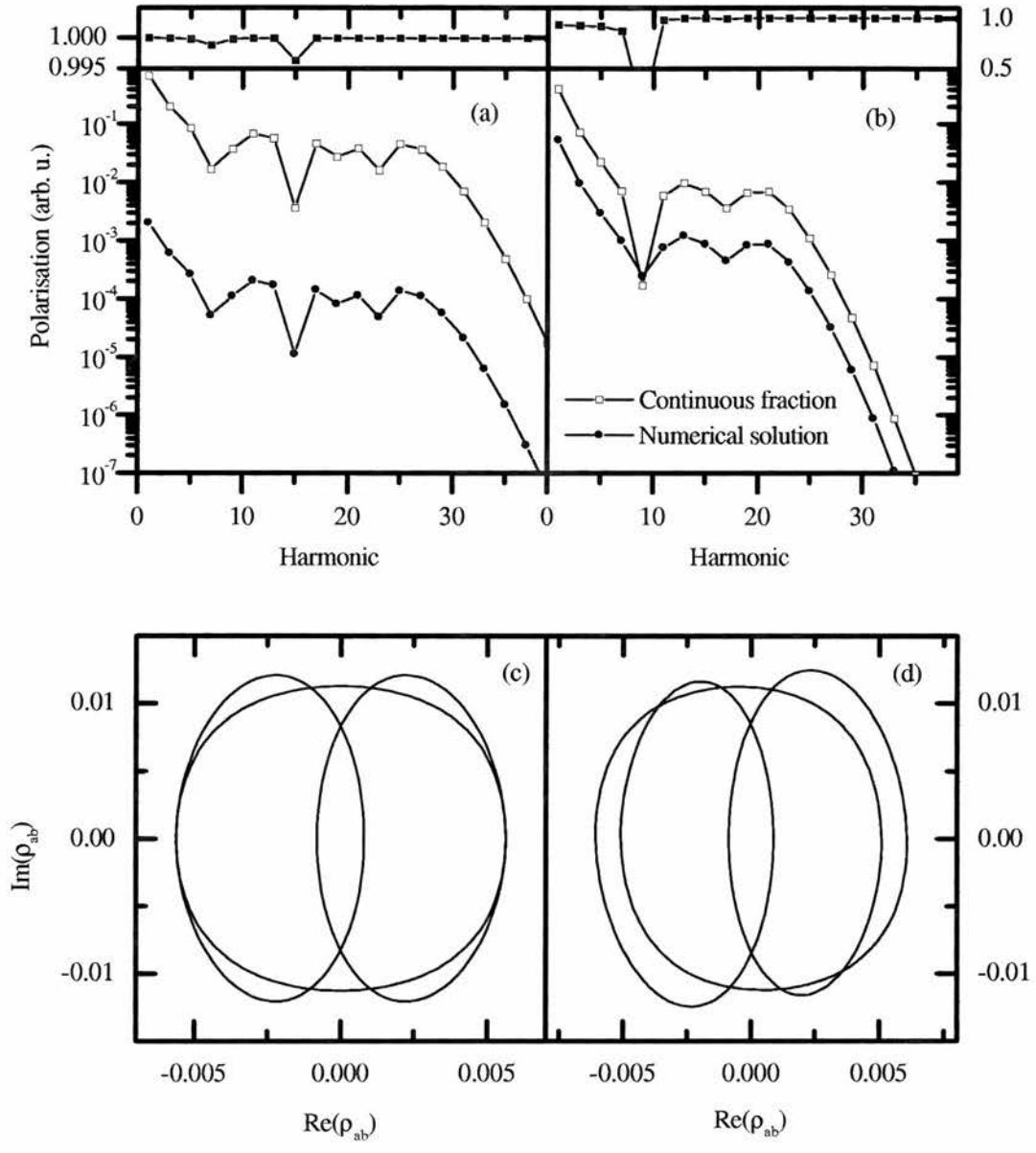

Figure 7.7: Polarisation intensity at the odd harmonics calculated with the continuous fraction method and with the numerical solution. (a) Resonant excitation ($V = 10$, $\Omega_0 = \omega_1 = 1$) and (b) non resonant excitation ($V = 1$, $\Omega_0 = 10\omega_1 = 1$). At the top, the ratio between the polarisations calculated by the two methods is represented.
A comparison of the two solutions in Bloch space is given by: (c) Solution obtained by the continous fraction method and (d) numerical solution.

excitation amplitude. This contradiction is due to the neglecting in the Fourier series of the terms having a different frequency from the harmonics of the excitation frequency that is to say the polarisations defined by

$$p(t) = e^{i\Delta\omega t} \sum_q p_q^{\Delta\omega} e^{iq\omega_1 t}, \tag{7.35}$$

with $\Delta\omega$ between 0 and the excitation frequency ω_1.

At this point, we are brought to consider a generalisation of the continuous fraction method (7.33) in order to include the terms (7.35) neglected in the literature. With these terms, the relation (7.31) can be written

$$\begin{aligned} -p_q^{\Delta\omega} \left(\frac{2(q\omega_1 + \Delta\omega)^2}{(q\omega_1 + \Delta\omega)^2 - \omega_1^2} + \frac{\Omega_0^2 - (q\omega_1 + \Delta\omega)^2}{V^2} \right) \\ = p_{q-2}^{\Delta\omega} \frac{q\omega_1 + \Delta\omega - 2\omega_1}{q\omega_1 + \Delta\omega - 1\omega_1} + p_{q+2}^{\Delta\omega} \frac{q\omega_1 + \Delta\omega + 2\omega_1}{q\omega_1 + \Delta\omega + 1\omega_1}. \end{aligned} \tag{7.36}$$

Introducing the non integer coefficient

$$r = \frac{q\omega_1 + \Delta\omega}{\omega_1} \tag{7.37}$$

at the place of the harmonic order q in the Fourier series we have the new continuous fraction

$$z_r^{\Delta\omega} = \frac{-(r-2)/(r-1)}{2r^2/(r^2-1) + (\Omega_0^2 - r^2\omega_1^2)/V^2 + [(r+2)/(r+1)] z_{r+2}^{\Delta\omega}}. \tag{7.38}$$

Finally, the complete solution can be constructed from all the terms $z_r^{\Delta\omega}$ defined for $\Delta\omega$ varying between 0 and ω_1.

7.6 Floquet expansion

As in the case of the continuous fraction, the Floquet expansion is applicable only in the case of Schrödinger's equations (for example (7.28)) and not for the density matrix equations. Thus, this method cannot explain the relaxation phenomena but has the advantage of introducing the notion of the dynamic state or the Floquet state. This kind of state is shown in the first part of this section when the numerical solution is searched for a two level system. The states correspond to the periodic solution. Here,

the Floquet expansion brings them forward in the general case of the n-level systems and for a monochromatic excitation (for bichromatic excitations see [86,87]).

The goal of the Floquet expansion is to transform the time dependent Schrödinger's equation

$$i\hbar\frac{dc_\alpha}{dt} = H_{\alpha\beta}c_\alpha + 2\cos(\omega_1 t)W_{\alpha\beta}c_\alpha \tag{7.39}$$

to a time independent equation. For this, it is necessary to use Floquet's theorem [88] that shows the existence of a solution of equation (7.39) in the form

$$c_\alpha = e^{-i\epsilon_n t/\hbar}c_\alpha^n, \tag{7.40}$$

where ϵ_n is the quasi-energy of the state. The Floquet state can also be introduced with the help of SU(2) symmetry [89].

Substituting (7.40) in equation (7.39), we find for each quasi-energy ϵ_n a modified Schrödinger equation

$$\epsilon_n c_\alpha^n + i\hbar\frac{dc_\alpha^n}{dt} = H_{\alpha\beta}c_\alpha^n + 2\cos(\omega_1 t)W_{\alpha\beta}c_\alpha^n. \tag{7.41}$$

Finally, the wave vector c_α^n is decomposed in a Fourier series with the fundamental frequency equal to the excitation one

$$c_\alpha^n = \sum_m e^{-im\omega_1 t}c_\alpha^{nm}. \tag{7.42}$$

This Fourier transformation gives the time independent equation

$$\epsilon_n c_\alpha^{nm} = \left(H_{\alpha\beta} - \hbar m\omega_1\right)c_\alpha^{nm} + W_{\alpha\beta}\left(c_\alpha^{nm-1} + c_\alpha^{nm+1}\right). \tag{7.43}$$

Defining the Hamiltonian operator

$$\mathcal{H} = \left(H_{\alpha\beta} - \hbar m\omega_1\right)\delta_{nm} + W_{\alpha\beta}\left(\delta_{nm-1} + \delta_{nm+1}\right) \tag{7.44}$$

and the wave vector associated with the Floquet state

$$\mathcal{C} = c_\alpha^n \tag{7.45}$$

Schrödinger's equation (7.39) can be written as a stationary equation

$$\epsilon_n \mathcal{C} = \mathcal{H}\mathcal{C}, \tag{7.46}$$

whose solution is composed of the eigen-vectors of $\mathcal{H}$. The eigen-values of $\mathcal{H}$ are the quasi–energies of Floquet states. One interesting property of these quasi–energies is their periodicity. Indeed, the Floquet Hamiltonian is invariant when adding a multiple of the energy of excitation

$$\mathcal{H} = \mathcal{H} + n\hbar\omega_1,$$

and consequently the eigen-values (quasi-energies) are also periodic.

The Floquet expansion method is based on the determination of the eigen-values of the Floquet Hamiltonian. The states associated with these eigen-values can be seen as forming a new quantum system composed of an n-level system and the excitation wave. These new states are indexed with the help of two quantum numbers, namely the state of the n-level system (α in equation (7.45)) and by the harmonic number of the excitation field (n in equation (7.45)). As this method is based on the search of eigen-values, it cannot directly be generalised to the case of density matrix equations which include the relaxation terms. This impossibility is due to the appearance in equation (7.46) of the free term associated with the thermodynamic equilibrium of the density matrix.

7.7 Summary

In this chapter, we studied, using the density matrix equations, the interaction between an n-level system and a monochromatic electromagnetic excitation. In order to define the evolution of the n-level system we used several methods for solving the equations. We started with a numerical solution method, where, taking advantage of the periodicity of the excitation, we could introduce a matrix operator linking the state of the system before and after one period of excitation. Using this matrix one can find the stationary and transient solutions of the density matrix equations. This numerical solution was then used as a reference against which we compared four other methods: perturbation expansion, rotating wave approximation, continuous fraction method and the Floquet

expansion. In this way we could show the limits of these methods as one increases the excitation amplitude.

Chapter 8

Stationary excitation of an n-level system

8.1 Introduction

In this chapter, we describe the behaviour of an n-level system in interaction with one or several monochromatic fields. In the preceding chapter, we illustrated the problems that arise when one searches for analytical solutions of the density matrix equations describing such systems. Usually, only a solution by quadrature can be found. Nevertheless, for special time dependent excitation fields one can find an analytical solution. This is the case of the Dirac excitation, meaning an infinitely brief excitation. Besides, the Fourier transformation of a real monochromatic wave is composed of two Dirac functions. Following these remarks, we develop a method for finding the solution of the density matrix equation of an n-level system under monochromatic excitation in this chapter. In order to do this, we use the Fourier transformation.

This chapter starts with a general introduction to our method. First, we treat the behaviour of a two level system as well as more generally of an n-level system interacting with only one monochromatic field. After the Fourier transformation, the density matrix equation becomes an infinite system of linear equations linking the density matrices at the different harmonic frequencies of the excitation. This system of equations can be written in a matrix form where the characteristic matrix has non-zero terms only on the principal and secondary diagonals. We show that the solution found from this truncated matrix at the N^{th} order, converges towards the solution of the infinite matrix as $1/N$.

We also give a recursive method for solving the truncated linear system. In the case of the n-level system this recursive solution takes the form of a generalised continuous fraction.

In the second section, the method used for the monochromatic excitation is generalised for the bichromatic excitation, namely the excitation by two beams of different wavelength and intensity. The bichromatic excitation presents, not only an interest in optoelectronic systems (for example [90,91]) but also in nuclear magnetic resonances [92] where the same kind of n-level quantum systems are considered. A fourth order tensor relation must be taken into account in order to treat the bichromatic excitation. Otherwise the method is the same as for the monochromatic excitation. The fourth order tensor relation links the density matrices at the harmonic frequencies obtained from the linear combinations of the two excitation frequencies.

8.2 The n-level system under monochromatic excitation

In this section, we deduce the stationary response of an n-level system under monochromatic excitation in the framework of the density matrix equation. In order to facilitate this study, we deduce the response of a two level system and of a more general n-level system in parallel. The difference between the two approaches resides in the order of the applied operators after the Fourier transformation. For the two level system, the calculation is made with the help of matrices, while for the n-level systems we need to use fourth order tensors. The following subsections are consequently divided into two parts. First the behaviour of a two level system is established and next the results are generalised for the n-level system.

In the first subsection, we start with the density matrix equation (6.9) including the relaxation terms (6.11). This equation is transformed with the help of the Fourier transformation and the resulting system of equations is solved after being truncated. Further, we show that this solution converges towards the exact solution. Finally, a recursive method of solution is developed.

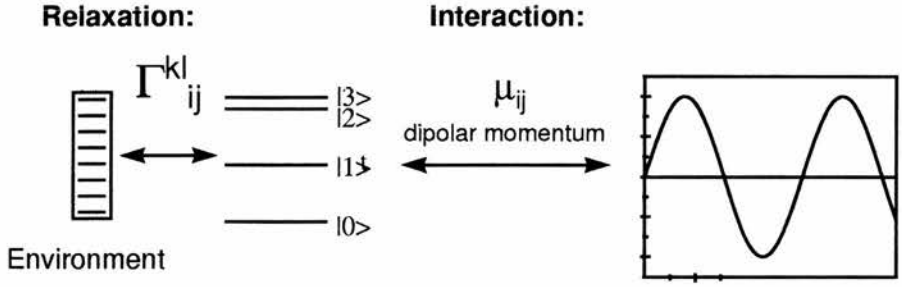

Figure 8.1: The elements considered in our model.

8.2.1 Description of the quantum system

The description of the quantum system in the density matrix formalism is presented in the preceding chapter. We remark here that at a given instant, the state of the system is characterised by the density matrix, that is to say by the populations and coherence of the eigen states of the Hamiltonian operator. The evolution of the density matrix is determined by equation (6.12) which links the different populations whilst keeping their sum constant.

Acting on the quantum system is the electromagnetic field. It intervenes in the evolution equation through the dipolar operator μ_{ij}. In this section, the considered excitation field is monochromatic

$$E(t) = E_1 \cos(\omega_1 t), \tag{8.1}$$

where ω_1 and E_1 are respectively its frequency and amplitude.

When the quantum system is excited, it absorbs energy. A part of this energy is dissipated by exchanges with the surrounding environment. This dissipation is modelled by the relaxation coefficients in the density matrix equation

$$\frac{d\rho_{ij}}{dt} = \frac{1}{i\hbar}(H_i^k \rho_{kj} - \rho_{ik} H_j^k) + \frac{1}{i\hbar} E_1 \cos(\omega_1 t)(\mu_i^k \rho_{kj} - \rho_{ik}\mu_j^k) - \Gamma_{ij}^{kl}(\rho_{kl} - \rho_{kl}^{(0)}). \tag{8.2}$$

In the following, we are interested in the stationary response of the quantum system that is to say the equilibrium state between the incoming energy from the electromagnetic field and the loss of energy due to the relaxation phenomena (see figure 8.1). This equilibrium state is determined by the density matrix equation (8.2) and is characterised by a periodic solution at the fundamental excitation frequency. This type of behaviour

is known in classical mechanics as a forced oscillation. The external force corresponds to the electromagnetic field and the dissipating force of the oscillator to the relaxation coefficients. This analogy, although very limited, can be used for a better comprehension of the behaviour of the quantum system at the time of the excitation.

For the two level system, equation (8.2) can be written in an explicit manner for the four elements of the density matrix

$$\frac{d\rho_{aa}}{dt} = +\frac{1}{i\hbar}E_1\cos(\omega_1 t)(\mu_{ab}\rho_{ba} - \rho_{ab}\mu_{ba}) - \Gamma_1(\rho_{aa} - \rho_{aa}^{(0)}), \tag{8.3a}$$

$$\frac{d\rho_{ab}}{dt} = \frac{1}{i\hbar}(H_{aa} - H_{bb})\rho_{ab} + \frac{1}{i\hbar}E_1\cos(\omega_1 t)\mu_{ab}(\rho_{bb} - \rho_{aa}) - \Gamma_2\rho_{ab}, \tag{8.3b}$$

$$\frac{d\rho_{ba}}{dt} = \frac{1}{i\hbar}(H_{bb} - H_{aa})\rho_{ba} + \frac{1}{i\hbar}E_1\cos(\omega_1 t)\mu_{ba}(\rho_{aa} - \rho_{bb}) - \Gamma_2\rho_{ba}, \tag{8.3c}$$

$$\frac{d\rho_{bb}}{dt} = +\frac{1}{i\hbar}E_1\cos(\omega_1 t)(\mu_{ba}\rho_{ab} - \rho_{ba}\mu_{ab}) - \Gamma_1(\rho_{bb} - \rho_{bb}^{(0)}), \tag{8.3d}$$

where a and b are the basic and excited states of the system respectively. The longitudinal relaxation coefficient Γ_1 implies, in the absence of excitation, the relaxation of populations ρ_{aa} and ρ_{bb} towards their equilibrium state $\rho_{aa}^{(0)}$ and $\rho_{bb}^{(0)}$. In this case, the solutions of equations (8.3a) and (8.3b) correspond to an exponential relaxation with the characteristic time $T_1 = 1/\Gamma_1$. The transverse relaxation coefficient Γ_2 has in effect the exponential relaxation of the coherence towards zero with a characteristic time $T_2 = 1/\Gamma_2$. Finally, the considered two level system is by hypothesis centro–symmetric and consequently the elements μ_{aa} and μ_{bb} of the dipolar interaction matrix are zero. The only allowed transitions are from state a to b and vice-versa. This implies also that all even-order susceptibilities are zero ($\chi^{2n} \equiv 0$) because the polarisation is an odd function with respect to the field $P(-E) = -P(E)$. The dipolar momentum of these transitions is given by the non diagonal terms of the dipolar operator $\mu_{ab} = \mu_{ba}^*$.

Equation (8.3) can also be written using a simpler matrix form as follows

$$
\begin{aligned}
-\Gamma_1 \begin{pmatrix} \rho_{aa}^{(0)} \\ 0 \\ 0 \\ \rho_{bb}^{(0)} \end{pmatrix} &= \frac{E(t)}{i\hbar} \begin{pmatrix} 0 & -\mu_{ba} & \mu_{ab} & 0 \\ -\mu_{ab} & 0 & 0 & \mu_{ab} \\ \mu_{ba} & 0 & 0 & -\mu_{ba} \\ 0 & \mu_{ba} & -\mu_{ab} & 0 \end{pmatrix} \begin{pmatrix} \rho_{aa} \\ \rho_{ab} \\ \rho_{ba} \\ \rho_{bb} \end{pmatrix} \\
&+ \begin{pmatrix} -\Gamma_1 & 0 & 0 & 0 \\ 0 & i\Omega_0 - \Gamma_2 & 0 & 0 \\ 0 & 0 & -i\Omega_0 - \Gamma_2 & 0 \\ 0 & 0 & 0 & -\Gamma_1 \end{pmatrix} \begin{pmatrix} \rho_{aa} \\ \rho_{ab} \\ \rho_{ba} \\ \rho_{bb} \end{pmatrix} - \frac{d}{dt} \begin{pmatrix} \rho_{aa} \\ \rho_{ab} \\ \rho_{ba} \\ \rho_{bb} \end{pmatrix}
\end{aligned} \tag{8.4}
$$

where the resonance frequency $\Omega_0/(2\pi)$ is defined by

$$\hbar\Omega_0 = H_{bb} - H_{aa}.$$

The n-level system

In the case of the n-level system, it is more convenient to use Liouville notation for the density matrix equation

$$L_{ij}^{kl}\rho_{kl} - \frac{d\rho_{ij}}{dt} - \Gamma_{ij}^{kl}\rho_{kl} + 2\cos(\omega_1 t)E_{ij}^{kl}\rho_{kl} = -\Gamma_{ij}^{kl}\rho_{kl}^{(0)}, \tag{8.5}$$

where the Liouville operator $\mathbf{L} = [\mathbf{H}, \bullet]$ is a fourth order tensor defined by

$$L_{ij}^{kl} = \frac{1}{i\hbar}\left(\delta_j^l H_i^k - \delta_i^k H_j^l\right). \tag{8.6}$$

The interaction with the electromagnetic field in the Liouville notation is described by the following tensor

$$E_{ij}^{kl} = \frac{E_1}{2i\hbar}\left(\delta_j^l \mu_i^k - \delta_i^k \mu_j^l\right). \tag{8.7}$$

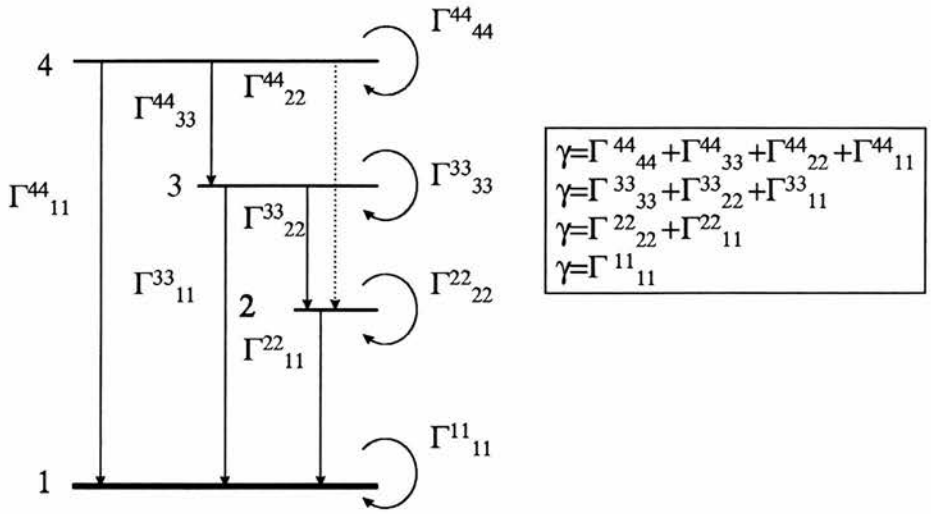

Figure 8.2: Example of the population relaxation (longitudinal relaxation) in the case of four levels (n=4) and in absence of thermalisation effects. The relaxation coefficient γ corresponds to the global relaxation time of the populations while the different Γ^{ii}_{jj} govern the relaxation between the different states of the quantum system.

The conservation of the total population

$$\begin{aligned} 0 &= Tr\left(\frac{d\rho_{ij}}{dt}\right) \\ &= -Tr\left(\Gamma^{kl}_{ij}(\rho_{kl}-\rho^{(0)}_{kl})\right) \\ &= -\sum_j\left(\Gamma^{kl}_{jj}(\rho_{kl}-\rho^{(0)}_{kl})\right), \end{aligned}$$

implies the following condition on the relaxation tensor Γ, more precisely on the longitudinal relaxation coefficients

$$\sum_i \Gamma^{jj}_{ii} = \gamma \tag{8.8}$$

for all $j = 1, \cdots, n$ (for an example see figure (8.2)). From a mathematical point of view, there is no special condition to be fulfilled by the transverse relaxation times. In order to determine this relation we took only transverse and longitudinal relaxation times into account(6.11) whilst the mixed terms (for example Γ^{22}_{12}) are neglected here. Physically, they would imply, for example, a relaxation from a stationary excited population towards the coherence of two states (in classical physics this would mean the relaxation of potential energy to give kinetic energy).

8.2.2 Fourier transformation

In the preceding chapter, we showed the difficulties to be overcome when searching for the solution of the density matrix equation in the case of the time dependent excitation. This equation (8.4) with a periodic excitation is a special case of time dependent excitation. The advantage of a periodic excitation in comparison with any other excitation is its simple representation in the frequency domain, that is to say after Fourier transformation. Consequently, the Fourier transformation is suitable for use in simplifying the density matrix equations

$$\hat{f}(\omega) = \mathcal{F}(f(t)) = \int_{-\infty}^{\infty} e^{-i\omega t} f(t) dt. \tag{8.9}$$

In the following, we use some properties of this transformation:

$$\mathcal{F}(\cos(\omega_1 t) f(t)) = \frac{1}{2}\hat{f}(\omega + \omega_1) + \frac{1}{2}\hat{f}(\omega - \omega_1), \tag{8.10a}$$

$$\mathcal{F}\left(\frac{df(t)}{dt}\right) = i\omega \hat{f}(\omega), \tag{8.10b}$$

$$\mathcal{F}(f_0) = \delta(\omega) f_0. \tag{8.10c}$$

With the help of the Fourier transformation (8.9) and of its properties (8.10), the evolution equation (8.4) can be written as

$$\frac{E_1}{2i\hbar} \begin{pmatrix} 0 & -\mu_{ba} & \mu_{ab} & 0 \\ -\mu_{ab} & 0 & 0 & \mu_{ab} \\ \mu_{ba} & 0 & 0 & -\mu_{ba} \\ 0 & \mu_{ba} & -\mu_{ab} & 0 \end{pmatrix} \left[\begin{pmatrix} \hat{\rho}_{aa}(\omega - \omega_1) \\ \hat{\rho}_{ab}(\omega - \omega_1) \\ \hat{\rho}_{ba}(\omega - \omega_1) \\ \hat{\rho}_{bb}(\omega - \omega_1) \end{pmatrix} + \begin{pmatrix} \hat{\rho}_{aa}(\omega + \omega_1) \\ \hat{\rho}_{ab}(\omega + \omega_1) \\ \hat{\rho}_{ba}(\omega + \omega_1) \\ \hat{\rho}_{bb}(\omega + \omega_1) \end{pmatrix} \right]$$

$$- \begin{pmatrix} \Gamma_1 + i\omega & 0 & 0 & 0 \\ 0 & \Gamma_2 + i(\omega - \Omega_0) & 0 & 0 \\ 0 & 0 & \Gamma_2 + i(\omega + \Omega_0) & 0 \\ 0 & 0 & 0 & \Gamma_1 + i\omega \end{pmatrix} \begin{pmatrix} \hat{\rho}_{aa}(\omega) \\ \hat{\rho}_{ab}(\omega) \\ \hat{\rho}_{ba}(\omega) \\ \hat{\rho}_{bb}(\omega) \end{pmatrix}$$

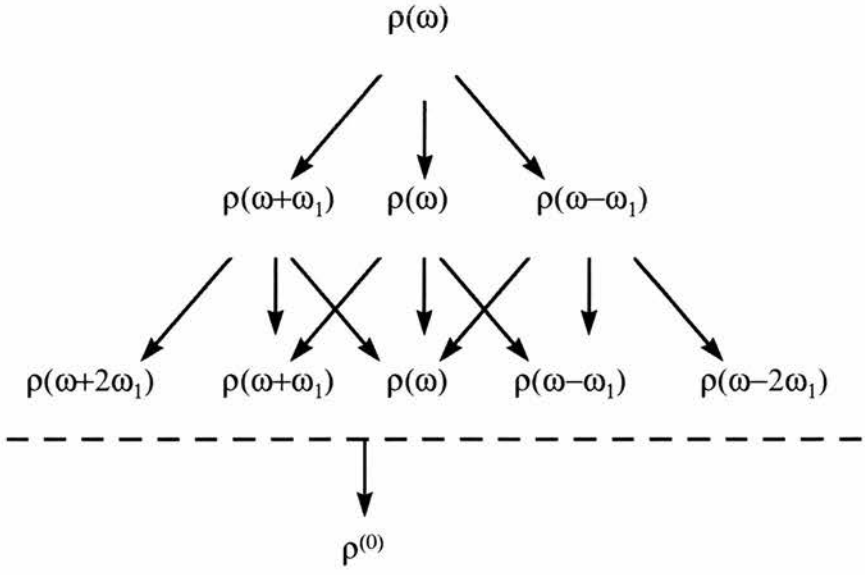

Figure 8.3: Relation between the different frequency components of the density matrix.

$$= -\Gamma_1 \delta(\omega) \begin{pmatrix} \rho_{aa}^{(0)} \\ 0 \\ 0 \\ \rho_{bb}^{(0)} \end{pmatrix}. \tag{8.11}$$

The Fourier transformation has changed the differential equation to an algebraic equation that links the different frequency components of the density matrix. Indeed, the density matrix at the frequency ω is coupled to the density matrix at the frequency $\omega - \omega_1$ and at the frequency $\omega + \omega_1$ (see figure 8.3). This "coupling" is more or less important according to the amplitude of the excitation field.

One can distinguish two different types of solution of equation (8.11) depending on whether the starting frequency ω is or isn't a multiple of the excitation frequency ω_1. In the first case, the solution of equation (8.11) corresponds to the Fourier transformation of the periodic special solution of the differential equation (8.4). In the second case, the solution corresponds to the homogeneous solution of the differential equation (8.4). This homogeneous solution is transient and corresponds to an exponential relaxation towards the thermodynamic equilibrium density matrix with the relaxation times T_1 and T_2. As we are interested in the stationary state of the system we discard this transient solution and study the solution corresponding to the special periodic solution. We remark that for this solution, in equation (8.11), only the harmonic frequencies of the excitation

intervene. Further this algebraic equation can be simplified if one defines

$$\begin{aligned}\hat{\rho}(\omega) &= \sum_{n=-\infty}^{\infty} \hat{\rho}^n \delta(n\omega_1 - \omega) \\ &= \sum_{n=-\infty}^{\infty} \begin{pmatrix} \hat{\rho}^n_{aa} \\ \hat{\rho}^n_{ab} \\ \hat{\rho}^n_{ba} \\ \hat{\rho}^n_{bb} \end{pmatrix} \delta(n\omega_1 - \omega)\end{aligned}$$

for the density matrix and

$$\hat{\rho}^{(0)} = -\Gamma_1 \begin{pmatrix} \hat{\rho}^{(0)}_{aa} \\ 0 \\ 0 \\ \hat{\rho}^{(0)}_{bb} \end{pmatrix}$$

for the thermodynamical equilibrium state.

The interaction matrices between the different harmonics of the density matrix are:

$$\mathbf{H}^n = \begin{pmatrix} \Gamma_1 + in\omega_1 & 0 & 0 & 0 \\ 0 & \Gamma_2 + i(n\omega_1 - \Omega_0) & 0 & 0 \\ 0 & 0 & \Gamma_2 + i(n\omega_1 + \Omega_0) & 0 \\ 0 & 0 & 0 & \Gamma_1 + in\omega_1 \end{pmatrix}$$

and

$$\mathbf{E} = \frac{E_1}{2\imath\hbar} \begin{pmatrix} 0 & -\mu_{ba} & \mu_{ab} & 0 \\ -\mu_{ab} & 0 & 0 & \mu_{ab} \\ \mu_{ba} & 0 & 0 & -\mu_{ba} \\ 0 & \mu_{ab} & -\mu_{ba} & 0 \end{pmatrix}.$$

Considering these notations, equation (8.11) can be written

$$\delta_{n0}\hat{\rho}^{(0)} = \mathbf{E}\hat{\rho}^{n+1} + \mathbf{E}\hat{\rho}^{n-1} + \mathbf{H}^n\hat{\rho}^n, \tag{8.12}$$

or in a matrix form

$$\begin{pmatrix} \vdots \\ 0 \\ 0 \\ 0 \\ 0 \\ 0 \\ \vdots \\ 0 \\ 0 \\ \hat{\rho}^{(0)} \\ 0 \\ 0 \\ \vdots \end{pmatrix} = \begin{pmatrix} \vdots & \cdots & \cdots & \cdots & \cdots & \cdots & \vdots & \cdots & \cdots & \cdots & \cdots & \cdots & \vdots \\ \vdots & \mathbf{H}^{n+2} & \mathbf{E} & 0 & 0 & 0 & \vdots & 0 & 0 & 0 & 0 & 0 & \vdots \\ \vdots & \mathbf{E} & \mathbf{H}^{n+1} & \mathbf{E} & 0 & 0 & \vdots & 0 & 0 & 0 & 0 & 0 & \vdots \\ \vdots & 0 & \mathbf{E} & \mathbf{H}^{n} & \mathbf{E} & 0 & \vdots & 0 & 0 & 0 & 0 & 0 & \vdots \\ \vdots & 0 & 0 & \mathbf{E} & \mathbf{H}^{n-1} & \mathbf{E} & \vdots & 0 & 0 & 0 & 0 & 0 & \vdots \\ \vdots & 0 & 0 & 0 & \mathbf{E} & \mathbf{H}^{n-2} & \vdots & 0 & 0 & 0 & 0 & 0 & \vdots \\ \vdots & \cdots & \cdots & \cdots & \cdots & \cdots & \vdots & \cdots & \cdots & \cdots & \cdots & \cdots & \vdots \\ \vdots & 0 & 0 & 0 & 0 & 0 & \vdots & \mathbf{H}^{2} & \mathbf{E} & 0 & 0 & 0 & \vdots \\ \vdots & 0 & 0 & 0 & 0 & 0 & \vdots & \mathbf{E} & \mathbf{H}^{1} & \mathbf{E} & 0 & 0 & \vdots \\ \vdots & 0 & 0 & 0 & 0 & 0 & \vdots & 0 & \mathbf{E} & \mathbf{H}^{0} & \mathbf{E} & 0 & \vdots \\ \vdots & 0 & 0 & 0 & 0 & 0 & \vdots & 0 & 0 & \mathbf{E} & \mathbf{H}^{-1} & \mathbf{E} & \vdots \\ \vdots & 0 & 0 & 0 & 0 & 0 & \vdots & 0 & 0 & 0 & \mathbf{E} & \mathbf{H}^{-2} & \vdots \\ \vdots & \cdots & \cdots & \cdots & \cdots & \cdots & \vdots & \cdots & \cdots & \cdots & \cdots & \cdots & \vdots \end{pmatrix} \begin{pmatrix} \vdots \\ \hat{\rho}^{n+2} \\ \hat{\rho}^{n+1} \\ \hat{\rho}^{n} \\ \hat{\rho}^{n-1} \\ \hat{\rho}^{n-2} \\ \vdots \\ \hat{\rho}^{2} \\ \hat{\rho}^{1} \\ \hat{\rho}^{0} \\ \hat{\rho}^{-1} \\ \hat{\rho}^{-2} \\ \vdots \end{pmatrix}. \tag{8.13}$$

The n-level system

In the general case of the n-level systems, the Fourier transformation gives the differential equation the following tensor form

$$\left(L_{ij}^{kl} - i\omega - \Gamma_{ij}^{kl}\right)\hat{\rho}_{kl}(\omega) + E_{ij}^{kl}\hat{\rho}_{kl}(\omega - \omega_1) + E_{ij}^{kl}\hat{\rho}_{kl}(\omega + \omega_1), = -\delta(\omega)\Gamma_{ij}^{kl}\rho_{kl}^{(0)}. \tag{8.14}$$

As for the two level system, we are interested in the periodic solutions of the differential equation (8.5). In this case, the solution of the equivalent equation (8.12) is composed only of the harmonic frequencies of the excitation frequency. We can thus decompose the density matrix with these harmonic frequencies

$$(\hat{\rho}_{ij}(\omega)) = \sum_{n=-\infty}^{\infty} \hat{\rho}^n \delta(n\omega_1 - \omega).$$

Defining the two interaction tensors between the different harmonics of the density matrix

$$\mathbf{L}^n = \left(L_{ij}^{kl} - in\omega_1 I_{ij}^{kl} - \Gamma_{ij}^{kl}\right)$$

and

$$\mathbf{E} = \left(E_{ij}^{kl}\right)$$

implies the following infinite system of linear equations

$$\begin{array}{ccccccc}
\vdots & \vdots & \vdots & \vdots & \vdots & \vdots & \vdots \\
\mathbf{E}\hat{\rho}^{N+2} & + & \mathbf{E}\hat{\rho}^{N} & + & \mathbf{L}^{N+1}\hat{\rho}^{N+1} & = & 0 \\
\mathbf{E}\hat{\rho}^{N+1} & + & \mathbf{E}\hat{\rho}^{N-1} & + & \mathbf{L}^{N}\hat{\rho}^{N} & = & 0 \\
\mathbf{E}\hat{\rho}^{N} & + & \mathbf{E}\hat{\rho}^{N-2} & + & \mathbf{L}^{N-1}\hat{\rho}^{N-1} & = & 0 \\
\vdots & \vdots & \vdots & \vdots & \vdots & \vdots & \vdots \\
\mathbf{E}\hat{\rho}^{2} & + & \mathbf{E}\hat{\rho}^{0} & + & \mathbf{L}^{1}\hat{\rho}^{1} & = & 0 \\
\mathbf{E}\hat{\rho}^{1} & + & \mathbf{E}\hat{\rho}^{-1} & + & \mathbf{L}^{0}\hat{\rho}^{0} & = & -\Gamma\rho^{(0)} \\
\mathbf{E}\hat{\rho}^{0} & + & \mathbf{E}\hat{\rho}^{-2} & + & \mathbf{L}^{-1}\hat{\rho}^{-1} & = & 0 \\
\vdots & \vdots & \vdots & \vdots & \vdots & \vdots & \vdots
\end{array} .$$

This system of equations can be written under a "matrix" form where each element is a fourth order tensor

$$\mathbf{M}_n^p \hat{\rho}^n = \delta_0^p \Gamma \rho^{(0)}, \tag{8.15a}$$

with

$$\mathbf{M}_n^p = \delta_n^p \mathbf{L}^n + \delta_{n+1}^p \mathbf{E} + \delta_{n-1}^p \mathbf{E}. \tag{8.15b}$$

8.2.3 The truncated solution

The method of solution for this infinite system of equations (8.13) that we adopt truncates the dependences between the higher harmonics. Indeed, from a certain harmonic order, the norm of the diagonal elements of the matrix $\mathbf{M}_n^p$ is bigger than that of the secondary diagonal (see figures 8.4). From this harmonic onward, we can neglect the "coupling" between the density matrix at one harmonic frequency and the following harmonic. This special truncation is described later. The error due to this approximation is established in the following subsection.

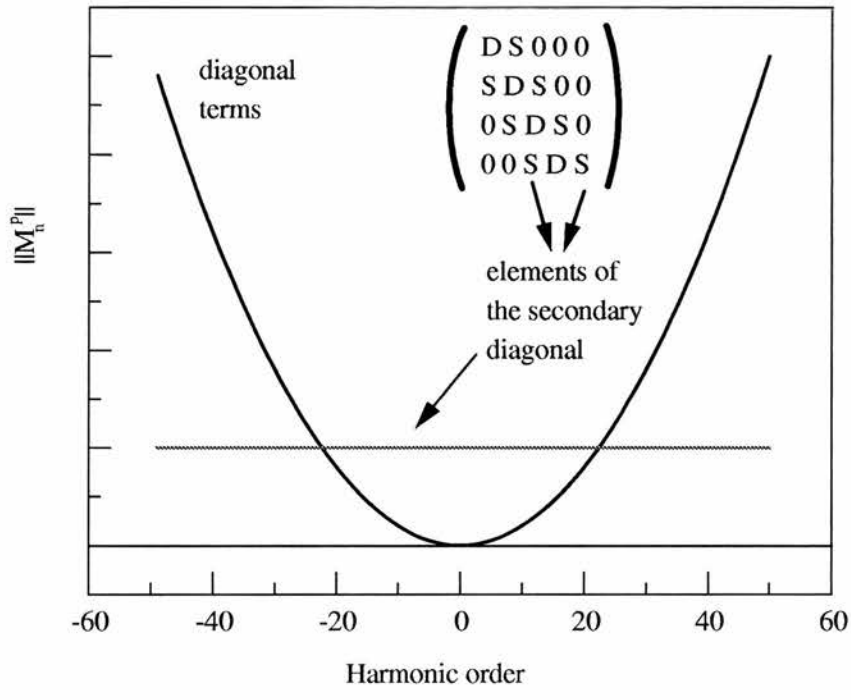

Figure 8.4: The norm of the principal and secondary diagonal of the matrix $||\mathbf{M}_n^p||^2$ (equation (8.15b)) as a function of the harmonic order n.

When truncating at a given harmonic order N, the matrices $\mathbf{E}$ (due to the excitation) are neglected in comparison with the matrix $\mathbf{H}^N$ (8.13). For that, the matrix (8.13) is decomposed into nine parts

$$
\begin{pmatrix}
\begin{pmatrix} \ddots & \vdots \\ \mathbf{H}^{N+2}\mathbf{E} & \\ \cdots\ \mathbf{E} & \mathbf{H}^{N+1} \end{pmatrix} & \begin{pmatrix} \vdots & & & & \\ 0 & & & & \\ \mathbf{E} & 0 & \cdots & \cdots & 0 \end{pmatrix} & \begin{pmatrix} \vdots & & & \\ 0 & & & \\ 0 & 0 & \cdots & \end{pmatrix} \\
\begin{pmatrix} \cdots\ 0 & \mathbf{E} \\ & 0 \\ & \vdots \\ & \vdots \\ & 0 \end{pmatrix} & \begin{pmatrix} \mathbf{H}^N & \mathbf{E} & \cdots & \cdots & 0 \\ \mathbf{E} & \mathbf{H}^{N-1} & & & \vdots \\ \vdots & & \ddots & & \vdots \\ \vdots & & & \mathbf{H}^{-N+1} & \mathbf{E} \\ 0 & \cdots & \cdots & \mathbf{E} & \mathbf{H}^{-N} \end{pmatrix} & \begin{pmatrix} 0 & & \\ \vdots & & \\ \vdots & & \\ 0 & & \\ \mathbf{E} & 0 & \cdots \end{pmatrix} \\
\begin{pmatrix} \cdots\ 0 & 0 \\ & 0 \\ & \vdots \end{pmatrix} & \begin{pmatrix} 0 & \cdots & \cdots & 0 & \mathbf{E} \\ & & & & 0 \\ & & & & \vdots \end{pmatrix} & \begin{pmatrix} \mathbf{H}^{-N-1} & \mathbf{E} & \cdots \\ & & \\ \mathbf{E} & \mathbf{H}^{-N-2} & \\ \vdots & & \ddots \end{pmatrix}
\end{pmatrix} =
$$

$$= \begin{pmatrix} \mathbf{M}_{11}^{\infty\times\infty} & \mathbf{M}_{12}^{\infty\times(2N+1)} & \mathbf{M}_{13}^{\infty\times\infty} \\ \mathbf{M}_{21}^{(2N+1)\times\infty} & \mathbf{M}_{22}^{(2N+1)\times(2N+1)} & \mathbf{M}_{23}^{(2N+1)\times\infty} \\ \mathbf{M}_{31}^{\infty\times\infty} & \mathbf{M}_{32}^{\infty\times(2N+1)} & \mathbf{M}_{33}^{\infty\times\infty} \end{pmatrix}.$$

These nine parts are themselves matrices of different orders. The matrices $\mathbf{M_{11}}$ and $\mathbf{M_{33}}$ are almost diagonal while the matrix $\mathbf{M_{22}}$ is tri-diagonal. The link between these three parts is made with the help of the matrices $\mathbf{M_{12}}$, $\mathbf{M_{21}}$, $\mathbf{M_{32}}$ and $\mathbf{M_{23}}$. In the same manner as for the matrix $\mathbf{M_n^P}$, the solution is divided into three parts

$$\begin{pmatrix} \begin{pmatrix} \vdots \\ \hat{\rho}^{N+1} \end{pmatrix} \\ \begin{pmatrix} \hat{\rho}^{N} \\ \hat{\rho}^{N-1} \\ \vdots \\ \hat{\rho}^{-N+1} \\ \hat{\rho}^{-N} \end{pmatrix} \\ \begin{pmatrix} \hat{\rho}^{-N-1} \\ \vdots \end{pmatrix} \end{pmatrix} = \begin{pmatrix} \hat{\rho}_1 \\ \hat{\rho}_2 \\ \hat{\rho}_3 \end{pmatrix}$$

and also the free term of the algebraic equation

$$\begin{pmatrix} \begin{pmatrix} \vdots \\ 0 \end{pmatrix} \\ \begin{pmatrix} 0 \\ \vdots \\ \hat{\rho}^{(0)} \\ \vdots \\ 0 \end{pmatrix} \\ \begin{pmatrix} 0 \\ \vdots \end{pmatrix} \end{pmatrix} = \begin{pmatrix} \hat{\rho}_1^{(0)} \\ \hat{\rho}_2^{(0)} \\ \hat{\rho}_3^{(0)} \end{pmatrix}.$$

Considering this segmentation, the equation (8.13) is written

$$\begin{pmatrix} \hat{\rho}_1^{(0)} \\ \hat{\rho}_2^{(0)} \\ \hat{\rho}_3^{(0)} \end{pmatrix} = \begin{pmatrix} \mathbf{M}_{11} & \mathbf{M}_{12} & \mathbf{M}_{13} \\ \mathbf{M}_{21} & \mathbf{M}_{22} & \mathbf{M}_{23} \\ \mathbf{M}_{31} & \mathbf{M}_{32} & \mathbf{M}_{33} \end{pmatrix} \begin{pmatrix} \hat{\rho}_1 \\ \hat{\rho}_2 \\ \hat{\rho}_3 \end{pmatrix} = \mathbf{M} \begin{pmatrix} \hat{\rho}_1 \\ \hat{\rho}_2 \\ \hat{\rho}_3 \end{pmatrix}. \tag{8.16}$$

In order to be able to neglect the dependencies between the higher harmonics, the matrices $\mathbf{M}_{11}$ and $\mathbf{M}_{33}$ are also divided into a diagonal and a non-diagonal part. This second part can be seen as being a perturbation on the diagonal part

$$\mathbf{M}_{11} = \begin{pmatrix} \ddots & & \vdots \\ & \mathbf{H}^{N+2} & 0 \\ \cdots & 0 & \mathbf{H}^{N+1} \end{pmatrix} + \begin{pmatrix} \ddots & & \vdots \\ & 0 & \mathbf{E} \\ \cdots & \mathbf{E} & 0 \end{pmatrix} = \mathbf{D}_{11} + \delta_{11}$$

and

$$\mathbf{M}_{33} = \begin{pmatrix} \mathbf{H}^{-N-1} & 0 & \cdots \\ 0 & \mathbf{H}^{-N-2} & \\ \vdots & & \ddots \end{pmatrix} + \begin{pmatrix} 0 & \mathbf{E} & \cdots \\ \mathbf{E} & 0 & \\ \vdots & & \ddots \end{pmatrix} = \mathbf{D}_{33} + \delta_{33}.$$

Using all of the above notations, the exact solution of the infinite system is a solution of equation

$$\begin{pmatrix} \hat{\rho}_1^{(0)} \\ \hat{\rho}_2^{(0)} \\ \hat{\rho}_3^{(0)} \end{pmatrix} = \begin{pmatrix} \mathbf{D}_{11} + \delta_{11} & \mathbf{M}_{12} & 0 \\ \mathbf{M}_{21} & \mathbf{M}_{22} & \mathbf{M}_{23} \\ 0 & \mathbf{M}_{32} & \mathbf{D}_{33} + \delta_{33} \end{pmatrix} \begin{pmatrix} \hat{\rho}_1 \\ \hat{\rho}_2 \\ \hat{\rho}_3 \end{pmatrix}. \tag{8.17}$$

The approximate solution obtained neglecting the perturbations δ_{11} and δ_{33} can be written

$$\begin{pmatrix} -\mathbf{D}_{11}^{-1}\mathbf{M}_{12}\sigma_2 \\ \sigma_2 \\ -\mathbf{D}_{33}^{-1}\mathbf{M}_{32}\sigma_2 \end{pmatrix} \tag{8.18}$$

with

$$\rho_2^{(0)} = \left(\mathbf{M}_{22} - \mathbf{M}_{21}\mathbf{D}_{11}^{-1}\mathbf{M}_{12} - \mathbf{M}_{23}\mathbf{D}_{33}^{-1}\mathbf{M}_{32}\right)\sigma_2. \tag{8.19}$$

The two matrices $\mathbf{M}_{21}\mathbf{D}_{11}^{-1}\mathbf{M}_{12}$ and $\mathbf{M}_{23}\mathbf{D}_{33}^{-1}\mathbf{M}_{32}$ link the superior and inferior diagonal parts of $\mathbf{M}_n^p$ in the solution σ_2. These two matrices can be evaluated as

$$\mathbf{M}_{21}\mathbf{D}_{11}^{-1}\mathbf{M}_{12} = \overbrace{\begin{pmatrix} \mathbf{E}\left(\mathbf{H}^{N+1}\right)^{-1}\mathbf{E} & 0 & \cdots & 0 \\ 0 & 0 & & \vdots \\ \vdots & & \ddots & \vdots \\ 0 & \cdots & \cdots & 0 \end{pmatrix}}^{(2N+1)} \Bigg\} (2N+1) \tag{8.20}$$

and

$$\mathbf{M}_{23}\mathbf{D}_{33}^{-1}\mathbf{M}_{32} = \overbrace{\begin{pmatrix} 0 & \cdots & \cdots & \cdots & 0 \\ 0 & \ddots & & & \vdots \\ \vdots & & & 0 & 0 \\ 0 & \cdots & \cdots & 0 & \mathbf{E}\left(\mathbf{H}^{-N-1}\right)^{-1}\mathbf{E} \end{pmatrix}}^{(2N+1)} \Bigg\} (2N+1). \tag{8.21}$$

Defining thus

$$\delta^N = \mathbf{E}\left(\mathbf{H}^{N+1}\right)^{-1}\mathbf{E}$$

and

$$\delta^{-N} = \mathbf{E}\left(\mathbf{H}^{-N-1}\right)^{-1}\mathbf{E}$$

the equation (8.19) giving the approximate solution σ_2, can be written as

$$\begin{pmatrix} 0 \\ 0 \\ \vdots \\ \hat{\rho}^{(0)} \\ \vdots \\ 0 \\ 0 \end{pmatrix} = \left(\begin{array}{ccc:ccc} \mathbf{H}^N - \delta^N & \mathbf{E} & 0 & 0 & 0 & 0 \\ \mathbf{E} & \mathbf{H}^{N-1} & \mathbf{E} & 0 & 0 & 0 \\ 0 & \mathbf{E} & \mathbf{H}^{N-2} & 0 & 0 & 0 \\ \cdots & \cdots & \cdots & \cdots & \cdots & \cdots \\ 0 & 0 & 0 & \mathbf{H}^{-N+2} & \mathbf{E} & 0 \\ 0 & 0 & 0 & \mathbf{E} & \mathbf{H}^{-N+1} & \mathbf{E} \\ 0 & 0 & 0 & 0 & \mathbf{E} & \mathbf{H}^{-N} - \delta^{-N} \end{array}\right) \begin{pmatrix} \sigma^N \\ \sigma^{N-1} \\ \sigma^{N-2} \\ \vdots \\ \sigma^{-N+2} \\ \sigma^{-N+1} \\ \sigma^{-N} \end{pmatrix}. \tag{8.22}$$

Finally using equation (8.18) we can deduce the approximate density matrices at the different harmonic orders valid for the two level system. This can be generalised for the n-level system.

The n-level system

In the case of the n-level system, we define the approximate solution, namely the solution where the dependences between the higher harmonic order are neglected, as follows

$$\sigma = \begin{cases} \vdots & \\ \sigma^{N+2} & = 0 \\ \sigma^{N+1} & = -\left(\mathbf{L}^{N+1}\right)^{-1} \mathbf{E}\sigma^N \\ \sigma^N & \\ \vdots & \\ \sigma^{-N} & \\ \sigma^{-N-1} & = -\left(\mathbf{L}^{-N-1}\right)^{-1} \mathbf{E}\sigma^{-N} \\ \sigma^{-N-2} & = 0 \\ \vdots & \end{cases} \tag{8.23}$$

where $\sigma^{-N} \cdots \sigma^{N}$ are the solutions of the finite linear system of equations:

$$\begin{array}{ccccccccc}
-\mathbf{E}\left(\mathbf{L}^{N+1}\right)^{-1}\mathbf{E}\sigma^{N} & + & \mathbf{E}\sigma^{N-1} & + & \mathbf{L}^{N}\sigma^{N} & = & 0 \\
\mathbf{E}\sigma^{N} & + & \mathbf{E}\sigma^{N-2} & + & \mathbf{L}^{N-1}\sigma^{N-1} & = & 0 \\
\vdots & \vdots & \vdots & \vdots & \vdots & \vdots & \vdots \\
\mathbf{E}\sigma^{2} & + & \mathbf{E}\sigma^{0} & + & \mathbf{L}^{1}\sigma^{1} & = & 0 \\
\mathbf{E}\sigma^{1} & + & \mathbf{E}\sigma^{-1} & + & \mathbf{L}^{0}\sigma^{0} & = & -\Gamma\rho^{(0)} \\
\mathbf{E}\sigma^{0} & + & \mathbf{E}\sigma^{-2} & + & \mathbf{L}^{-1}\sigma^{-1} & = & 0 \\
\vdots & \vdots & \vdots & \vdots & \vdots & \vdots & \vdots \\
\mathbf{E}\sigma^{-N+2} & + & \mathbf{E}\sigma^{-N} & + & \mathbf{L}^{-N+1}\sigma^{N} & = & 0 \\
\mathbf{E}\sigma^{-N+1} & - & \mathbf{E}\left(\mathbf{L}^{-N-1}\right)^{-1}\mathbf{E}\sigma^{-N} & + & \mathbf{L}^{-N}\sigma^{-N} & = & 0.
\end{array}$$

This solution is a generalisation of the solution valid for a two level system. In the following we show that these two solutions have the same properties.

8.2.4 Convergence of the truncated solution

In this subsection, we estimate the error due to the truncation of the algebraic system. A preliminary graphical study of the approximate solution for different truncation orders as a function of the excitation amplitude shows that the solution found by truncation is valid up to a given amplitude (see figure 8.5). From this excitation amplitude, the approximate solution truncated at the order N shows a different behaviour from the approximated solutions at a higher order. In this graphical study, we plot the population of the excited state at zero frequency.

Figure 8.5 shows a series of oscillations. These oscillations are better displayed when the order of the truncation is greater. In other words, for a given excitation amplitude, the result obtained is almost the same for all truncation orders greater than a certain given truncation order. In the following, this hypothesis is demonstrated from a mathematical point of view. Therefore the induced error by truncation of the matrices $\mathbf{M}_{11}$ and $\mathbf{M}_{33}$ is evaluated by calculating the difference between the exact solution ρ

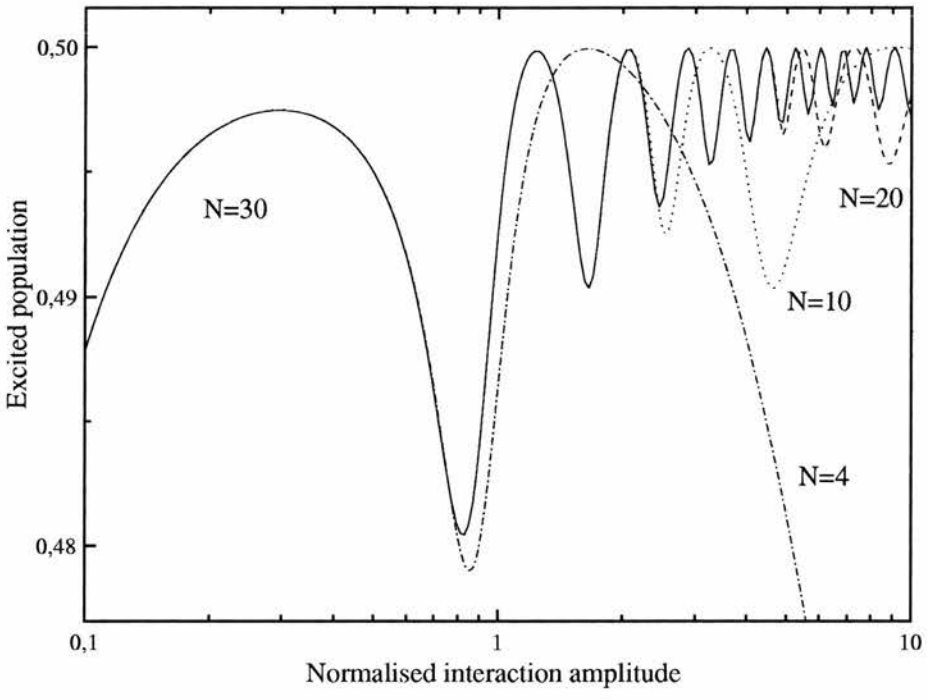

Figure 8.5: Population of the excited state at zero frequency for different excitation amplitudes and for different truncation orders.

and the approximated one σ

$$\begin{pmatrix} \mathbf{D}_{11}+\delta_{11} & \mathbf{M}_{12} & 0 \\ \mathbf{M}_{21} & \mathbf{M}_{22} & \mathbf{M}_{23} \\ 0 & \mathbf{M}_{32} & \mathbf{D}_{33}+\delta_{33} \end{pmatrix} \left[\begin{pmatrix} \rho_1 \\ \rho_2 \\ \rho_3 \end{pmatrix} - \begin{pmatrix} -\mathbf{D}_{11}^{-1}\mathbf{M}_{12}\sigma_2 \\ \sigma_2 \\ -\mathbf{D}_{33}^{-1}\mathbf{M}_{32}\sigma_2 \end{pmatrix} \right] = \begin{pmatrix} -\delta_{11}\mathbf{D}_{11}^{-1}\mathbf{M}_{12}\sigma_2 \\ 0 \\ -\delta_{33}\mathbf{D}_{33}^{-1}\mathbf{M}_{32}\sigma_2 \end{pmatrix}. \tag{8.24}$$

Let λ_M be the smallest eigen value of matrix $\mathbf{M}$ and m the biggest element of the matrices $\delta_{33}\mathbf{D}_{33}^{-1}\mathbf{M}_{32}$ and $\delta_{11}\mathbf{D}_{11}^{-1}\mathbf{M}_{12}$. Then we can find the upper value for the difference between the exact solution ρ and the approximate solution σ

$$\begin{aligned} ||\rho_2 - \sigma_2|| &\leq \left|\left| \begin{pmatrix} \rho_1 \\ \rho_2 \\ \rho_3 \end{pmatrix} - \begin{pmatrix} -\mathbf{D}_{11}^{-1}\mathbf{M}_{12}\sigma_2 \\ \sigma_2 \\ -\mathbf{D}_{33}^{-1}\mathbf{M}_{32}\sigma_2 \end{pmatrix} \right|\right| \\ &\leq 2\frac{m}{|\lambda_M|}||\sigma_2||. \end{aligned} \tag{8.25}$$

The factor m can be calculated from the matrix $\delta_{11}\mathbf{D}_{11}^{-1}\mathbf{M}_{12}$, which means from

$$\delta_{11}\mathbf{D}_{11}^{-1}\mathbf{M}_{21} = \left.\overbrace{\begin{pmatrix} \vdots & & \\ 0 & 0 & \cdots \\ \mathbf{E}\left(\mathbf{H}^{N+1}\right)^{-1}\mathbf{E} & 0 & \cdots \\ 0 & 0 & \cdots \end{pmatrix}}^{(2N+1)}\right\} \infty. \tag{8.26}$$

For a two level system, this implies

$$m = \left| \frac{\mu_{ab}\mu_{ba}E_1^2/(4\hbar^2)}{\Gamma_2 + i((N+1)\omega_1 + \Omega_0)} \right|.$$

Consequently, the relative error induced by the approximate solution decreases as $1/N$, that is to say inversely proportional to the truncation order

$$||\rho_2 - \sigma_2|| \leq \frac{\mathcal{O}(1/N)}{|\lambda_M|}||\sigma_2||. \tag{8.27}$$

The n-level system

In the case of the n-level system the difference between the approximate and the exact solutions can be evaluated from

$$\mathbf{M}_n^p\left(\hat{\rho}^n - \sigma^n\right) = -\delta_{N+2}^p\mathbf{E}\left(\mathbf{L}^{N+1}\right)^{-1}\mathbf{E}\sigma^N - \delta_{-N-2}^p\mathbf{E}\left(\mathbf{L}^{-N-1}\right)^{-1}\mathbf{E}\sigma^{-N}. \tag{8.28}$$

Let us define, as for the two level system, the smallest eigen value λ_M of $\mathbf{M}_n^p$ and the biggest element m of $\mathbf{E}\left(\mathbf{L}^{N+1}\right)^{-1}\mathbf{E}$ and $\mathbf{E}\left(\mathbf{L}^{-N-1}\right)^{-1}\mathbf{E}$. Then the difference between the two solutions has an upper value given by the inequality

$$||\hat{\rho} - \sigma|| \leq 2\frac{m}{|\lambda_M|}||\sigma||,$$

where m is proportional to $1/N$. Consequently, the relative error diminishes with the truncation order.

8.2.5 The recursive solution method

The recursive resolution method consists of the triangularisation of matrix $\mathbf{M}$ after the above discussed truncated approximation. We define a recursion sequence giving the terms of the diagonal of $\mathbf{M}$ after subtraction of the influence of the following harmonic. With this method we generalise the continuous fraction method described in the preceding chapter.

Let the initial term of diagonal be

$$\mathbf{D}^N = \mathbf{H}^N - \delta^N, \tag{8.29a}$$

the general recursive term be

$$\mathbf{D}^n = \mathbf{H}^n - \mathbf{E}\left(\mathbf{D}^{n+1}\right)^{-1}\mathbf{E}, \tag{8.29b}$$

and the last term of this sequence be

$$\mathbf{D}^{-N} = \mathbf{H}^{-N} - \delta^{-N} - \mathbf{E}\left(\mathbf{D}^{-N+1}\right)^{-1}\mathbf{E}. \tag{8.29c}$$

During the triangularisation of the matrix $\mathbf{M}$, the free term changes also, giving a sequence of terms with the first term given by

$$\eta^0 = \hat{\rho}^{(0)}, \tag{8.30a}$$

and the general recursive term by

$$\eta^n = -\mathbf{E}\left(\mathbf{D}^{n+1}\right)^{-1}\hat{\eta}^{n+1}. \tag{8.30b}$$

With the help of these two sequences, equation (8.22) can be written as

$$\begin{pmatrix} 0 \\ 0 \\ \vdots \\ \eta^{0} \\ \vdots \\ \eta^{-N+1} \\ \eta^{-N} \end{pmatrix} = \begin{pmatrix} \mathbf{D}^{N} & \mathbf{E} & 0 & \vdots & 0 & 0 & 0 \\ 0 & \mathbf{D}^{N-1} & \mathbf{E} & \vdots & 0 & 0 & 0 \\ 0 & 0 & \mathbf{D}^{N-2} & \vdots & 0 & 0 & 0 \\ \cdots & \cdots & \cdots & \vdots & \cdots & \cdots & \cdots \\ 0 & 0 & 0 & \vdots & \mathbf{D}^{-N+2} & \mathbf{E} & 0 \\ 0 & 0 & 0 & \vdots & 0 & \mathbf{D}^{-N+1} & \mathbf{E} \\ 0 & 0 & 0 & \vdots & 0 & 0 & \mathbf{D}^{-N} \end{pmatrix} \begin{pmatrix} \sigma^{N} \\ \sigma^{N-1} \\ \sigma^{N-2} \\ \vdots \\ \sigma^{-N+2} \\ \sigma^{-N+1} \\ \sigma^{-N} \end{pmatrix} \tag{8.31}$$

Consequently, the approximate solution can be defined as a sequence with the first term given by

$$\sigma^{-N} = \left(\mathbf{D}^{-N}\right)^{-1} \eta^{-N}, \tag{8.32a}$$

and the general recursive term by

$$\sigma^{n} = \left(\mathbf{D}^{n}\right)^{-1} \left(\eta^{n} - \mathbf{E}\sigma^{n-1}\right). \tag{8.32b}$$

With the help of these three recursive sequences we define the solution of equation (8.22). This method can be generalised to the case of the n-level system.

The n-level system

In the case of the n-level system, we can again define two sequences. The first sequence gives the diagonal terms $\mathbf{D}^{n}$ with the first term

$$\mathbf{D}^{N} = \mathbf{L}^{N} - \mathbf{E}\left(\mathbf{L}^{N+1}\right)^{-1}\mathbf{E}, \tag{8.33a}$$

the general recursive term

$$\mathbf{D}^{n} = \mathbf{L}^{n} - \mathbf{E}\left(\mathbf{D}^{n+1}\right)^{-1}\mathbf{E}, \tag{8.33b}$$

and the last term

$$\mathbf{D}^{-N} = \mathbf{L}^{-N} - \mathbf{E}\left(\mathbf{L}^{-N-1}\right)^{-1}\mathbf{E} - \mathbf{E}\left(\mathbf{D}^{-N+1}\right)^{-1}\mathbf{E}. \tag{8.33c}$$

The free member sequence is defined by the first term

$$\eta^0 = \Gamma\rho^{(0)}, \tag{8.34a}$$

and the general recursive term

$$\eta^n = -\mathbf{E}\left(\mathbf{D}^{n+1}\right)^{-1}\eta^{n+1}. \tag{8.34b}$$

From these two recursive sequences, the solution can be determined in a recursive manner with the initial term

$$\sigma^{-N} = \left(\mathbf{D}^{-N}\right)^{-1}\eta^{-N} \tag{8.35a}$$

and the general recursive term

$$\sigma^n = \left(\mathbf{D}^n\right)^{-1}\left(\eta^n - \mathbf{E}\sigma^{n-1}\right). \tag{8.35b}$$

In this section, we rigorously deduced the solution of the density matrix equations in the frequency domain. This solution can be defined as the limit of a convergent sequence. The terms of this sequence are the approximate solutions, calculated from the interaction matrices between the different harmonics, truncated at the order N. We showed that this sequence converges as $1/N$ as well for the two level system as for the general case of a n-level system. Finally, a recursive resolution method is described for determining the solutions at the order N.

8.3 The n-level system under bichromatic excitation

In the preceding section, we treated the case of an n-level system under monochromatic excitation. We established that such an excitation at high intensity induces high harmonic generation of the electromagnetic field (the response of the system is at frequencies which are multiples of the excitation field). Likewise a bichromatic excitation

induces the response of the system at the frequencies corresponding to the linear combinations of the two excitation frequencies ω_1 and ω_2 with whole number coefficients (see also [93, 94])

$$\omega_{response} = n\omega_1 + m\omega_2 \quad with \;\; n, m \in \mathbb{N}.$$

This response of the system, at new frequencies, can be used in the characterisation of materials presenting non-linear optical effects. From an experimental point of view, the creation of new frequencies allows the spectral filtering of the response of the system and thus the measurement of a background free measure. Furthermore, when the difference between the two excitation frequencies is the same order of magnitude as the inverse of one of the relaxation times of the system, the response of the system presents a phenomena of "resonances". From these phenomena, the relaxation times can be deduced even if the length of the impulse is longer than the relaxation time. For this reason we have generalised the monochromatic solution method to the case of the bichromatic excitations.

The solution of the density matrix equation is more complex in the case of a bichromatic excitation. Contrary to monochromatic excitation, bichromatic excitation is generally non periodic. This is the case if the two frequencies are not commensurable [95]. This non periodicity induces, after the Fourier transformation of the density matrix equation, an algebraic equation that can no longer be written under the simple form of a matrix relation between the density matrices at different harmonic frequencies. In the following, we generalise the method form monochromatic excitation to the bichromatic case. This generalisation consists of a change of a matrix relation (second order tensor) to a relation using a fourth order tensor. Finally, the result is verified for the case where the two frequencies are commensurable and therefore the periodic excitation for this case can be treated as a generalised monochromatic excitation.

8.3.1 The Fourier transformation

A bichromatic excitation is characterised by the two amplitudes E_1 and E_2 and the two frequencies ω_1 and ω_2 of two sinusoidal fields. The sum of these two fields forms the

excitation

$$E(t) = E_1 \cos(\omega_1 t) + E_2 \cos(\omega_2 t). \tag{8.36}$$

The density matrix equation (6.12) with this excitation field is written

$$\begin{aligned} \frac{d\rho_{ij}}{dt} &= \frac{1}{i\hbar}(H_i^k \rho_{kj} - \rho_{ik} H_j^k) - \Gamma_{ij}^{kl}(\rho_{kl} - \rho_{kl}^{(0)}) \\ &+ \frac{1}{i\hbar} E_1 \cos(\omega_1 t)(\mu_i^k \rho_{kj} - \rho_{ik}\mu_j^k) \\ &+ \frac{1}{i\hbar} E_2 \cos(\omega_2 t)(\mu_i^k \rho_{kj} - \rho_{ik}\mu_j^k). \end{aligned} \tag{8.37}$$

Its Fourier transformation has the following tensor form

$$\begin{aligned} -\delta(\omega)\Gamma_{ij}^{kl}\rho_{kl}^{(0)} &= \left(L_{ij}^{kl} - i\omega - \Gamma_{ij}^{kl}\right)\hat{\rho}_{kl}(\omega) + E_{ij}^{kl}\hat{\rho}_{kl}(\omega - \omega_1) \\ &+ E_{ij}^{kl}\hat{\rho}_{kl}(\omega + \omega_1) + F_{ij}^{kl}\hat{\rho}_{kl}(\omega - \omega_2) + F_{ij}^{kl}\hat{\rho}_{kl}(\omega + \omega_2) \end{aligned} \tag{8.38}$$

with

$$E_{ij}^{kl} = \frac{E_1}{2i\hbar}\left(\delta_j^l \mu_i^k - \delta_i^k \mu_j^l\right) \tag{8.39a}$$

$$F_{ij}^{kl} = \frac{E_2}{2i\hbar}\left(\delta_j^l \mu_i^k - \delta_i^k \mu_j^l\right). \tag{8.39b}$$

Equation (8.38) shows the links between the composing frequencies of the density matrix. This dependence is similar to the one outlined in figure 8.3 for the monochromatic excitation. In this case the dependence makes the system respond at the frequencies $\omega - \omega_1$, $\omega + \omega_1$, $\omega - \omega_2$ and $\omega + \omega_2$.

As for the monochromatic excitation, we are interested in the stationary solutions of the differential equation (8.37). The Fourier transformation of the density matrix equation implies a decomposition of the spectral response following the two frequencies of excitation. In other words, a non zero solution of equation (8.38) can only be found for

$$\omega_{nm} = n\omega_1 + m\omega_2 \quad \text{with } n, m \in \mathbb{N}. \tag{8.40}$$

This decomposition of the spectrum into frequencies indexed by two whole numbers is unique only if the two frequencies are not commensurable. In the case where the two frequencies are commensurable, an infinity of pairs (n, m) give the same frequency ω_{nm}. In the following, we decompose the response of the system onto these two frequencies. Therefore, a unique decomposition is useful. We show at the end of this section that this decomposition remains valid for the bichromatic excitations with commensurable frequencies.

In the case of a non commensurable bichromatic excitation, the solution of the density matrix equation is composed only of terms at the frequency ω_{nm} corresponding to the mixed harmonic of the two excitation frequencies

$$(\hat{\rho}_{ij}(\omega)) = \sum_{n,m=-\infty}^{\infty} \hat{\rho}^{nm}\delta(\omega_{nm} - \omega). \tag{8.41}$$

The interaction between the harmonics of the two frequencies occurs through the following three tensors:

$$\mathbf{L}_{nm} = \left(L_{ij}^{kl} - i\omega_{nm} I_{ij}^{kl} - \Gamma_{ij}^{kl}\right), \tag{8.42a}$$

$$\mathbf{E_1} = \left(E_{ij}^{kl}\right), \tag{8.42b}$$

$$\mathbf{E_2} = \left(F_{ij}^{kl}\right). \tag{8.42c}$$

With the help of these tensors, equation (8.38) can be put into the form of a infinite system of linear equations that can be written in a tensor form

$$\mathbf{M}_{nm}^{pq}\hat{\rho}^{nm} = \delta_0^p\delta_0^q\Gamma\rho^{(0)}, \tag{8.43a}$$

with

$$\mathbf{M}_{nm}^{pq} = \delta_n^p\delta_m^q\mathbf{L}_{nm} + \delta_{n+1}^p\mathbf{E_1} + \delta_{n-1}^p\mathbf{E_1} + \delta_{m+1}^q\mathbf{E_2} + \delta_{m-1}^q\mathbf{E_2}. \tag{8.43b}$$

In these relations, we notice the similarity between the equations found while treating the monochromatic case (8.15). The bichromatic excitation is simply the generalisation of the monochromatic one by transforming a second order tensor relation (matrix relation) into a fourth order tensor relation for the two level system and by transforming

a fourth order tensor relation into a sixth order tensor relation for the general n-level system.

The generalisation of this procedure to any number of monochromatic excitations r adds to the equation (8.43b) the supplementary terms $\mathbf{E_i}$ (with $i = 3...r$) and changes the order of the tensor $\mathbf{M}$ to $2r$ (the order tensor relation is then $2r + 2$).

In the case where the two frequencies are commensurable, their ratio is a rational number. This property implies that the frequencies ω_{nm} for different indices n and m correspond to the same frequency. Let the ratio between the two frequencies be defined by the denominator q and the numerator p

$$\frac{\omega_1}{\omega_2} = \frac{p}{q} \tag{8.44}$$

where p and q have no common factor. Then the frequencies

$$\omega_{(n+jq)(m-jp)} = (n + jq)\omega_1 + (m - jp)\omega_2 \quad \text{with } n, m, j \in \mathbb{N}. \tag{8.45}$$

are the same frequency.

Using this property, equation (8.38) can be written in a matrix form as in the case of the monochromatic excitation. Physically, this form is possible because the bichromatic excitation is periodic in the case of commensurable sinusoidal fields. Consequently, this case can be treated in the same manner as the monochromatic case. The basic frequency of this commensurable excitation is given by

$$\Delta\omega = \frac{\omega_1}{p} = \frac{\omega_2}{q} \tag{8.46}$$

which allows us to introduce the decomposition of the spectrum following the multiple frequencies of $\Delta\omega$. The new decomposition of the frequency is

$$\omega_n = n\Delta\omega \quad \text{with } n \in \mathbb{N}. \tag{8.47}$$

Between this new decomposition and the one with two indices we have the following relation

$$\begin{aligned} \omega_{nm} &= p\omega_n + q\omega_m \\ &= \omega_{p*n+q*m} \end{aligned}$$

which implies that all the mixed harmonics of the two frequencies are in reality the simple harmonics of the fundamental frequency given by $\Delta\omega$. Defining the new Lagrangian operator

$$\mathbf{L}_n = \left(L_{ij}^{kl} - i\omega_n I_{ij}^{kl} - \Gamma_{ij}^{kl}\right),$$

and using the interaction tensors $\mathbf{E_1}$ and $\mathbf{E_2}$ defined in equations (8.42b) and (8.42c) the infinite system of linear equations can be written

$$\mathbf{M}_n^p \hat{\rho}^n = \delta_0^p \Gamma \rho^{(0)}, \tag{8.48a}$$

with

$$\mathbf{M}_n^p = \delta_n^p \mathbf{L}_n + \delta_{n+p}^p \mathbf{E_1} + \delta_{n-p}^p \mathbf{E_1} + \delta_{n+q}^q \mathbf{E_2} + \delta_{n-q}^q \mathbf{E_2} \tag{8.48b}$$

where

$$(\hat{\rho}_{ij}(\omega)) = \sum_{n=-\infty}^{\infty} \hat{\rho}^n \delta(\omega_n - \omega). \tag{8.49}$$

This relation between the harmonic frequencies of $\Delta\omega$ written in a matrix form (see equation (8.13)) is composed of a diagonal part originating in the tensors $\mathbf{L}_n$ and of two secondary diagonals offset with respect to the principal diagonal by p and of q and originating respectively from the tensors $\mathbf{E_1}$ and $\mathbf{E_2}$.

The system of equations (8.43) is equivalent to the system of equations (8.48). To show this equivalence it is necessary to define the relation between the density matrices ρ^n and ρ^{nm}. For this, the solutions (n_i, m_i) of the Diophantine equation must be used

$$pn_i + qm_i = j. \tag{8.50}$$

Then the density matrix defined in the equation (8.49) is

$$\rho^j = \sum_i \rho^{n_i m_i}. \tag{8.51}$$

Using this same summation rule on the system of equations (8.43), we can verify that it transforms into the system of equations (8.48).

A direct application of this property follows from the demonstration itself. The equivalence between these two representations makes possible the usage of our general non-commensurable resolution method for the commensurable bichromatic excitations. This is the case for experiments where the pump and the probe are degenerate ($\omega_1 = \omega_2$) or at another harmonic frequency ($\omega_1 = 2\omega_2$ for example).

8.4 Summary

In this chapter, we obtained a method for finding the solution of the density matrix equations for an n-level system. This method is based on the joint employment of the continuous fraction method and the Fourier transformation. The method is illustrated in the case of a two level system and more generally n-levels excited by monochromatic and bichromatic excitations.

Chapter 9

Applications: Chromatic excitation

9.1 Introduction

We review in this chapter some effects that can be explained by the n-level density matrix equations solved using our method. These effects include the saturation of the response of the system at the fundamental frequency when it is submitted to high intensity excitation. During the saturation phenomena the energy received by the system is redistributed to the higher harmonics. Thus, we show the observed plateau in the generation of the high harmonics. With our method, we deduce, from the polarisations at the fundamental and at the third harmonic, the saturation intensity and the dynamic Stark shift. We also show, the multiple photon resonances as well as their reciprocal Stark shift as a function of the excitation intensity. This last effect helps to understand the oscillation effects of the system response as a function of the excitation amplitude. Further, we apply this method to two concrete cases of bichromatic excitations. First, we study the "non degenerate pump-probe" configuration which is modelled with the help of the general relations obtained in the second section. The considered bichromatic excitation is composed of a low and a high intensity beam. The first can be treated as a first order perturbation (method similar to [95]), whereas, the second beam is treated with our method and is valid also for high intensities. The second configuration studied corresponds to the "non-degenerate four-wave mixing" setup. In this case the two beams are of high intensity [96,97] and must be treated using the fourth order tensor formalism.

For quantum systems we use an ideal two level system and an excitonic system (n-level system). Further, from the general solution, we deduce a simplified version taking

into account the properties of the physical system (for example $\omega_1 \approx \Omega_0 \gg \Gamma_2 \gg \Gamma_1$). This facilitates the comparison with experimental results.

9.2 One wave excitation

In the following, the recursive resolution method is applied to the two level system. To simplify the solution in the form of a continuous fraction, we use a centro-symmetric system ($\mu_{aa} = \mu_{bb} = 0$). Considering this symmetry, the interaction between two adjacent harmonics in the sequence (8.29), characterised by the matrix $\mathbf{E}\,(\mathbf{D})^{-1}\,\mathbf{E}$, has a special form where only two terms A_p and B_p can be distinguished

$$\mathbf{E}\left(\mathbf{D}^{p+1}\right)^{-1}\mathbf{E} = \begin{pmatrix} A_p & 0 & 0 & -A_p \\ 0 & B_p & -B_p & 0 \\ 0 & -B_p & B_p & 0 \\ -A_p & 0 & 0 & A_p \end{pmatrix}. \tag{9.1}$$

Introducing the following notation:

$$\alpha_n = \frac{1}{\frac{1}{\Gamma_2+i(\omega_0+n\omega_1)} + \frac{1}{\Gamma_2+i(n\omega_1-\Omega_0)}}, \tag{9.2a}$$

$$\beta_n = \frac{1}{2}(\Gamma_1 + in\omega_1), \tag{9.2b}$$

$$a = \frac{E_1\mu}{2\hbar}, \tag{9.2c}$$

the expressions of the density matrices at the different harmonics can be simplified. When using the point symmetry property (9.1) and the above notation (9.2), one can write the recurrent sequence (8.29) as

$$A_n = \frac{a^2}{B_{n+1} - \alpha_{n+1}} \tag{9.3a}$$

and

$$B_n = \frac{a^2}{A_{n+1} - \beta_{n+1}} \tag{9.3b}$$

where only the two distinct elements of the matrix (9.1) are treated. This sequence can also be written in the form of a continuous fraction

$$A_n = \cfrac{a^2}{\cfrac{a^2}{\cfrac{a^2}{\cfrac{a^2}{\vdots}-\alpha_{n+3}}-\beta_{n+2}}-\alpha_{n+1}} \tag{9.4a}$$

and

$$B_n = \cfrac{a^2}{\cfrac{a^2}{\cfrac{a^2}{\cfrac{a^2}{\vdots}-\beta_{n+3}}-\alpha_{n+2}}-\beta_{n+1}}. \tag{9.4b}$$

With the help of these matrix elements, we can specify the solution of the density matrix at zero frequency

$$\hat{\rho}^0 = \frac{1}{2A - \Gamma_1}(A\mathbb{I} - \Gamma_1\rho^{(0)}) \tag{9.5}$$

with

$$A = A_0 + c.c. \tag{9.6}$$

and where *c.c.* designates the complex conjugate and $\mathbb{I}$ the unity matrix.

From the density matrix at zero frequency, we can deduce the response at the fundamental frequency, that is to say the response having the same frequency as the excitation. For that, it is necessary to use the triangular matrix of equation (8.31). With the help of this matrix and putting

$$\gamma_n = \Gamma_2 + i(\omega_0 + n\omega_1) \tag{9.7}$$

the populations and the coherences at the first harmonic are respectively

$$\hat{\rho}^1_{aa} = \hat{\rho}^1_{bb} = 0, \tag{9.8a}$$

$$\hat{\rho}^1_{ab} = -\frac{i\Gamma_1\rho^{(0)}_D\gamma_1 A_0}{a(2A - \Gamma_1)(\gamma_1 + \gamma^*_{-1})}, \tag{9.8b}$$

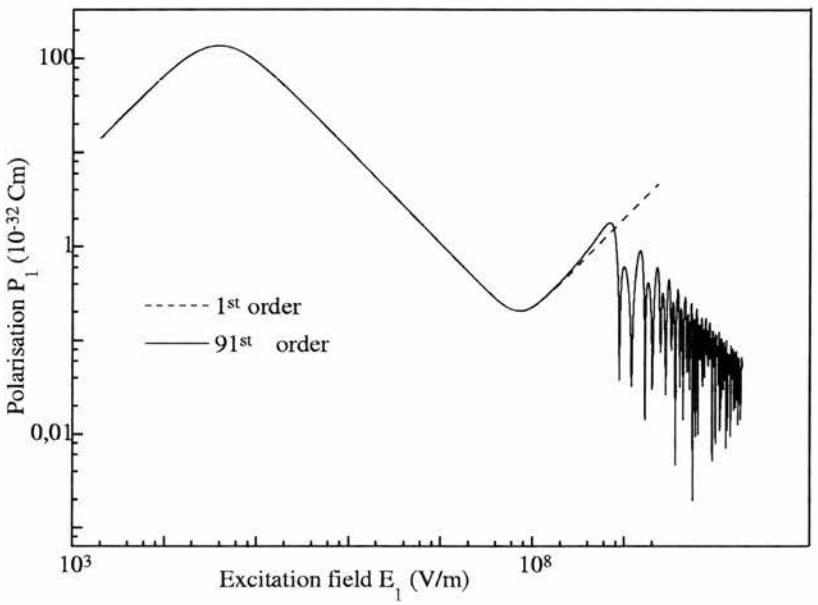

Figure 9.1: Polarisation response of the two level system at the first harmonic as a function of the excitation amplitude on a logarithmic scale.

$$\hat{\rho}^1_{ba} = \frac{i\Gamma_1 \rho_D^{(0)} \gamma^*_{-1} A_0}{a(2A - \Gamma_1)(\gamma_1 + \gamma^*_{-1})}. \tag{9.8c}$$

The point symmetry of the two level system gives no population at this frequency while the coherences give the induced polarisation

$$P_{\omega_1}(E_1, \omega_1) = \frac{\Gamma_1 \Omega_0 \rho_D^{(0)} A_0}{a(2A - \Gamma_1)(\gamma_1 + \gamma^*_{-1})} \tag{9.9}$$

that is represented in figure 9.1. In this figure we observe several distinct domains of the polarisation response. For the weak excitation amplitudes, the response of the system is linear. In this domain, the solution found corresponds to the one calculated with the help of the perturbation theory. From a certain amplitude of excitation E_1^{sat}, a saturation of the response becomes visible. For higher excitation, the amplitude of the polarisation response diminishes. This last amplitude domain can no longer be treated by the perturbation theory. It corresponds to the instant when the amplitude of the exciting field implies that the terms of the secondary diagonal in equation (8.15a) become greater than the term $\mathbf{M_0^0}$ (first diagonal term). In order to find a solution that demonstrates this saturation behaviour, it is necessary to take into account the dependence between the different harmonics at least to first order.

When introducing the different definitions in equation (9.9) and in the case where

$$\omega_1 \approx \Omega_0 \gg \Gamma_2 \gg \Gamma_1 \tag{9.10}$$

the polarisation at the first and at the third harmonic can be written

$$\hat{P}_1(E_1,\omega_1) \approx \frac{E_1\Gamma_1\hbar\mu_{ab}\mu_{ba}\Omega_0\rho_D^{(0)}\Gamma_1\left[E_1^2\mu_{ab}\mu_{ba}+2\hbar^2\gamma_1^*\gamma_{-1}\right]}{2\Gamma_1\hbar^4\gamma_1^*\gamma_{-1}\gamma_1\gamma_{-1}^*+4E_1^2\mu_{ab}\mu_{ba}\Gamma_2\hbar^2(\Omega_0^2+\omega_1^2)}, \tag{9.11a}$$

$$\hat{P}_3(E_1,\omega_1) \approx \frac{E_1^2\mu_{ab}\mu_{ba}}{2\hbar^2\gamma_3\gamma_{-3}^*}\hat{P}_1(E_1,\omega_1). \tag{9.11b}$$

We remark here that the dielectric susceptibility $\chi_1(\omega_1)$ defined from this polarisation fulfils the Kramers-Kronig relation (see §I.C) in the case where the terms in E_1^2 are neglected. Moreover, in this case, the dielectric susceptibility fulfils the condition

$$\chi(-\omega_1) = \chi^*(\omega_1)$$

which corresponds to a real polarisation after Fourier transformation.

In the case where the terms in E_1^2 are no longer negligible (high excitation intensity), the Kramers-Kronig relation is no longer fulfilled because the system is becoming non-linear. The response of the system cannot then be described by the convolution of the Dirac response and excitation field. This is the case for excitation amplitudes greater than

$$E_{max} = \sqrt{\frac{\Gamma_1\hbar^2(\omega_1^2-\Omega_0^2)^2+2\Gamma_1\Gamma_2^2\hbar^2(\omega_1^2+\Omega_0^2)}{2\mu_{ab}\mu_{ba}\Gamma_2(\Omega_0^2+\omega_1^2)}}. \tag{9.12}$$

With the help of the measurement of this saturation amplitude as a function of the excitation frequency, we can determine the product of relaxation times (transverse and longitudinal). In fact, by virtue of (9.12), this product is proportional to the minimal saturation amplitude (see figure 9.2). Further, their ratio is proportional to the slope of the asymptote of this saturation graph.

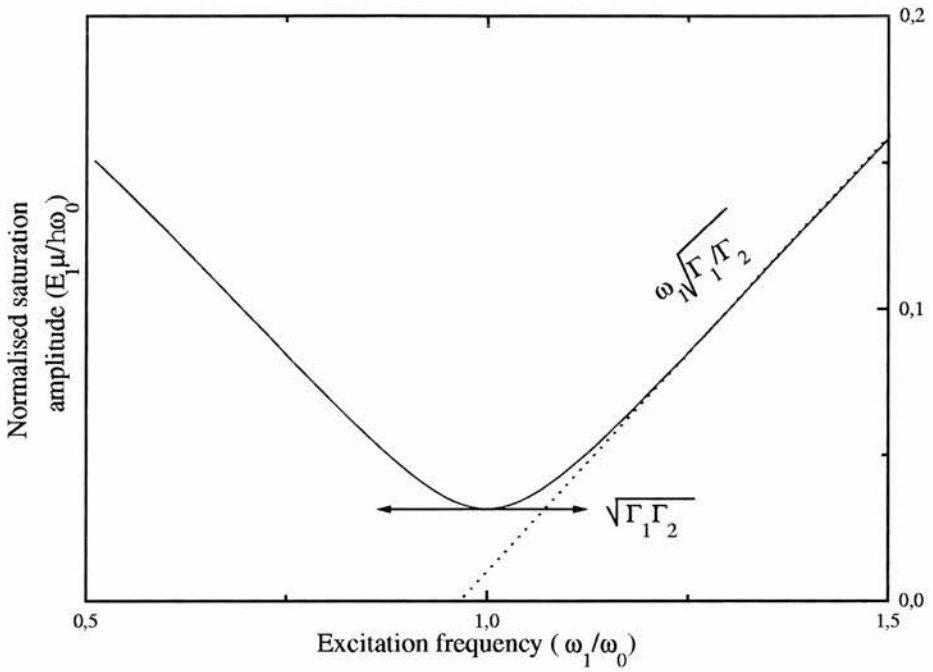

Figure 9.2: The saturation amplitude of a two level system as a function of the excitation frequency. From this graph, the ratio and the product of the two relaxation times (transverse $T_2 = 1/\Gamma_2$ and longitudinal $T_1 = 1/\Gamma_1$) can be determined.

With the help of equation (9.11a), we determine the amplitude from which the response of the system begins to grow again

$$E_{min} = \frac{\sqrt{2}\hbar}{\sqrt{\mu_{ab}\mu_{ba}}}\sqrt[4]{4\omega_1^2\Gamma_2^2 + (\Omega_0^2 - \omega_1^2)^2}. \tag{9.13}$$

For excitation amplitudes greater than E_{min}, the response at the fundamental harmonic exhibits a succession of periodic peaks (see figure 9.3). The excitation amplitude for the n^{th} saturation peak is given by

$$E_n^{sat} \approx \Omega_0\hbar\frac{n^2 - 1}{\sqrt{2\mu_{ab}\mu_{ba}}n}. \tag{9.14}$$

Mathematically, this periodicity can be explained by the almost periodic structure of the interaction matrix between the different harmonics of the density matrix. This periodicity appears also in the expression for the different elements (9.4).

This periodicity of response at the fundamental frequency can be explained by considering the behaviour of the system as a function of the excitation frequency for different excitation amplitudes. Figure 9.4 shows such a spectrum. For weak excitation ampli-

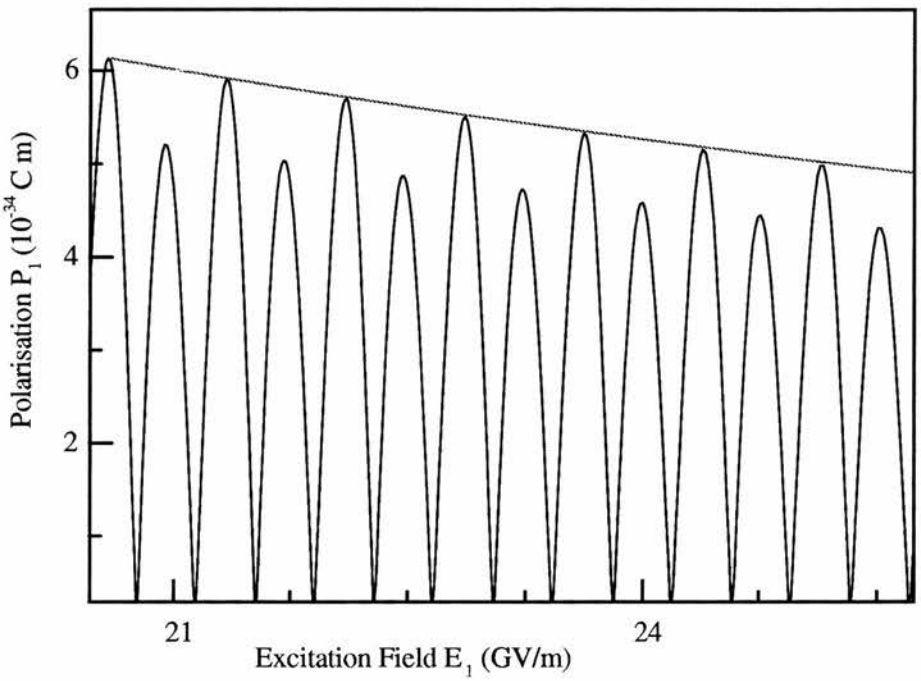

Figure 9.3: The response of the system at the fundamental harmonic as a function of the excitation amplitude for an excitation much greater than the saturation amplitude (9.12).

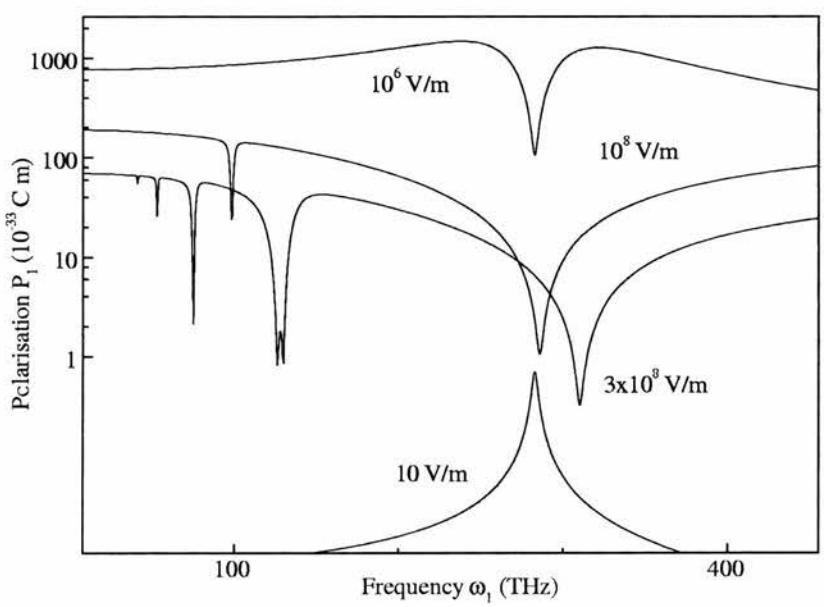

Figure 9.4: The response of a two level system at the fundamental frequency as a function of the excitation frequency for different excitation amplitudes.

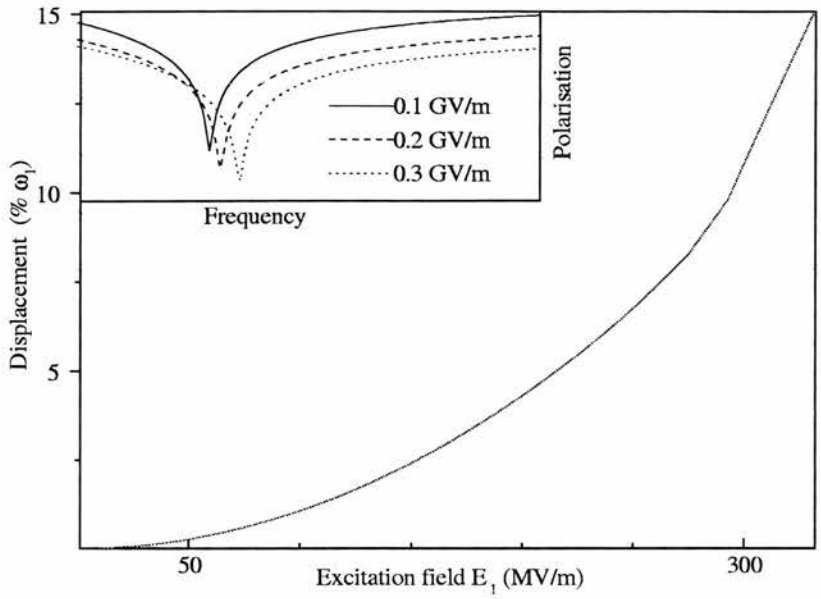

Figure 9.5: Shift towards the blue of the saturation frequency of the fundamental harmonic (figures 9.4) as a function of the excitation amplitude.

tudes, corresponding to a linear regime, the response of the system has a Lorentzian behaviour where the maximal response is given when the excitation frequency is in resonance with the system eigen-frequency $\Omega_0/(2\pi)$. Increasing the amplitude of the excitation, a saturation phenomenon appears first at resonance and next when an odd number of photons are in resonance ($\omega = \Omega_0/3$, $\omega = \Omega_0/5$, ...). This saturation corresponds to the absorption of several photons.

To the multi-photon absorption phenomenon one has to add the optical Stark shift which corresponds to a shift towards the blue of the fundamental resonance (figures 9.5)

$$\hbar\omega_{Stark} = \sqrt{\hbar^2\Omega_0^2 + 2E^2\mu_{ab}\mu_{ba}}, \tag{9.15}$$

which is also present in the multi-photon resonances.

With the help of these two effects (the multi-photon resonances fig. 9.4 and the shift towards the blue fig. 9.5) we can explain the periodic amplitude oscillations of the response of the system when the excitation amplitude increases (9.3). To show the link between these two phenomena, let us look at the behaviour of the saturation of the three photon absorption ($\omega = \Omega_0/3$). When the amplitude of the excitation increases, this saturation undergoes a movement towards the blue. For sufficiently large

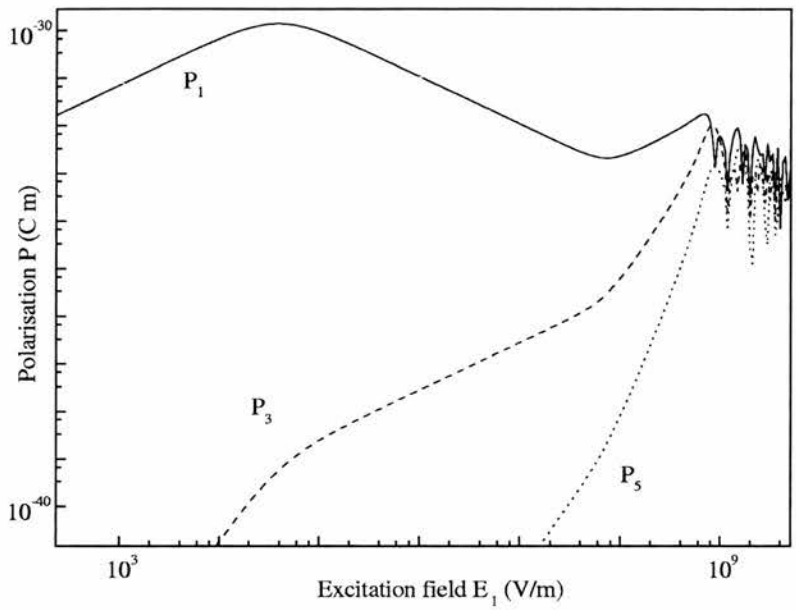

Figure 9.6: Response of a two level system at the fundamental frequency, at the third harmonic ($\omega = 3\omega_1$) and at the fifth harmonic ($\omega = 5\omega_1$) as a function of the excitation amplitude.

amplitudes, this shift makes the three photon saturation correspond to the fundamental resonance of the system. We notice then a new saturation of the fundamental resonance of the system ($\omega = \Omega_0$). This corresponds in reality to the saturation of the shifted three photon resonance towards the blue. This effect repeats itself for all the multi-photon resonances. Whenever such a resonance crosses the fundamental resonance, a fast decrease of the response can be observed.

So far, we were interested in the response of the system at the fundamental harmonic. In order to evaluate the polarisations for other harmonics, it is necessary to employ the recurrent sequence (8.32). Considering the new notation, the elements of the density matrix for the odd harmonics (centro-symmetrical system) can be written:

$$\hat{\rho}_{ab}^{n+2} = -\frac{B_n \gamma_{n+2} (\hat{\rho}_{ab}^{n} - \hat{\rho}_{ba}^{n}) A_{n+2}}{(\gamma_{n+2} + \gamma_{-n-2}^{*}) a^2} \tag{9.16a}$$

and

$$\hat{\rho}_{ba}^{n+2} = \frac{B_n \gamma_{-n-2}^{*} (\hat{\rho}_{ab}^{n} - \hat{\rho}_{ba}^{n}) A_{n+2}}{(\gamma_{n+2} + \gamma_{-n-2}^{*}) a^2}. \tag{9.16b}$$

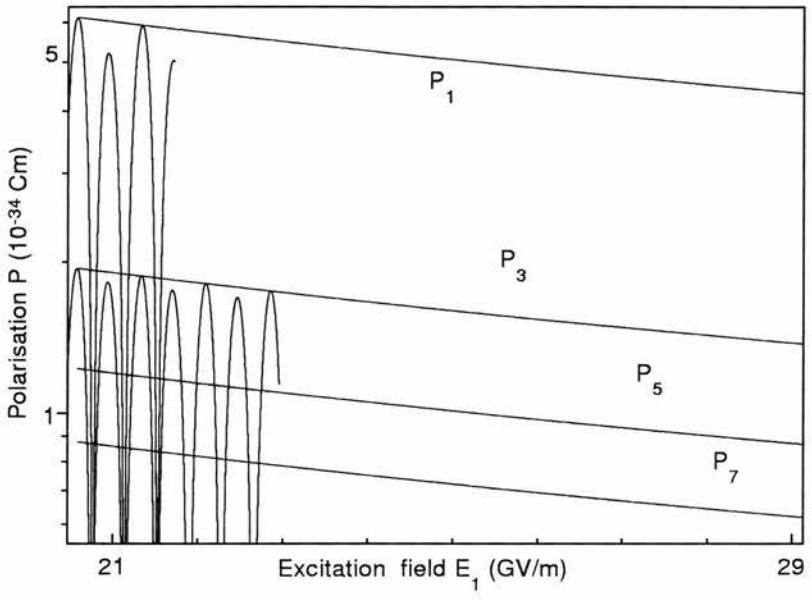

Figure 9.7: Response of a two level system at the fundamental frequency, at the third harmonic ($\omega = 3\omega_1$) and at the fifth harminic ($\omega = 5\omega_1$) as a function of the excitation amplitude which is largely above the saturation amplitude (9.12).

The populations $\hat{\rho}_{aa}^{n+2}$ and $\hat{\rho}_{bb}^{n+2}$ are zero for these harmonics. From these expressions, the response at the fundamental harmonic as well as at the third ($\omega = 3\omega_1$) and at the fifth ($\omega = 5\omega_1$) are represented in the case of weak excitations (figure 9.6) and of strong excitation (figure 9.7).

As for the fundamental frequency, the responses at higher harmonics show several regimes of the system depending on the excitation amplitude. For weak excitations, the behaviour is linear for the first harmonic, cubic for the third harmonic and generally at the power n for the n^{th} harmonic. For amplitudes higher than the saturation amplitude (9.2), all the polarisation responses change as the amplitude to the power $n-2$. For example the third harmonic is proportional to the excitation amplitude. When the excitation increases even more in amplitude, the different harmonics undergo periodic oscillations similar to the fundamental harmonic..

In order to better understand these periodic oscillations, we represent in figure (9.8) the behaviour of the response up to the 21^{st} harmonic for two different excitation amplitudes. Two possible responses appear: a "plateau" followed by a fast decrease of the response as a function of the harmonic order. The harmonics being part of this plateau are those that are saturated and that present an identical oscillating behaviour. As the

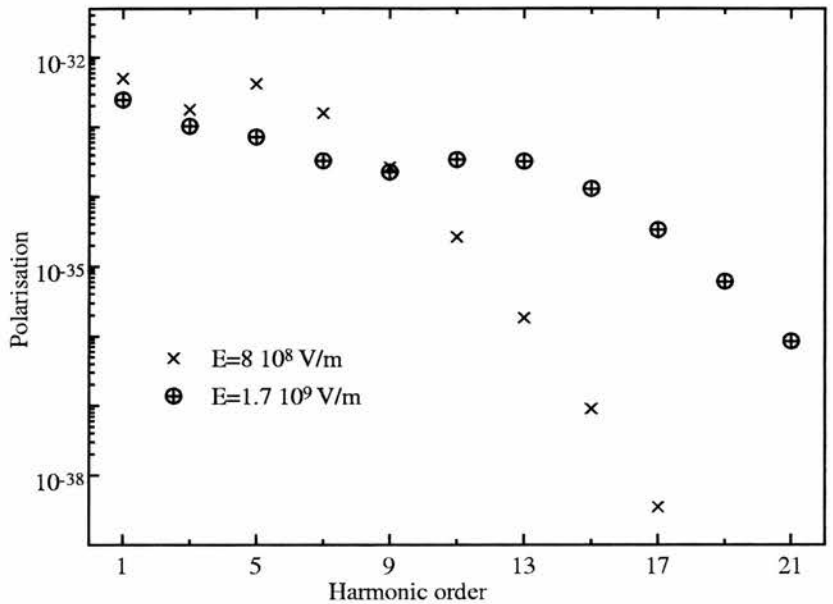

Figure 9.8: The relative amplitudes of the response of a two level system at different harmonics as a function of the harmonic number for two excitation amplitudes.

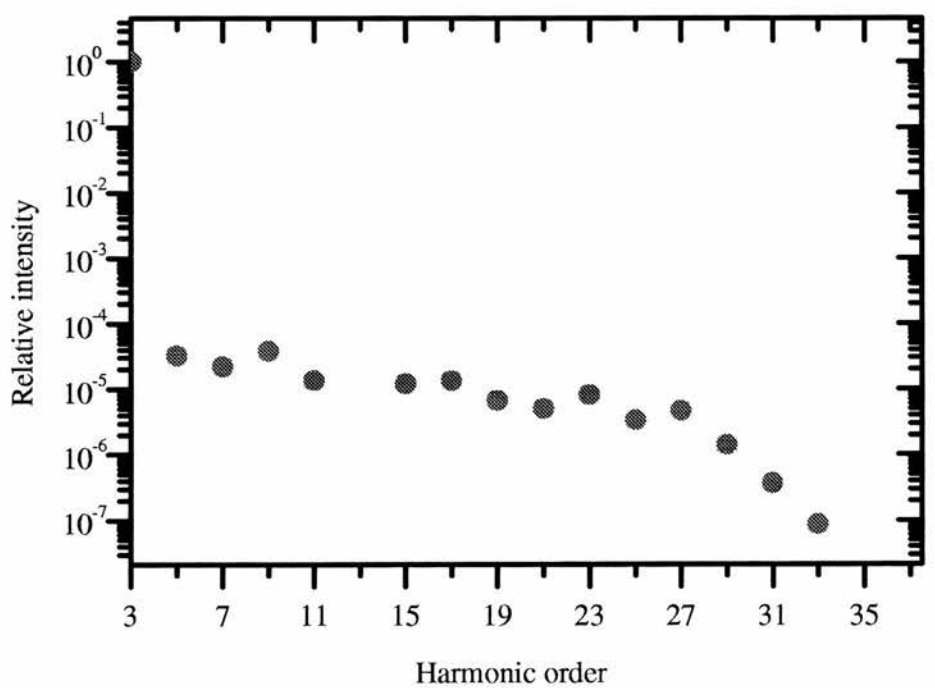

Figure 9.9: The relative amplitudes of the high harmonics generated in argon with the help of a Nd:YAG laser [98].

excitation amplitude increases, this plateau includes more and more harmonic orders. This phenomenon is observed experimentally in gases such as xénon, krypton and argon (density between 10^{17} and 10^{18} atoms/cm^3), excited at a wavelength of 1064nm (intensity between 10^{13} and 10^{14} W/cm^2). In this case, a very effective high harmonic generation can be measured (see figures 9.9 and [99]) reaching the 31^{st} order. This result completes those obtained for an excitation at a smaller wavelength in these same systems [100]. More recently, this generation of high harmonic orders has been observed up to order 135 in neon and 57 in argon [98,101]).

Several [102] theoretical approaches are used to model this phenomenon. They can be divided into several groups. On one side we have the research of the direct solution to Schrödinger's time dependent equation. This is solved numerically for a one dimensional atom [103,104] but also for the more elaborate case of three dimensions [105–107]. This numerical solution in three dimensions is used in the case of a semiconductor [108] where high harmonic generation can be observed. As an alternative to the direct solution of Schrödinger's time dependent equation, this phenomenon can be treated using the Floquet states [109,110]. Yet, another possible approach is the classical treatment of an electron in the field of a proton subject [109,111] to a monochromatic excitation. This method uses the classical trajectory of the electron and the Monte-Carlo solution to show a plateau in the high harmonic generation. Finally, alternative models are proposed in the literature which approximate the atomic potential by a short range interaction [112] or the numerical solution of Bloch's equation (without taking relaxation terms into account) for a two level system [79].

Our result, shown in figure 9.8, corresponds to this last approach, generalised to include relaxation phenomena and solved in an analytical manner. The advantage of such a solution is the possibility of determining the harmonic order "cut off". This cut off corresponds to the order N at which one can truncate the dependence between the different harmonics. It can be evaluated as

$$n_{cutoff} = \frac{1}{\omega_1}\sqrt{\frac{E_1^2}{\mu_{ab}\mu_{ba} + \Omega_0^2}}. \tag{9.17}$$

9.2.1 Monochromatic excitation of an excitonic system

Excitonic systems in semiconductors give a good example of n-level systems. These correspond principally to an electron-hole pair created in our case by optical means (absorption of a photon) and held together by Coulomb interaction. The energy levels E_n of such an electron-hole pair can be calculated in the same manner as those of a hydrogen atom [63]

$$E_n = E_g - \frac{\mu e^4}{2\epsilon^2 \hbar^2} \frac{1}{n^2} \tag{9.18}$$

where μ is the reduced effective mass of the electron and hole, e the charge of the electron, ϵ the dielectric constant and E_g the energy gap of the semiconductor. For low dimensional semiconductors such as quantum dots, the excitonic energy levels change in comparison with those of hydrogen due to the confinement of the exciton [113, 114]. These excitonic systems can be modelled, to a first approximation, by a two level system, made out of a ground level (no exciton) and the first excitonic level E_1 (n = 1).

When these quantum systems interact with the electromagnetic wave the exciton appears. Further, this corresponds to the induced polarisation that represents the response of the system to the applied external field. Usually, the excitonic levels reveal themselves by a series of resonance peaks (in transmission or reflection) when the photonic energy of the excitation equals the energy of the excitonic levels (9.18).

In order to show the differences between the response of a two level system and an n-level system, we take a look at the response of a four level system at the excitation frequency (figures 9.10). The four considered levels correspond, in energy and dipole moment, to the first three levels of an exciton [113].

In this case we use the same procedure as for the two level system treated previously. The solution for an n-level system is determined with the help of recursive relations

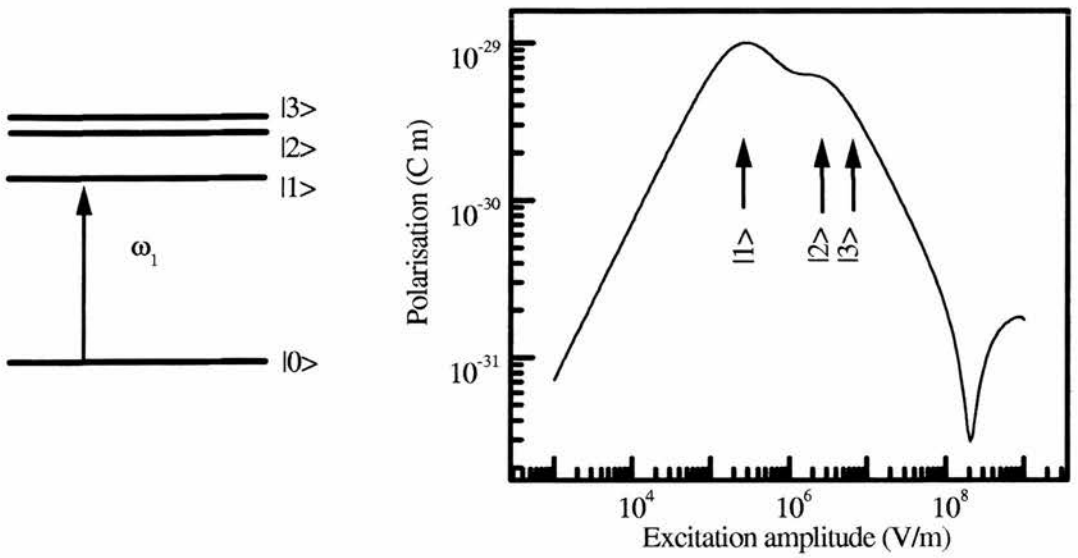

Figure 9.10: Response of an excitonic system at the excitation frequency as a function of the excitation amplitude. The three first excitonic levels are taken into account.

(8.33). In the case of the truncation at the first order, the different terms are:

$$\begin{aligned}
\mathbf{D}^1 &= \mathbf{L}^1 - \mathbf{E}\left(\mathbf{L}^2\right)^{-1}\mathbf{E} \\
\mathbf{D}^0 &= \mathbf{L}^0 - \mathbf{E}\left(\mathbf{D}^1\right)^{-1}\mathbf{E} \\
\mathbf{D}^{-1} &= \mathbf{L}^{-1} - \mathbf{E}\left(\mathbf{L}^{-2}\right)^{-1}\mathbf{E} - \mathbf{E}\left(\mathbf{D}^0\right)^{-1}\mathbf{E} \\
\eta^0 &= \Gamma\rho^{(0)} \\
\eta^{-1} &= -\mathbf{E}\left(\mathbf{D}^0\right)^{-1}\Gamma\rho^{(0)}
\end{aligned}$$

Consequently, the solution is

$$\sigma^{-1} = -\left(\mathbf{D}^{-1}\right)^{-1}\mathbf{E}\left(\mathbf{D}^0\right)^{-1}\Gamma\rho^{(0)}. \tag{9.19}$$

We notice (figures 9.10) that for weak excitation amplitudes, we have, as for the two level system, a linear response of the system followed by saturation and by characteristic oscillations. This phenomenon is comparable [115] to the suppression of ionisation in atoms when excited at high intensities [116–119]. In conclusion, the general phenomena shown in the two level system remain valid for the n-level system where other phenomena superpose.

9.3 Pump-probe configuration

In the following, we consider a bichromatic excitation. The solution in the case of these kinds of excitation is the generalised Fourier-Floquet matrix in a tensor relation (8.43). We apply this formalism in the case where the amplitude of one of the two exciting beams is in the linear regime. This corresponds to a "pump-probe configuration". Practically, a high intensity beam is exciting the sample while a second weak beam is used to measure the refractive index changes induced in the sample. This can be seen as an interaction between the two beams. The magnitude of this interaction depends on the non-linear part of the response of the sample which itself depends on the intensity of the pump beam. During such an interaction, several effects can appear such as the dynamic Stark shift, induced absorption or transmission. These effects are explained by the saturation of the system under the high intensity pump beam. In this subsection, we study these effects in the framework of the Fourier-Floquet transformation for a bichromatic excitation.

In order to solve the system of equations (8.43) in the case of a pump-probe configuration, we take into account only the terms ρ^{n0} and ρ^{n1} of the density matrix. This means that the pump is treated to the order N (as its high intensity implies a non linear response) while the probe is treated at the zeroth order. This approximation is in agreement with the amplitudes of the two beams and implies for its description two systems of equations each similar to the monochromatic excitation equations

$$\mathbf{M}^{p0}_{n0}\hat{\rho}^{n0} = \delta^{p}_{0}\Gamma\rho^{(0)}, \tag{9.20a}$$

$$\mathbf{M}^{p1}_{n1}\hat{\rho}^{n1} = -\mathbf{E_2}\rho^{p0}. \tag{9.20b}$$

In the tensor $\mathbf{M}^{pq}_{nm}$ defined by (8.43b), the terms $\mathbf{E_1}$ and $\mathbf{E_2}$ correspond respectively to the pump and to the probe excitations. The first equation (9.20a) describes the effects of the pump on the system. It can be resolved by the recursive method described in the preceding section. The second equation (9.20b) takes into account the linear interaction of the probe with the system in equilibrium with the pump excitation. With the help of these two equations, the saturation effects, induced by the pump, can be studied.

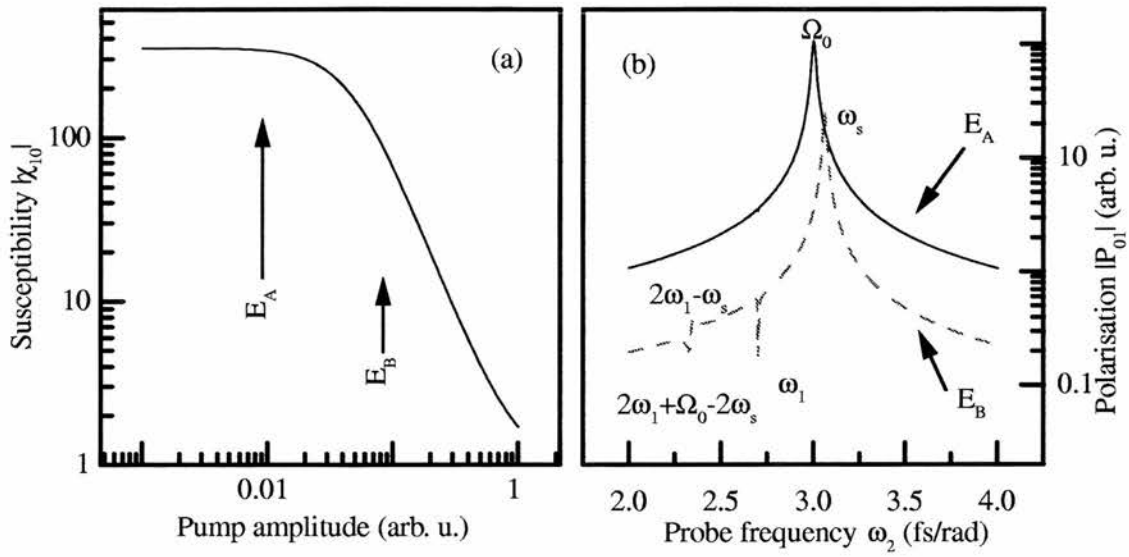

Figure 9.11: (a) The susceptibility due to the pump as a function of the pump amplitude. (b) The polarisation due to the probe for the amplitudes E_A and E_B of the pump. The frequency of the pump is $\omega_1 = 2.7$rad/fs. The resonance frequency of the system is $\Omega_0 = 3$rad/fs in the absence of excitation and ω_s in the presence of the dynamic Stark shift.

9.3.1 Two level system

In the following, we develop the behaviour of a two level system in the pump-probe configuration. As in the preceding section, the approximation conditions (9.10) are taken into account. Further, the solution developed to first order shows the effects of the dynamical Stark shift.

In order to simplify the notation we use the following definitions:

$$\begin{aligned}
\gamma_1 &= \Gamma_2 + i\Omega_0 + i\omega_1, \\
\gamma_{-1} &= \Gamma_2 + i\Omega_0 - i\omega_1, \\
g_1 &= \Gamma_1 - i\omega_1 + i\omega_2, \\
g_2 &= \Gamma_2 - i\omega_1 + i\omega_2, \\
g_3 &= \Gamma_2 - i\Omega_0 + i\omega_2, \\
g_4 &= \Gamma_2 + i\Omega_0 - 2i\omega_1 + i\omega_2, \\
g_5 &= (2\Gamma_2\Omega_0\chi_{10} + i\Gamma_2\chi_{-10}g_4 + \Omega_0\chi_{-10}g_4 - \Omega_0\chi_{10}g_4).
\end{aligned}$$

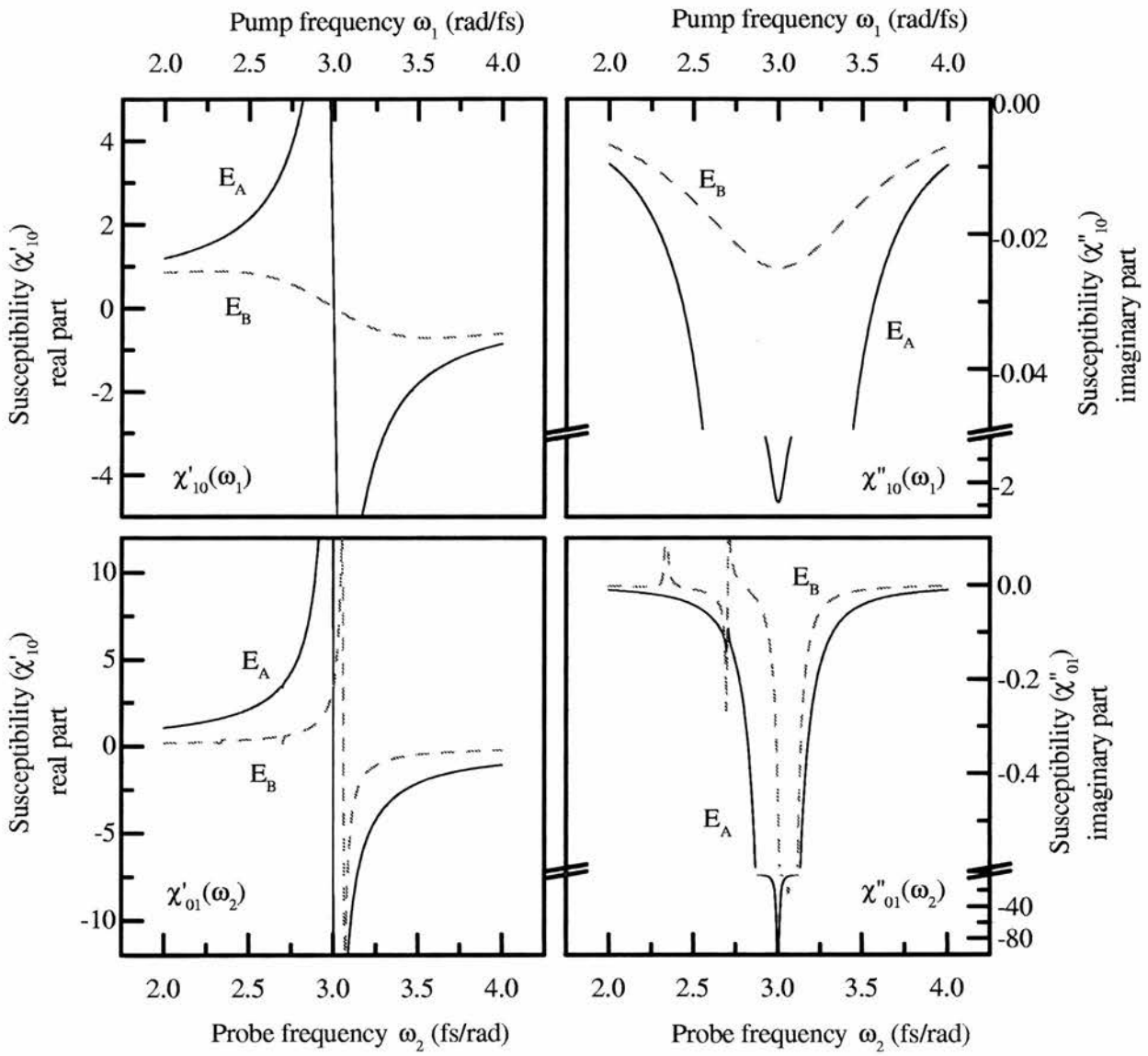

Figure 9.12: Susceptibility (real part χ'_{10} and imaginary part χ''_{10} (b)) induced by the pump, as a function to its frequency, for different pump intensities. These intensities are defined in figure 9.11. The susceptibility (real part χ'_{01} (c) and imaginary part χ''_{01} (d)) induced by the probe for different pump intensities. In the figures (c) and (d) the frequency of the pump is $\omega_1 = 2.7$rad/fs and the frequency of the resonance of the system is $\Omega_0 = 3$rad/fs

The susceptibility induced by the pump can be determined with the help of the first equation in the system of equations (9.20). This susceptibility depends not only on the frequency of the pump but also on its amplitude

$$\chi_{10}(E_1,\omega_1) = \frac{\Gamma_1|\mu|^2\Omega_0\rho_D^{(0)}(2\hbar^2\gamma_{-1}\gamma_1^* + E_1^2|\mu|^2)}{2\hbar^3\Gamma_1|\gamma_1|^2|\gamma_{-1}|^2 + 4\hbar E_1^2|\mu|^2\Gamma_2(\Omega_0^2+\omega_1^2)} \tag{9.21a}$$

$$\chi_{-10}(E_1,\omega_1) = \frac{\Gamma_1|\mu|^2\Omega_0\rho_D^{(0)}(2\hbar^2\gamma_{-1}^*\gamma_1 + E_1^2|\mu|^2)}{2\hbar^3\Gamma_1|\gamma_1|^2|\gamma_{-1}|^2 + 4\hbar E_1^2|\mu|^2\Gamma_2(\Omega_0^2+\omega_1^2)}. \tag{9.21b}$$

Figure 9.11a represents the norm of the susceptibility as a function of the intensity of the pump. This figure allows the definition of the two pump intensities used in the calculation of the induced polarisation by the probe (figure 9.11b). The polarisation due to the probe shows a resonance at the eigen-frequency of the system (Ω_0 for low pump intensities and ω_s for high pump intensities due to the dynamical Stark shift), at the pump frequency and at the sum and difference frequencies $2\omega_1 + \Omega_0 - 2\omega_s$ and $2\omega_1 - \omega_s$. These last resonances are of Fano type [120] while the resonance at the pump frequency ($\omega = \omega_1$) was also found in a similar theoretical treatment [121, 122].

The susceptibilities (9.21) are used to define the right hand term of equation (9.20b). From this last equation the susceptibility of the probe is found (9.22) to be

$$\chi_{01}(E_1,\omega_1,\omega_2) = -\frac{4\hbar^2\Gamma_2\Omega_0\chi_{10}\chi_{-10}g_4g_1 + E_1^2|\mu|^2\chi_{-10}g_5}{2\Omega_0(\chi_{10}-\chi_{-10})(\hbar^2g_4g_3g_1 + E_1^2|\mu|^2g_2)}. \tag{9.22}$$

Figure (9.12) summarises these results while representing the induced susceptibility by a high intensity beam (pump) and one induced by the probe in the pump-probe configuration.

When increasing the intensity of the pump, we observe two effects. On the one hand we have the appearance of virtual resonances induced by the pump and on the other the dynamical Stark shift of the principal resonance as well as the other induced resonances. These effects are represented in figure 9.13. We notice in this figure the behaviour of resonances described in figure 9.11, namely the shifts of the induced absorption $2\omega_1 - \omega_s$ and induced transmission $2\omega_1 + \Omega_0 - 2\omega_s$.

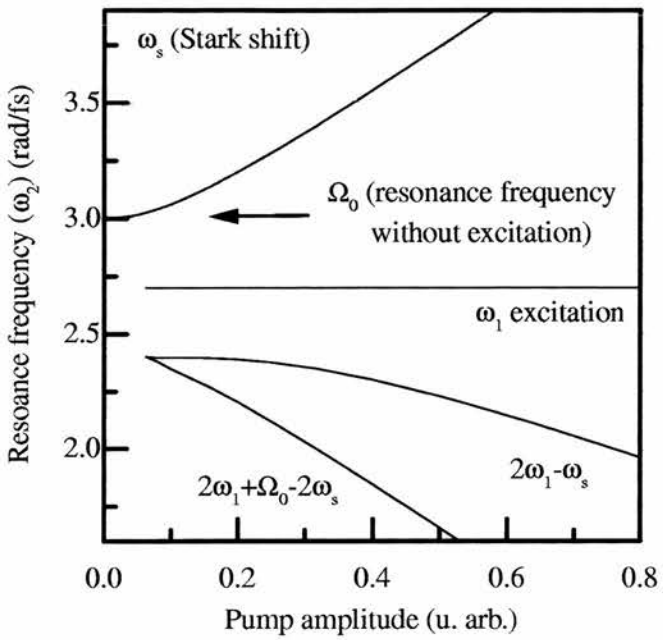

Figure 9.13: Stark shift of the different resonances as a function of the pump amplitude. The frequency of the pump is $\omega_1 = 2.7\text{rad/fs}$ and the resonance frequency of the system is $\Omega_0 = 3\text{rad/fs}$

9.3.2 Three level system

In the following we explain the induced absorption in a three level system. In order to model such a system it is necessary to use the tensor notations introduced in the above sections. The two equations (9.20) are:

$$\Gamma \begin{pmatrix} 0 \\ \rho^{(0)} \\ 0 \end{pmatrix} = \begin{pmatrix} \mathbf{L_{10}} & \mathbf{E_1} & 0 \\ \mathbf{E_1} & \mathbf{L_{00}} & \mathbf{E_1} \\ 0 & \mathbf{E_1} & \mathbf{L_{-10}} \end{pmatrix} \begin{pmatrix} \rho^{10} \\ \rho^{00} \\ \rho^{-10} \end{pmatrix}, \tag{9.23a}$$

$$-\mathbf{E_2} \begin{pmatrix} \rho^{10} \\ \rho^{00} \\ \rho^{-10} \end{pmatrix} = \begin{pmatrix} \mathbf{L_{11}} & \mathbf{E_1} & 0 \\ \mathbf{E_1} & \mathbf{L_{01}} & \mathbf{E_1} \\ 0 & \mathbf{E_1} & \mathbf{L_{-11}} \end{pmatrix} \begin{pmatrix} \rho^{11} \\ \rho^{01} \\ \rho^{-11} \end{pmatrix}. \tag{9.23b}$$

Introducing the first recursive term of the diagonal

$$\mathbf{D_{00}} = \mathbf{L_{00}} - \mathbf{E_1}\mathbf{L_{10}^{-1}}\mathbf{E_1} - \mathbf{E_1}\mathbf{L_{-10}^{-1}}\mathbf{E_1}, \tag{9.23c}$$

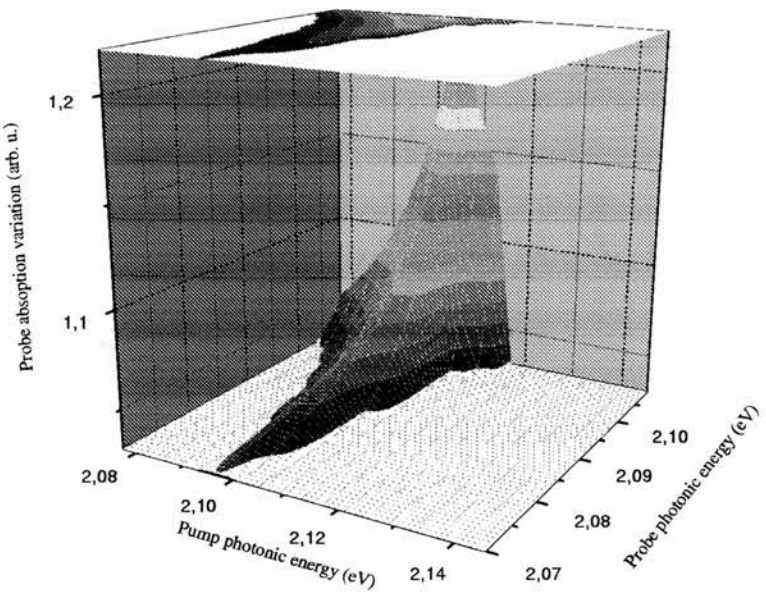

Figure 9.14: Theoretical simulation of the saturation of the intermediate level of a three level system. This saturation implies an apparent shift of the absorption edge.

we can deduce the other harmonics of the density matrix for the frequencies ω_1, 0 and $-\omega_1$

$$\rho^{10} = -\mathbf{L}_{10}^{-1}\mathbf{E_1}\mathbf{D}_{00}^{-1}\Gamma\rho^{(0)}, \tag{9.24a}$$

$$\rho^{00} = \mathbf{D}_{00}^{-1}\Gamma\rho^{(0)}, \tag{9.24b}$$

$$\rho^{-10} = -\mathbf{L}_{-10}^{-1}\mathbf{E_1}\mathbf{D}_{00}^{-1}\Gamma\rho^{(0)}. \tag{9.24c}$$

Finally, it is necessary to determine the diagonal term $\mathbf{D}_{01}$. For this we use the density matrices defined above (9.24) as well as the diagonal recursive term defined by (9.23b)

$$\mathbf{D}_{01} = \mathbf{L}_{01} - \mathbf{E_1}\mathbf{L}_{11}^{-1}\mathbf{E_1} - \mathbf{E_1}\mathbf{L}_{-11}^{-1}\mathbf{E_1}. \tag{9.25}$$

The density matrix, corresponding to the response induced by the probe is then

$$\rho^{01} = -\mathbf{D}_{01}^{-1}\left(\mathbf{E_2}\rho^{00} - \mathbf{E_1}\mathbf{L}_{11}^{-1}\mathbf{E_2}\rho^{10} - \mathbf{E_1}\mathbf{L}_{-11}^{-1}\mathbf{E_2}\rho^{-10}\right). \tag{9.26}$$

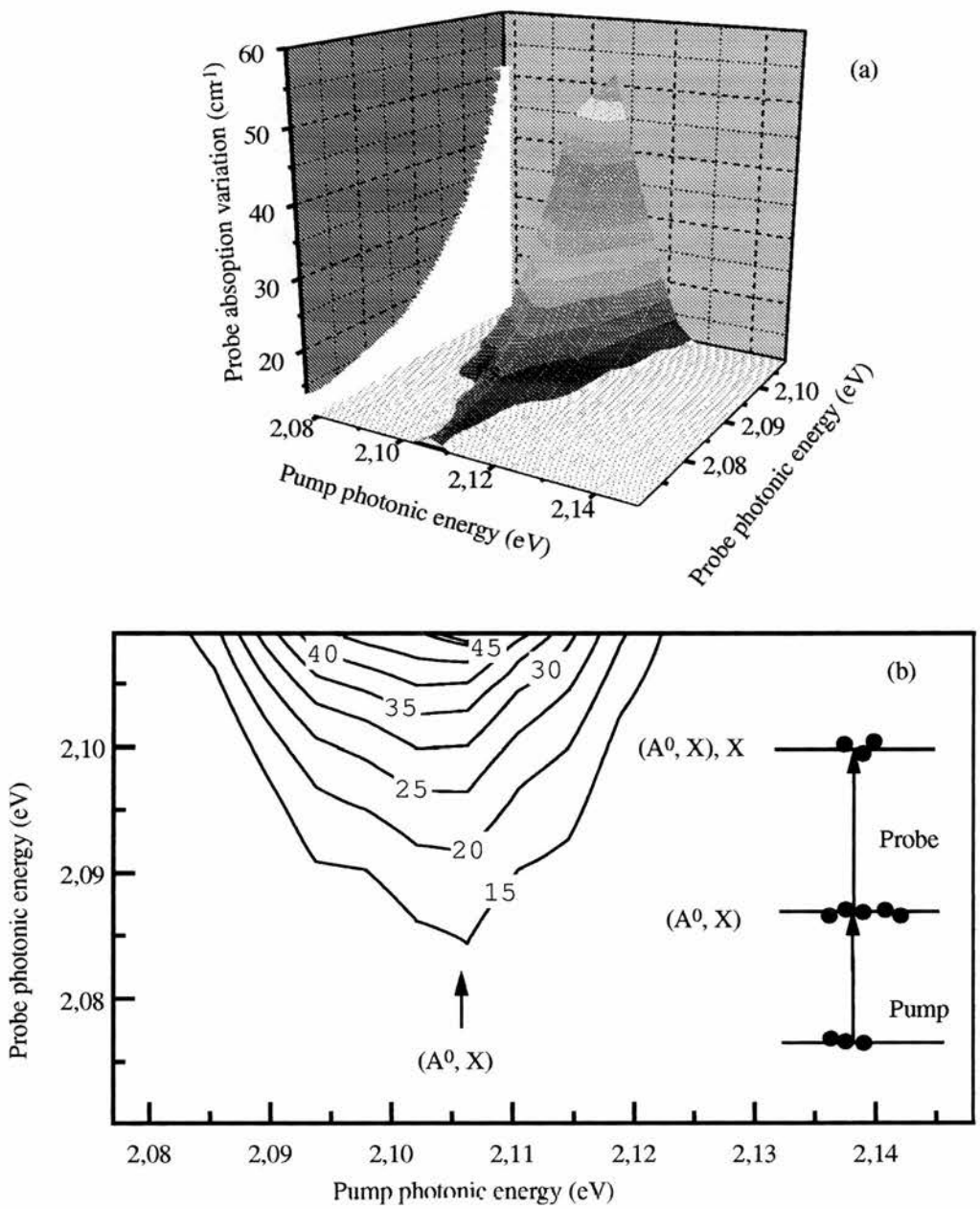

Figure 9.15: Measure in pump-probe configuration of the absorption edge shift in $Cd_xZn_{1-x}Te$ [123, 124]. (a) Absorption edge shift as a function of the pump frequency of the pump and probe. (b) Contour plot of the induced transmission allowing us to deduce the energy of the pump inducing a maximum absorption of the probe.

With the help of this density matrix, the polarisation, the susceptibility and finally the absorption can be calculated easily. Figure 9.14 represents the theoretical result of our approach where the three considered levels model an excitonic level and a trapped biexcitonic level in a $Cd_xZn_{1-x}Te$ [123,124] compound. This figure can be compared to figure 9.15 which summarises the experimental results obtained in $Cd_xZn_{1-x}Te$. These experiments were done with the help of a variable wavelengh dye laser for the pump and of a spectrally large probe. The amplitude of the pump is maintained constant while its wavelength is varied. With the help of this experiment, we show the existence of this trapped biexcitonic third level. In fact, in a system having only two levels (9.22) the induced absorption by the pump in such a configuration does not show such a behaviour. On the other hand, the experimental results are comparable with the simulation of a three level system.

9.4 Non-degenerate four-wave mixing

In this subsection we treat the excitation of an n-level with two beams having different frequencies. This kind of excitation generalises the pump-probe configuration as the second beam can have any amplitude. Such a configuration corresponds to the non-degenerate four-wave mixing and is useful in order to measure the transverse relaxation time [125,126]. The theoretical treatment of this configuration must take into account the higher harmonic orders of the density matrix for both beams. On the other hand, the use of a higher harmonic order implies more difficulties in the determination of approximated analytical solutions valid for the n-level system. Consequently, we deduce, as a first step, the analytical formulas for a two level system while the study of the more general n-level system remains numerical.

For the two level system, its evolution equations (8.3) can be simplified. This simplification transforms the system into a new system of equations whose treatment no longer resembles that of the n-level system of the preceding section. Furthermore, the treated two level system is point symmetric which implies further simplification. The excitation is bichromatic, and corresponds to the sum of two monochromatic waves

$$E(t) = \frac{1}{2}(E_1 e^{-i\omega_1 t} + E_1^* e^{i\omega_1 t} + E_2 e^{-i\omega_2 t} + E_2^* e^{i\omega_2 t}). \tag{9.27}$$

Each of the two excitation fields is decomposed into two complex conjugated amplitudes. This allows a study of the effects induced by the relative phase of the two fields. The system of equations giving the evolution of the elements of the density matrix is

$$\begin{aligned}
i\omega\hat{\rho}_D(\omega) &= \frac{i}{\hbar}(E_1\mu_{ab}\hat{\rho}_{ba}(\omega+\omega_1) + E_1^*\mu_{ab}\hat{\rho}_{ba}(\omega-\omega_1) \\
&\quad -E_1\mu_{ba}\hat{\rho}_{ab}(\omega+\omega_1) - E_1^*\mu_{ba}\hat{\rho}_{ab}(\omega-\omega_1)) \\
&\quad +\frac{i}{\hbar}(E_2\mu_{ab}\hat{\rho}_{ba}(\omega+\omega_2) + E_2^*\mu_{ab}\hat{\rho}_{ba}(\omega-\omega_2) \\
&\quad -E_2\mu_{ba}\hat{\rho}_{ab}(\omega+\omega_2) - E_2^*\mu_{ba}\hat{\rho}_{ab}(\omega-\omega_2)) \\
&\quad -\Gamma_1(\hat{\rho}_D(\omega) - \delta(\omega)\rho_D^{(0)}) \qquad (9.28a) \\
i\omega\hat{\rho}_{ba}(\omega) &= \frac{i}{2\hbar}\mu_{ba}[E_1\hat{\rho}_D(\omega+\omega_1) + E_1^*\hat{\rho}_D(\omega-\omega_1)] \\
&\quad +\frac{i}{2\hbar}\mu_{ba}[E_2\hat{\rho}_D(\omega+\omega_2) + E_2^*\hat{\rho}_D(\omega-\omega_2)] \\
&\quad -(\Gamma_2 + i\Omega_0)\,\hat{\rho}_{ba} \qquad (9.28b) \\
i\omega\hat{\rho}_{ab}(\omega) &= -\frac{i}{2\hbar}\mu_{ab}[E_1\hat{\rho}_D(\omega+\omega_1) + E_1^*\hat{\rho}_D(\omega-\omega_1)] \\
&\quad -\frac{i}{2\hbar}\mu_{ab}[E_2\hat{\rho}_D(\omega+\omega_2) + E_2^*\hat{\rho}_D(\omega-\omega_2)] \\
&\quad -(\Gamma_2 - i\Omega_0)\,\hat{\rho}_{ab}, \qquad (9.28c)
\end{aligned}$$

with $\rho_D = \rho_{bb} - \rho_{aa}$ and $\rho_D^{(0)} = \rho_{bb} - \rho_{aa}$. Algebraic manipulation of this system transforms it into a new system of equations depending only on the polarisation at different frequencies. In fact, in adding (9.28b) and (9.28c) we obtain the following relation between the two coherences $\hat{\rho}_{ab}$ and $\hat{\rho}_{ba}$

$$\mu_{ba}\hat{\rho}_{ab}(\omega) = -\mu_{ab}\hat{\rho}_{ba}(\omega)\frac{\Gamma_2 + i(\Omega_0+\omega)}{\Gamma_2 + i(-\Omega_0+\omega)}. \qquad (9.29)$$

After Fourier transformation, the polarisation of the system can be written as a function of the matrix element ρ_{ba}

$$\begin{aligned}
\hat{P}(\omega) &= \mu_{ba}\hat{\rho}_{ab}(\omega) + \mu_{ab}\hat{\rho}_{ba}(\omega) \\
&= \mu_{ab}\hat{\rho}_{ba}(\omega)\frac{-2i\Omega_0}{\Gamma_2 + i(-\Omega_0+\omega)}, \qquad (9.30)
\end{aligned}$$

and the difference between $\hat{\rho}_{ab}$ and $\hat{\rho}_{ba}$ as a function of the polarisation

$$\mu_{ba}\hat{\rho}_{ab}(\omega) - \mu_{ab}\hat{\rho}_{ba}(\omega) = -\hat{P}(\omega)\frac{\Gamma_2 + i\omega}{-i\Omega_0}. \qquad (9.31)$$

Using these two relations and equation (9.28a), we can determine the relation between the population difference $\hat{\rho}_D$ and the polarisation

$$\begin{aligned}\hat{\rho}_D(\omega)(\Gamma_1+i\omega) &= -\frac{1}{\hbar\Omega_0}[E_1\hat{P}(\omega+\omega_1)(\Gamma_2+i(\omega+\omega_1))\\ &\quad E_1^*\hat{P}(\omega-\omega_1)(\Gamma_2+i(\omega-\omega_1))]\\ &\quad -\frac{1}{\hbar\Omega_0}[E_2\hat{P}(\omega+\omega_2)(\Gamma_2+i(\omega+\omega_2))\\ &\quad E_2^*\hat{P}(\omega-\omega_2)(\Gamma_2+i(\omega-\omega_2))]\\ &\quad +\delta(\omega)\rho_D^{(0)}\Gamma_1.\end{aligned}$$

The substitution of this relation in equation (9.28b) simplifies the evolution equation so as to depend only on the polarisation

$$\begin{aligned}&\hat{P}(\omega)\frac{\Gamma_2+i(-\Omega_0+\omega)}{-i2\Omega_0\mu_{ab}}(\Gamma_2+i(\Omega_0+\omega))\\ &+\frac{i\mu_{ba}}{2\hbar}\frac{1}{\hbar\Omega_0}*\Bigg[E_1E_1\hat{P}(\omega+2\omega_1)\frac{(\Gamma_2+i(\omega+2\omega_1))}{(\Gamma_1+i(\omega+\omega_1))}\\ &+E_1^*E_1^*\hat{P}(\omega-2\omega_1)\frac{(\Gamma_2+i(\omega-2\omega_1))}{(\Gamma_1+i(\omega-\omega_1))}\\ &+E_1E_1^*\hat{P}(\omega)\left(\frac{(\Gamma_2+i\omega)}{(\Gamma_1+i(\omega+\omega_1))}+\frac{(\Gamma_2+i\omega)}{(\Gamma_1+i(\omega-\omega_1))}\right)\\ &+E_2E_2\hat{P}(\omega+2\omega_2)\frac{(\Gamma_2+i(\omega+2\omega_2))}{(\Gamma_1+i(\omega+\omega_2))}+E_2^*E_2^*\hat{P}(\omega-2\omega_2)\frac{(\Gamma_2+i(\omega-2\omega_2))}{(\Gamma_1+i(\omega-\omega_2))}\\ &+E_2E_2^*\hat{P}(\omega)\left(\frac{(\Gamma_2+i\omega)}{(\Gamma_1+i(\omega+\omega_2))}+\frac{(\Gamma_2+i\omega)}{(\Gamma_1+i(\omega-\omega_2))}\right)\\ &+E_1E_2\hat{P}(\omega+\omega_1+\omega_2)\left(\frac{(\Gamma_2+i(\omega+\omega_1+\omega_2))}{(\Gamma_1+i(\omega+\omega_1))}+\frac{(\Gamma_2+i(\omega+\omega_1+\omega_2))}{(\Gamma_1+i(\omega+\omega_2))}\right)\\ &+E_1E_2^*\hat{P}(\omega+\omega_1-\omega_2)\left(\frac{(\Gamma_2+i(\omega+\omega_1-\omega_2))}{(\Gamma_1+i(\omega+\omega_1))}+\frac{(\Gamma_2+i(\omega+\omega_1-\omega_2))}{(\Gamma_1+i(\omega-\omega_2))}\right)\\ &+E_1^*E_2\hat{P}(\omega-\omega_1+\omega_2)\left(\frac{(\Gamma_2+i(\omega-\omega_1+\omega_2))}{(\Gamma_1+i(\omega-\omega_1))}+\frac{(\Gamma_2+i(\omega-\omega_1+\omega_2))}{(\Gamma_1+i(\omega+\omega_2))}\right)\\ &+E_1^*E_2^*\hat{P}(\omega-\omega_1-\omega_2)\left(\frac{(\Gamma_2+i(\omega-\omega_1-\omega_2))}{(\Gamma_1+i(\omega-\omega_1))}+\frac{(\Gamma_2+i(\omega-\omega_1-\omega_2))}{(\Gamma_1+i(\omega-\omega_2))}\right)\Bigg]\\ =\ &\frac{i\mu_{ba}\rho_D^{(0)}}{2\hbar}(E_1\delta(\omega-\omega_1)\delta(\omega_2)+E_1^*\delta(\omega+\omega_1)\delta(\omega_2)\\ &+E_2\delta(\omega-\omega_2)\delta(\omega_1)+E_2^*\delta(\omega+\omega_2)\delta(\omega_1)).\end{aligned} \tag{9.32}$$

As we already mentioned in the preceding sections, in the system of equations (9.32) only the polarisation at the harmonic frequencies of the excitation interact. In this case, the polarisation of the frequency ω is coupled to the polarisations with the frequency

$\omega + j\omega_1 + k\omega_2$ (where $j + k = 0, \pm 2, \pm 4, ...$). The free term is proportional to $(E_1\delta(\omega - \omega_1) + E_1^*\delta(\omega + \omega_1 + E_2\delta(\omega - \omega_2) + E_2^*\delta(\omega + \omega_2))$. This implies that the polarisation can be written as a sum of Dirac functions corresponding to the harmonics of the frequencies of ω_1 and ω_2,

$$\hat{P}(\omega) = \sum_{n=-\infty}^{\infty} \sum_{m=-\infty}^{\infty} \hat{P}_{nm}\delta(\omega - n\omega_1 - m\omega_2), \tag{9.33}$$

with $\hat{P}_{nm} = 0$ for $n + m = 2k$. This allows the determination of a system of equations for the polarisation. This system corresponds to the relation (8.43) in its general case

$$\begin{aligned}
&\hat{P}_{nm}\frac{\Gamma_2 + i(-\Omega_0 + \omega_{nm})}{-i2\Omega_0\mu_{ab}}\left(\Gamma_2 + i(\Omega_0 + \omega_{nm})\right) \\
&+\frac{i\mu_{ba}}{2\hbar}\frac{1}{\hbar\Omega_0} * \left[E_1E_1\hat{P}_{n+2m}\frac{(\Gamma_2 + i\omega_{n+2m})}{(\Gamma_1 + i\omega_{n+1m})} + E_1^*E_1^*\hat{P}_{n-2m}\frac{(\Gamma_2 + i\omega_{n-2m})}{(\Gamma_1 + i\omega_{n-1m})}\right. \\
&+E_1E_1^*\hat{P}_{nm}\left(\frac{(\Gamma_2 + i\omega_{nm})}{(\Gamma_1 + i\omega_{n+1m})} + \frac{(\Gamma_2 + i\omega_{nm})}{(\Gamma_1 + i\omega_{n-1m})}\right) \\
&+E_2E_2\hat{P}_{nm+2}\frac{(\Gamma_2 + i\omega_{nm+2})}{(\Gamma_1 + i\omega_{nm+1})} + E_2^*E_2^*\hat{P}_{nm-2}\frac{(\Gamma_2 + i\omega_{nm-2})}{(\Gamma_1 + i\omega_{nm-1})} \\
&+E_2E_2^*\hat{P}_{nm}\left(\frac{(\Gamma_2 + i\omega_{nm})}{(\Gamma_1 + i\omega_{nm+1})} + \frac{(\Gamma_2 + i\omega_{nm})}{(\Gamma_1 + i\omega_{nm-1})}\right) \\
&+E_1E_2\hat{P}_{n+1m+1}\left(\frac{(\Gamma_2 + i\omega_{n+1m+1})}{(\Gamma_1 + i\omega_{n+1m})} + \frac{(\Gamma_2 + i\omega_{n+1m+1})}{(\Gamma_1 + i\omega_{nm+1})}\right) \\
&+E_1E_2^*\hat{P}_{n+1m-1}\left(\frac{(\Gamma_2 + i\omega_{n+1m-1})}{(\Gamma_1 + i\omega_{n+1m})} + \frac{(\Gamma_2 + i\omega_{n+1m-1})}{(\Gamma_1 + i\omega_{nm-1})}\right) \\
&+E_1^*E_2\hat{P}_{n-1m+1}\left(\frac{(\Gamma_2 + i\omega_{n-1m+1})}{(\Gamma_1 + i\omega_{n-1m})} + \frac{(\Gamma_2 + i\omega_{n-1m+1})}{(\Gamma_1 + i\omega_{nm+1})}\right) \\
&\left.+E_1^*E_2^*\hat{P}_{n-1m-1}\left(\frac{(\Gamma_2 + i\omega_{n-1m-1})}{(\Gamma_1 + i\omega_{n-1m})} + \frac{(\Gamma_2 + i\omega_{n-1m-1})}{(\Gamma_1 + i\omega_{nm-1})}\right)\right] \\
&= \frac{i\mu_{ba}\rho_D^{(0)}}{2\hbar}(E_1\delta_{1n}\delta_{0m} + E_1^*\delta_{-1n}\delta_{0m} + E_2\delta_{0n}\delta_{1m} + E_2^*\delta_{0n}\delta_{-1m}).
\end{aligned} \tag{9.34}$$

From the system of equations (9.34) developed to first order and using the following notation, we can deduce the polarisation at the frequency of one of the two beams:

$$\begin{aligned} c_{nm} &= \frac{\Gamma_2 + i\omega_{nm}}{i\Omega_0}, \\ q_{nm} &= i\Omega_0(1 - c_{nm}^2), \\ \gamma_{nm} &= -\Gamma_1 - i\omega_{nm}, \\ a_1 &= \frac{E_1\mu}{2\hbar}, \\ a_2 &= \frac{E_2\mu}{2\hbar}, \end{aligned}$$

$$\begin{aligned} n_1 &= -2iq_{-10}q_{0-1}q_{10}\gamma_{-11}\gamma_{1-1}, \\ n_2 &= 8iq_{10}(c_{-10}q_{0-1}\gamma_{1-1} - c_{0-1}q_{-10}\gamma_{-11}), \\ n_3 &= -8iq_{0-1}(c_{10}q_{-10}\gamma_{-11} + c_{-10}q_{10}\gamma_{1-1}), \\ d_1 &= q_{-10}q_{0-1}q_{01}q_{10}\gamma_{-11}\gamma_{00}\gamma_{1-1}, \\ d_2 &= 4(c_{0-1}q_{-10}q_{01}q_{10}\gamma_{-11}\gamma_{00} + c_{10}q_{-10}q_{0-1}q_{01}\gamma_{-11}\gamma_{1-1} \\ &\quad + c_{-10}q_{0-1}q_{01}q_{10}\gamma_{-11}\gamma_{1-1} + c_{01}q_{-10}q_{0-1}q_{10}\gamma_{00}\gamma_{1-1}), \\ d_3 &= 4(c_{10}q_{-10}q_{0-1}q_{01}\gamma_{-11}\gamma_{00} + c_{01}q_{-10}q_{0-1}q_{10}\gamma_{-11}\gamma_{1-1} \\ &\quad + c_{0-1}q_{-10}q_{01}q_{10}\gamma_{-11}\gamma_{1-1} + c_{-10}q_{0-1}q_{01}q_{10}\gamma_{00}\gamma_{1-1}), \\ d_4 &= 16(c_{-10}c_{10}q_{0-1}q_{01}\gamma_{-11} - 2c_{0-1}c_{10}q_{-10}q_{01}\gamma_{-11} \\ &\quad + c_{0-1}c_{01}q_{-10}q_{10}\gamma_{-11} + c_{01}c_{10}q_{-10}q_{0-1}\gamma_{00} \\ &\quad + c_{-10}c_{0-1}q_{01}q_{10}\gamma_{00} + c_{-10}c_{10}q_{0-1}q_{01}\gamma_{1-1} \\ &\quad + c_{0-1}c_{01}q_{-10}q_{10}\gamma_{1-1} - 2c_{-10}c_{01}q_{0-1}q_{10}\gamma_{1-1}), \\ d_5 &= 16(c_{0-1}c_{10}q_{-10}q_{01}\gamma_{-11} + c_{-10}c_{0-1}q_{01}q_{10}\gamma_{-11} \\ &\quad + c_{0-1}c_{01}q_{-10}q_{10}\gamma_{00} + c_{01}c_{10}q_{-10}q_{0-1}\gamma_{1-1} + c_{-10}c_{01}q_{0-1}q_{10}\gamma_{1-1}), \\ d_6 &= 16(c_{01}c_{10}q_{-10}q_{0-1}\gamma_{-11} + c_{0-1}c_{10}q_{-10}q_{01}\gamma_{-11} \\ &\quad + c_{-10}c_{10}q_{0-1}q_{01}\gamma_{00} + c_{-10}c_{01}q_{0-1}q_{10}\gamma_{1-1} + c_{-10}c_{0-1}q_{01}q_{10}\gamma_{1-1}). \end{aligned}$$

The polarisation is then

$$\hat{P}_{01} = -\frac{\Gamma_1(a_2 n_1 + a_1^2 a_2 n_2 + a_2^3 n_3)}{d_1 + a_1^2 d_2 + a_2^2 d_3 + a_1^2 a_2^2 d_4 + a_1^4 d_5 + a_2^4 d_6}. \tag{9.35}$$

This analytical formula is a generalisation of the monochromatic case as well as of the pump-probe configuration. Indeed, if the amplitude a_1 is zero then this equation describes the polarisation induced by one excitation beam (9.11a). In the case where the intensity of the second beam is small we can neglect a_2^2 and the susceptibility found corresponds to the pump-probe configuration (9.22).

Another easily measurable quantity in the case of the non-degenerate four-wave mixing is the response at the frequency $(2\omega_1 - \omega_2)$. The advantage of such a measure resides in the spectral resolution of the response with respect to the excitations. Further, in the case where the two beams are not collinear we also have a spatial separation between the excitation beams and the response at the frequency $(2\omega_1 - \omega_2)$.

In order to determine the polarisation $\hat{P}_{2-1}$ to a first approximation, it is necessary to use the relation (9.34) as well as the polarisation at the fundamental harmonic (9.35). From the relation (9.34), we find the following relations between $\hat{P}_{2-1}$ and $\hat{P}_{1-2}$. The higher orders of polarisation $\hat{P}_{21}$, $\hat{P}_{30}$, $\hat{P}_{4-1}$, $\hat{P}_{3-2}$, $\hat{P}_{2-3}$, $\hat{P}_{1-4}$, $\hat{P}_{0-3}$ and $\hat{P}_{-1-2}$ are

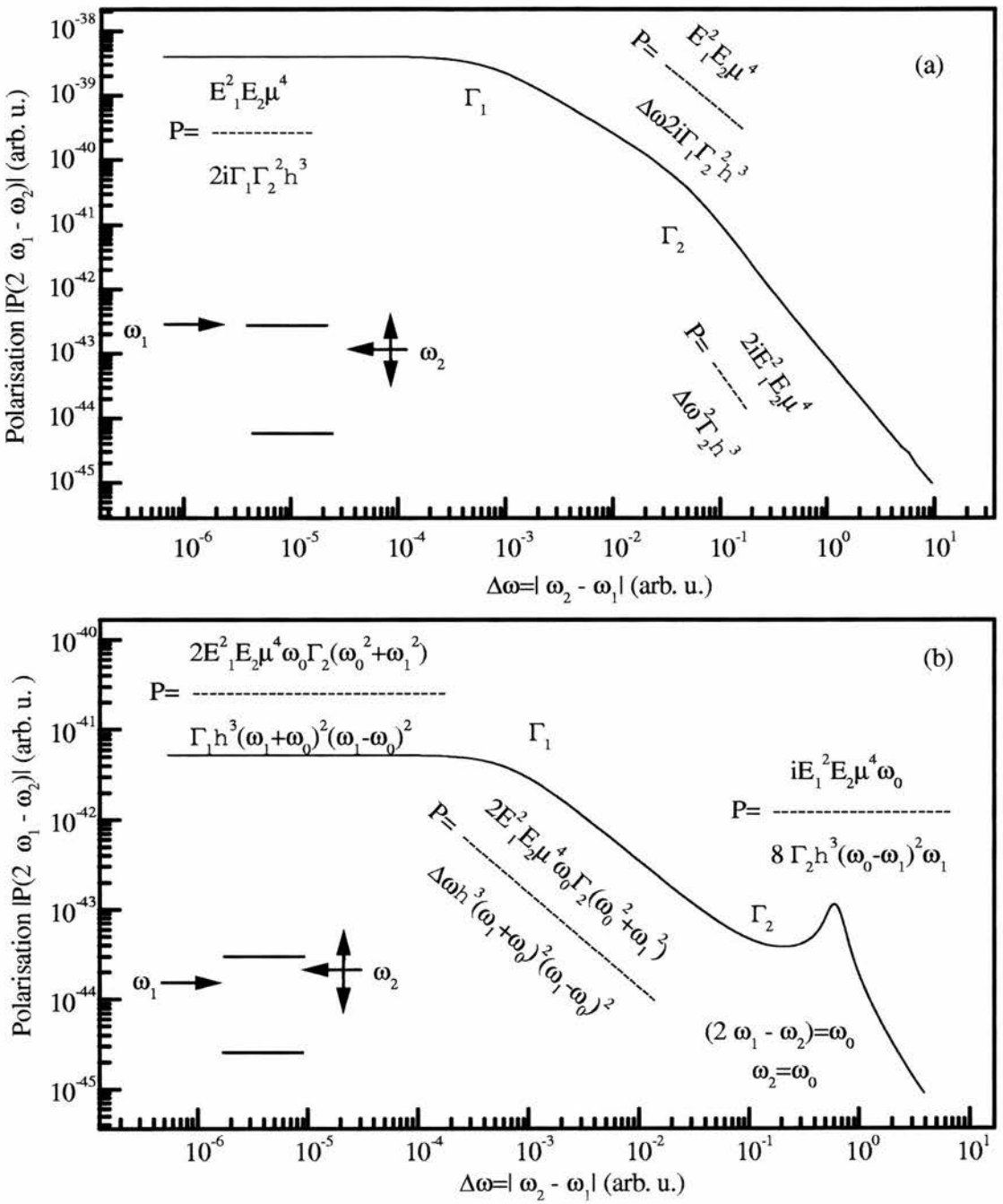

Figure 9.16: Simulation of the response of a two level system excited (a) in resonance or (b) out of resonance in the four-wave mixing configuration.

neglected in the following relations:

$$\begin{aligned}
&\hat{P}_{2-1}\ \left[\frac{\Gamma_2+i(-\Omega_0+\omega_{2-1})}{-i2\Omega_0\mu_{ab}}\left(\Gamma_2+i(\Omega_0+\omega_{2-1})\right)\right.\\
&\quad+\frac{i\mu_{ba}}{2\hbar}\frac{1}{\hbar\Omega_0}E_1E_1^*\left(\frac{2\left(\Gamma_1+i\omega_{2-1}\right)\left(\Gamma_2+i\omega_{2-1}\right)}{\left(\Gamma_1+i\omega_{3-1}\right)\left(\Gamma_1+i\omega_{1-1}\right)}\right)\\
&\quad\left.+\frac{i\mu_{ba}}{2\hbar}\frac{1}{\hbar\Omega_0}E_2E_2^*\left(\frac{2\left(\Gamma_1+i\omega_{2-1}\right)\left(\Gamma_2+i\omega_{2-1}\right)}{\left(\Gamma_1+i\omega_{2-2}\right)\left(\Gamma_1+i\omega_{20}\right)}\right)\right]\\
+\ &\hat{P}_{1-2}\ E_1^*E_2^*\frac{i\mu_{ba}}{2\hbar}\frac{1}{\hbar\Omega_0}\left(\frac{2\left(\Gamma_1+i\omega_{1-2}\right)\left(\Gamma_2+i\omega_{1-2}\right)}{\left(\Gamma_1+i\omega_{2-2}\right)\left(\Gamma_1+i\omega_{1-1}\right)}\right)\\
=-\frac{i\mu_{ba}}{2\hbar}\frac{1}{\hbar\Omega_0}&\left[\hat{P}_{10}E_1^*E_2\left(\frac{2\left(\Gamma_1+i\omega_{10}\right)\left(\Gamma_2+i\omega_{10}\right)}{\left(\Gamma_1+i\omega_{20}\right)\left(\Gamma_1+i\omega_{1-1}\right)}\right)\right.\\
&\left.+\hat{P}_{0-1}E_1^*E_1^*\frac{\left(\Gamma_2+i\omega_{0-1}\right)}{\left(\Gamma_1+i\omega_{1-1}\right)}\right]
\end{aligned}\tag{9.36a}$$

$$\begin{aligned}
&\hat{P}_{1-2}\ \left[\frac{\Gamma_2+i(-\Omega_0+\omega_{1-2})}{-i2\Omega_0\mu_{ab}}\left(\Gamma_2+i(\Omega_0+\omega_{1-2})\right)\right.\\
&\quad+\frac{i\mu_{ba}}{2\hbar}\frac{1}{\hbar\Omega_0}E_1E_1^*\left(\frac{2\left(\Gamma_1+i\omega_{1-2}\right)\left(\Gamma_2+i\omega_{1-2}\right)}{\left(\Gamma_1+i\omega_{0-2}\right)\left(\Gamma_1+i\omega_{2-2}\right)}\right)\\
&\quad\left.+\frac{i\mu_{ba}}{2\hbar}\frac{1}{\hbar\Omega_0}E_2E_2^*\left(\frac{2\left(\Gamma_1+i\omega_{1-2}\right)\left(\Gamma_2+i\omega_{1-2}\right)}{\left(\Gamma_1+i\omega_{1-3}\right)\left(\Gamma_1+i\omega_{1-1}\right)}\right)\right]\\
+\ &\hat{P}_{2-1}\ E_1^*E_2^*\frac{i\mu_{ba}}{2\hbar}\frac{1}{\hbar\Omega_0}\left(\frac{2\left(\Gamma_1+i\omega_{2-1}\right)\left(\Gamma_2+i\omega_{2-1}\right)}{\left(\Gamma_1+i\omega_{2-2}\right)\left(\Gamma_1+i\omega_{1-1}\right)}\right)\\
=-\frac{i\mu_{ba}}{2\hbar}\frac{1}{\hbar\Omega_0}&\left[\hat{P}_{0-1}E_1^*E_2\left(\frac{2\left(\Gamma_1+i\omega_{0-1}\right)\left(\Gamma_2+i\omega_{0-1}\right)}{\left(\Gamma_1+i\omega_{0-2}\right)\left(\Gamma_1+i\omega_{1-1}\right)}\right)\right.\\
&\left.+\hat{P}_{10}E_2E_2\frac{\left(\Gamma_2+i\omega_{10}\right)}{\left(\Gamma_1+i\omega_{1-1}\right)}\right]
\end{aligned}\tag{9.36b}$$

In figure 9.16 we have represented the response of a two level system excited by two beams in the non-degenerate four-wave mixing configuration. This response of the system can be described by simple formulae each valid over a frequency domain. These formulae are represented on the graphs.

Further, figure 9.16a shows the response at the frequency $(2\omega_1 - \omega_2)$ of a two level system when the first beam is in resonance with the two level system. Three different domains can be distinguished when varying the difference in frequency between the two beams. The transition between these regimes occurs when the difference in frequency implies a beating with a frequency comparable to the relaxation coefficients Γ_1 and Γ_2.

In the same manner, several regimes can be observed in figure 9.16b where the theoretical simulation shows the case where the first beam is off resonance with respect to the two level system. When the detuning of the two beams is varied (see also [127,128])

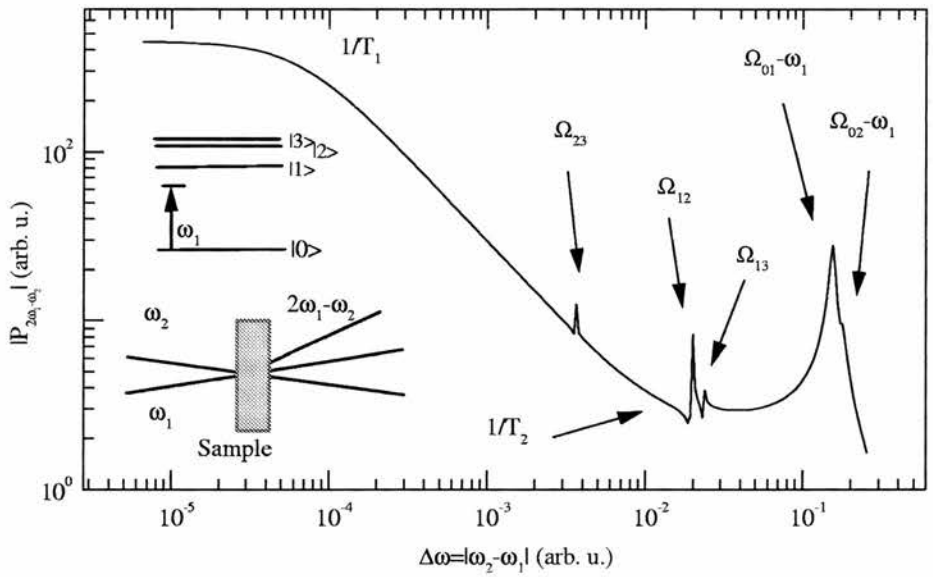

Figure 9.17: Reponse of an excitonic system to a bichromatic excitation out of resonance.

two different slopes can be observed. In addition to the two slope changes, there is a "resonance" effect between the detuning $(\omega_1 - \omega_2)$ and the relaxation coefficients Γ_1 and Γ_2. Further, we have a resonance at the moment where the detuning of the two beams corresponds to the difference in frequency between the first beam and the resonace of the two level system.

9.4.1 N-level system

In the case of an n-level system, the analytical formulae giving the polarisation in the non-degenerate four-wave mixing configuration become more complicated. We then need to use the general equations and tensors in order to describe the relation between the different harmonics of the density matrix. Figure 9.17 represents the response of an excitonic system where we took into account the first three levels with their energy and dipolar moment [113]. In comparison with the two level system excited out of resonance, the excitonic system shows additional resonances corresponding to the different excitonic levels. With the help of such a configuration, we can determine in this case the transverse and longitudinal relaxation times as well as to spectrally resolve energy levels.

Figure 9.18a shows the experimentally measured non-degenerate four-wave mixing signal for CdSe [129] quantum dots. Experimentally, we observe a resonance when the difference between the two frequencies is 26meV. The numerical simulation of this

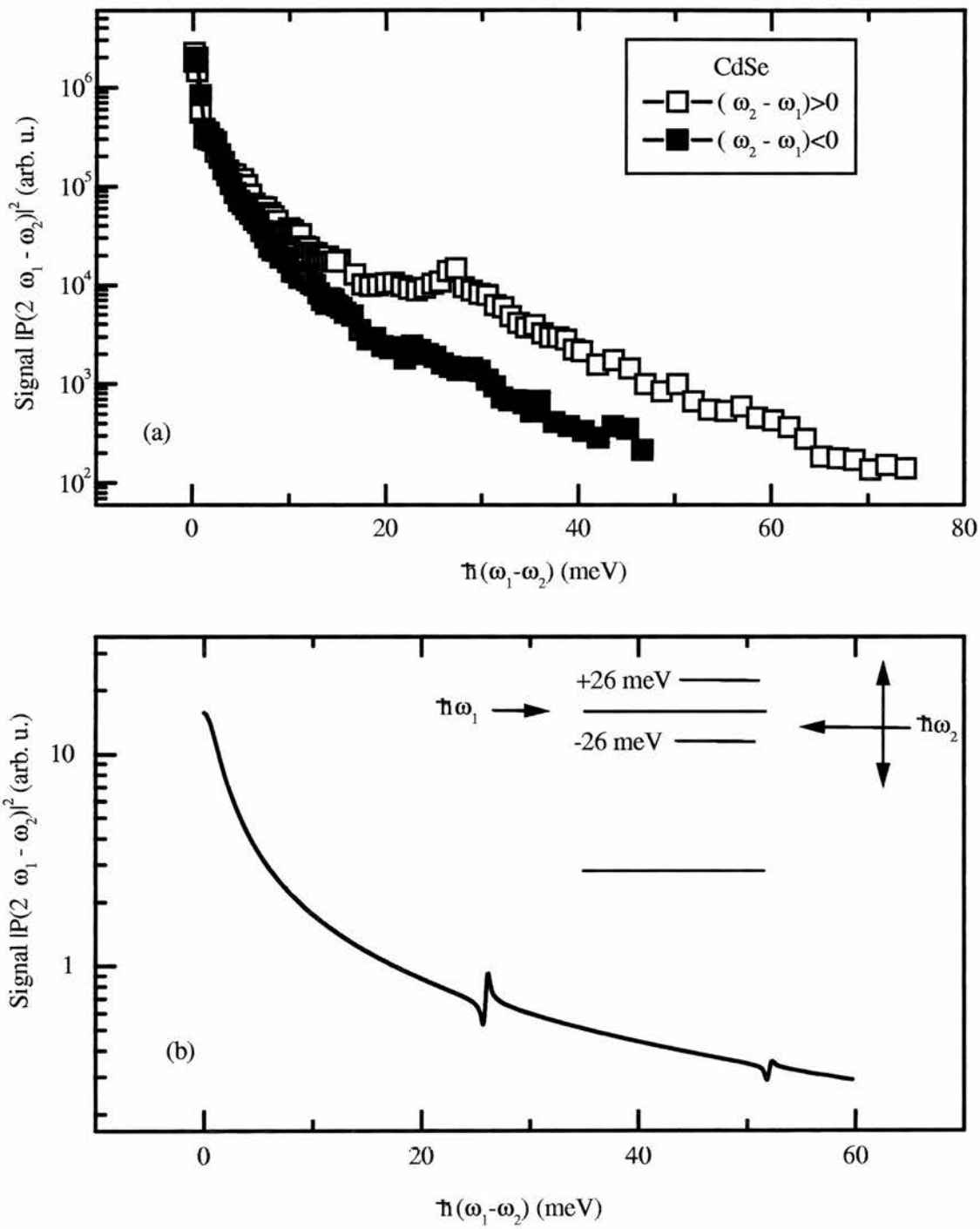

Figure 9.18: (a) Response of the dispersed CdSe quantum dots in glass to a bichromatic excitation in the non-degenerate four-wave mixing configuration. The measured signal is at the frequency $(2\omega_1 - \omega_2)$ [129]. (b) Numerical simulation of the response at the frequency $(2\omega_1 - \omega_2)$ of a four level system excited with two frequencies.

experiment is represented in figure 9.18b where we considered a four level system in which the three superior levels are equidistant in energy and their difference is 26meV (phonon energy). The theoretical simulation shows a resonance when the detuning of the two frequencies is 26meV but it cannot explain the difference between the two possible cases $(\omega_2 - \omega_1) > 0$ and $(\omega_2 - \omega_1) < 0$. Further experiments are necessary to confirm this difference.

9.5 Summary

The application to two level systems show several phenomena that appear in the presence of high intensity excitations. The pump-probe configuration is considered as a special case of a bichromatic excitation where one of the beams is of weak intensity and treated to zeroth order. In non-degenerate four-wave mixing, the two excitation beams are treated in the same manner, namely with the help of the truncated matrix obtained in the bichromatic case. In all these cases, simplified forms of the solution are deduced of which some are compared to the experimental results.

Chapter 10

Conclusion and future work

In this work we have dealt with the propagation of plane waves through multilayer structures and their interaction with electronic systems in these multilayers.

We started by deducing a novel method for the calculation of the optical properties of multilayer structures. This method (**LTR**) is solely based on physically meaningful quantities such as the transmission and reflection coefficients. The method is based on an addition operator that allows the formal combination of two multilayer elements resulting in the determination of the overall optical response of the structure. Further, we defined a multiplication operator suited to the treatment of periodic structures.

An important conclusion deduced from the properties of the multiplication operator is that a periodic structure can be treated as a single period and then the results can be broken up into surface and bulk properties. As one considers more and more periods of the structure the importance of the bulk properties increases whereas the surfaces are less and less important. In the case of optoelectronic structures the bulk properties give rise to band structures. When combining two different structures, the properties of the surface become important and greatly influences its immediate environment. One can thus introduce a surface band structure. This property can be applied to photonic crystals and in future work we plan to expand the formalism to be able to treat electronic structures in the same unique formalism.

Another important expansion of our **LTR** method is the inclusion of interface roughness effects. These roughness effects are treated as a statistical distribution of the position of the interface. Optically, our model of the roughness can be observed in the transmission and reflection spectra as a decrease in the contrast of Fabry-Perot fringes.

In the case of high finesse cavities such as LEDs or VCSELs the roughness changes the emission mode through broadening and decreased intensity. Applied to selectively oxidised structures we could deduce the effective roughness introduced by the oxidation. Further, comparing, for a monolayer sample, the roughness model with the roughness measured by atomic force microscopy we showed that these were in good agreement. Our optical method overestimates the roughness effects which are due to the greater sampling domain of the structure.

Another use of the **LTR** formalism is the treatment of continuous refractive index variations and non linear propagation. In the latter case we arrived at the conclusion that one can find the solutions to non-linear intensity-dependent propagation equations by defining a sequence of solutions as a function of the intensity. This sequence corresponds to the evolution of the system when slowly increasing the intensity.

We showed that our **LTR** formalism is in reality a more general formalism by applying it to various different cases. Indeed, the formalism always works when we are in the presence of an interface at which we have continuity conditions of two functions on one side and of one function on the other side of the interface. This configuration leads to the consideration of reflection and transmission coefficients of these functions. Using this general approach we demonstrate the use of our formalism to find the propagation modes in plane waveguides and the eigen states in multiple quantum wells.

Starting from the eigen states in multiple quantum wells we used the density matrix formalism to study the interaction between light and a quantum n-level system. We showed that using standard procedures to solve the density matrix equations the solution breaks down when treating high intensity excitations. In order to address this problem we developed a recursive solution method based on a combination between the continuous fraction method and the Floquet expansion. This method can be used to treat monochromatic as well as bichromatic excitations in or out of resonance with the quantum system.

We applied our recursive solution method to different configurations such as the single beam excitation, the pump-probe configuration and the non-degenerate four wave mixing case. In conclusion we showed that many of the non-linear effects present at high intensity can be understood in the framework of a single and unique model. This allowed the explanation of the link between the plateau observed in the generation of high harmonic frequencies and the saturation of the population inversion of the system.

In short this effect originates in the impossibility of the system to store the energy received at high intensities in the population inversion. The energy is then mostly converted into the higher harmonics. This induces abnormally high harmonic generation at high intensities. Further, using our recursive solution method we could show a quantum behaviour as a function of the excitation intensity. Indeed, as one increases the intensity oscillations appear in the response of the system. These oscillations take place when the electromagnetic energy of the interaction is a multiple of the resonance frequency and correspond to the successive saturation of the multi-photon absorption. In the pump probe configuration we showed the appearance of pump induced virtual resonance. Finally, we showed the possibility of measuring coherence relaxation times using the frequency detuning between the two beams in the nondegenerate four-wave mixing configuration. The spectra obtained in this setup shows that resonance effects become observable when the beating period between the two beams is comparable to the coherence relaxation times. It is thus possible to measure relaxation times which are smaller than the pulse duration of the pulse.

In future work, we plan to combine in a unique framework the **LTR** formalism and the quantum n-level systems. With this model we hope to study more complex periodic and non periodic devices where we have an intrinsic coupling between the electromagnetic wave and the electronic wave. Another promising direction of study is the generalisation of our methods to three dimensional structures such as photonic crystals and induced gratings. Finally, we wish to expand our results to treat the propagation of short pulses through these structures.

Acknowledgements

To my parents and fiancée for their help, patience, encouragement and moral support.

To Alan Miller for giving me the opportunity to work in his group and to write this thesis.

To Bernd Hönerlage (Strasbourg) for getting me started on the study of the n-level systems and for showing me how treat this problem.

To Dominique Ohlmann, Philippe Riblet and Vesko Donchev for their experimental work and helpful discussions when trying to understand the results.

To the rest of the A-Team, Dawn, Julia, Jonathan, Steve and John-Mark for their friendly help.

To the Strasbourg team, B. Hönerlage, J.-B. Grun, C. Hirlimann, R. Levy, and P. Gilliot for letting me work in their group and for all their help.

To my colleagues from Strasbourg, Dominique, Jean-Frederic, Philippe, Stephane, Paul and Dirk for sharing so much with me.

To David M. Finlayson for proof reading the thesis and for all his interesting conversations.

Bibliography

[1] K. Ishiguro and T. Kato. *J. Phys. Soc. Jap.*, 8(1):77, 1953.

[2] H.A. MacLeod. *Thin-Film Optical Filters.* Adam Hilger, London, 1969.

[3] Z. Knittl. *Optics of Thin Films.* John Willy & Sons, London, 1976.

[4] O.S. Heavens. *Optical Properties of Thin Solid Films.* Butterworth Scientific Publications, London, 1950.

[5] A. Vasicek. *Optics of Thin Films.* North Holland, Amsterdam, 1960.

[6] H. Anders. *Thin Films in Optics.* Focal Press, London, 1967.

[7] S.D. Smith. Design of multilayer filters by considering two effective interfaces. *J. Opt. Soc. Am.*, 48:43, 1958.

[8] P. Lorrain, D.R. Corson, and F. Lorrain. *Electromagnetic Fields and Waves.* W.H. Freeman and Company, New York, 1988.

[9] M. Born and E. Wolf. *Principles of Optics, Electromagnetic Theory of Propagation, Interference and Diffraction of Light.* Pergamon Press, Oxford, 1980.

[10] F. Abeles. *Ann. de Physique*, 5:777, 1950.

[11] Y. Fu, Y.-M. Mu, and M. Willander. *Superlattices and Microstr.*, 23:417, 1998.

[12] P.J. Leurgans. *J. Opt. Soc. Am.*, 41:714, 1951.

[13] J.A. Berning and P.H. Berning. *J. Opt. Soc. Am.*, 50:805, 1960.

[14] T. J. Cui and C. H. Liang. Inverse scattering method for arbitrary fractal cantor bar multilayers. *J. Phys. D-Applied Physics*, 26:1843–1850, 1993.

[15] L. Brillouin. *Wave Propagation in Periodic Structures.* Mc Graw-Hill Book Company, New York, 1946.

[16] A.V. Andreev and J.R. Prudnikov. *Crystallogr. Rep.*, 41:203, 1996.

[17] M. Afromowitz. *Solid State Commun.*, 15:59–63, 1974.

[18] A Xu and B.L. Evans. The performance simulation of multilayer reflectors in soft-x-ray and EUV regions. *Mod. and Sim. in Mat. Sci. and Eng.*, 2(5):1079–1092, 1994.

[19] V. V. Konotop. On wave propagation in periodic structures with smoothly varying parameters. *J. Optical Soc. America B-Optical Phys.*, 14:364–369, 1997.

[20] G. T. Kiehne, A. E. Kryukov, and J. B. Ketterson. A numerical study of optical second-harmonic generation in a one-dimensional photonic structure. *Applied Phys. Letters*, 75:1676–1678, 1999.

[21] T. Hattori, N. Tsurumachi, and H. Nakatsuka. Analysis of optical nonlinearity by defect states in one- dimensional photonic crystals. *J. Optical Soc. America B-Optical Phys.*, 14:348–355, 1997.

[22] A.W. Snyder and J.D. Love. *Optical waveguide theory.* Chapman and Hall, 1983.

[23] M. Lehman and M. Garavaglia. Beam reflection from multilayers with periodic and fractal distributions. *J. Modern Optics*, 46:1579–1593, 1999.

[24] W. M. Robertson, S. A. Boothroyd, and L. Chan. Photonic band-structure calculations using a 2-dimensional electromagnetic simulator. *J. Modern Optics*, 41:285–293, 1994.

[25] A. Rosenberg, R. J. Tonucci, H. B. Lin, and E. L. Shirley. Photonic-band-structure effects for low-index-contrast two- dimensional lattices in the near-infrared. *Phys. Review B-Condensed Matter*, 54:R5195–R5198, 1996.

[26] R. Biswas, M.M. Sigalas, G. Subramania, and K.M. Ho. Photonic band gaps in colloidal systems. *Phys. Review B-Condensed Matter*, 57(7):3701–3705, 1998.

[27] A. J. Ward and J. B. Pendry. Refraction and geometry in Maxwell's equations. *J. Modern Optics*, 43:773–793, 1996.

[28] D. Barchiesi. A 3-d multilayer model of scattering by nanostructures. Application to the optimisation of thin coated nano-sources. *Optics Comm.*, 126:7–13, 1996.

[29] H. Nishihara, M. Haruna, and T. Suhara. *Optical integrated circuits.* McGraw-Hill, 1985.

[30] E. Yablonovitch. Inhibited spontaneous emission in solid-state physics and electronics. *Phys. Review Letters*, 58:2059–2062, 1987.

[31] S. John. Strong localization of photons in certain disordered dielectric superlattices. *Phys. Review Letters*, 58:2486–2489, 1987.

[32] P. M. Hui, W. M. Lee, and N. F. Johnson. Theory of scalar wave-propagation in periodic composites - a k·p approach. *Solid State Comm.*, 91:65–69, 1994.

[33] A. Figotin and V. Gorentsveig. Localized electromagnetic waves in a layered periodic dielectric medium with a defect. *Phys. Review B-Condensed Matter*, 58:180–188, 1998.

[34] N. H. Liu. Defect modes of stratified dielectric media. *Phys. Review B-Condensed Matter*, 55:4097–4100, 1997.

[35] E. Özbay, M. S. Islam, B. Onat, M. Gükkavas, O. Aytür, G. Tuttle, E. Towe, R.H. Henderson, and M. S. Ünlü. http://photon.bu.edu/selim/papers/ptl-97/ptl.html.

[36] D. Ohlmann, O. Cregut, I. Pelant, R. Granger, R. Triboulet, and B. Honerlage. *Journal of Luminescence*, 54:357, 1993.

[37] V. Netiksis, B. Honerlage, R. Weil, J.L. Loison, J.B. Grun, and R. Levy. *J. Appl. Phys.*, 74:5729, 1993.

[38] D. Ohlmann, M. Mazilu, R. Levy, and B. Honerlage. *Appl. Phys.*, 82:1335, 1997.

[39] M. Mazilu, D. Ohlmann, and B. Honerlage. *Journal of Luminescence*, 72-74:824, 1997.

[40] R. Weil, M. Joucla, J.L. Loison, M. Mazilu, D. Ohlmann, M. Robino, and G. Schwalbach. *Appl. Phys.*, 37:2681, 1998.

[41] F. Yang, M. Wilkinson, E. J. Austin, and K. P. ODonnell. *Phys. Rev. Lett.*, 70:323, 1993.

[42] Y.-G. Zhao, Y.-H. Zou, Y.-D. Qin, and X.-L. Nuang. *Appl. Phys. Lett.*, 72:97, 1998.

[43] W. Braun, L. V. Kulik, T. Baars, M. Bayer, and A. Forchel. *Phys. Rev. B*, 57:7196, 1998.

[44] T. G. Dargam and B. Koiller. *Solid State Commun.*, 105:211, 1998.

[45] Y. Fu, Y.-M. Mu, and M. Willander. *Superlattices and Microstr.*, 23:417, 1998.

[46] H.-E. Shin, Y.-G. Ju, H.-W. Song, D.-S. Song, I.-Y. Han, J.-H. Ser, H.-Y. Ryu, and Y.-H. Lee. *Appl. Phys. Lett.*, 72:2205, 1998.

[47] T. Takamori, K. Takamesa, and T. Kamijoh. *Appl. Phys. Lett*, 69:659, 1996.

[48] S. Guha, F. Agahi, B. Pezeshki, J. A. Kash, D. W. Kisker, and N.A. Bojarczuk. *Appl. Phys. Lett*, 68:906, 1996.

[49] Z. Liliental-Weber, M. Li, G. S. Li, C. Chang-Hasnain, and E. R. Weber. *Proc. Microscopy and Microanalysis.* San Francisco Press, San Francisco, 1996. (Eds. G. W. Bailey, J. M. Corbett, R. V. W. Dimlich, J. R. Michael, and N. J. Zaluzec).

[50] M. H. MacDougal, H. Zhao, P. D. Dapkus, M. Ziari, and W. H. Steier. *Electronics Lett.*, 30:1147, 1994.

[51] P. Heremans, M. Kuijk, R. Windisch, J. Vanderhaegen, H. De Neve, R. Vounckx, and G. Borghs. *J. Appl. Phys.*, 82:5265, 1997.

[52] M. Mazilu, V. Donchev, O. Blum, and A. Miller. *Appl. Phys. B*, 68:633, 1999.

[53] M. Mazilu, V. Donchev, O. Blum, and A. Miller. *paper presented at the conference EQEC99, Baltimore, USA*, 1999.

[54] M. Mazilu, V. Donchev, O. Blum, and A. Miller. *paper presented at the conference QE14, Manchester, UK*, 1999.

[55] T.D.S. Hamilton, I.H. Munro, and G. Walker. *Luminescence Spectroscopy.* Academic Press, London, 1978.

[56] V. Donchev, M. Mazilu, and A. Miller. *paper presented at the conference LEOS, Orlando, USA*, 1998.

[57] M. Afromowitz. *Solid State Commun.*, 15:59–63, 1974.

[58] R. E. Fern and A. Onton. *J. Appl. Phys.*, 42:3499, 1971.

[59] A. Messiah. *Quantum Mechanics*, volume 1. North-Holland Publishing Company, 1967.

[60] L. Landau and E. Lifshitz. *Mécanique Quantique*, volume 3. MIR, 1967.

[61] C. Cohen-Tannoudji, B. Diu, and F. Laloë. *Mécanique Quantique*, volume 1. Hermann, 1977.

[62] L. Mandel and E. Wolf. *Optical coherence and quantum optics.* Cambridge University Press, 1995.

[63] C. Kittel. *Quantum theory of solids.* John Wiley & Sons, 1987.

[64] J. Pankove. *Optical processes in semiconductors.* Dover Publications, 1971.

[65] E. Schrödinger. Quantisierung als eigenwertproblem. *Ann. Phys.*, 79:361 and 489, 1925.

[66] H.B. Callen and T.A. Welton. *Phys. Rev.*, 83:34, 1951.

[67] A. Yariv. *Quantum Electronics, 2^{nd} Edition.* John Wiley & Sons, Inc., 1975.

[68] L. Landau and E. Lifshitz. *Statistical physics.* North Holland, Amsterdam, 1980.

[69] C. Cohen-Tannoudji, B. Diu, and F. Laloë. *Mécanique Quantique*, volume 2. Hermann, 1986.

[70] D.C. Hutchings, M. Sheik-Bahae, D.J. Hagan, and W. Van Stryland. Kramers-Kronig relations in nonlinear optics. *Opt. and Quantum Elec.*, 24:1–30, 1992.

[71] S. Scandolo and F.Bassani. Kramers-Kronig relation and sum-rules for the 2^{nd}-harmonic susceptibility. *Phys.Rev.B*, 51(11):6925–6927, 1995.

[72] W. A. Harrison. *Solid State Theory.* McGraw-Hill, 1970.

[73] P. Y. Yu and M. Cardona. *Fundaments of Semiconductors.* Springer, 1996.

[74] E. Diez, A. Sanchez, F. Dominguezadame, and G. P. Berman. Electron dynamics in intentionally disordered semiconductor superlattices. *Phys. Review B-Condensed Matter*, 54:14550–14559, 1996.

[75] M. W. Street, N. D. Whitbread, D. C. Hutchings, J. M. Arnold, J. H. Marsh, J. S. Aitchison, G. T. Kennedy, and W. Sibbett. Quantum-well intermixing for the control of second-order nonlinear effects in AlGaAs multiple-quantum-well waveguides. *Optics Letters*, 22:1600–1602, 1997.

[76] A. Würger. Non-linear dynamics of a driven two-level tunnelling defect. *Z.Phys.B*, 93:109–118, 1993.

[77] R. Bavli and Y.Dakhnovskii. Two-level system in a strong laser field: A comparative analysis between the Landau-Lifshitz solution and an exact numerical one. *Phys.Rev.A*, 48(2):R886–R889, 1993.

[78] J.M. Gomez Llorente and J. Plata. Tunnelling control in a two-level system. *Phys.Rev.A.*, 45(10):R6958–R6961, 1992.

[79] P. Sundaram and P.W.Milonni. High-order harmonic generation:simplified model and relevance of single-atom theories to experiment. *Phys.Rev.A.*, 41(11):6571–6573, 1990.

[80] M. Dörr and R.Shakeshaft. Resonance enhancement of above-threshold peaks in multiphoton ionization. *Phys.Rev.A.*, 38(1):543–546, 1988.

[81] M. Dörr, O. Latinne, and C.J. Joachain. Time evolution of a hydrogen atom in a strong, ultrashort, high-frequency laser pulse. *Phys.Rev.A.*, 52(5):4289–4292, 1995.

[82] G. Arfken. *Mathematical Methods for Physicists.* Academic Press, Orlando, Florida, third edition, 1985.

[83] P. Bergé, Y. Pomeau, and Ch. Vidal. *L'ordre dans le chaos.* Herman Editeurs des Sciences et des Arts, Paris, 1984.

[84] R. Dandoloff, R. Balakrishnan, and A.R. Bishop. Two-level system: space curve formalism, Berry's phase and Gauss-Bonnet theorem. *J.Phys.A.Math.Gen.*, 25:L1105–L1110, 1992.

[85] L. Plaja and L. Roso-Franco. Adiabatic theory for high-order harmonic generation in a two-level atom. *J. Opt. Soc. Am. B*, 9(12):2210–2213, 1992.

[86] T.S. Ho and J. Tietz. Semiclassical many-mode Floquet theory. *Chemical Phys.Lett.*, 96(4):464–471, 1983.

[87] T.-S. Ho and S. Chu. Semiclassical many-mode Floquet theory: II. non-linear multiphoton dynamics of a two-level system in a strong bichromatic field. *Phys.A.*, 17:2101–2128, 1984.

[88] J.H. Shirley. Solution of the Schrödinger equation with a Hamiltonian periodic in time. *Phys.Rev.*, 138(4B):B979–B987, 1965.

[89] X.-G. Zhao. Quasienergy and Floquet in a time-periodic driven two-level system. *Phys.Rev.B*, 49(23):16753–16756, 1994.

[90] N. Nayak. Squeezing in nondegenerate two-photon processes in a cavity quantum electrodynamics of a three-level and a two-level Rydberg atom. *Phys.Rev.A.*, 47(3):2276–2280, 1993.

[91] M.W. Beijersbergen, R.J.C. Spreeuw, L. Allen, and J.P. Woerdman. Multiphoton resonances and Bloch-Siegert shifts observed in a classical two-level system. *Phy.Rev.A*, 45(3):1810–1815, 1992.

[92] N.B. Manson, C. Wei, and J.P.D. Martin. Response of a two-level system driven by two strong fields. *Phys.Rev.Lett.*, 46(21):3943–3946, 1996.

[93] G.S. Agarval, Y.Zhu, D.J.Gauthier, and T.W.Mossberg. Spectrum of radiation from two-level atoms under intense bichromatic excitation. *J.Opt.Soc.Am.B*, 8(5):1163–1167, 1991.

[94] W.M. Ruyten. Some analytical results for the fluorescence spectrum of a two-level atom in a bichromatic field. *J.Opt.Soc.Am.*, 9(10):1892–1894, 1992.

[95] M. Dörr, R.M.Potvliege, D.Prolux, and R.Shakeshaft. Multiphoton processes in a intense laser field. VI. two-color ionization with incommensurable frequencies. *Phys.Rev.A.*, 44(1):574–583, 1991.

[96] Z. Ficek and H.S.Freedhof. Resonance-fluorescence and absorption spectra of a two-level atom driven by a strong bichromatic field. *Phys.Rev.A*, 48(4):3092–3104, 1993.

[97] S.P. Goreslavskii and V.P.Krainov. Two-level atom in a bichromatic resonance field. *Sov.Phys.JETP*, 49(1):13–17, 1979.

[98] C.-G. Wahlström. High-order harmonic generation using high-power lasers. *Physica Scripta*, 49:201–208, 1994.

[99] M. Ferray, A. L'Huillier, X.F. Li, and L.A. Lompre. Multiple-harmonic conversion of 1064 nm radiation in rare gases. *J. Phys. B*, 21:L31, 1988.

[100] A. McPherson, G. Gibson, H. Java, U. Johann, T.S. Luk, I.A. McIntyre, K. Boyer, and C.K. Rhodes. Studies of multiphoton production of vacuum-ultraviolet radiation in the rare gases. *J. Opt. Soc. Am. B*, 4:595, 1987.

[101] A. L'Huillier and Ph.Balcou. High-order harmonic generation in rare gases with a 1-ps 1053-nm laser. *Phys.Rev.Lett.*, 70(6):774–777, 1993.

[102] A. L'Huillier, K.J. Schafer, and K.C. Kulander. Theoretical aspects of intense field harmonic generation. *J.Phys.B.*, 24:3315–3341, 1991.

[103] J.H. Eberly and Q. Su. Nonlinear light scattering accompanying multiphoton ionization. *Phys.Rev.Lett.*, 62(8):881–884, 1989.

[104] R.A. Sacks and A. Szöke. Generation of harmonic radiation during electron scattering from piece-wise constant potential in an intense electromagnetic field. *J. Opt. Soc. Am. B*, 8(9):1987–1998, 1991.

[105] K.C. Kulander and B.W. Shore. Calculations of multiple-harmonic conversion of 1064-nm radiation in Xe. *Phys.Rev.Lett.*, 62(5):524–526, 1989.

[106] P.L. DeVries. Calculation of harmonic generation during multiphoton ionization of the hydrogen atom. *J. Opt. Soc. Am. B*, 7:517–520, 1990.

[107] K.J. LaGattuta. Laser effects in photoionization II. numerical solution of coupled equations for atomic hydrogen. *Phys. Rev. A*, 41:5110–5116, 1990.

[108] L. Plaja and L.Roso-Franco. High-order harmonic generation in a crystalline solid. *Phys.Rev.B.*, 45(15):8334–8341, 1992.

[109] S.I. Chu, K. Wang, and E. Layton. Nonperturbative treatments of level shifts of excited states and high-order harmonic generation in strong fields. *J. Opt. Soc. Am. B*, 7:425–432, 1990.

[110] R.M. Potvliege and R. Shakeshaft. Multiphoton processes in a intense laser field: Harmonic generation and total ionization rates for atomic hydrogen. *Phys.Rev.A.*, 40(6):3061–3079, 1989.

[111] G. Bandarage, A.Maquet, and J.Cooper. Harmonic generation by a classical hydrogen atom in the presence of an intense radiation field. *Phys.Rev.A.*, 41(3):1744–1746, 1990.

[112] W. Becker, S. Long, and J.K. McIver. Higher-harmonic production in a model atom with short range potential. *Phys. Rev. A*, 41(7):4112–4115, 1990.

[113] Al.L. Éfros and A. L. Éfros. Interband absorption of light in a semiconductor sphere. *Sov. Phys. Semicond.*, 16(7):772–775, 1982.

[114] H. Haug and S.W. Koch. *Quantum Theory of the Optical and Electronic Properties of Semiconductors.* World Scientific, 1990.

[115] M. Combescot. Optical stark effect of the exciton. II. polarization effects and exciton splitting. *Phy.Rev.B*, 41(6):3517–3533, 1990.

[116] R. Shakeshaft, R.M.Potvliege, M.Dörr, and W.E.Cooke. Multiphoton processes in a intense laser field. iv the static- field limit. *Phys.Rev.A.*, 42(3):1656–1668, 1990.

[117] M. Dörr, R.M.Potvliege, and R.Shakeshaft. Tunneling ionization of atomic hydrogen by an intense low-frequency field. *Phys.Rev.Lett*, 64(17):2003–2006, 1990.

[118] K. Burnett, P.L. Knight, B.R.M. Piraux, and V.C. Reed. Suppression of ionization in strong laser fields. *Phys.Rev.Lett.*, 66(3):301–304, 1991.

[119] R.R. Jones and P.H. Bucksbaum. Ionization suppression of Stark states in intense laser fields. *Physical Review Letters*, 67(23):3215–3218, 1991.

[120] U. Fano. Effects of configuration interaction on intensities and phase shifts. *Phys. Rev.*, 124(6):1860–1878, 1961.

[121] J.Y. Bigot and B.Hönerlage. On the dielectric function of three-level systems under high excitation. *Phys.stat.sol.(b)*, 121:649–659, 1984.

[122] B. Hönerlage and J.Y.Bigot. On the dielectric function of three-level systems under high excitation ii. *Phys.stat.sol.(b)*, 123:201–208, 1984.

[123] D. Ohlmann, M. Mazilu, R. Levy, and B. Hönerlage. Tunable optical nonlinearities in $Cd_{1-x}Zn_xTe$ ternary alloys. *J. of Appl. Phys.*, 82(3):1355–1358, 1997.

[124] M. Mazilu, D. Ohlmann, and B. Hönerlage. Adjustable optical nonlinearities in $Cd_{1-x}Zn_xTe$ alloys. *J. of Lum.*, 72(4):824–825, 1997.

[125] T. Yajima and Y.Taira. Spatial optical parametric coupling of picosecond light pulses and tranverse relaxation effect in resonant media. *J.of Phys.Soc. of Japan*, 47(5):1620–1626, 1979.

[126] E. Hanamura. Effects of trapped states on spectra of four-wave mixing and differential transmission. *Phys.Rev.B*, 46(8):4718–4731, 1992.

[127] G.I. Toptygina and E.E. Fradkin. Theory of subradiative absorption structure in the interaction between two intense waves in a nonlinear medium. *Sov.Phys.JETP*, 55(2):246–251, 1982.

[128] A.M. Bonch-Bruevich, T.A.Vartanyan, and N.A.Chigir. Subradiative structure in the absorption spectrum of a two-level system in a biharmonic radiation field. *Sov.Phys.JETP*, 50(5):901–906, 1979.

[129] P. Riblet. *Etude comparée des nonlinéarités optiques de nanocristaux et monocristaux de CdS et CdSe.* Université Louis Pasteur, Strasbourg, 1995.

Publications

- A. Miller, P. Riblet, M. Mazilu, S. White, T.M. Holden, A.R. Cameron and P. Perozzo, Exciton saturation in GaAs multiple quantum wells at room temperature, J. Appl. Phys. **86**(7), pp 3734-3744, 1999

- M. Mazilu M, V. Donchev, O. Blum and A. Miller, Optical determination of interface roughness in multilayered semiconductor structures, Appl. Phys. B-Lasers Opt. **68**(3), pp 633-636, 1999

- R. Weil, M. Joucla, J.L. Loison, M. Mazilu, D. Ohlmann, M. Robino and G. Schwalbach, Preparation of optical quality ZnCdTe thin films by vacuum evaporation, Appl. Opt. **37**(13), pp 2681-2686, 1998

- D. Ohlmann, M. Mazilu, R. Levy and B. Honerlage, Tunable optical nonlinearities in $Cd_{1-x}Zn_xTe$ ternary alloys, J. Appl. Phys. **82**(3), pp 1355-1358, 1997

- M. Mazilu and B. Honerlage, Exact solution for excitons in intense laser fields, J. Lumines. **74**(4), pp 802-803, 1997

- M. Mazilu, D. Ohlmann and B. Honerlage, Adjustable optical nonlinearities in $Cd_{1-x}Zn_xTe$ alloys, J. Lumines. **74**(4), pp 824-825, 1997

- E. Vanagas, J. Moniatte, M. Mazilu, P. Riblet, B. Honerlage, S. Juodkazis, F. Paille, J.C. Plenet, J.G. Dumas, M. Petrauskas and J. Vaitkus, Dynamics of optical nonlinearities induced by strong light illumination in CdS nanocrystallites, J. Appl. Phys. **81**(8), pp 3586-3591, 1997

List of Figures